Vol. 52, No.2 / 2017

e: ISSN 2068 – 2239
p: ISSN 2068 – 4215

INMATEH -

AGRICULTURAL ENGINEERING

MAY - AUGUST

Editorial

The National Institute of Research-Development for Machines and Installations designed to Agriculture and Food Industry - INMA Bucharest has the oldest and most prestigious research activity in the field of agricultural machinery and mechanizing technologies in Romania.

Short History

- In 1927, the first research **Center for Agricultural Machinery** in Agricultural Research Institute of Romania - ICAR (Establishing Law was published in O.D. no. 97/05.05.1927) was established;
- In 1930, was founded **The Testing Department of Agricultural Machinery and Tools** by transforming Agricultural Research Centre of ICAR - that founded the science of methodologies and experimental techniǎues in the field (Decision no. 2000/1930 of ICAR Manager - GHEORGHE IONESCU ŞIŞEŞTI);
- In 1952, was established the Research Institute for Mechanization and Electrification of Agriculture - ICMA Băneasa, by transforming the Department of Agricultural Machines and Tools Testing;
- In 1979, the Research Institute of Scientific and Technological Engineering for Agricultural Machinery and Tools – ICSITMUA was founded - subordinated to Ministry of Machine Building Industry - MICM, by unifying ICMA subordinated to MAA with ICPMA subordinated to MICM;
- In 1996 the National Institute of Research-Development for Machines and Installations designed to Agriculture and Food Industry – INMA was founded – according to G.D. no.1308/25.11.1996, by reorganizing ICSITMUA, G.D no. 1308/1996 coordinated by the Ministry of Education and Research G.D. no. 823/2004;
- In 2008 INMA has been accredited to carry out research and developing activities financed from public funds under G.D. no. 551/2007, Decision of the National Authority for Scientific Research - ANCSno. 9634/2008.

As a result of widening the spectrum of communication, dissemination and implementation of scientific research results, in 2000 was founded the institute magazine, issued under the name of SCIENTIFIC PAPERS **(INMATEH)**, ISSN 1583 – 1019.

Starting with volume 30, no. 1/2010, the magazine changed its name to **INMATEH - Agricultural Engineering**, appearing both in print format (ISSN 2068 - 4215), and online (ISSN online: 2068 - 2239). The magazine is bilingual, being published in Romanian and English, with a rhythm of three issues / year: January-April, May-August, September-December and is recognized by CNCSIS – with B^{+} category. Published articles are from the field of AGRICULTURAL ENGINEERING: technologies and technical equipment for agriculture and food industry, ecological agriculture, renewable energy, machinery testing, environment, transport in agriculture etc. and are evaluated by specialists inside the country and abroad, in mentioned domains.

Technical level and performance processes, technology and machinery for agriculture and food industry increasing, according to national reǎuirements and European and international regulations , as well as exploitation of renewable resources in terms of efficiency, life, health and environment protection represent referential elements for the magazine „**INMATEH - Agricultural Engineering**".

We are thankful to all readers, publishers and assessors.

Editor in chief,
Ph.D. Eng. Vladut Nicolae-Valentin

In the present, *INMATEH - Agricultural Engineering* journal is indexed in the next international databases:
ULRICHS Web: Global Serials Directory, CABI, SCIPIO, ELSEVIER /SciVerse SCOPUS, Index COPERNICUS International, EBSCO Publishing, Elektronische Zeitschriftenbibliothek

INMATEH - Agricultural Engineering
vol. 52, no.2/ 2017
NATIONAL INSTITUTE OF RESEARCH-DEVELOPMENT FOR MACHINES AND INSTALLATIONS DESIGNED TO AGRICULTURE AND FOOD INDUSTRY - INMA Bucharest

6 Ion Ionescu de la Brad Blvd., sector 1, Bucharest

Three issues per year,
eISSN: 2068 – 2239
pISSN: 2068 – 4215

Edited by: INMA Bucharest

CONTENT

		Pag.
1.	**INFLUENCE OF EQUAL-AREA PROJECTION OF THE CYLINDER DRUM'S CROSS-SECTION HEIGHT ON THE DESCRIPTION ACCURACY OF ITS OVERCOMING THE AIR RESISTANCE FORCE /** ***ВПЛИВ ЕКВІВАЛЕНТНОЇ ПРОЕКЦІЇ ВИСОТИ ПЕРЕТИНУ БАРАБАНА НА ТОЧНІСТЬ ОПИСУ ПОДОЛАННЯ НИМ СИЛИ ОПОРУ ПОВІТРЯ*** **Lect.Ph.D.Eng. Bohatyrov D.V., Doctor of Technical Sciences, Professor Salo V.M., Lect.Ph.D.Eng. Kyslun O.A., Lect. Ph.D. Eng. Skrynnik I.O., Asst.Ph.D. Stud. Eng. Kisilov R.V.** Kirovohrad National Technical University / Ukraine	7
2.	**THEORETICAL GROUNDING OF SEEDS VALVE OPENER SETTINGS FOR SUBSOIL-SPREADING SOWING METHOD /** ***ТЕОРЕТИЧНЕ ОБҐРУНТУВАННЯ ПАРАМЕТРІВ РОЗПОДІЛЬНИКА НАСІННЯ СОШНИКА ДЛЯ ПІДҐРУНТОВО-РОЗКИДНОГО СПОСОБУ СІВБИ*** **Ph.D. Eng. Zayets M., Ph.D. Eng. Sukmaniuk E, Ph.D. Eng. Grudovyi R.** Zhytomyr National Agroecological University / Ukraine	13
3.	**GEOSTATISTICAL APPROACH TO DETERMINE THE EFFECTS OF DIFFERENT SOIL TILLAGE METHODS ON PENETRATION RESISTANCE IN A CLAYEY SOIL /** ***KİLLİ TOPRAKTA FARKLI TOPRAK İŞLEME YÖNTEMLERİNİN PENETRASYON DİRENCİNE ETKİSİNİN BELİRLENMESİ İÇİN JEOİSTATİSTİKSEL BİR YAKLAŞIM*** **Assist.Prof.Dr. Selvi K.Ç.*1), Assoc.Prof.Dr.Sağlam M2), Prof.Dr.Dengiz O2)** 1)Department of Agriculture Machinery and Technologies Engineering, Faculty of Agriculture, OndokuzMayıs University, Atakum, Samsun / Turkey; 2) Dep. of Soil Science and Plant Nutrition, Faculty of Agriculture, OndokuzMayıs University, Samsun / Turkey	19
4.	**THE RESEARCH CONCEPT ON THE WEEDING PROCESS AND THE CONTACT ACTION MACHINES /** ***ФОРМУВАННЯ КОНЦЕПЦІЇ ДОСЛІДЖЕННЯ ПРОЦЕСУ ЗНИЩЕННЯ БУР'ЯНІВ І МАШИНИ КОНТАКТНОГО СПОСОБУ ДІЇ*** **Ph.D. Eng. Bundza O.Z. 1), Prof. Ph.D. Eng. Nalobina O.O. 1), Assoc.Prof. Ph.D. Eng. Nikitin V.G. 1), Ph.D. Eng. Tkachuk O.L. 2)** 1) National University of Water Management and Nature Resources Use, Rivne / Ukraine 2) Lutsk National Technical University, Lutsk / Ukraine	27
5.	**GROUNDING OF CONSTRUCTION PARAMETERS OF PSEUDOFLUIDIZED LAYER DRYER WORKING CHAMBER /** ***ОБОСНОВАНИЕ КОНСТРУКТИВНЫХ ПАРАМЕТРОВ РАБОЧЕЙ КАМЕРЫ СУШИЛКИ ПСЕВДООЖИЖЕННОГО СЛОЯ*** **Prof. PhD. Eng.Sc. Kuznetsov Y.A., Assoc. Prof. D.Eng.Sc. Volzhentsev A.V., Prof. PhD. Eng.Sc. Kolomeichenko A.V., Prof. PhD. Eng.Sc. Kalashnikova L.V.** Orel State Agrarian University named after N.V. Parakhin / Russia	33
6.	**DESIGN AND PERFORMANCE TEST OF THE HALF-FED AND SELF-PROPELLED GARLIC HARVESTER /** ***半喂入自走式大蒜收获机的设计及性能测试*** **Ph.D. Eng. LÜ Xiaolian*1), Prof. Ph.D. Eng. HU Zhichao2), Prof. Ph.D. Eng. LÜ Xiaorong3), Prof. Eng. PENG Baoliang2)** 1) Chuzhou University, College of Machinery and Automotive Engineering / China; 2) Nanjing Research Institute for Agricultural Mechanization Ministry of Agriculture / China; 3) Sichuan Agricultural University, College of Machinery & Electronics / China	39
7.	**A PRAGMATIC METHODOLOGY TO ESTIMATE HOURLY ENERGY DEMAND PROFILE OF A CASE STUDIED DAIRY FARM; PRIMARY STEP TOWARD PV APPLICATION /** یک روش عملی برای تخمین پروفیل ساعتی برق مصرفی در یک گاوداری گاو شیری مورد مطالعه: گام نخستین در بکار گیری برق فتوولتاییک **Ph.D. Stud. Eng.Sarnavi H.J.1), Assoc.Prof.Ph.D. Eng. Nikbakht A.M.1), Assoc.Prof.Ph.D. Eng. Hasanpour A.1), Assoc.Prof.Ph.D. Eng. Shahbazi F.2), Assoc.Prof.Ph.D. Eng. Aste N.3), Assoc.Prof. Ph.D. Eng. Adhikari R.S.3)** 1)Department of Mechanical Engineering of Biosystems, Urmia University / Iran, 2)Department of Mechanical Engineering of Biosystems, Lorestan University / Iran, 3)Dep. of Architecture, Built Environment and Construction Engineering, Politecnico di Milano University / Italy	47

		Pag.
8.	**RESEARCH ON THE DYNAMICS OF SAPROPEL UNLOADING FROM A CABLE INSTALLATION BUCKET /** ***ДОСЛІДЖЕННЯ ДИНАМІКИ РОЗВАНТАЖЕННЯ САПРОПЕЛЮ ІЗ КОВША КАНАТНОЇ УСТАНОВКИ*** **Prof. Ph.D. Eng. Hevko B.M., Lect. Ph.D. Eng. Diachun A.Y., Lect. Ph.D. Eng. Dzyura V.O., Lect. Ph.D. Eng. Skyba O.P., Mel'nychuk S.L.** Ternopil Ivan Pul'uj National Technical University, Ruska Str., 56, Ternopil, Ukraine	55
9.	**STUDY OF THE PRESSURE REGULATOR WORK WITH A SPRING-DAMPER SYSTEM APPLIED TO MILKING MACHINE /** ***ДОСЛІДЖЕННЯ РОБОТИ РЕГУЛЯТОРА ТИСКУ З ПРУЖИННО-ДЕМПФЕРНОЮ СИСТЕМОЮ СТОСОВНО ДО ДОЇЛЬНИХ УСТАНОВОК*** **Assoc. Prof., Dr.Sc.Eng. Dmytriv V.T.[*1)], Lect. Ph.D.Eng. Dmytriv I.V.[1)], Lect. Ph.D.Eng. Lavryk Y.M.[1)], Postgraduate Krasnytsia B.[1)], Assoc. prof., Dr.Sc.Eng. Bubela T.Z.[2)], Prof., Dr.Sc.Eng. Yatsuk V.O.[2)]** [1)] Lviv National Agrarian University, Faculty of Mechanic and Power Engineering, Lviv-Dubliany / Ukraine [2)] Lviv Polytechnic National University, Department of Metrology, Standardization and Certification, Lviv / Ukraine	61
10.	**KINETIC FEATURES OF VIBRATING AND FILTRATION DEWATERING OF FRESH-PEELED PUMPKIN SEEDS /** ***ОСОБЛИВОСТІ КІНЕТИКИ ВІБРАЦІЙНО-ФІЛЬТРАЦІЙНОГО ЗНЕВОДНЕННЯ СВІЖЕОЧИЩЕН НАСІННЯ ГАРБУЗА*** **Ph.D. Tsurkan O.V. [1)], Eng. Gerasimov O.O.[1)], Ph.D. Polyevoda Y.A.[1)], Ph.D. Tverdokhlib I.V.[1)], Ph.D. Rimar T.I.[2)], Ph.D. Stanislavchuk O.V.[3)]** [1)]Vinnitsa National Agrarian University / Ukraine; [2)]National University "Lviv Polytechnic" / Ukraine, [3)]Lviv State University of Life Safety / Ukraine	69
11.	**RESEARCH ON REVERSIBLE HEAT PUMP INSTALLATION FOR GREENHOUSE HEATING /** ***ИЗСЛЕДВАНЕ НА РЕВЕРСИВНА ТЕРМОПОМПЕНА ИНСТАЛАЦИЯ ЗА ОТОПЛЕНИЕ НА ОРАНЖЕРИИ*** **Lecturer Ph.D. Eng. Kolev Z. D.[1)], Lecturer Ph.D. Eng. Kadirova S. Y.[*2)], Student Nenov T. R.[3)]** [1)] Rousse University "Angel Kunchev", Agrarian – Industrial Faculty / Bulgaria [2)] Rousse University "Angel Kunchev", Faculty of Electrical Engineering, Electronics and Automation / Bulgaria [3)] Rousse University "Angel Kunchev", Faculty of Electrical Engineering, Electronics and Automation / Bulgaria	77
12.	**MODELLING THE WORK OF CLOSED SYSTEM OF HEATING AND VENTILATION OF GREENHOUSES /** ***МОДЕЛЮВАННЯ РОБОТИ ЗАМКНУТОЇ СИСТЕМИ ОПАЛЕННЯ І ВЕНТИЛЯЦІЇ ТЕПЛИЦЬ*** **Doctor of Engineering Science Golub G.A.[1)], Ph.D. Eng. Kepko O.I.[2)]** [1)]National University of Life and Environmental Sciences of Ukraine, Kyiv / Ukraine, [2)] Uman National University of Horticulture, Uman', Ukraine	85
13.	**STRUCTURAL OPTIMIZATION OF A HANDHELD TILLER HANDRAIL BY VIBRATION MODAL ANALYSIS /** *基于振动模态分析的微耕机扶手架结构优化* **Ph.D. Niu P.[1)], Prof. Yang M.J.*[1)], Prof. Chen J.[1)], Ph.D. Yang L.[1)], Prof. Xie S.Y.[1)], Prof. Chen X.B.*[2)]** [1)] Southwest University, College of Engineering and Technology, Chongqing Key Laboratory of Agricultural Equipment for Hilly and Mountainous Regions / P. R. China; [2)] Agricultural Machinery Quality Control and Inspection Technology Centre, Nanjing Research Institute for Agricultural Mechanization Ministry of Agriculture / P. R. China	91
14.	**A THEORETICAL RESEARCH OF THE GRAIN MILLING TECHNOLOGICAL PROCESS FOR ROLLER MILLS WITH TWO DEGREES OF FREEDOM /** ***ТЕОРЕТИЧНЕ ДОСЛІДЖЕННЯ ТЕХНОЛОГІЧНОГО ПРОЦЕСУ ПОДРІБНЕННЯ ЗЕРНА У ВАЛЬЦЕВИХ СТАНКАХ З ДВОМА СТУПЕНЯМИ ВІЛЬНОСТІ*** **Prof.PhD.Eng. Bulgakov V.[1)], Prof.PhD.Eng.Holovach I.[1)], Prof.PhD. Eng. Bandura V.[2)], PhD.Eng. Ivanovs S.[3)]** [1)]National University of Life and Environmental Sciences / Ukraine, [2)]Vinnytsia National Agrarian University /Ukraine, [3)]Latvia University of Agriculture / Latvia	99
15.	**STUDY OF LONG HAUL TRUCK MOVEMENT ALONG THE CURVILINEAR TRAJECTORY WHILE STEERING A CARRYALL SEMI-TRAILER - CONTAINER BY BRAKING THE WHEELS OF ONE AXLE /** ***ДОСЛІДЖЕННЯ РУХУ АВТОПОЇЗДА ПО КРИВОЛІНІЙНІЙ ТРАЄКТОРІЇ ПРИ УПРАВЛІННІ УНІВЕРСАЛЬНИМ НАПІВПРИЧІПОМ-КОНТЕЙНЕРОВОЗОМ ШЛЯХОМ ГАЛЬМУВАННЯ КОЛІС ОДНІЄЇ ОСІ*** **Prof. Dr. Eng. Sakhno V.P.[1)], Prof. Ph.D. Eng. Marchuk M.M. [2)], Lect. Ph.D. Eng. Marchuk R.M.[2)].** [1)] National Transport University, Suvorova Str., 1, Kiev / Ukraine [2)] National University of Water and Environmental Engineering, Rivne / Ukraine	107

		Pag.
16.	**INFLUENCE OF ORGANIC OPERATION ENVIRONMENT ON CORROSION PROPERTIES OF METAL STRUCTURE MATERIALS OF VEHICLES /** ***ВПЛИВ ОРГАНІЧНИХ РОБОЧИХ СЕРЕДОВИЩ НА КОРОЗІЙНІ ХАРАКТЕРИСТИКИ МАТЕРІАЛІВ МЕТАЛОКОНСТРУКЦІЙ ТРАНСПОРТНИХ ЗАСОБІВ*** **Prof. Ph.D. Eng. Popovych P.V. [1], Prof. Ph.D. Eng. Lyashuk O.L. [1], Lect. Ph.D. Eng. Shevchuk O.S. [1], Lect. Ph.D. Eng. Tson O.P. [1], Lect. Ph.D. Eng. Poberezhna L.Ya. [2], Bortnyk I. M. [1]** [1]Ternopil Ivan Pul'uj National Technical University, Ternopil / Ukraine [2]Ivano-Frankivsk National Medical University, Ivano-Frankivsk / Ukraine	113
17.	**QUERY ALGORITHM OF AGROMETEOROLOGICAL BIG DATA BASED ON DISTRIBUTED MATCHING /** ***基于分布式匹配的农业气象大数据查询算法研究*** **Assoc. Professor Liu X.C.*[1], Ph.D. Chen S.[2], Ph.D. Wen L.Y.[3]** [1] Department of Information Engineering, Anhui Vocational and Technical College, Hefei/China; [2] Institute of Intelligent Machines, Chinese Academy of Sciences, Hefei/China; [3]Department of Computer Science and Electrical Engineering, West Virginia University, Morgantown/USA	119
18.	**A PRODUCTIVE POTENTIAL ESTIMATION OF FIVE GENOTYPES OF THE MISCANTHUS ANDERSS GENUS IN THE UKRAINIAN STEPPE ZONES CONDITIONS /** ***ОЦІНКА ПРОДУКТИВНОГО ПОТЕНЦІАЛУ П'ЯТИ ГЕНОТИПІВ МІСКАНТУСУ ANDERSS GENUS В УМОВАХ СТЕПОВОЇ ЗОНИ УКРАЇНИ*** **Prof. Ph.D. Agri.Sci. Kharytonov M.[1], Dr. Ph.D. Biol.Sci.Martynova N.[1], Dr. Assoc. Prof. Ph.D. Biol.Sci.Sitnyk S.[1], Dr. Assoc. Prof. Ph.D. Eng.Sci. Naumenko M. [1], Prof. Ph.D. Biol.Sci. Pidlisnyuk V.[2], Assoc. Prof. Ph.D. Biol.Sci.Stefanovska T.[3],** [1] Dnipropetrovsk State Agrarian and Economic University, Dnipro / Ukraine [2] Jan Evangelista Purkyne University in Ústí nad Labem, Ústí nad Labem / Czech Republic [3] National University of Life & Environmental Sciences, Kiev / Ukraine	129
19.	**SYNTHESIS OF SELF-CENTRING GRIPPERS /** ***SINTEZA MECANISMELOR DE PREHENSIUNE AUTOCENTRANTE*** **Prof. Ph.D. Eng. Moise V., Asoc.Prof. Ph.D.Eng.Tabără I., Lect. Ph.D. Eng. Dudici C.L., As. Ph.D. Stud. Eng. Bănică E., As. Ph.D. Stud. Eng. Rotaru Al., Eng. Boureci Gh. A., Eng. Stroe I.** University Politehnica of Bucharest / Romania	137
20.	**DETERMINATION OF RATIONAL OPERATING PARAMETERS FOR A VIBRATING DYSK-TYPE GRINDER USED IN ETHANOL INDUSTRY** ***ВИЗНАЧЕННЯ РАЦІОНАЛЬНИХ ЕКСПЛУАТАЦІЙНИХ ПАРАМЕТРІВ ВІБРОДИСКОВОЇ ДРОБАРКИ СПИРТОВОЇ ГАЛУЗІ*** **Ph.D. Yanovich V.P., Assist. Kupchuk I.M.** Vinnitsa National Agrarian University	143

INFLUENCE OF EQUAL-AREA PROJECTION OF THE CYLINDER DRUM'S CROSS-SECTION HEIGHT ON THE DESCRIPTION ACCURACY OF ITS OVERCOMING THE AIR RESISTANCE FORCE
/
ВПЛИВ ЕКВІВАЛЕНТНОЇ ПРОЕКЦІЇ ВИСОТИ ПЕРЕТИНУ БАРАБАНА НА ТОЧНІСТЬ ОПИСУ ПОДОЛАННЯ НИМ СИЛИ ОПОРУ ПОВІТРЯ

Lect.Ph.D.Eng. Bohatyrov D.V., Doctor of Technical Sciences, Professor Salo V.M., Lect.Ph.D.Eng. Kyslun O.A., Lect. Ph.D. Eng. Skrynnik I.O., Asst.Ph.D. Stud. Eng. Kisilov R.V.
Kirovohrad National Technical University / Ukraine
Tel: +380504572446; E-mail: profbdv@gmail.com

Keywords: *Crimper-roller, cylinder drum with blades, resistance area, equal-area height.*

ABSTRACT
The article presents a theoretical research on the influence of introducing height equal-area projection on the calculation accuracy of the air resistance power of the cylinder drum with blades. The effort was made to specify the resistance area depending on the angle setting and the number of blades of the crimper-roller. Research on the introduction of the equal-area projection of the height on the description accuracy of the crimper-roller air resistance power showed that the fractional error decreases by 1.5 times. This is explained by the absence of the uncertainty influence of the cylinder drum initial angle setting.

РЕЗЮМЕ
Стаття присвячена теоретичному дослідженню впливу внесення еквівалентної проекції висоти на точність визначення сили опору повітря барабану з ножом. Зроблено спробу уточнити площу опору в залежності від кутового положення та кількості ножів барабана котка-подрібнювача. Дослідження внесення еквівалентної проекції висоти на точність опису сили опору повітря барабану з ножами показали, що відносна похибка зменшується у 1,5 рази, що пояснюється виключенням впливу невизначеності початкового кутового положення барабану.

INTRODUCTION
In the last few years Ukraine was filled with non-traditional and in some cases unknown technologies of crop science *(Bohatyrov D.V., 2012; Vasylkovska K.V., 2016)*. The changes started by using imported harvesters which left practically all residues on the field. This practice allowed increasing the productivity of picking processes and shortening the terms of harvest period but there appeared the problem of plant residues further processing. The Ukrainian producers chose the simplest way to solve it and used disc equipment for soil cultivation. As a result, the structure of surface soil was damaged, valuable agro-technical aggregates were mashed, which led to their transformation into dusty unstructured condition. There was also over-tamping of subsoil, dysfunction of the aeration and infiltration processes, decrease of the storage of productive soil water in lower levels *(Salo V.M., 2014)*. Special machines (Fig. 1) are usually used in these cases abroad which are debris pulverisers *(Bohatyrov D.V., 2012; Salo V.M., 2016)*. In Ukraine, these machines are not well-known; they are expensive and perceived by agricultural producers as part of the technological process which needs extra costs, which are not obligatory *(Sysolin P.V., 2001)*. Besides, according to the special design of each of these machines, they do not provide necessary pulverization for Ukraine production technologies (*Salo V.M., 2014*).

In order to determine the accurate draught of the crimper-roller it is necessary to take into account the force to overcome air resistance. In the well-known works *(Ashford D.L., 2003; Korniecki T.S., 2006)* this issue was not studied in full details. For the first time, H. Tagaev suggested to take into account, the air resistance for the equipment that destroys weeds in the rice bays (*Tagaev Kh., 2015*).

The objective of the research is to determine theoretical projection of the height of cylinder drum's cross-section on the accuracy of description of its overcoming the air resistance force.

MATERIAL AND METHODS
The experimentally determined range of velocities from 15 to 24 km/h takes into account the peculiarities of the crimper-roller operation in field conditions, particularly the movement of the aggregate on

ground slopes and humps in vertical as well as in horizontal planes *(Bohatyrov D.V., 2015)*. Having these values of movement velocity, it is worthwhile taking into account the force of air resistance *(Bohatyrov D.V., 2015)*. A drum with knives is similar to a lobed wheel. At working speeds, knives create resistance to its rotation both in soil and in the air. It is established that the traction resistance increases by 12% at speeds of 15-25 km/h (*Tagaev Kh., 2015*).

Fig. 1 - Crimper-roller KP-4.5

Let us consider height b_B of the half cylinder drum with blades cross-section with the angle values $-\frac{\beta}{2} \le \varphi \le \frac{\beta}{2}$ (Fig. 2).

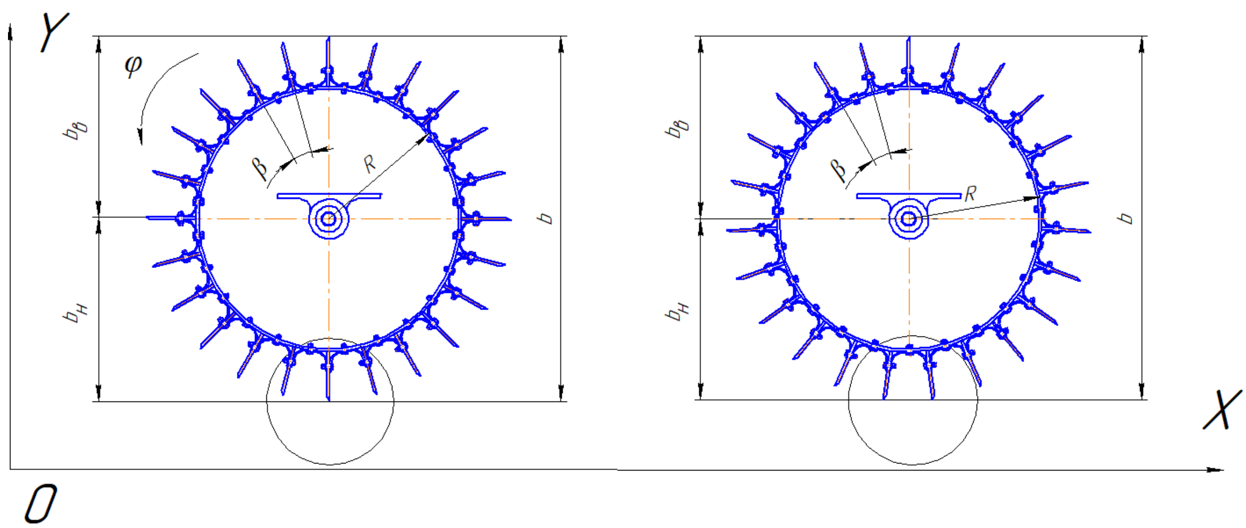

a) b)

Fig. 2 - Cases with blade placement

a) even number of blades (z=24 pieces); b) odd number of blades (z=23 pieces);

β – angle between the blades, $\beta = \frac{2 \cdot \pi}{z}$; *b* - cross-section of the height of half cylinder drum with blade on the axis OY.

We determine the height projection $b_в$ in relation to the angle φ if $b_в \ge R$,

$$b_B = (h + R) \cdot \cos\varphi \text{ [m]} \tag{1}$$

where: R – radius of the cylinder drum, m;

h – height of the blade, m.

When the crimper-roller operates with a certain number of blades *z* it may happen that the surface of the cylinder drum is seen between the blades $b_B < R$ (Fig. 2, b), then $b_B = R$.

Let us consider the cases with even and odd numbers of blades *z*. With even number of blades, the value of the height projection b_B on the axis OY is $b_н = b_B$. Let us consider the case with odd number of blades on the cylinder drum of the crimper-roller.

With odd number of blades:

$b_н = (h+R)\cdot\cos\left(\frac{\beta}{2}-\varphi\right)$, where $0 \le \varphi \le \frac{\beta}{2}$; $b_н = (h+R)\cdot\cos\left(\frac{\beta}{2}+\varphi\right)$, where $-\frac{\beta}{2} \le \varphi \le 0$.

So, we have general expression to determine the height projection of the half cylinder drum's cross-section with a blade, where $-\frac{\beta}{2} \le \varphi \le \frac{\beta}{2}$:

$$b_н = (h+R)\cdot\cos\left(\frac{\beta}{2}-|\varphi|\right) \text{ [m]} \tag{2}$$

Much the same, when the crimper-roller is operating with a certain number of blades *z* it may happen that the surface of the cylinder drum is seen between the blades $b_н < R$, then $b_н = R$.

Mechanically, the blades are fixed on the cylinder drum of the crimper-roller in such a way that the case when $b_в < R$ and $b_н < R$ cannot be possible.

In general situation, the height projection of the cylinder drum's cross-section with even and odd numbers of blades z will be determined in the following way:

$$b(\varphi) = (h+R)\cdot\left(\frac{3-(-1)^{z+1}}{2}\cdot\cos(\varphi)+\frac{1-(-1)^{z}}{2}\cdot\cos\left(\frac{\pi}{z}-|\varphi|\right)\right), \text{ [m]} \tag{3}$$

where the angle value will be in the limits of $-\frac{\pi}{z} \le \varphi \le \frac{\pi}{z}$.

There is no sense to use formula (3) for further calculations because it is impossible to set the initial angle of the cylinder drum with blades. There is a need to have additional calculations which will take into account the calculation's errors. That will enable introducing equal-area projection of the height of cylinder drum's cross-section.

Let us determine the equal-area height $b_{ек}$ for

$$b_{ек} = \frac{z}{2\cdot\pi}\cdot\int_{\frac{\pi}{z}}^{\frac{\pi}{z}} b(\varphi)\,d\varphi, \text{ [m]} \tag{4}$$

For an even number of blades

$$b_{ек} = \frac{z}{2\cdot\pi}\cdot\int_{\frac{\pi}{z}}^{\frac{\pi}{z}} b(\varphi)\,d\varphi = \frac{2\cdot z\cdot(R+h)}{\pi}\cdot\sin\left(\frac{\pi}{z}\right), \text{ [m]} \tag{5}$$

Let us find the ratio error δ, which is formed as a result of taking into account equal-area projection of the height of the bladed cylinder drum's cross-section during one complete revolution.

The function $\cos\left(\varphi-\frac{\pi}{2\cdot z}\right)$ where $-\frac{\pi}{z} \le \varphi \le 0$ increases to its highest level value, if $\varphi = 0$.

Let us consider the cylinder drum revolution on one blade $-\frac{\pi}{z} \le \varphi \le \frac{\pi}{z}$ for the even number of blades

$$\frac{b(\varphi)}{b_{ек}} = \frac{2\cdot(R+h)\cdot(\cos\varphi)}{\frac{2}{\pi}\cdot(R+h)\cdot z\cdot\sin\left(\frac{\pi}{z}\right)} = \frac{\pi\cdot\cos(\varphi)}{z\cdot\sin\left(\frac{\pi}{z}\right)}$$

where $-\frac{\pi}{z} \le \varphi \le \frac{\pi}{z}$.

The highest value of the error δ is when the cylinder drum is rotating with the values of the angle $\varphi = -\frac{\pi}{z}$ та $\varphi = \frac{\pi}{z}$, will be

$$\delta = \left| 1 - \frac{\pi \cdot \cos\frac{\pi}{z}}{z \cdot \sin\frac{\pi}{z}} \right| \cdot 100\% = \left| 1 - \frac{\pi}{z} \cdot ctg\frac{\pi}{z} \right| \cdot 100\% \quad [\%] \tag{6}$$

Let us assess the error of the accuracy of the force determination as a result of introduction of $b_{ек}$ for the odd number of blades when $-\frac{\pi}{z} \le \varphi \le 0$

$$\frac{b(\varphi)}{b_{ек}} = \frac{\pi \cdot \cos\left(-\frac{\pi}{2 \cdot z}\right) \cdot \cos\left(\varphi + \frac{\pi}{2 \cdot z}\right)}{z \cdot \sin\frac{\pi}{z}}.$$

where $0 \le \varphi \le \frac{\pi}{z}$

$$\frac{b(\varphi)}{b_{ек}} = \frac{\pi \cdot \cos\left(\frac{\pi}{2 \cdot z}\right) \cdot \cos\left(\varphi - \frac{\pi}{2 \cdot z}\right)}{z \cdot \sin\frac{\pi}{z}}.$$

The highest value of the error δ is when the cylinder drum is rotating with the values of the angle $\varphi = -\frac{\pi}{z}$, $\varphi = 0$ and $\varphi = \frac{\pi}{z}$:

$$\delta = \left| 1 - \frac{\pi}{2 \cdot z} \cdot ctg\frac{\pi}{2 \cdot z} \right| \cdot 100\%. \quad [\%] \tag{7}$$

Let us determine the error δ_t, which is introduced by the indeterminateness of the initial angle set of the cylinder drum with blades while applying the exact determination of the height projection of the cylinder drum's cross-section b. For the even number of blades

$$\delta_t = \left| 1 - \frac{2 \cdot (h+R) \cdot \cos 0^o}{2 \cdot (h+R) \cdot \cos\frac{\pi}{z}} \right| \cdot 100\% = \left| 1 - \frac{1}{\cos\frac{\pi}{z}} \right| \cdot 100\%. \quad [\%] \tag{8}$$

For the odd number of blades

$$\delta_t = \left| 1 - \frac{(h+R) \cdot \left(\cos\varphi_{\max} + \cos\left(\frac{\pi}{z} - |\varphi_{\max}| \right) \right)}{(h+R) \cdot \left(\cos\varphi_{\min} + \cos\left(\frac{\pi}{z} - |\varphi_{\min}| \right) \right)} \right| \cdot 100\% = \left| 1 - \frac{1}{\cos\frac{\pi}{2 \cdot z}} \right| \cdot 100\%, \quad [\%] \tag{9}$$

where: $\varphi_{\min} = 0 = -\frac{\pi}{z}$, $\varphi_{\max} = -\frac{\pi}{2 \cdot z}$.

RESULTS

Graphic interpretations (Fig. 3) of the research findings of the influence of the equal-area projection of the height $b_{ек}$ on the accuracy of the description of the air resistance force showed that the ratio error decreases by 1.5 times. That is explained by the indeterminateness of the initial angle set of the cylinder drum with blades and equals: for the odd number of blades δ=1%, δ_t=1.6%; for the even number of blades is (z=24 pieces) (z=23 pieces) δ=2.2%, δ_t=3.5%.

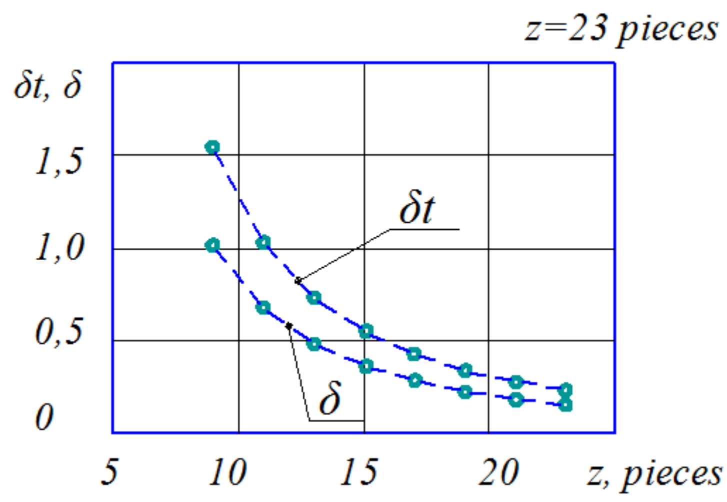

a)

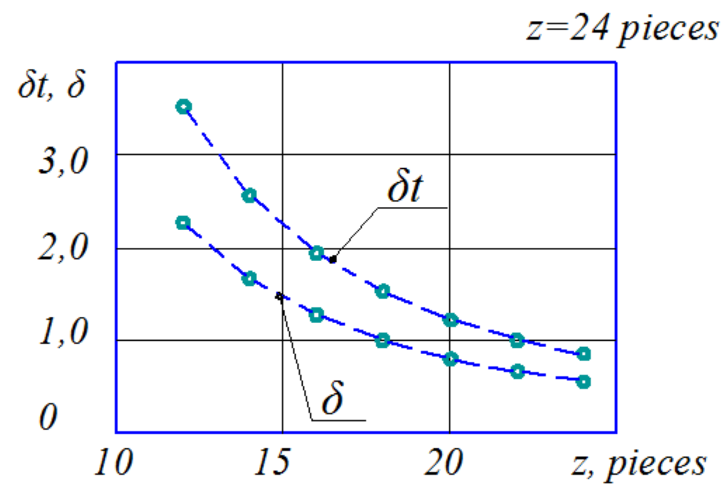

b)

Fig. 3 - Dependence of the ratio errors δ and δ_T on the number of blades *z*

a) odd number of blades (z=11…23 pieces); b) even number of blades (z=10…24 pieces).

δ – the error which is formed as a result of introduction of $b_{ек}$ equal-area projection of the height of the cylinder drum with blades;

δ_T – the error which is formed as a result of the indeterminateness of the initial angle set of the cylinder drum with blades;

Taking into consideration formulae (5, 6) the force to overcome the air resistance can be determined in the following way

$$P_c = k \cdot k_0 \cdot L_н \cdot b_{ек} \cdot \left(\vartheta_0 - \vartheta_{агр}\right)^2 \text{, [N]} \tag{11}$$

where: k is the number of cylinder drums with blades on the crimper-roller, pieces;

k_0 is a coefficient which takes into account the type of environment;

$L_н$ is the length of the blade, m;

ϑ_0 is the wind speed, m/s;

$\vartheta_{агр}$ is the speed of the aggregate, m/s.

CONCLUSIONS

Theoretical determination of the equal-area height projection depending on the angle setting and the number of blades will enable determining the value of the effort to overcome the air resistance force by the crimper-roller. Theoretical dependencies were obtained for the first time. They allow taking into account the required amount of energy and fuel used to overcome the resistance to air at speeds of 15-25 km/h. Given the research, further theoretical grounding of the rational design and technological parameters of the crimper-roller is necessary.

REFERENCES

[1] Ashford D.L., Reeves D.W., (2003), Use of a mechanical roller-crimper as an alternative kill method for cover crop, *American Journal of Alternative Agriculture,* Vol.18(1), USA, pp.37-45;

[2] Bohatyrov D.V., Salo V.M., Nosulenko V.I., Martynenko D.V., (2012) Grounding of prospect trends of the designs of crimper-rollers for plant residues, *Design, Production and Exploitation of Agricultural Machines: Collection of Scientific Works,* Vol. 42, pp. 39-44, Kirovohrad/Ukraine;

[3] Bohatyrov D.V., Salo V.M., Leshchenko S.M., Machok Y.V. (2015), Experimental research on the influence of the crimper-roller movement velocity on the corn residues pulverization quality, *Collection of scientific works of Lutsk National Technical University: Agricultural machinery*, Vol.31, pp.10-17, Lutsk/Ukraine;

[4] Bohatyrov D.V., Salo V.M., (2015) Technical support grinding process plant remains. *Propozytsia,* № 9, pp. 42-47, Kyiv/Ukraine;

[5] Bohatyrov D.V., Salo V.M., Kyslun O.A. (2016), Definition projection height equivalent of crossing the drum with an even number of knives, *International Scientific and Practical Conference "WORLD SCIENCE",* pp.78-85, Ajman/UAE;

[6] Korniecki T.S., Price A.J., (2006), Perfomance of Different Roller Designs in terminating rye cover crop and reducing vibration, Applied Eng. Agric., Vol. 22(5), pp.633-641, Alabama/USA;

[7] Vasylkovska K.V., Leshchenko S.M., Vasylkovskyi O.M., Petrenko D.I., (2016), Improvement of equipment for basic tillage and sowing as initial stage of harvest forecasting, *INMATEH - Agricultural Engineering,* Vol. 50, No.3, pp.13-20, Bucharest/Romania;

[8] Salo V.M., Bohatyrov D.V., Leshchenko S.M., Savytskyi, (2014), National technical support of modern processes in plant growing, *Engineering and Technology of APK*. *Scientific and production journal,* №10 (61)*,* pp.16-19, Kyiv/Ukraine;

[9] Salo V.M., Leshchenko S.M., Machok Y.V., Luzan P.G., Bohatyrov D.V., (2016), *Machines for soil cultivation and fertilizer*, Edited by Salo V.M., Amosov V.V., pp.22-31, Kharkiv/Ukraine;

[10] Sysolin P.V., Salo V.M, Kropivnyy V.M., (2001), Agricultural machines: theoretical bases, design, engineering, Book 1. *Arable farming machines*, Edited by Chernovol M.I., p.384, Kyiv/Ukraine;

[11] Tagaev Kh., (2015), The formula of Tagaev to determine the hydro-dynamic resistance of water, *Technical science,* pp.32-37, Dubai/UAE.

THEORETICAL GROUNDING OF SEEDS VALVE OPENER SETTINGS FOR SUBSOIL-SPREADING SOWING METHOD
/
ТЕОРЕТИЧНЕ ОБҐРУНТУВАННЯ ПАРАМЕТРІВ РОЗПОДІЛЬНИКА НАСІННЯ СОШНИКА ДЛЯ ПІДҐРУНТОВО-РОЗКИДНОГО СПОСОБУ СІВБИ

Ph.D. Eng. Zayets M., Ph.D. Eng. Sukmaniuk E, Ph.D. Eng. Grudovyi R.
Zhytomyr National Agroecological University / Ukraine
E-mail: sukmanyukolena@gmail.com

Keywords*: speed, sowing, distributor, generators uniformity*

ABSTRACT
In the article, we examine the determination of the distributor optimal shape and the seeds distribution process by combined distributor in the form of a curved prism. Based on calculations we found out that seeds distribution uniform for bandwidth depends on the distributor shape that is sown with the opener for cereals continuous sowing. Formulas for determining the seed speed on the distributor surface were recorded, depending on changes of structurally technological parameters including generating circle prism diameter. It was recorded the mathematical model of the coordinates and the seed trajectory and the range flight seed of ideal forms. Uniformity of seeds distribution for opener widths will be characterized by the seeds flow speed on the distributor sloping plot of guiding and coordinates falling on the distributor surface. The effect of the distributor sloping plot length on seeds uniformity distribution was researched, the obtained dependences of the flight distance determining on the seeds distributor sloping plot length and seeds uprising speed through which the optimal lengths of sloping plot was selected. The paper presents the main results of theoretical studies and recommendations for this type of passive distributors use in opener for subsoil-spreading crops sowing method.

РЕЗЮМЕ
В статті розглядається визначення оптимальної форми розподільника та процес розподілу насіння комбінованим розподільником у виді криволінійної призми. На основі розрахунків встановлено, що від форми розподільника залежить рівномірність розподілу насіння за шириною смуги, яка засівається сошником для суцільної сівби зернових колосових культур. Записано формули для визначення швидкості руху насінини по поверхні розподільника, в залежності від зміни констукційно-технологічних параметрів, зокрема, діаметру твірного кола призми. Записано математичну модель визначення координат і траєкторії руху посівного матеріалу та дальності польоту насінини ідеальної форми. Рівномірність розподілу насіння за шириною захвату сошника буде характеризуватися швидкістю надходження насіння на похилу ділянку розподільника з направляча та координатами потрапляння на поверхню розподільника. Досліджено вплив довжини похилої ділянки розподільника на рівномірність розподілу насіння, отримані залежності визначення дальності польоту насіння від довжини похилої ділянки розподільника і швидкості його сходу, по яких обране оптимальне значення довжини похилої ділянки. В роботі представлені основні результати теоретичних досліджень та рекомендації щодо використання даного типу пасивних розподільників в сошниках для підґрунтово-розкидної сівби зернових культур.

INTRODUCTION
Appreciable difference between the current seeding machine for ground slightly spreading method of sowing is the construction of seeding machines, in particular their distribution adjustment (*Hevko B. M. et. al., 2014; Sysolin P. V. and Sysolina I. P., 2014).* Seeding machines for ground slightly spreading method of sowing mostly are in form of cultivator share with different sweeping distance. Seed spreader is one of the main seeding machine elements, which influence at equability of spreader of technologic material on the field surface and increase of the width of sowing line. Different forms of the bafflers and seeding machine spreader adjustments constructions for ground slightly spreading sowing method caused by seeds increasing on the field area equability (*Romanyshyn O. Y. and Zayets M. L., 2006; Hevko B. M. and Pavelchuk Yu. F., 2016; Lisovyi I. O. et. at., 2016)*.

Advantages of the spreaders with non-rectilinear shape performance on the working surface the seed of which change direction of its moving with minimal kinetic energy wastes and moves to the seeding machine area and saw on the furrow bottom – were proved by analysts (*Vasylenko P.M., 1960; Heege H. J. 1993*). Such a design of the opener allows to reduce its effect on the seed, that is, the micro- and macrocracks formation (*Derevianko D. A., 2015*).

To reach maximal speed of moving in point of convergence of curve line, the curve line must be capable of the terms requiring of the quickest moving of elements during certain interval. Such a curve line accordant to the determination is called brachistochrone (*Zayets M. L. and Zhyvega M. M., 2015)*.

Zayets M. L. *(Zayets M.L. et. al., 2014*) devoted his work to the theoretical and experimental researches of the seed moving on the curve lines. He examines the brachistochrone as compatibility of rectilinear area and circle of the permanent radius r, and moving of seeds on the curve as a moving of seeds on this circle.

MATERIAL AND METHODS

Using the method of machines, work items and processes mathematical modelling, using computational differential equations, conversion and graphical definition on the basis of mechanics laws let us consider seed moving on a sloping surface (sloping area) of the combined distributor (fig. 1). At time t_0 seed comes down from the curvilinear areas of the combined distributor and starts moving with an initial velocity $V \ (V_0)$ at an angle β_0. Gravity and friction acts on a seed as the direction of movement will occur along some curve.

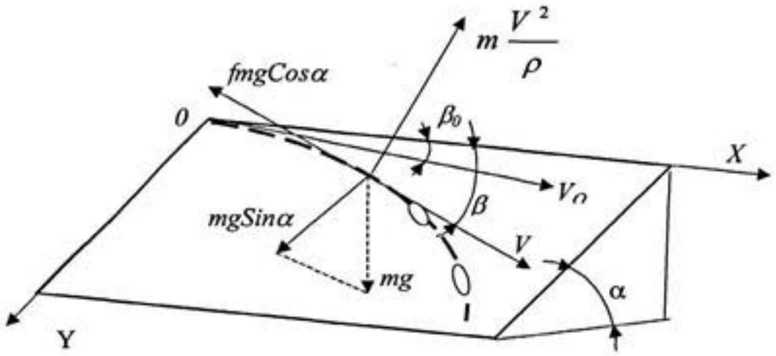

Fig. 1 – Forces calculation model, acting on the seed during its moving on the distributor sloping plot

Let us complete differential equations of the seed moving in projections on the normal line and tangent line to the trajectory. These equations are as follows (*Romanyshyn O. Y. and Zayets M. L., 2006*):

$$m\frac{dV}{dt} = mg \times \sin\alpha - fmg \times \cos\alpha, \tag{1}$$

$$m\frac{m^2}{\rho} = mg \times \sin a \times \cos\beta \tag{2}$$

Where: V – speed of the seed moving on the inclined surface at the moment t, [m/s];

α – the angle of the horizontal curve section, [rad];

β – the angle between moving elements at the moment *t* and OX Cartesian axes, [rad];

ρ – curve radius of the movement pattern on the curve section at the moment, [m]

f – seed moving coefficient on the steel.

Kindly note, that:

$$\rho = \frac{dS}{d\beta} = \frac{V \cdot dt}{d\beta} \tag{3}$$

where, $\frac{dS}{d\beta}$ – increasing of distance, [m].

If we mention ρ in equation (2) and determine dt, we obtain:

$$dt = \frac{V \cdot d\beta}{g \cdot \sin\alpha \cdot \cos\beta} \tag{4}$$

Substitute the value dt in the equation (1), we obtain as follows:

$$\frac{dV}{V \cdot d\beta} mg \cdot \sin\alpha \cdot \cos\beta = mg \cdot \sin\alpha \cdot \sin\beta - fmg \cdot \cos\alpha \tag{5}$$

Using mathematical calculations, we obtain:

$$\frac{dV}{V} = tg\beta \cdot d\beta - f \cdot ctg\alpha \frac{1}{\cos\beta} \cdot d\beta \tag{6}$$

The difference equation obtained is the equation with articulate modulars.

The general solution to the equation is as follows:

$$V = \frac{C}{\cos\beta} \cdot \left(\frac{1 - tg\dfrac{\beta}{2}}{1 + tg\dfrac{\beta}{2}} \right)^{f \cdot ctg\alpha} \tag{7}$$

where C – permanent data.

Arbitrary constant shall be determined from the permanent terms $\beta = \beta_0 V = V_{cx}$:

$$C = \frac{V_{cx}}{\cos\beta_0} \cdot \left(\frac{1 + tg\dfrac{\beta_0}{2}}{1 - tg\dfrac{\beta_0}{2}} \right)^{f \cdot ctg\alpha} \tag{8}$$

RESULTS

As a result of theoretical research, we got the differential equation for determining structural and technological parameters of the combined distributor:

- speed descent of the curvilinear generatrix;
- the range distribution of seeds;
- the design parameters of the sloping area (length of the sloping area and installation angle to the horizon) the use of which allows to determine the optimal parameters of the distributor and the sloping sections.

Substitute the value C in equation (7) and after calculation we get defining formula for determining the seed speed on the curve section:

$$V = \frac{V_{cx}}{\cos\beta_0 \cdot \cos\beta} \cdot \left[\left(\frac{1 + tg\dfrac{\beta_0}{2}}{1 - tg\dfrac{\beta_0}{2}} \right) \cdot \left(\frac{1 - tg\dfrac{\beta}{2}}{1 + tg\dfrac{\beta}{2}} \right) \right]^{f \cdot ctg\alpha} \tag{9}$$

Movement pattern of the speed in the curve section shall be determined as follows:

$$dx = V \cdot \cos\beta \cdot dt, dy = V \cdot \sin\beta \cdot dt \tag{10}$$

Or according to the following equation: (4):

$$dx = \frac{V^2 \cdot d\beta}{g \cdot \sin\alpha}$$
$$dy = \frac{V^2 \cdot tg\beta \cdot d\beta}{g \cdot \sin\alpha} \tag{11}$$

The general consensus of the simultaneous equations (11) is as follows:

$$C_1 = -\frac{2V_{cx}^2}{g\cdot\sin\alpha\cdot\cos^2\beta_0}\cdot\left(\frac{1+tg\frac{\beta_0}{2}}{1-tg\frac{\beta_0}{2}}\right)^{2\cdot f\cdot ctg\alpha}\cdot\left(\frac{1}{2\cdot f\cdot ctg\alpha-1}\cdot\left(\frac{1+tg\frac{\beta_0}{2}}{1-tg\frac{\beta_0}{2}}\right)^{2\cdot f\cdot ctg\alpha-1}+\frac{1}{2\cdot f\cdot ctg\alpha+1}\cdot\left(\frac{1-tg\frac{\beta_0}{2}}{1+tg\frac{\beta_0}{2}}\right)^{2\cdot f\cdot ctg\alpha+1}\right)$$

$$C_2 = -\frac{V_{cx}^2}{g\cdot\sin\alpha\cdot\cos^2\beta_0}\cdot\left(\frac{1+tg\frac{\beta_0}{2}}{1-tg\frac{\beta_0}{2}}\right)^{2\cdot f\cdot ctg\alpha}\cdot\left(\frac{1}{2\cdot f\cdot ctg\alpha-2}\cdot\left(\frac{1-tg\frac{\beta_0}{2}}{1-tg\frac{\beta_0}{2}}\right)^{2\cdot f\cdot ctg\alpha-2}-\frac{1}{2\cdot f\cdot ctg\alpha-2}\cdot\left(\frac{1-tg\frac{\beta_0}{2}}{1+tg\frac{\beta_0}{2}}\right)^{2\cdot f\cdot ctg\alpha+2}\right) \quad (12)$$

where C_1 and C_2 – are the variables.

$$x = -\frac{2\cdot V_{cx}^2}{g\cdot\sin\alpha\cdot\cos^2\beta_0}\cdot\left(\frac{1+tg\frac{\beta_0}{2}}{1-tg\frac{\beta_0}{2}}\right)^{2\cdot f\cdot ctg\alpha}\cdot\left(\frac{1}{2\cdot f\cdot ctg\alpha-1}\cdot\left(\frac{1-tg\frac{\beta}{2}}{1+tg\frac{\beta}{2}}\right)^{2\cdot f\cdot ctg\alpha-1}+\frac{1}{2\cdot f\cdot ctg\alpha+1}\cdot\left(\frac{1-tg\frac{\beta}{2}}{1+tg\frac{\beta}{2}}\right)^{2\cdot f\cdot ctg\alpha+1}\right)+C_1$$

Constant variables shall be determined according to the initial data:

If $\beta = \beta_0 ... x = 0, y = 0$:

$$y = -\frac{V_{cx}^2}{g\cdot\sin\alpha\cdot\cos^2\beta_0}\cdot\left(\frac{1+tg\frac{\beta_0}{2}}{1-tg\frac{\beta_0}{2}}\right)^{2\cdot f\cdot ctg\alpha}\cdot\left(\frac{1}{2\cdot f\cdot ctg\alpha-2}\cdot\left(\frac{1-tg\frac{\beta}{2}}{1-tg\frac{\beta}{2}}\right)^{2\cdot f\cdot ctg\alpha-2}-\frac{1}{2\cdot f\cdot ctg\alpha+2}\cdot\left(\frac{1-tg\frac{\beta}{2}}{1+tg\frac{\beta}{2}}\right)^{2\cdot f\cdot ctg\alpha+2}\right)+C_2$$

Analysis of equation (13), confirms that maximal X axis stroke (ranging of the seed spreader on the sowing width) shall be in case of coincidence of the speed direction at time zero with axis X $(\beta = 0)$..

Data of the constant variables are determined from the following equations:

$$C_1 = \frac{2\cdot V^2{}_{cx}}{g\cdot\sin\alpha}\cdot\left(\frac{1}{2\cdot f\cdot ctg\alpha-1}+\frac{1}{2\cdot f\cdot ctg\alpha+1}\right)$$

$$C_2 = \frac{V^2{}_{cx}}{g\cdot\sin\alpha}\cdot\left(\frac{1}{2\cdot f\cdot ctg\alpha-2}-\frac{1}{2\cdot f\cdot ctg\alpha+2}\right) \quad (14)$$

When installing of the distributor with eccentricity, relative to the axis coordinate counting X seed wire we lead from point O (fig. 1) (the point of seed falling on a sloping plot) coordinate Y of the distributor axial line (fig. 2).

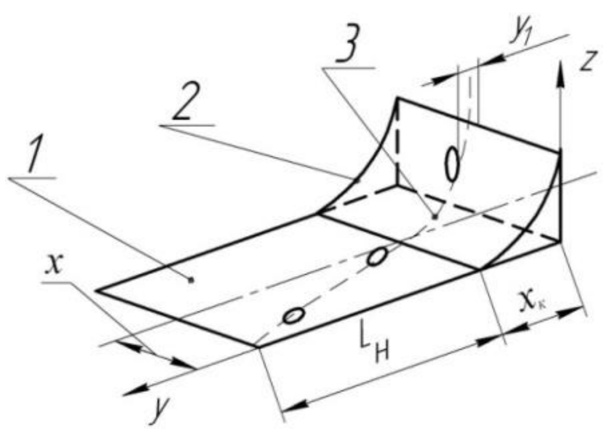

Fig. 2 – Scheme of the spreader with the curve section

1 – curve section, 2 – spreader, 3 – movement pattern of a seed

So, we can write the following:

$$x = x(\beta) + C_1 + x_k$$
$$y = y(\beta) + C_2 \pm y_1 \qquad (15)$$

where:

$x(\beta)$ and $y(\beta)$ – functions x and y depending on the parameter β (13);

C_1 and C_2 – data of constant variables (14);

x_k – projection of the curve moving line of the spreader on the curve section, [m];

y_1 – distance from the axis line of a spreader to the point of a seed impact on the curve section, [m] (Fig. 2).

During the sowing moving, under the inertial force, data of the seed movement pattern on the curve section differs from theoretical data and it will influence the line width, which the seeding machine sows.

This fact shall be mentioned and calculated due to the correction factor.

After plugging in the equation system (15) data points β_0, $x(\beta)$, $y(\beta)$, C_1 and C_2, note that the length of the curve section is datum by the line $L_н$, get the equation of seed moving on the curve section in the following parametric form:

$$x = K \cdot \left[-\frac{2V_{cx}^2}{g \cdot \sin\alpha \cdot \cos^2\beta_0} \cdot \left(\frac{1}{2 \cdot f \cdot ctg\alpha - 1} \cdot \left(\frac{1 - tg\frac{\beta}{2}}{1 + tg\frac{\beta}{2}} \right)^{2 \cdot f \cdot ctg\alpha - 1} + \frac{1}{2 \cdot f \cdot ctg\alpha + 1} \cdot \left(\frac{1 - tg\frac{\beta}{2}}{1 + tg\frac{\beta}{2}} \right)^{2 \cdot f \cdot ctg\alpha + 1} \right) + \frac{2 \cdot V_{cx}^2}{g \cdot \sin\alpha} \cdot \left(\frac{1}{2 \cdot f \cdot ctg\alpha - 1} + \frac{1}{2 \cdot f \cdot ctg\alpha + 1} \right) + x_k \right] \qquad (16)$$

$$L_H = -\frac{V_{cx}^2}{g \cdot \sin\alpha \cdot \cos^2\beta_0} \cdot \left(\frac{1}{2 \cdot f \cdot ctg\alpha - 2} \cdot \left(\frac{1 - tg\frac{\beta}{2}}{1 + tg\frac{\beta}{2}} \right)^{2 \cdot f \cdot ctg\alpha - 2} - \frac{1}{2 \cdot f \cdot ctg\alpha + 2} \left(\frac{1 - tg\frac{\beta}{2}}{1 + tg\frac{\beta}{2}} \right)^{2 \cdot f \cdot ctg\alpha + 2} \right) + \frac{V_{cx}^2}{g \cdot \sin\alpha} \cdot \left(\frac{1}{2 \cdot f \cdot ctg\alpha - 2} - \frac{1}{2 \cdot f \cdot ctg\alpha + 2} \right) \pm y_1$$

where K – modifying factor, determined in an experimental way.

$$k = \frac{B_{еккс}}{2 \cdot x} \qquad (17)$$

where $B_{експ}$ – observed width of line sowing by the seeding-machine.

According to the received system of equations the main parameters, which characterize propagation distance of seed, are the following: length of the curved section $L_н$ speed of seed movement from the curve sector of the spreader to the curve section V, angle of incidence of the curve section to the horizon α.

Analyzing the received equations, let's determine the minimal angle of incidence of the curve section in case of plugs deficiency on the curve section:

$$f \cdot ctg\alpha < 1 \qquad (18)$$

Or

$$f \cdot tg\alpha > 1 \qquad (19)$$

Due to the value of traction coefficient 0.36...0.37 for spiked cereals, we determine that the minimal angle of incidence of the curve section is 19.8°...20.3°.

If length of the curve section is $L_{н}$, the speed moving of a seed is V_{cx}, the slope angle is α and due to the system of equations, we determine the seed distribution x, about a symmetric axis of the seeding machine. Using received equations (16), we determine that the line width, sewed by the seeding machine is nearly 95…100 mm while the length of the curve section is nearly 30...70 mm.

CONCLUSIONS

The following theoretical dependence for determining the constructive parameters of the compound spreader is obtained: moving speed from the curved line to the diameter of the brachistochrone circle line; propagation distance of seed (in parametric form) from the constructive parameters of the curve section (length of the curve section and angle of its adjustment to the horizon), usage of which allows to determine optimal parameters of the spreader and curve section to secure seed diffusion in the operating width of a seeding machine with necessary ranging and steadiness.

Length of the curved section selected according to the ranging and steadiness of the seed spreading shall be 60 mm. Compound spreader spreads crop seeds on the width 95-100 mm.

REFERENCES

[1] Derevianko D. A., (2015), Influence of technical means and technological processes on seeds injury and quality: Monograph (Вплив технічних засобів та технологічних процесів на травмування і якість насіння: Монографія), *Zhytomyr: Polissya,* p. 774, Zhytomyr/ Ukraine;

[2] Heege H. J., (1993), Sowing methods performance for cereals, rape, and beans. *Transactions of the ASAE*, Vol. 36(3). pp. 653–661;

[3] Hevko B.M., Ljasuk A. L., Pavelchuk Yu. F. et. al., (2014), Technological bases of designing and manufacturing of sowing machines: monograph (Технологічні основи проектування та виготовлення посівних машин: монографія), *Ternopil National Tech. University of I. Puluj*., p.236, Ternopil/Ukraine;

[5] Hevko B.M., Pavelchuk Yu. F., (2016), Investigation of the Seed Distribution Process of Cereal Cultures in the Substrate-Scattering Sowing Method: Theoretical Analysis (Дослідження процесу розподілу насіння зернових культур при підґрунтово-розкидному способі сівби: теоретичний аналіз), Collection of scientific works of the Podilsky State Agricultural and Technical University. Technical sciences, (*Збірник наукових праць Подільського державного аграрно-технічного університету. Технічні науки*), Vol. 24 (2), pp. 25-32;

[6] Lisovyi I. O., Boyko A. I., Banny O. O., Pushk O. S., (2016), Justification of the working bodies for the cultivation of the cultivator parameters for direct sowing: Monograph, *FOP Alexandrova M.V.*, p.160, Kirovograd/ Ukraine;

[7] Romanyshyn O.Y., Zayets M.L., (2006) Sowing machine for spreading method of corn sowing (Сошник для розкидного способу сівби зернових культур), *REPORTER of Poltava State Agriculture Academy*, Vol. 4, pp.87 - 89, Poltava/Ukraine;

[8] Sysolin P.V., Sysolina I.P., (2014), Modern methodology of agricultural machinery creation (on the example of a seed machine): monograph (Сучасна методологія створення сільськогосподарської техніки (на прикладі висівного апарата) монографія), *Kirovogr National Tech. University.* Lysenko V.F., p. 120, Kirovograd/Ukraine;

[9] Vasylenko P.M., (1960), Theory of material elements movements on the rough surface of the agricultural machines, *Ukrainian Academy of Agricultural Sciences*, p.282, Kiev/Ukraine;

[4] Zayets M. L. and others, (2014), Technological bases of sowing machines designing and manufacturing (Технологічні основи проектування та виготовлення посівних машин), *Ternopil Nat. Tech. University of I. Puluj*., p. 238, Ternopil/Ukraine;

[10] Zayets M.L., Zhyvega M.M., (2015), Determination of the seeds speed moving on the spreader seeding machine for subareal spread sowing (Визначення швидкості руху насіння по розподільнику сошника для підгрунтово-розкидного способу сівби*), Collection of research papers. Seria “Technique and engineering of agro-industrial complex*, Vol. 226. pp. 307-315, Kyiv/Ukraine.

GEOSTATISTICAL APPROACH TO DETERMINE THE EFFECTS OF DIFFERENT SOIL TILLAGE METHODS ON PENETRATION RESISTANCE IN A CLAYEY SOIL
/
KİLLİ TOPRAKTA FARKLI TOPRAK İŞLEME YÖNTEMLERİNİN PENETRASYON DİRENCİNE ETKİSİNİN BELİRLENMESİ İÇİN JEOİSTATİSTİKSEL BİR YAKLAŞIM

Assist.Prof.Dr. Selvi K.Ç.[*1)], Assoc.Prof.Dr. Sağlam M[2)], Prof.Dr. Dengiz O[2)]
[1)]Department of Agriculture Machinery and Technologies Engineering, Faculty of Agriculture, Ondokuz Mayıs University, Atakum, Samsun / Turkey;
[2)] Department of Soil Science and Plant Nutrition, Faculty of Agriculture, OndokuzMayıs University, Samsun / Turkey
Tel: + 90362312199 / 1259; E-mail:kcselvi@omu.edu.tr

Keywords: *tillage methods, penetration resistance, geostatistical approach*

ABSTRACT
In this study carried out in 2011 and 2012, the effects of four different tillage practices [plow + disc harrow + rotary tiller + direct seeding machine (TP_1), chisel + disc harrow + rotary tiller + direct seeding machine (TP_2), plow + rotary tiller + direct seeding machine (TP_3), direct drilling (TP_4)] and control plot without planting (TP_5) on the soil bulk density (BD), moisture content and penetration resistance of a clayey textured soil were evaluated in the central Black Sea Region of Turkey with a geostatistical approach. The values of soil compaction indicators were significantly greater under the TP_4 treatment than in the case of TP_1 and TP_2 after harvest, especially at 20-40 cm depth in 2011 and 2012. Overall, our results suggest the avoidance of direct seeding practices in high clay content soils.

ÖZET
Bu çalışma ile 2011-2012 yıllarında, Türkiye'nin Orta Karadeniz Tarımsal Bölgesinde killi bünyeye sahip bir toprakta, dört farklı toprak işleme metodunun [(pulluk+diskaro+rotatiller+doğrudan ekim makinası;($Tİ_1$), çizel+diskaro+rotatiller+doğrudan ekim makinası;($Tİ_2$), (pulluk+rotatiller+doğrudan ekim makinası; ($Tİ_3$) ve doğrudan ekim; (DE)] ve ekim yapılmayan kontrol parselinin hacim ağırlığı, nem içeri ve penetrasyon direncine etkileri jeo-istatistiksel yaklaşım metodu ile değerlendirilmeye çalışılmıştır. Bu çalışmanın sonuçlarına göre ağır bünyeli topraklarda Doğrudan Ekim (DE) uygulamasından kaçınılması gerektiği söylenebilir.

INTRODUCTION
Soil is one of the necessary requirements for human existence and an essential contributor to human civilization. It is a fundamental prerequisite for agricultural production and is closely connected with food supply *(Badalikova B., 2010)*. Compacted soil can be a serious problem in agriculture as it can restrict access of the root system to water and nutrients, thus decreasing crop yields *(Clark et al. 2003).* Sustainable use of agricultural lands for optimal plant production is closely related to agricultural practices. Many soil properties are affected to some degree by soil management practices *(AksakalandÖztaş, 2010)*. Soil tillage, which requires high-energy inputs at considerable expense, creates favourable conditions for good stand establishment and development, and crop yields. Tillage practices play a crucial role in soil conservation *(El Titi., 2003)*. One of the main goals of soil tillage is to influence soil processes, predominantly modification of soil chemical, physical and biological properties *(Badalikova B., 2010; Botta et al., 2010).* However, from soil preparation to harvest, field operations can damage soil structure by compaction which is a major problem for agricultural lands *(Stafford and Hendrick, 1988)*.
Soil compaction is basically the reduction in volume of a given soil mass. It is commonly defined as an increase in soil bulk density (BD) that is manifested through closer packing of solid particles, and decreased porosity, especially the proportion of large pores *(Arslan S., 2006; Pınar et al, 2008; Çelik A., 2011)*. The relationship between soil compaction and penetration resistance (PR) has been described in many studies *(Utsetand Cid, 2001; Kılıç et al, 2004; Hamza and Anderson, 2005; Arslan S., 2006; Carrara et al, 2007; UsowiczandLipiec, 2009).* Soil compaction is an important physical limiting factor for root growth and plant emergence and is one of the major causes of reduced crop yield in worldwide *(Utsetand Cid, 2001; Hamza and Anderson, 2005; Pınar et al. 2008; Tekin et al, 2008)*. In soils compacted to more than 2 MPa resistance, root growth is extremely difficult *(Botta et al, 2006).* Sometimes, however, compaction is desirable, because it can lead to improved seed-soil contact, and hence better germination and growth of the seedling *(Çelik İ., 2011).*

As far as the determination of soil compaction and related soil properties, the determination of these properties and the spatial distribution of the soil compaction level in the vicinity are of great importance in terms of effective soil management practices. For precision agriculture applications, it is essential to determine the level of yield and productivity parameters change, including soil compressibility, and to prepare area indicator maps.

Geostatistical techniques, together with classical statistics, constitute an important tool in determining the spatial effects of soil management practices *(Usowicz andLipiec, 2009).* Traditional statistics assume that the spatial variability of soil is random and without spatial correlations, therefore they are not suitable for analysing spatially varying soil properties. However, geostatistical techniques accept that samples taken in close proximity are generally more similar than samples taken from a greater distance apart, and spatially analyse the relationships between soil properties *(Isaaksand Srivastava, 1989)*. Spatial continuity exists in most earth science data sets. Two data in close proximity are more likely to have similar values than two data that are far apart *(Isaaksand Srivastava, 1989)*.

Geostatistical techniques can be divided into two groups, namely semivariogram for spatial modelling and kriging for spatial interpolation. To estimate the unsampled values, it is essential to know the semivariogram function associated with the soil properties evaluated. Kriging is a statistical procedure for interpolating values at unsampled locations between locations with measured values. It is one of many procedures available to estimate unknown values within a domain based on already known values *(Nielsen and Wendroth, 2003).* Geostatistical techniques have become widely used for the analysis of soil data *(Lopez-Granados et al, 2005; Sağlam M., 2015).*

Knowledge of the spatial distribution of PR can be helpful in identifying zones with soil compaction (strength) problems and developing management strategies that minimize the harmful impacts of infield traffic on crop production. The aim of this study was to examine the effects of different soil tillage methods on PR by using geostatistical techniques.

MATERIAL AND METHODS

The experiment was conducted on alluvial soil at the Karadeniz Agricultural Research Institute, Samsun, Turkey in 2011 and 2012. Average annual rainfall was 1045.2 mm. The soil of the study area had a clayey texture (67% clay, 18% silt and 15% sand) and according to its soil taxonomy, it was classified as Vertisol *(Soil Survey Staff, 1999).*

Four different tillage practices, namely plow+disc harrow+rotary tiller+direct seeding machine (TP_1), chisel+disc harrow+rotary tiller+ direct seeding machine (TP_2), plow+rotary tiller+direct seeding machine (TP_3) and direct drilling (TP_4), and an unplanted control plot (TP_5) were applied to experimental plots of 11 m x 50 m with three replicates. A Ford 6600 tractor (77 horsepower, 2.750 kg) was used for all soil tillage treatments. After the tillage treatments, maize (*Zea mays, L.*) was planted in all study plots in May and harvested in October.

Penetration resistance was measured with an Eijelkamp handheld penetrometer of 16.60 mm diameter and 30° cone angle. This instrument can measure a penetration force ranging from 0 to 1 kN (with a resolution of 0.02 kN) up to a maximum depth of 0.45 m. Penetration resistance was determined with the following equation *(Selvi K Ç., 2003):*

$$PR = \frac{F}{A} \text{ x } 0.0981 \tag{1}$$

where:

PR is penetration resistance [MPa];
F is the reading; the value of force [daN];
A is the base area of cone [cm^2].

Before tillage, soil *BD* was determined with the cylinder method *(Blake and Hartge, 1986).* Soil gravimetric moisture content at 0-20 cm and 20-40 cm was determined for 100 cm^3 of undisturbed soil samples taken with rollers 24 h and dried in an oven at 105 °C.

The spatial variability of soil *PR* was examined with semivariogram models and the following equation was used to estimate the models.

$$\gamma(h) = \frac{1}{2N}\sum_{i=1}^{N}\left(Z_x - Z_{x+h}\right)^2 \tag{2}$$

where:

z (x_i) and *z(x_i + h)* are the variables of interest at locations xi and x_i + h, respectively,

N(h) is the number of pairs at locations separated by a distance 'h' *(Isaaksand Srivastava, 1989),* the theoretical spherical semivariogram model was used to establish the spatial variability of PR.

The isotropic spherical model:

$$\gamma(h) = \begin{cases} C_o + C\left[\frac{3h}{2a} - \frac{1}{2}\left(\frac{h}{a}\right)^3\right] & 0 \le h \le a \\ C_o + C & h > a \end{cases} \tag{3}$$

where:

C_0 is the nugget variance,

C is the structural variance,

C_0+C is the sill variance,

h is the lag distance,

a is the range of spatial correlation.

While selecting the best fit model, the model with the smallest residual sum of squares (RSS), the highest coefficient of determination (r^2) and the best cross-validation result was controlled. The semivariogram and spatial structure analyses for PR were performed with geostatistical software *(Robertson G P, 2008).*

RESULTS

The soil BD (g cm^{-3}) and volumetric water content (VWC) (%) before tillage and after harvesting in the experimental plots at 0-20 cm and 20-40 cm for both experimental years are shown in Table 1.

Table 1

Values of some soil properties before tillage and after harvesting for different soil tillage methods on the Black Sea coast of Turkey

Years	Tillage Practices	Depth, [cm]	Bulk Density, [gcm^{-3}]		Volumetric Water Content, [%]	
			BT	AH	BT	AH
2011	TP_1	0-20	1.28	1.07	37	43
	TP_2		1.28	1.08	36	45
	TP_3		1.24	1.12	33	46
	TP_4		1.27	1.12	31	48
	TP_5		1.28	1.12	25	48
	TP_1	20-40	1.30	1.12	36	52
	TP_2		1.30	1.14	38	54
	TP_3		1.32	1.21	40	52
	TP_4		1.36	1.22	40	55
	TP_5		1.30	1.21	38	54
2012	TP_1	0-20	1.23	1.21	35	38
	TP_2		1.23	1.20	41	44
	TP_3		1.22	1.17	42	44
	TP_4		1.22	1.20	41	42
	TP_5		1.21	1.20	42	44
	TP_1	20-40	1.28	1.24	34	56
	TP_2		1.26	1.23	42	54

Years	Tillage Practices	Depth, [cm]	Bulk Density, [gcm^{-3}]		Volumetric Water Content, [%]	
			BT	AH	BT	AH
	TP_3		1.26	1.28	42	56
	TP_4		1.28	1.28	44	56
	TP_5		1.26	1.27	44	54

TP_1: plow+disc harrow+rotary tiller+direct seeding machine. TP_2: chisel+disc harrow+rotary tiller+direct seeding machine. TP_3: plow+rotary tiller+direct seeding machine. TP_4: direct drilling. TP_5: control plot without planting. BT= before tillage; AH= after harvesting.

The average *BD* for 0-20 cm for all experimental plots before soil tillage and after harvesting in 2011 were 1.27 g cm^{-3} and 1.10g cm^{-3}, respectively, and in 2012, 1.22 g cm^{-3} and 1.20g cm^{-3}, respectively. For 0-20 cm, the mean moisture content for treatments before tillage and after harvesting in 2011 were 32.4% and 46.0%, respectively, and in 2012, 40.2% and 42.4%, respectively. For 20-40 cm, the mean moisture content for treatments before tillage and after harvesting in 2011 were 34.4% and 53.4%, respectively, and in 2012, 40.2% and 42.4%, respectively. Differences in soil moisture among tillage methods were not statistically significant ($P>0.05$).

Values of soil *PR* ranged between 0.51 MPa and 1.97 MPa for 0-20 cm and 0.70 MPa and 1.37 MPa for 20-40 cm before tillage in 2011. Penetration resistance ranged between 0.76 MPa and 1.41 MPa for 0-20 cm and 0.91 MPa and 3.10 MPa for 20-40 cm after harvesting in 2011. Values of PR ranged between 0.61 MPa and 1.35 MPa for 0-20 cm and 0.61 MPa and 1.23 MPa for 20-40 cm before tillage in 2012. Penetration resistance ranged between 0.66 MPa and 1.33 MPa for 0-20 cm and 0.77 MPa and 2.07 MPa for 20-40 cm after harvesting in 2012.

The semivariogram model was fitted to empirical values with a determination coefficient >0.9 in all cases. In this study, only selected semivariograms are presented for 0-20 cm and 20-40 cm before tillage and after harvesting in 2011 and 2012. Semivariogram models of PRs evaluated in terms of both sampling times and sampling depths were fitted as spherical models, and all models fitted had a high coefficient of determination and small RSS which indicated that all the models were reliable (Table 2).

Table 2

Parameters of semivariogram models for different soil tillage methods on the Black Sea coast of Turkey

Year	Time	Depth	Model	Nugget	Sill	Range	R^2	RSS	r [for cross validation]
2011	BT	0-20	Sph	0.0001	0.108	20.28	0.98	2.203×10^{-4}	0.8
		20-40	Sph	0.0001	0.035	21.76	0.99	1.909×10^{-5}	0.76
	AH	0-20	Sph	0.00001	0.016	17.91	0.96	8.467×10^{-6}	0.92
		20-40	Sph	0.0001	0.223	22.44	0.94	1.281×10^{-3}	0.93
2012	BT	0-20	Sph	0.0001	0.041	15.16	0.97	2.486×10^{-6}	0.81
		20-40	Sph	0.00008	0.020	14.18	0.97	1.984×10^{-5}	0.8
	AH	0-20	Sph	0.00061	0.029	16.96	1.00	7.029×10^{-7}	0.77
		20-40	Sph	0.0039	0.067	4232	1.00	1.030×10^{-5}	0.81

Sph: spherical; BT=before tillage; AH= after harvesting; RSS: residual sum of squares

Semivariogram maps of *PR* for the two depths indicated the occurrence of spatial dependence with different values of semivariance, as affected by tillage methods.

The effects of different tillage methods on distribution of *PR* in 2011 and 2012 are given in Figures 1 and 2, respectively.

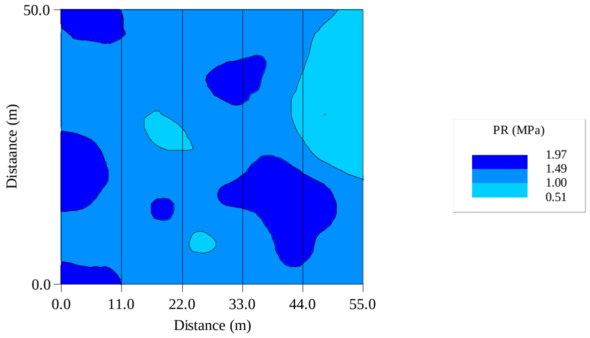

a. before tillage (0-20 cm)

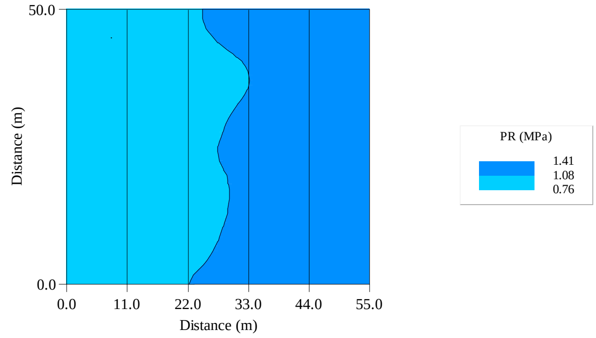

b. after harvesting (0-20 cm)

c.

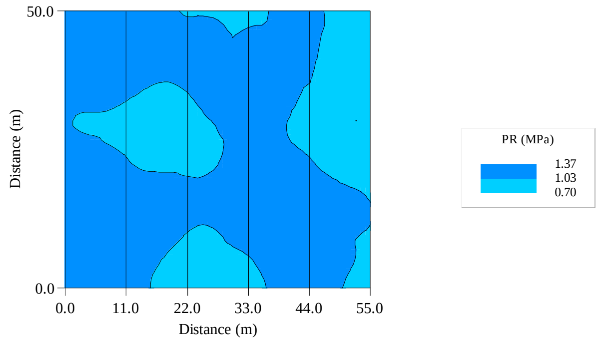

d. before tillage (20-40 cm)

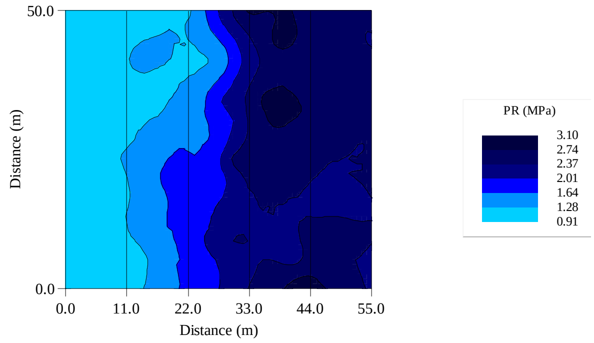

e. after harvesting (20-40 cm)

Fig 1 - The effects of different soil tillage methods on distribution of PR in 2011

TP_1: plow+disc harrow+rotary tiller+direct seeding machine. TP_2: chisel+disc harrow+rotary tiller+direct seeding machine. TP_3: plow+rotary tiller+direct seeding machine. TP_4: direct drilling. TP_5: control plot without planting; 0.0 m-11.0 m = TP_1; 11.0 m-22.0m = TP_2; 22.0 m-33.0 m= TP_3; 33.0 m-44.0 m= TP_4; 44.0 m-55.0 m= TP_5.

In 2011, for 0-20 cm, the *PR* values were heterogeneous in all experimental plots before tillage. Penetration resistance values obtained after harvesting (AH) showed that they were most reduced by the TP_1 method. For 20-40 cm before tillage, *PR* values were more homogeneous and the average values of PR were lower than for 0-20 cm.

However, after harvesting, *PR* values were high enough to limit the crop yield *(Botta et al, 2006)* in the TP_3 and TP_4 plots at 20-40 cm. Penetration resistances for TP_1 decreased at both depths.

This result may be explained by inversion of the soil by the plow, which increases pore size. These results support the results of Çetin et al. (2009) and Doğan and Çarman (1997).

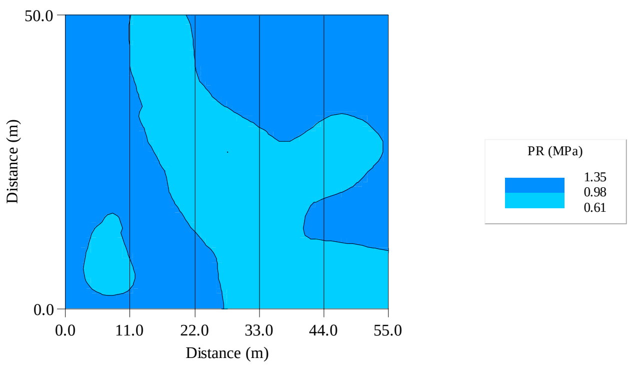

a. before tillage (0-20 cm)

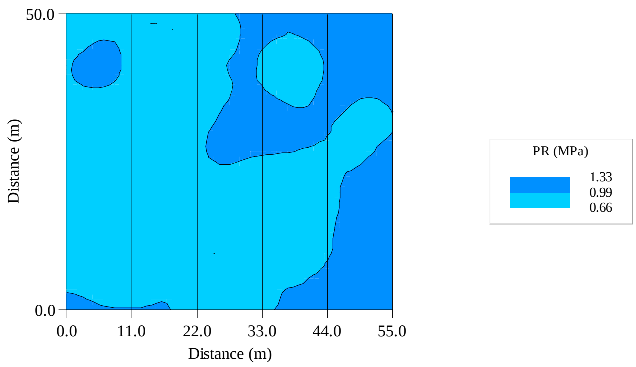

b. after harvesting (0-20 cm)

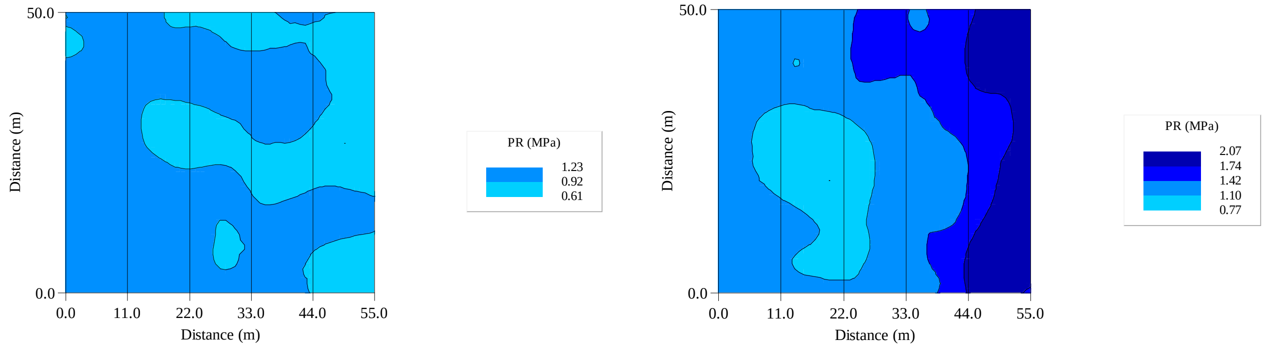

c. before tillage (20-40 cm) d. after harvesting (20-40 cm)

Fig. 2 -The effects of different soil tillage methods on distribution of PR in 2012

TP_1: plow+disc harrow+rotary tiller+direct seeding machine. TP_2: chisel+disc harrow+rotary tiller+direct seeding machine. TP_3: plow+rotary tiller+direct seeding machine. TP_4: direct drilling. TP_5: control plot without planting; 0.0 m-11.0 m = TP_1; 11.0 m-22.0m = TP_2; 22.0 m-33.0 m= TP_3; 33.0 m-44.0 m= TP_4; 44.0 m-55.0 m= TP_5.

The average *PR* values before soil tillage in 2012 were lower than in 2011. In 2012, the *PR* values at 0-20 cm were more homogenous than in 2011 in all experimental plots. In 2012, the PR values obtained at 0-20 cm after harvesting for the TP_1 and TP_2 methods were lower than for 2011. In addition, after harvesting, *PR* values were higher for the TP_3 and TP_4 methods for 20-40 cm in 2011 than in 2012. The TP_1 method decreased the *PR* at 0-20 cm. That result can be attributed to the short term loosening effect of tillage. However, the TP_3 and TP_4 methods increased the *PR* at 20-40 cm. These results were in good agreement with those of Scwartz et al. (2003) and Çelik (2011).

Penetration resistances for the two soil depths were the highest under the TP_4 method and the lowest under the TP_1 method in both experimental years, relative to TP_5 (Control). This result supported those of Alvarez et al. (2009) and Çelik (2011) and the lowest values of PR were obtained for the TP_1 method. In our study, the *PR* increased with soil depth for all methods, which supported the results of Boydaş and Turgut (2007) and Amin et al. (2014).

CONCLUSIONS

The results of the current study showed that the use of the TP_1 and TP_2 methods for two years in maize growing resulted in lower bulk densities than for other tillage operations on a heavy clayey soil (Vertisol). The *BD* and *PR* were significantly greater under TP_3 and TP_4, especially TP_4, than those under TP_1 and TP_2 at 0-20 and 20-40 cm. The values of *BD* and *PR* were lower in the surface layers. The TP_4 method had detrimental effects that varied according to the sampling period and soil depth.

Overall, soil properties influencing *PR* in all plots were water content, *BD* and clay content. Our results suggest that since the *PR* was adversely affected, direct seeding (TP_4) should be avoided on high clay content soils under the Black Sea Region climatic regime.

ACKNOWLEDGEMENT

The authors are grateful to The Scientific Research Council of OndokuzMayıs University for financial support (project number PYO.ZRT.1901.011.013) and Gregory T. Sullivan of GPEM, University of Queensland in Brisbane, Australia for editing the English in an earlier version of this manuscript.

REFERENCES

[1] Aksakal E.L., Öztaş T., (2010), Changes in distribution patterns of soil penetration resistance within a silage-corn field following the use of heavy harvesting equipment, *Turkish Journal of Agriculture and Forestry.* doi:10.3906/tar-0906-189;

[2] Alvarez C.R., Taboada M.A, Gutierrez B.F.H, Bono A., Fernandez P.L., Prystupa P, (2009), Topsoil properties as affected by tillage systems in the Rolling Pampa Region of Argentina, *Soil Science Society of America Journal,* vol.73, pp.1242-1250;

[3] Amin M., Khan M.J., Jan M.T., Rehman M., Tariq J.A., Hanif M, Shah Z., (2014), Effect of different tillage practices on soil physical properties under wheat in semi-arid environment, *Soil Environ*, vol.33, pp.33–37;

[4] Arslan S, (2006), An alternative method for preventing soil compaction: controlled traffic, *K.S.U. Journal of Science and Engineering,* vol.9, pp.135-141;

[5] Badalikova B, (2010), Influence of soil tillage on soil compaction. Berlin: Heidelberg. Chapter 2, *Soil Engineering: Soil Biology,* pp. 19-30, doi: 10.1007/978-3-642-03681-1_2;

[6] Blake G.R., Hartge K.H., (1986), Methods of soil analysis: physical and mineralogical analysis. *Madison (WI): American Society of Agronomy. Chapter 14*, Bulk density and particle density, pp.363-381;

[7] Botta G.F., Jorajuria J., Balbuena R., Ressia M., Ferreo J., Rosatto H., Tourn M, (2006), Deep tillage and traffic effects on subsoil compaction and sunflower (Helianthus annus L.) yields. *Soil & Tillage Research,* doi:10.1016/j.still.2005.12.011;

[8] Botta G.F., Tolon-Becerra A., Lastra-Bravo X., Tourn M,(2010), Tillage and traffic effects (planters and tractors) on soil compaction and soybean (Glycine max L.) yields in Argentinean pampas. *Soil & Tillage Research.* doi:10.1016/j.still.2010.07.001;

[9] Boydas M.G., Turgut N, (2007), Effect of tillage implements and operating speeds on soil physical properties and wheat emergence. *Turkish Journal of Agriculture and Forestry*, vol.31, pp.399–412;

[10] Carrara M., Castrignanò A, Comparetti A., Febo P., Orlando S, (2007), Mapping of penetrometer resistance in relation to tractor traffic using multivariate geostatistics, *Geoderma.* doi:10.1016/j.geoderma.2007.08.020;

[11] Clark L.J., Whalley W.R., Barraclough P.B, (2003), How roots penetrate strong soil?, *Plant and Soil,* vol*.*25, pp.93-104;

[12] Çetin M., Akbaş T., Şimşek E., (2009), Determination of the effects of different soil tillage equipment on soil penetration resistance*. 25th National Agricultural Mechanization Congress*; 2009 October 1-3; Isparta Turkey;

[13] Çelik İ., (2011), Effects of tillage methods on penetration resistance, bulk density and saturated hydraulic conductivity in a clayey soil conditions. *Journal of Agricultural Sciences,* vol.17, pp.143–156;

[14] Doğan H., Çarman K., (1997), Effects of seedbed preparation application on some soil physical properties and fuel consumption at grain farming in Konya region. *Agricultural Mechanization 17nd National Congress*; 1997 September 17-19, Tokat /Turkey;

[15] El Titi A, (2003), Soil tillage in agro-ecosystem. *Secaucus (NJ): Taylor and Francis*;

[16] Hamza M.A., Anderson, W.K, (2005), Soil compaction in cropping systems: A review of the nature, causes and possible solutions. *Soil and Tillage Research,* vol. 82, pp.121-145;

[17] Isaaks E.H, Srivastava R.M, (1989), An introduction to applied geostatistics. New York (NY): Oxford University Press;

[18] Kılıç K., Özgöz E., Akbaş F, (2004), Assessment of spatial variability in penetration resistance as related to some soil physical properties of two fluvents in Turkey. *Soil & Tillage Research.* doi:10.1016/j.still.2003.08.009;

[19] Lopez G.F., Jurado E.M., Pena B.J.M., Garcia T.L, (2005), Using geostatistical and remote sensing approaches for mapping soil properties. *Europ J Agronomy*, vol.23, pp.279–289;

[20] Nielsen D.R., Wendroth O, (2003), Spatial and temporal statistics. Sampling field soils and their vegetation*. Reiskirchen: GeoScience Publisher*;

[21] Pınar Y., Selvi K.Ç., Yılmaz S, (2008), Effect of soil compaction (plough pan) on soybean yield at Samsun conditions*. Journal of Agricultural Machinery Science*, vol.4, pp.165-170;

[22] Robertson G.P, (2008), GS^+: geostatistics for the environmental sciences. *Plainwell (MI): Gamma Design Software;*

[23] Sağlam M, (2015), Evaluation of the physico chemical properties of alluvial and colluvial soils formed under ustic moisture regime using multivariate geostatistical techniques. *Archives of Agronomy and Soil Science*, vol.61, pp. 943-957;

[24] Schwartz R.C., Evett S.R., Unger P.W, (2003), Soil hydraulic properties of cropland compared with re-established and native grassland. *Geoderma,* vol.116, pp.47-60;

[25] Selvi K.Ç., Kirişci V., Korucu T., (2003), The effects of plow pan on cotton production in terms of soil dynamics. *21th National Agricultural Mechanization Congress,* 2003 September 3-5, Konya/Turkey;

[26] Stafford J.V., Hendrick J.G, (1988), Dynamic sensing of soil pans. *Transactions of the ASAE*, vol.31. pp.9-13;

[27] Soil Survey Staff, (1999), Soil taxonomy: a basic of soil classification for making and interpreting soil survey. 2nd ed. Washington (DC): *NRCS, USDA, Agriculture Handbook* No.436;

[28] Tekin Y., Kul B., Okursoy R, (2008), Sensing and 3D mapping of soil compaction. *Sensors*. 8:3447-3459. doi: 10.3390-s8053447;

[29] Usowicz B., Lipiec J, (2009), Spatial distribution of soil penetration resistance as affected by soil compaction: The fractal approach. *Ecological Complexity*. doi:10.1016/j.ecocom. 2009.05.005;

[30] Utset A., Cid G, (2001), Soil penetrometer resistance spatial variability in a Ferralsol at several soil moisture conditions, *Soil & Tillage Research*, vol.61. pp.193–202.

THE RESEARCH CONCEPT ON THE WEEDING PROCESS AND THE CONTACT ACTION MACHINES
/
ФОРМУВАННЯ КОНЦЕПЦІЇ ДОСЛІДЖЕННЯ ПРОЦЕСУ ЗНИЩЕННЯ БУР'ЯНІВ І МАШИНИ КОНТАКТНОГО СПОСОБУ ДІЇ

Ph.D. Eng. Bundza O.Z. [1], Prof. Ph.D. Eng. Nalobina O.O. [1], Assoc.Prof. Ph.D. Eng. Nikitin V.G. [1], Ph.D. Eng. Tkachuk O.L. [2]

[1] National University of Water Management and Nature Resources Use, Rivne / Ukraine
[2] Lutsk National Technical University, Lutsk / Ukraine
E-mail: olegbundza@gmail.com

Keywords: *analysis, weeds, herbicide, contact application, oblique cut*

ABSTRACT
The article deals with the kinetics of the weeding process. The authors analyse the key figures to evaluate the effectiveness of machines for contact application; they also present the equation to calculate the final accuracy of the process.

РЕЗЮМЕ
Досліджено кінетику технологічного процесу знищення бур'янів. Розглянуто показники, якими можна оцінити якість роботи машини для контактного нанесення. Виведено вираз для визначення показника чистоти обробки.

INTRODUCTION
Agriculture means provide certain conditions, notably well-timed and effective weeding. The analyses of the production processes in the agricultural enterprises in Ukraine and abroad has shown that this task is accomplished mainly with the help of chemical methods *(Lysov A.K., 2012; Melezhyk O.I., 2010; Onyschenko B.V., 2011)*.

Herbicide spraying means serious undesirable losses caused by wind, evaporation, dropping, working solution drops settling on the soil *(Lysov A.K., 2009)*. Besides, the existing processes aimed to eliminate the weeds have low effectiveness caused by numerous technical reasons and physical and mechanical characteristics of the plants.

The current scientific and practical task is to develop the new equipment of weed infestation decrease that will allow to increase the process effectiveness by reducing unproductive losses and destroy both the stalks and the roots of the weeds *(Lemus R., Mowdy M., Davis A., 2013)*. It is important to develop the weeding technologies *(Joseph M. DiTomaso., Drewitz J., 2008; Thomas J. Monaco, 2002)* because the existing equipment and machinery have low productivity. The comparative analysis of the present technology has shown the perspectives of contact method of herbicide application on the plants *(Moyo C., Harrington K. C., Kemp P. D., Eerens J. P., 2008; Kotov A.A., 2009)*.

However, the weeding technology with already known contact action equipment can't be used on the areas with big slopes or on the fields and pastures overgrown with weeds having rough stem.

The solution of the current scientific and practical task of more effective weeding process should be based on the system analysis of interaction between the working tools of the machine for contact herbicide application and the stems; it will allow to indicate the process regularities, investigate the reasons of unproductive losses, scientifically explain the way to increase the effectiveness and constructive design of working tools.

MATERIAL AND METHODS
The analysis in literature and statistical reports has proven that the contact method is becoming widely used *(Bundza O.Z., Kravets S. V., Nalobina O. O., Nikitin V. G., 2015; Lvov S.M., Putianin Y.P., Shashova M.V., 1990)*. Its principle is that certain amount of working solution is applied directly on the plant. In comparison with other method it allows: to avoid the loses caused by wind (compared to irrigation); minimize losses caused by dropping and evaporation; eradicate high weeds without damaging low plants; decrease

the loss of working solution; avoid using expensive herbicides of selective effect. This method is successfully used to control high weeds on grazing and agricultural lands. It allows to reduce pollution of agricultural plants with chemicals.

The analysis of the existing machine constructions and their working tools for contact herbicide application has helped conclude the following:

1) the work of this equipment is characterized by the significant losses of working solution that causes:
- environmental pollution;
- great herbicide losses;
- transfer of the chemicals to the agricultural plants.

2) actual equipment is not effective for eradication of the weeds with thick stems when their roots must be destroyed.

In order to eliminate these drawbacks, the authors have designed the weeding machine construction of contact action; the scheme of the working tool is represented in figure 1 *(Bundza, O.Z. and Nikitin, V.H., 2010; Bundza O.Z., Kravets S. V., Nalobina O. O., 2015)*. The machine for contact weeding in combined method consists of three working tools: cutting device, collector of the cut plants and unit for the contact herbicide application.

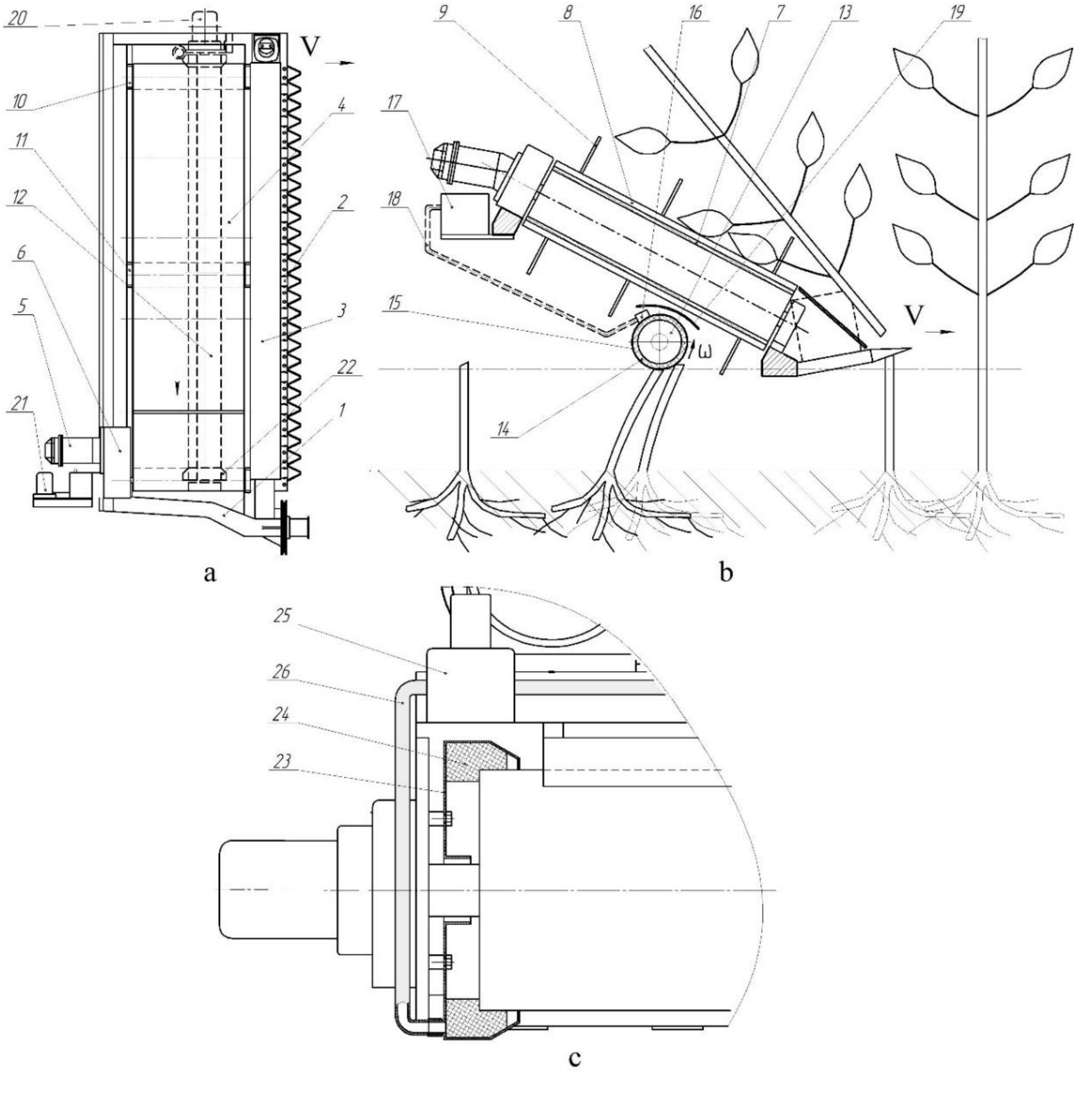

Fig. 1 - Scheme of the working tools of the contact action weeding mechanism

top view (a), working scheme (b), unused solution collector (c):
1-frame, 2-cutting device, 3-plate, 4-collector; 5-collector drive hydraulic motor; 6-collector drive gearbox; 7-conveyor belt; 8-cleat; 9-fingers; 10-tension mechanism; 11-supporters; 12-couplant mechanism; 13-drum; 14-porous-capillary material; 15-synthetical net; 16-feeder; 17-dosing pump; 18-pipe lines; 19-casing; 20-shaft drive; 21-pump drive; 22-unused solution collectors; 23-jar; 24-circle made of porous material; 25-draining pump; 26-pipe line

While in operation, the cut plants fall on the collector *4* and they are taken away; the drum *13* applies the herbicide solution directly on the cut plants by the couplant method. The herbicide moves to the plant root through the capillaries and causes their destruction or significant loss of vital functions without polluting the environment. The dosing pump *17* regulates the herbicide flow in order to ensure the supply of the necessary amount of herbicide and to avoid dropping.

The suggested construction has following advantages: possibility to destroy above ground part of the weeds and their roots, possibility to reuse the weed stems, selective action (only high plants are cut down, crop plants and grass are saved), ecological compatibility (chemicals that are used in solutions don't settle on the soil or crops), minimal non-productive losses (dropping, evaporation, wind).

According to the chosen topic, the authors research the kinetics of the weeding process in order to formulate the concept for further examining the weeding machine construction.

The authors study the technological process of weeding as the one that is done sequentially and consists of two technological operations: weeds stem cutting and herbicide application on the cut stems. As a result, we get two products – weed stubbles with herbicide applied on the top and cut weed stems on the field surface.

The authors examine the kinetics of weeding technological process in order to form the concept for further research of machine construction for contact weeding method. The analysis of the weeding process is done in accordance with the theory of biological populations' propagation and death *(Sychuhov N.P., 1970; Ventsel E.S., 2003)*.

The authors regard the weeding process as homogenous, set in time and deterministic. The subpopulation of weed stems may be in the following states – cut but without herbicide covering (stubbles, non-covered); cut and covered with herbicide (stubbles, covered); non-cut covered with herbicide (stems, covered). These assemblages are characterized with initial and current inclusion in total weed amount on a certain field area. If these assumptions are correct, then the equation of material balance is true in any random moment of time:

$$Q(t)+Z(t)+\alpha(t)=Q_0 \tag{1}$$

where *Q(t)* is the number of uncut plants that are not covered with the herbicide and remain on the field, *Z(t)* is the number of uncut plants but covered with the herbicide, *α(t)* is the amount of cut and covered with the herbicide weeds, Q_0 is the total number of weeds before the beginning of the process.

The authors introduce the limitation for further research:

- in the initial moment of the process(*t=0*) $Q(t)= Q_0$;
- weed stems cutting is performed simultaneously with the herbicide application on the tops of the stubbles;
- the contact herbicide application process takes place under unchangeable environmental conditions.

We can write the differential equation of weeds number change on the processed area:

$$\frac{dQ(t)}{dt}=-k_1\cdot Q(t) \tag{2}$$

where k_1 is the intensity of the weeds cutting process with the cutting unit of the contact action machine for weeding.

The number of weeds that are not cut but covered with the herbicide can be calculated with the help of the equation:

$$\frac{dZ(t)}{dt}=\frac{Q(t)}{dt}-\frac{d\alpha(t)}{dt}=k_1\cdot Q(t)-\frac{d\alpha(t)}{dt} \tag{3}$$

The number of the stems where herbicide was applied is proportional to the number of cut and uncut stems:

$$\frac{d\alpha(t)}{dt}=k_2\cdot Q(t)+k_3\cdot Z(t) \tag{4}$$

where k_2 indicates the intensity of uncut stems processing and k_3 – the intensity of cut stems processing.

The indices k_1, k_2, k_3 can be defined experimentally or theoretically.

The equations for total change of weeds amount that was processed with the contact action machine are the following:

$$\left.\begin{array}{l} \frac{dQ(t)}{dt} = -k_1 \cdot Q(t) \\ \frac{d\alpha(t)}{dt} = k_2 \cdot \frac{dQ(t)}{dt} + k_3 \cdot \frac{dZ(t)}{dt} \\ \frac{dZ(t)}{dt} = k_1 \cdot Q(t) - (k_2 \cdot Q(t) - k_3 \cdot Z(t)) \\ \frac{dQ(t)}{dt} + \frac{d\alpha(t)}{dt} + \frac{dZ(t)}{dt} = 0 \end{array}\right\} \tag{5}$$

We solve these equations.

The first equation of the system (5) shows the change in number of uncut weeds where herbicide was applied with the drum. The solution of this equation is:

$$\frac{dQ(t)}{Q} = -k_1 \cdot dt \text{, hence } \ln Q_{(t)} = -k_1 \cdot t + C \tag{6}$$

If we assume that $C=lnC_1$, we will get $\ln Q_{(t)} - \ln C_1 = -k_1 \cdot t$.

If the processing time $t=0$, then $Q(t) = Q_0$ and $C_1 = Q_0$, we have

$$Q(t) = Q_0 e^{-k_1 \cdot t} \tag{7}$$

The equation (7) is an exponential function. Before the start of the process $t=0$ $Q(t) = Q_0$. If the machine starts functioning moving along the field, the number of uncut stems covered with the herbicide reduces and tends to zero. The speed of herbicide application is determined by intensity (k_1). The variable k_1 depends on the design parameters of the machine and working regime. Also, the variable k_1 depends on the roughness and height of the weed stems.

The weed stems are processed by the cutting device knives in one second. The cutting device cuts *m* number of weeds in one second.

The cutting device cuts *N* stems on working width. According to *(Letoshnev M.N., 1949)*:

$$N = t_0 hK \cdot 10^{-4} \tag{8}$$

where t_0 is the distance between the blades of cutting device, mm; *h* is delivery, cm; *K* is number of weed stems per m^2, units.

We examine the key figures to evaluate the working quality of the machine for contact application.

For the evaluation of the process we take the key figures (the equations that we have got after the analysis of the functions above):

1. the number of unprocessed weed stems:

$$\varphi_u(t) = \frac{Q(t)}{Q_0} = e^{-k_1 \cdot t} \tag{9}$$

If t=0, we get $\varphi_u(t) = 1$.

2. the number of cut weed stems that are covered with herbicide – finish accuracy:

taking the condition that $t=0$ $\varphi_u(t)=1$, we get $\varphi_y(t) = 1 - \frac{Q(t)}{Q_0} = 1 - e^{-k_1 \cdot t}$, (10)

3. the number of destroyed weeds:

$$Y(t) = \frac{\alpha(t)}{Q_0} \tag{11}$$

If $t=0$, $Y(t)=0$.

The intensity coefficients κ_1, κ_2, κ_3 do not show their complete dependence on design parameters and operation mode of the working tools of the contact action weeding machines. With this purpose, the authors establish general correspondences between plant stems and some parameters of machine working tools.

To calculate the intensity coefficient k_1 we assume that the cutting device effectively cuts on working width:

$$\lambda_1 = \frac{k_1 \cdot t}{N}\text{, or } \lambda_1 N = k_1 \cdot t \tag{12}$$

If we assume that the cutting effectiveness on each area is the same, we will have an equation for finish accuracy (10):

$$\varphi_y(t) = 1 - e^{-\lambda_1 \cdot N} \tag{13}$$

Here we see that the cutting device is determined by the effectiveness index on a certain area. The higher λ_1 is, the faster φ_y becomes maximal.

On the other side, the process effectiveness is determined by the number of weed stubbles covered with herbicide. The drum contacts with m cut stems in one second:

$$m = \frac{L_d \omega_d}{2\pi \cdot v_m} \tag{14}$$

where L_d is the drum length, m; ω_d is its rotational speed, c^{-1}; v_m is the machine speed, m per s.

We calculate the intensity of weeds cutting k_1. We solve the equations (7), (9), (12). According to (12) we write the equation for finish accuracy (10):

$$\varphi_y(N) = 1 - e^{-\lambda_1 \cdot N} \tag{15}$$

Then the equation $\varphi_y(N) = 1 - \varphi_u^N$ is true (according to (14) and (15)) if the whole length of the cutting device cuts.

We get:

$$\varphi_y(N) = 1 - e^{-k_1 \cdot N} \text{ and } \varphi_u(N) = e^{-k_1 \cdot N} \tag{16}$$

Taking into consideration this equation and transformation (7), (9), (12), we can calculate:

$$k_1 = -\frac{\ln \varphi_y(N)}{t}, \tag{17}$$

where t is the processing time, s.

$\varphi_y(N)$ is determined in experimental way.

RESULTS

The effectiveness of the weeding process by suggested contact action machine can be evaluated with k_1, that is the process intensity. It is a physical quantity that describes the kinetics of the process.

CONCLUSIONS

The above-mentioned equations (4), (9), (11), (12), (14) allow to formulate the concept of further research: explain the main parameters of the contact application machine in accordance with the physical and mechanical characteristics of the stems, namely roughness, cutting height, weed stems diameter that depends on the development stage of the weed. It allows providing the effective work of the suggested equipment.

REFERENCES

[1] Bundza O.Z., Kravets S. V., Nalobina O. O., Nikitin V. G., (2015), Theoretical reasoning of the couplant equipment drum position respectively the cut plants, *INMATEH-Agricultural Engineering*, vol.46, no 2., pp. 95–100, Bucharest/Romania;

[2] Bundza, O.Z.& Nikitin, V.H., (2010), *Equipment for plant and weed destruction*, Patent, No. 47259, Ukraine;

[3] Joseph M. DiTomaso., Drewitz J., (2008), Jubatagrass (Cortaderia Jubata) control using chemical and mechanical methods, *Kyser invasive plant science and management*, vol.1, no.1., pp. 82–90, Davis/California;

[4] Kotov A.A., (2009), Research of solution losses from the working tool surface of the contact herbicide machine (Исследование потерь препарата из покрытия рабочего органа контактной гербицидной машины), *Annals of the Moscow State University,* no.2, pp. 124–128, Moscow;

[5] Kotov A.A., (2009), *Technology perfection and creation of new mechanisms for forest nurseries and forest crops,* Phd. Eng. dissertation, Moscow State Forest University/ Russia;

[6] Lemus R., Mowdy M., Davis A., (2013), Herbicide evaluation for Smutgrass control using the weed wiper method, *Journal of the American Society of Farm managers and rural appraisers*, Vol. 6., issue 1, Mississippi State / U.S.A.;

[7] Letoshnev M.N., (1949), Agricultural machines. Theory, calculation, design, tests (Сельськохозяйственные машины. Теория, расчет, проектирование и испытание), "*State publishing of agricultural literature*", Moscow – St. Petersburg, 856p;

[8] Lvov S.M., Putianin Y.P., Shashova M.V., (1990), Contact method of herbicide and arboricide application, *Forest Management*, no. 12, p.45-50;

[9] Lysov A.K., (2009), Reduction of the pesticide losses during spraying (Снижение потерь пестицидов при опрыскивании), *Agricolist*, no. 2, p.138, Kyiv / Ukraine;

[10] Lysov A.K., (2012), New technology for plants spraying (Новая техника для опрыскивания растений), *Plants protection and quarantine*, *Agricolist*, no.5, pp. 55 – 57, Kyiv / Ukraine;

[11] Melezhyk O.I., (2010), *Improvement of pesticide spraying dispersion (Покращення дисперсності розпилення пестицидів*), PhD Science Thesis, National university of bio-resources and natural use of Ukraine, Kyiv / Ukraine;

[12] Moyo C., Harrington K. C, Kemp P. D, Eerens J. P., (2008), Herbicide deposition on weeds from weed wipers*, New Zealand Plant Protection*, (vol.61), p. 395, Henderson/ New Zealand;

[13] Onyschenko B.V., (2011), Explanation of the spraying device with the step-type dispersion controller (Обґрунтування розпилювального пристрою обприскувача з ступеневим регулюванням дисперсності розпилення), PhD Science Thesis, National University of Life and Environmental Sciences of Ukraine, Kyiv / Ukraine;

[14] Sychuhov N.P., (1970), Pneumatic transport mounting. Classification, theory, calculation of principal blocks and examples of mounting calculations (Установки пневматического транспорта. Классификация, основы теории, расчет основных узлов и пример расчета установки), Moscow, p. 68;

[15] Thomas J. Monaco, (2002), Weed science. Principles and Practices, John Wiley & Sons.inc., 685p., New York/U.S.A.;

[16] Ventsel E.S., (2003), Theory of probability and its application in engineering (Теория вероятностей и ее инженерные приложения), "Publishing centre "Academy", p. 464;

[17] ***Weed wipers (2014). Available at: http://www.smuckermfg.net/pages/ weedwipers.aspx (Accessed: 28 March 2015).

GROUNDING OF CONSTRUCTION PARAMETERS OF PSEUDOFLUIDIZED LAYER DRYER WORKING CHAMBER
/
ОБОСНОВАНИЕ КОНСТРУКТИВНЫХ ПАРАМЕТРОВ РАБОЧЕЙ КАМЕРЫ СУШИЛКИ ПСЕВДООЖИЖЕННОГО СЛОЯ

Prof. PhD. Eng.Sc. Kuznetsov Y.A., Assoc. Prof. D.Eng.Sc. Volzhentsev A.V.,
Prof. PhD. Eng.Sc. Kolomeichenko A.V., Prof. PhD. Eng.Sc. Kalashnikova L.V.
Orel State Agrarian University - N.V. Parakhin / Russia
Tel: +79208289219; E-mail: kentury@rambler.ru

Keywords: *drying, dryer, method, grain, pseudofluidization, gas distribution grid*

ABSTRACT
A new method for assessing the quality of fluidization is proposed, which allows providing more uniform heating of grain material and intensify its drying process.

РЕЗЮМЕ
Предложен новый метод оценки качества ожижения, позволяющий обеспечить более равномерный нагрев зернового материала и интенсифицировать процесс его сушки.

INTRODUCTION
Grain harvesting period in many regions of Russia coincides with autumn precipitation falls, thus as a result the harvested grain has high humidity *(Zhuravlev A.P., 2014).*

Now, convection drying of grain material by combustion products of organic matter used as a fuel with comparatively high combustion temperature are used in agricultural industry. The disadvantage of such dryers is high energy consumption *(Tarasenko A.P., 2008; Pilipyuk V.L. 2009).*

This provides the necessity to develop new, less energy consuming, environmentally friendly technologies of grain drying *(Shhitov S.V. et al, 2016; Bibik G.A., 2016; Volkov A.V., 2017).* The application of food dehydration method in pseudofluidized layer allows significantly speeding up the process that is very important for increasing technical and economic indicators of drying installations.

The grain layer description in dryers functioning according to its pseudofluidization principle *(Volzhentsev A.V., 2014; Kalashnikova N.V. and Volzhentsev A.V., 2009)* can be at best estimated only visually, which is not quite objective.

For this reason, there were many attempts to find more precise definition of pseudofluidization quality.

However, in known methods foreign objects should be plunged into pseudofluidized layer. It influences the pseudofluidization nature.

MATERIAL AND METHODS
The intensity of light flow when determining grain layer uniformity was detected by lux meter Ю-116, the readings of which were recorded by Panasonic NV-GS80EE-S video camera.

The installation response time of test and periodical running time were recorded by dual interruptible stop watch “С-II-16” with clock-driven mechanism.

We suggested the method of determining pseudofluidization uniformity consisting in determining light beam intensity, penetrating through grain layer.

Experimental tests were performed on the developed and manufactured installation presented in figure 1.

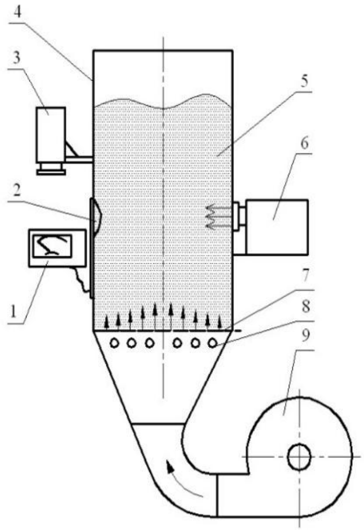

Fig. 1 – Scheme of experimental installation and devices arrangement to determine the pseudofluidization uniformity degree

1 – lux meter; 2 – selenium sensor; 3 – video camera; 4 – drying chamber; 5 – grain layer; 6 – light source; 7 – gas distribution device; 8 – electric heating elements; 9 – ventilator

Under the influence of heating with electric heating elements *8,* the air flow created by ventilator *9* on grain layer *5* which is located on gas distribution grid *7* the inter-grain contacts become weak, bed void fraction increases and its structure is destructed under certain conditions.

Dense grain layer in working chamber *4* merges into condition that reminds boiling liquid h.e. pseudo-fluidization condition. At that point, the uniformity degree of pseudofluidized grain layer produces the main effect on drying quality.

Light emission produced by directed light source *6* was detected by selenium sensor *2*, registered by lux meter *1* and recorded by video camera *3*.

Oscillograph recordings of lux meter readings have the form presented in figure 4, and allow obtaining detailed amplitude and frequency data. Different lines and hatchings in figure 5 present the processing of these recordings to obtain the necessary information.

Thus, distinguishing definite sufficiently large time interval T , we summarized the area under curve $\delta(t)$ and determined the mean average deviation $\bar{\delta}$ of light emission:

$$\bar{\delta} = \frac{1}{T}\int_0^T \delta(t)dt \; . \tag{1}$$

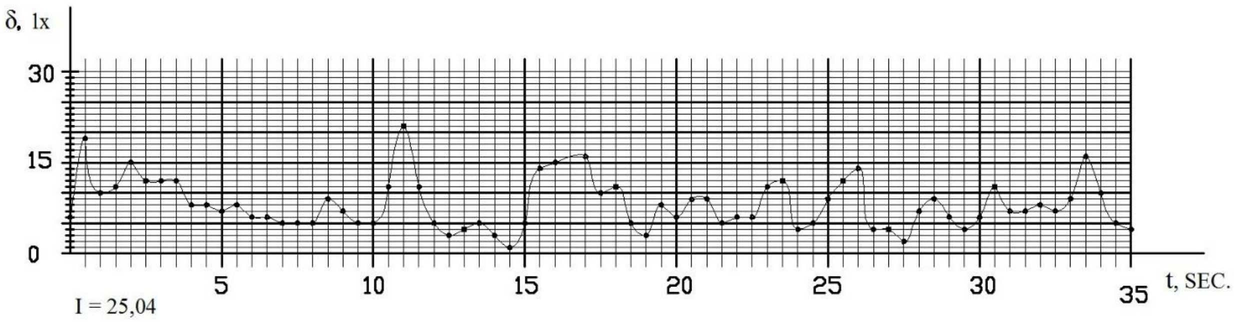

abscissa – test duration t, sec; ordinate – light flow δ, lux; I – uniformity index (I = 25.04)

Fig. 2 – Determining the fluidization uniformity index

Further we drew the corresponding horizontal that separated areas with $\delta > \bar{\delta}$ (spaces with sign «+») from areas $\delta < \bar{\delta}$ (spaces with sign «–»).

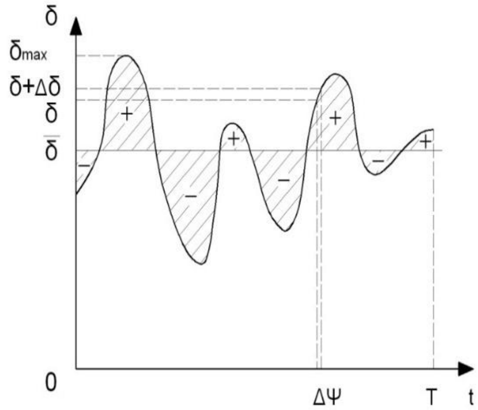

Fig. 3 – Processing of lux meter readings

Integrating separately the areas of truncated positive and negative spaces, we determine the average absolute deviation:

$$\left|\Delta\bar{\delta}\right| = \frac{1}{T}\int_0^T \left|\delta(t) - \bar{\delta}\right| dt = \frac{2}{t}\int_0^T \Delta\delta + dt = \frac{2}{t}\int_0^T \Delta\delta\_dt\,. \tag{2}$$

Drawing in the same figure the number of horizontals corresponding to neighbouring values δ and $\delta + \Delta\delta$, it is possible to add up continuances $\Delta\psi$, during which the light intensity was enclosed in this interval, and to determine this event relative probability $\Delta\omega(\delta) = \sum \Delta\psi / T$.

Uniformity index I is determined as relation of average deviation $\bar{\delta}$, to oscillation frequency ν: $I = \bar{\delta}/\nu$, where v – oscillation frequency.

Uniformity index I was interpreted as the relation of average deviation $\bar{\delta}$, to oscillation frequency ν: $I = \bar{\delta}/\nu$, where ν oscillation frequency.

According to the experiment, uniformity indexes were connected with pseudofluidization quality in the following way: high degree of uniformity corresponds to index 7, satisfactory – index from 7 to 15, low, with increasing piston flow – from 15 to 32.

RESULTS

Experimental investigations were done in order to ground the drying chamber structural parameters providing the specified variation limits of uniformity index I of wheat seeds pseudofluidized layer, which was determined according to intensity variation of light beam penetrating through the grain layer. In this regard, it was necessary to study the effect of the variation of diameter *d* and pitch *h* of drying chamber gas distribution grid holes on the uniformity index I of grain seeds pseudofluidized layer.

Hole diameter was chosen according to the following values: d = 2; 2.2; 2.4; 2.6; 2.8; 3 mm. The hole pitch was equal to h = 1; 1.5; 2 mm.

Experimental results of the study of the above-mentioned factors, effects on uniformity index of pseudofluidized material in the drying chamber are presented in the form of characteristic curves in figures 6 and 7. The obtained uniformity index dependences of the fluidized material on holes diameter of gas distribution grid (figure 4) at different pitch of the given holes have linear character.

Sharp decrease of uniformity index I with grid hole diameter increase takes place to the specified value and then its continuous increase occurs. Minimum value of index I corresponds to the grid diameter values arranged in the interval from 2.4 to 2.6 mm.

On the ground of the obtained results it is necessary, in further investigations and also in practical usage, to apply grids with hole diameter from 2 to 3 mm. Further increase of grid hole diameter is unreasonable because of spillage of part of the grain material through them.

Characteristic curves (figure 5) of uniformity index I from grid hole pitch *h* indicates that with increase *h* uniformity index decreases and reaches the minimum value at h = 1.5 mm.

The sequential increase of holes pitches results in gradual increase of uniformity index at any specified values of grid diameter.

We consider that further holes pitches increase in gas distribution grid is impossible because of reduction of grid open space and as a result of considerable increase of its hydraulic resistance. The type of the dependence obtained in the course of investigations with sufficient high accuracy corresponds to the theoretical one.

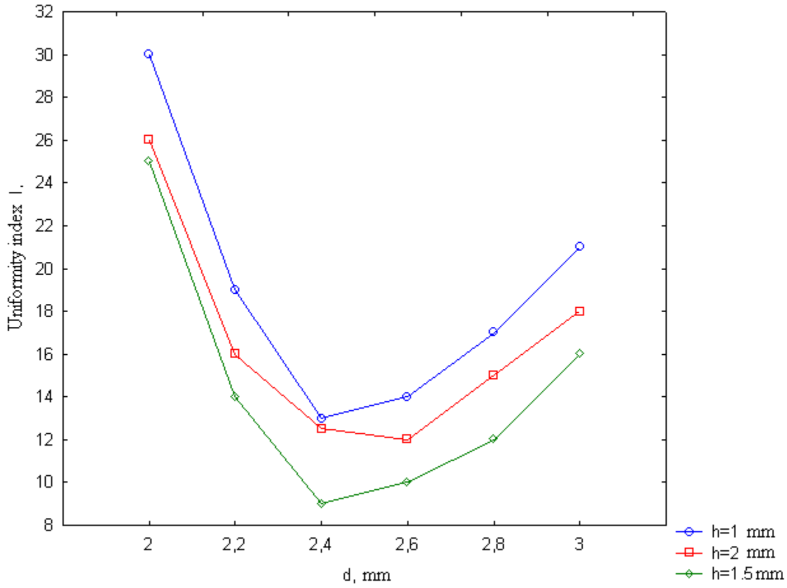

Fig. 4 – Dependence of uniformity index I on hole diameter *d* of gas distribution grid at different values of holes pitch *h*

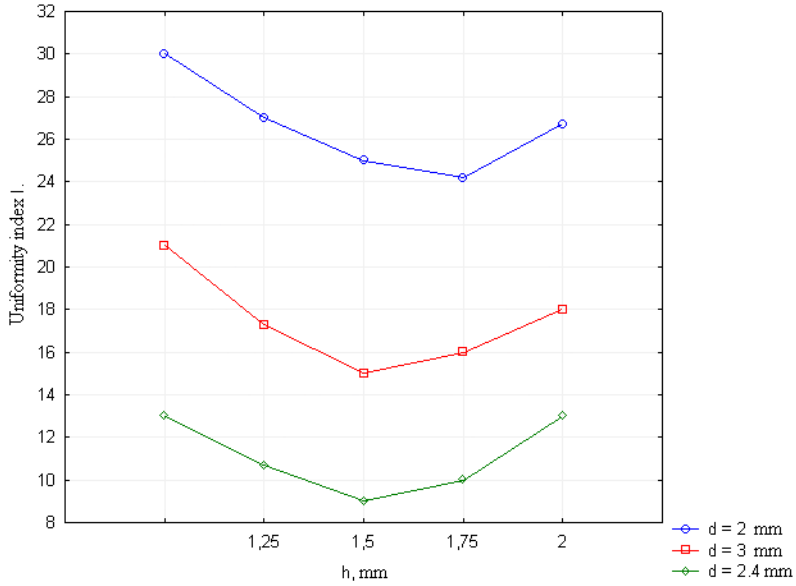

Fig. 5 – Dependence of uniformity index I on hole pitch *h* gas distribution grid at different values of hole diameter *d*

Pseudofluidization characteristic also depends on the relation of grain layer height L to diameter D. Minimum relation q = L/D was admitted equal to 1, further decrease of this value is unreasonable due to economic reasons, because dryer capacity decreases significantly. Maximum value of height to grain layer diameter relation, which does not violate fluidization stability, was determined by test and was admitted L/D = 2. Characteristic curve analysis of uniformity index I from relation L/D value (figure 6) at different gas distribution grid hole diameters *d* indicates that the process of grain material fluidization at the value of relation L/D = 2 is stable.

Further increase of L/D value results in transition from fluidized state to piston flow and grain material emission from drying chamber, h.e. at L/D > 2, grain drying is impossible.

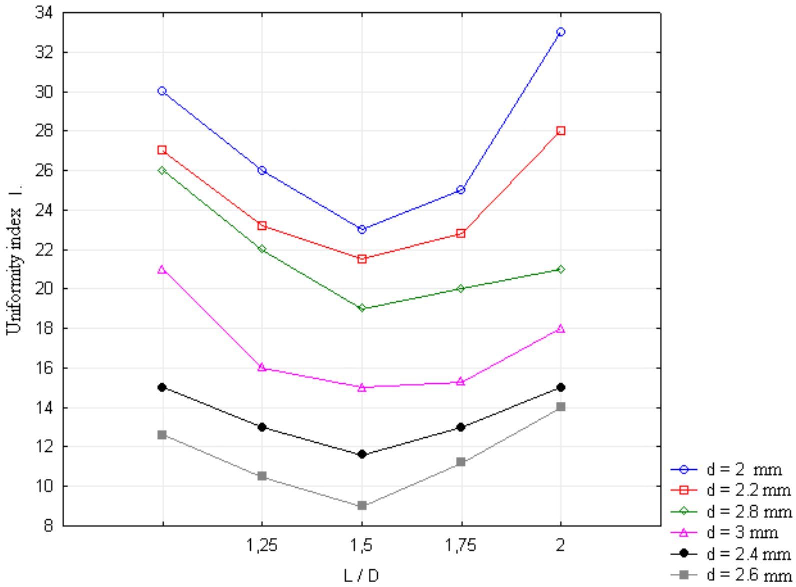

Fig. 6 – Dependence of uniformity index I on L/D relation value

The most qualitative fluidization at minimum uniformity index was observed at L/D =1.5.

Thus, while designing experimental dryer it is necessary to limit the relation range L/D from 1 to 2.

To provide the interaction and effect estimation of experimental dryer constructive and operation parameters with pseudofluidized grain layer on fluidization uniformity index, a full factorial experiment was carried out and the regression equation of the following type was obtained:

$$I = 432{,}741 - 240{,}586d - 35.178h + 57.468dq - 200.766q + 39.252d^2 + 72.912q^2 + 11.1h^2 - 21.552dq^2 \quad (3)$$

After substitution of the corresponding values of the main factors, factorial change dependence of fluidization uniformity index *I* by grain dryer is drawn diagrammatically (figure 7).

It is obviously seen from diagramming analysis of the obtained results that grain material most qualitative fluidization can be obtained at gas distributive device holes diameter d = 2.5 mm and holes pitch h = 1,5 mm. Optimal value of grain layer height-diameter ratio can be accepted as *L/D* = 1.5.

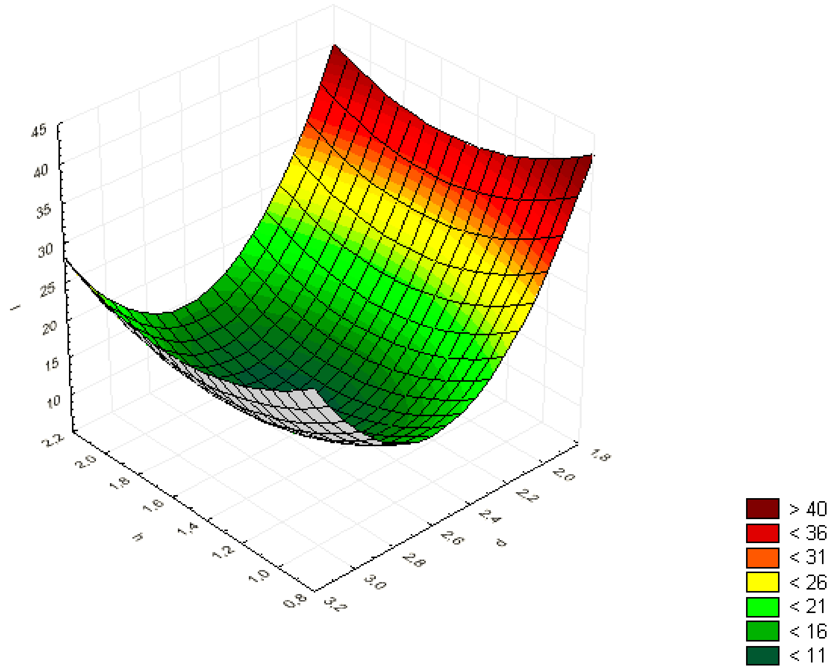

Fig. 7 – Factorial dependence of pseudofluidization uniformity index by experimental dryer

CONCLUSIONS

1. The optimal parameters of gas distribution device of dryers are determined: diameter and holes pitch of the grid, ratio of grain layer height to drying chamber diameter.

2. At the sake of the specified parameters the best distribution of air flow in pseudofluidized grain layer is performed, its uniformity is increased, the active surface values of heat exchange between separate grain and dryer agent are increased, drying enhancement and more uniform heat penetration of grain are carried out.

REFERENCES

[1] Bibik G.A., (2016), Grain drying processes optimization (Оптимизация процесса сушки зерна), *Materials of International science and practice conference «Optimization of electrotechnologies in Agro Industrial Complex»*, Yaroslavl / Russia, pp. 8-12;

[2] Kalashnikova N.V., Volzhentsev A.V., (2009), Improvement of technological process of wheat grain drying with grounding of pseudofluidized layer dryer parameters (Совершенствование технологического процесса сушки зерна пшеницы с обоснованием параметров сушилки с псевдоожиженным слоем), *Bulletin of Federal State Budgetary Educational Establishment of Higher Education Orel State Agrarian University (Вестник ФГОУ ВПО ОрелГАУ),* Issue number 1(16), pp. 44-45, Orel / Russia;

[3] Kalashnikova N.V., Volzhentsev A.V., (2009), Optimal constructional parameters of driers with pseudofluidization of grain material (Оптимальные конструктивные параметры сушилок с псевдоожижением зернового материала), *Mechanization and electrification of agriculture (Механизация и электрификация сельского хозяйства),* Issue number 3, pp. 6-7, Moscow / Russia;

[4] Kalashnikova N.V., Volzhentsev A.V., (2009), Grounding of parameters of gas distribution grids in grain driers with pseudofluidized layer (Обоснование параметров газораспределительных решет в зерносушилках с псевдоожиженным слоем), *Mechanization and electrification of agriculture (Механизация и электрификация сельского хозяйства*), Issue number 8, pp. 4-6, Moscow / Russia;

[5] Pilipyuk V.L., (2009), Grain and seeds storage technique *(Технология хранения зерна и семян)*, M.: Vuz. Study book, 457 p., Moscow / Russia;

[6] Shhitov S.V., Krivutsa Z.F., Kozlov A.V., (2016), Improvement of grain drying technology at the account of het-mass-exchange processes optimization (Совершенствование технологии сушки зерна за счет оптимизации процессов тепломассообмена), *Agroecoinfor (Агроэкоинфо),* Issue number 8, p. 24, Moscow / Russia;

[7] Tarasenko A.П., (2008), Modern machines for post-harvest treatment of grain and seeds (Современные машины для послеуборочной обработки зерна и семян), M.: KolosS, 232 p., Moscow/ Russia;

[8] Volzhentsev A.V., (2014), Determination of quality of grain fluidization in dryers (Определение качества ожижения зерна в сушилках), *Education, science and production (Образование, наука и производство)*, Issue number 4, pp. 4-7, Moscow / Russia;

[9] Volkov A.V. (2017). Ways of grain drying intensification (Пути интенсификации сушки зерна), Materials of VIII International science and practice conference «Agrarian science and education on the modern period of development: experience, problems and ways of their solutions», Yaroslavl / Russia, pp. 63-65;

[10] Zhuravlev A.P., (2014), Grain drying and grain driers: monograph *(Зерносушение и зерносушилки: монография),* Kinel: RIC Samara State Agricultural Academy, 293 p., Kinel / Russia.

DESIGN AND PERFORMANCE TEST OF THE HALF-FED AND SELF-PROPELLED GARLIC HARVESTER

/

半喂入自走式大蒜收获机的设计及性能测试

Ph.D. Eng. Lü Xiaolian*[1], Prof. Ph.D. Eng. Hu Zhichao[2], Prof. Ph.D. Eng. Lü Xiaorong[3], Prof. Eng. Peng Baoliang[2]

[1] Chuzhou University, College of Machinery and Automotive Engineering / China;
[2] Nanjing Research Institute for Agricultural Mechanization Ministry of Agriculture / China;
[3] Sichuan Agricultural University, College of Machinery & Electronics / China
Tel: 13516412415; E-mail: lxl500@163.com

Keywords: *garlic combine harvester, working principle, structural design, slign-cut device, performance testing*

ABSTRACT

Garlic harvesting is an important part during the garlic production process. Currently, the major obstacles of the garlic industry development are labour intensity, high farming time, significant losses and low efficiency. According to the characteristics of garlic cultivation in China and based on the current design experience, a half-fed and self-propelled garlic harvester, suitable for garlic producing within most areas of China, was developed. The main working parts contain the devices of stalk-dividing, stalk-lifting, stalk-clamping and conveying, clod-removing, align-cut seedling, as well as garlic collecting system, etc. To ensure the digging effect and improve working quality and stability of the machine, the combined working principle of digging and lifting has been adopted. The functions of garlic align-cut device are to align garlic and cut garlic from seedling; the handle length of cut garlic is accordance with production requirements at the same time. Through the field performance test of the garlic harvester, the operation performance is tested for stalk lifting device and align-cut device in different operating conditions. The operating performance in field is assessed through testing the machine's key performance indicators for different operating speeds. Solutions were suggested after analysing the main causes that impact its operating performance. Testing results showed: the machine has good manoeuvrability and high working efficiency; garlic loss rate≤1.8%, garlic picking broken rate≤2.1%, containing soil rate≤12.8%; all the performance indexes met the design requirements.

摘要

大蒜收获作业是其生产过程的重要部分。当前，人工劳动强度大、占用农时多、损失大、效率低等已成为影响大蒜产业发展的主要问题。针对我国大蒜种植特点，在现有研究的基础上，研制了一种适合于我国大蒜主产区收获的半喂入自走式大蒜收获机。该机主要工作部件包括：分禾装置、扶禾装置、挖掘装置、夹持输送装置、清土装置、对齐切秧装置和集果系统等。采用挖拔组合式工作原理，保证了大蒜收获中挖掘效果，提高了整机的作业质量和稳定性；设计的对齐切秧装置实现了对齐及果秧分离，同时蒜果的留柄长度满足生产要求。通过该机田间作业性能试验，测试了不同作业条件下扶禾装置及对齐切秧装置的作业效果。通过对不同作业速度下该机的主要性能指标的检测，考核该机的田间作业性能，分析影响其作业性能的主要原因及解决办法。试验结果可知：该机工作灵活、作业效率高，作业中果实损失率不大于 1.8%，破损率不大于 2.1%，含土率不大于 12.8%，各项性能指标均满足设计要求。

INTRODUCTION

Garlic is the cultivation crop of labour intensity, harvesting operations being an important part during its production process. Currently, the major obstacles of the garlic industry development are labour intensity, high farming time, significant losses and low efficiency. The mature production technology and equipment abroad are difficult to adapt to the actual needs in China *(Hu Z.C. and Wang H.O., 2007; Zhang H.J. and Hu Z.C., 2010).* Some garlic planting machine and garlic harvester have been developed by some research institutes and enterprises in our country, such as: the 2ZDS-5type and 2ZDC-5 type self-propelled garlic planter, the 4S-60 type garlic harvesting machine, the 4DS-1000 type garlic excavator *(Lü X.L. and Hu Z.C., 2015; Badoiu D., Petrescu M. and Toma G., 2014; Guan M., Chen Z.Y. and Gao L.X., 2015; Hu Z.C. and Wu*

F., 2007; Hu Z.C., Wang H.O. and Wang J.N., 2010; Jiang J.C., 2007). At present, garlic harvesting mainly relies on artificial work in China, the garlic mining plow is used in some areas. Garlic harvesting machine is used in few areas, such as Shandong, Henan provinces etc., but the garlic harvester needs to be developed. Overall, the garlic mechanized harvesting technology and equipment in our country is still in the initial stages, most part of the equipment is still in prototype testing stage. They need to be improved in the quality, adaptability, reliability and economic performance. Therefore, the research and development of the garlic harvesting equipment have important significance to accelerate garlic mechanized production in China.

MATERIAL AND METHODS

Overall structure and working principle

The half-fed and self-propelled garlic harvester has been developed by Nanjing Research Institute for Agricultural Mechanization Ministry of Agriculture. At present, the production and testing of the prototype have been completed. The main working parts of the garlic harvester contained the stalk-dividing device, stalk-lifting device, digging shovel, clod-removing device, clamping and conveying chain, align-cut seedling device, cleaning device, garlic collecting system, etc.(Fig.1).

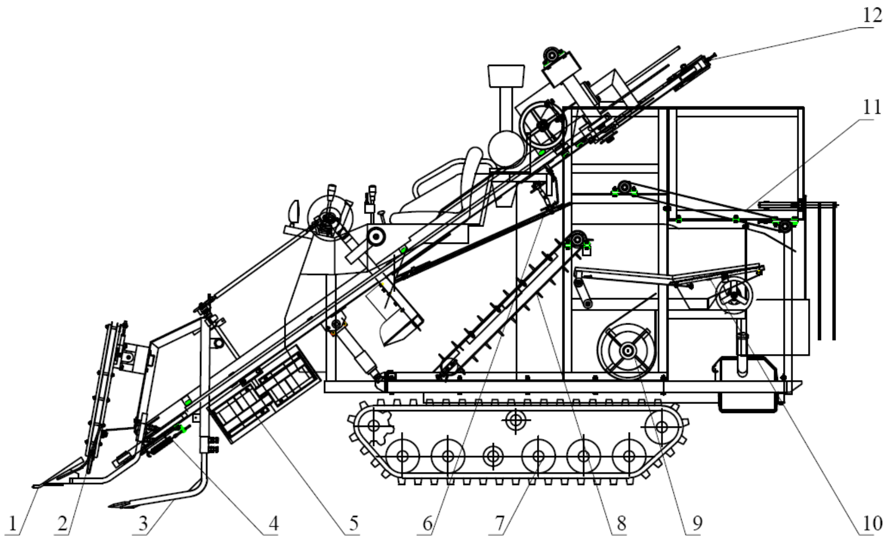

Fig. 1 - Structural scheme of the garlic harvester

1 - Stalk dividing device; 2 - Stalk lifting device; 3 - Digging shovel; 4 - Clamping and conveying chain; 5 - Removing clod device; 6 - Align-cut device; 7 - Chassis; 8 - Conveying belt ; 9 - Fan; 10 - Cleaning sieve; 11 - Seedling conveying belt; 12 - Seeding throwing chain

The harvester can complete the garlic lifting and digging, garlic seedling clamping and conveying, garlic and soil separating, garlic seedlings cutting, garlic cleaning, automatically collecting garlic, etc. *(D. R. LIU, X. J. WANG and Y.S. WANG, 2010; B. F. Li, 2008)*. When the harvester is working, garlic seedlings are separated from both sides seeding and lifted by the stalk lifting device; the digging shovel takes off the garlic roots. The garlic seeding is clamped and backward conveyed by the clamping and conveying chain. The removing clod device eliminates the soil on the garlic root. The garlic seeding is conveyed into the align-cut device with the clamping and conveying chain, and the stem according to the requirements of garlic stem length is cut off with the disc cutter. The garlic drops onto the conveying belt, and conveyed to the cleaning sieve to remove clod, fall into the collecting box at the rear of the cleaning sieve. The seedling continues to be backward conveyed, and discharged from the harvester rear.

Chassis

The chassis mainly consists of engine, speed transmission system, working system and console. The engine is of 490 Diesel type, with 33 kW set power and 2700 r/min output speed. Variable speed system includes the gearbox and hydraulic CVT. The CVT is used to adjust the speed or rotation direction of the gears. The working system is of rubber tracks style. The track centre distance is 950 mm, the track length on the ground is 1230 mm, the width is 400 mm, pitch is 90 mm and the section number is 45. Two transmission lines are designed according to the requirements of the driving system of the machine. In order to efficiently solve the power shortage, the belt tensioning wheel clutch is used. Removing clod device, conveying belt, fan, cleaning sieve, seeding throwing chain and seedling conveying belt use a transmission line of driving system. The output power is directly supported by the engine and its speed is directly controlled by the engine. The clamping and conveying system, align-cut device and stalk lifting device use another transmission line of driving system. The power is outputted from the gearbox, and the speed varies with the working speed of the harvester.

Stalk dividing and stalk lifting device

The stalk-dividing and stalk-lifting devices separate plants on each row or furrow, upwardly lifts stalk, and feed seeding into the clamping and conveying chain (Fig.2).

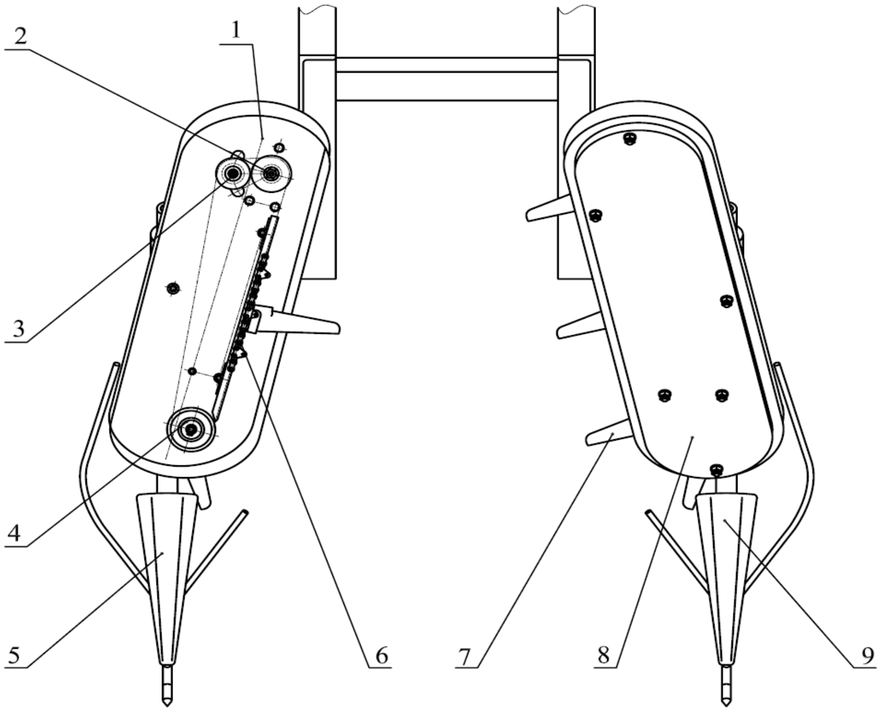

Fig. 2 - Structural scheme of the stalk dividing and lifting device

1 - Left finger chain box; 2 - Drive sprocket; 3 - Tension wheel; 4 - Pulley; 5 - Left stalk dividing device; 6 - Transmission chain; 7 - Finger; 8 - Right finger chain box; 9 - Right stalk dividing device

The stalk-dividing device is a fixed-guide structure, mounted on the front of dig-pull conveying device. The points and angle into the soil of the Digging shovel can be adjusted according to the different working conditions. The left and right finger chain boxes of the stalk lifting device have a symmetric configuration, and contain a drive sprocket, tensioned wheel, pulley, drive chain. The centre distance can be adjusted according to the garlic planting mode between the symmetrical pulley and drive chain of the stalk lifting device. The finger has two speed gears, and the gears can be chosen for the required speed of the harvester.

Dig-pull conveying device

Dig-pull conveying device is composed of the digging shovels, clamping and conveying device (Fig.3). During working, dug shovel touches the garlic fibrous roots, loosens soil and lifts up the garlic. In order to meet enough dug depth and reduce forward resistance, the digging shovel is designed with rectangular shape and inclined plane. The shovel handle is fixed onto the tube holder of the rack on both sides. The digging point and dug depth can be adjusted according to the production requirement. The main design parameters are: the entry soil angle is 30°, the between spaces of the shovels is 0~45 cm, the digging width is 40~95 cm, the digging depth is 0~12 cm. The entrance of the clamping and conveying chain is in the V shape, the garlic seedling is clamped at about 20° to vertical direction and backward conveyed. In order to adjust the extracting height of the garlic seedling, the hydraulic lifting and the depth-limiting mechanic structure are designed. The opening size at entrance can be adjusted with the adjusting wheel, and the tension force of the clamping and conveying chain can be adjusted with the tension spring.

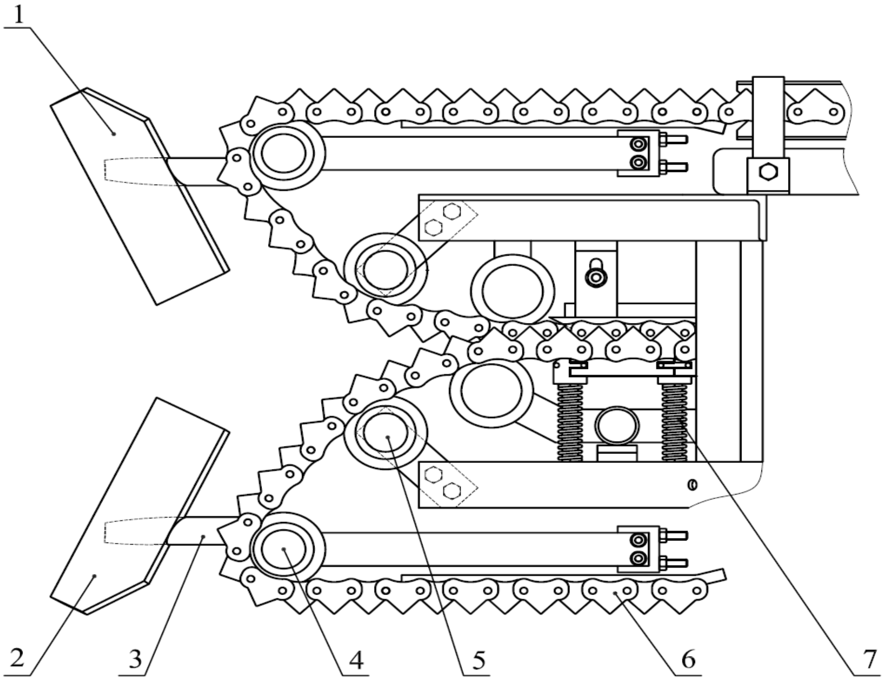

Fig. 3 - Structural scheme of the dig-pull device

1 - Left digging shovel; 2 - Right digging shovel; 3 - Shovel handle; 4 - Adjustment wheel I; 5 - Adjustment wheel II; 6 - Clamping and conveying chain; 7 - Tensioned spring

Align-cut seedling device

The device mainly composed of the left and right guide rod, upper clamping chain, alignment chain, arranged disk of garlic, hook, disk cutter, etc. (Fig.4). The garlic seeding is clamped with upper clamping chain and backward conveyed, and orderly arranged at the entrance on the guide bar. Each hook grabs a garlic seedling through combined action of arranged disk. The garlic is conveyed backward through combined action of the upper clamping chain and alignment chain, aligned and cut by the disc cutter. The garlic seedling continues to be backward conveyed by the clamping chain. The garlic remain handle length is determined by the position of the disc cutter.

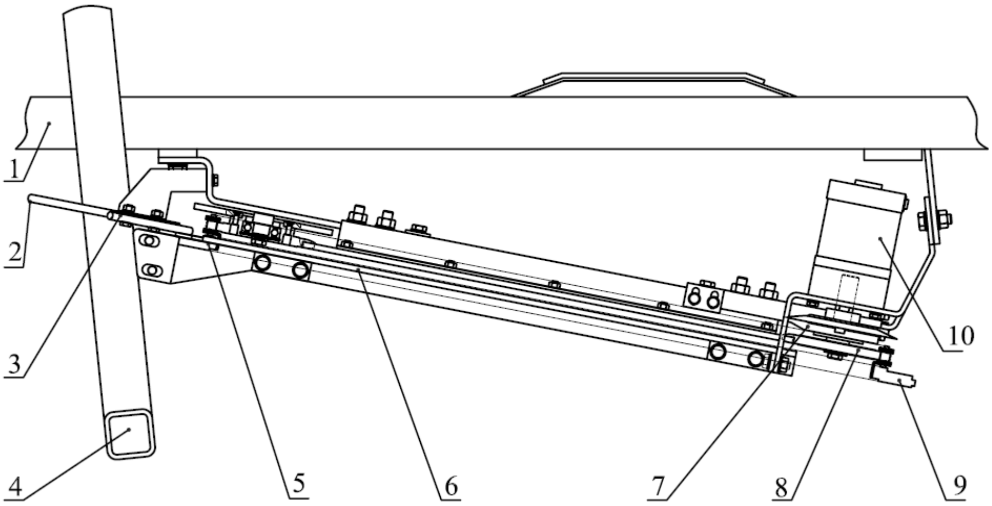

Fig. 4 - Structural scheme of the align-cut device

1 - The upper clamping chain; 2 - Left guide rod; 3 - Right guide rod; 4 – Rack; 5 –arranged disk of Garlic; 6. Align chain; 7 - Disc cutter; 8 – Sprocket; 9 - Hook; 10 - Motor

Performance test

Test content: (1) the performance test of the working parts. The operating performance of the stalk lifting device and align-cut device in different conditions are tested respectively. (2) the operations quality test of the whole machine. This test is destined mainly to assess the operation effect of the garlic combined harvester and provides the basis for further optimized and improved machine design.

Test conditions: the test is carried out at Pizhou City, Jiangsu province; it is in sand soil; the garlic planting pattern is wide and narrow planter suitable for mechanized operations, the narrow row space is 20 cm, the wide row space is 40 cm; the growth characteristic parameters of the garlic, soil compaction and moisture content are measured; the results are shown in Table 1.

Table 1

Garlic growing characteristics and soil conditions

Parameter	Measurement results
Height of garlic seeding, [cm]	34
The flower stalks diameter, [cm]	1.6
Bulb diameter, [cm]	6.5
Bulb height, [cm]	4.7
Garlic depth, [cm]	0-10
Plant spacing, [cm]	19.6
Row spacing, [cm]	13.3
10-15 cm soil moisture [%]	48.64
10-15 cm soil compaction, [kN/cm^2]	0.085

The indexes of the operations quality of the whole machine are as follows: injury garlic rate, loss rate, containing soil rate and the productivity. During the test process, the speed of the harvester is set at 0.36 m/s or 0.54 m/s, the digging depth is 120~130 mm. The test zero is 30 m long, and three testing cells are randomly chosen from the test zero.

The length of each test cell is 5 m. In the test cell, the garlic dug up manually in field (as buried garlic), the garlic dug up by the harvester but not clamped (as loss garlic), garlic harvesting by the harvester in the testing cell (as harvested garlic) and all the trauma of the garlic (as damaged garlic), were weighed. Harvested garlic weight is w_1, garlic loss weight is w_2, buried garlic weight is w_3, damaged garlic weight is w_4, the soil weight of harvested garlic is w_5, test indicators are shown as follows *(Liu J.J., 2008; Li S. X., 2015; Li Z.X., 2010; LU Z.M., 2011)*:

Loss rate：

$$r_1 = \frac{w_2 + w_3}{w_1 + w_2 + w_3} \times 100\% \tag{1}$$

Damaged garlic rate:

$$r_2 = \frac{w_4}{w_1 + w_2 + w_3} \times 100\% \tag{2}$$

Containing soil garlic rate:

$$r_3 = \frac{w_5}{w_1 + w_5} \times 100\% \tag{3}$$

Productivity:

$$P = \frac{LH/10000}{T/3600} = \frac{0.36LH}{T} \quad [\text{hm}^2/\text{h}] \tag{4}$$

In the formula:

P- Productivity [hm^2/h]; *T*- The time used by the prototype to pass through the testing zero, [s];

L- The length of the testing zero, [m]; *H*- Operating width, [m].

RESULTS

Performance test results

The performance of the stalk lifting device is tested in the garlic upright and lodging status (Fig. 5). The testing results show that more upright the garlic is, the better the operating effect of the stalk lifting device is.

(a) Plants upright *(b) Plants lodging*

Fig. 5 - Working effect of the stalk lifting device

The working quality of the align-cut device is mainly affected by the arranged status of plants, the clamping position and the feed quantity.

The effects of remain handle length is tested in different conditions. From the harvested garlic in test zero, 20 are randomly selected to test their handle length in each condition. The handle length is measured from the garlic fake stems to the top of the garlic bulb. The handle length is set 5 cm. In the test, the align-cut device performs better with plants upright status, the statistical results of the handle length in different conditions being shown in Table 2.

Table 2

Statistics result of garlic handle length

Plant status	Gear	Maximum (cm)	Minimum (cm)	Mean (cm)	Variance
Upright	I	6.50	4.58	5.01	0.421
	II	6.50	4.60	5.06	0.447
Lodging	I	6.80	4.54	5.41	0.579
	II	7.00	4.58	5.46	0.696

Operating quality *test results*

The test results are shown in Table 3. Machinery harvest effect is shown in Fig. 6 and Fig. 7.

Table 3

Test result of the garlic combine harvester

Test parameters		Test indexes			
Speeds (m/s)	Digging depth (mm)	Loss rate (%)	Rate of injuries garlic (%)	Containing soil rate (%)	Productivity (hm^2/h)
0.36	130	≤1.8	≤2.1	≤12.8	0.078
0.54	120	≤3.1	≤3.8	≤14.5	0.116

Fig. 6 - The effect of the machine harvesting the garlic

Fig. 7 - The situation after the harvesting in field

CONCLUSIONS

The developed half-fed and self-propelled garlic combined harvester can complete a variety of functions from digging, cleaning clod, clamping and conveying, align-cutting to collecting, etc. The test results are shown:

(1) The upright status of the garlic seedlings has a more significant influence on the harvester operating effect. The better the garlic upright status is, the better stalk lifting device propped the garlic seedlings. The garlic can be orderly conveyed to the align-cut device, so that the uniformity of the garlic handle length is improved, and the harvester performance is stable and reliable. When the lodging status of the garlic is more serious, the stalk lifting device cannot propel the garlic seedlings. The garlic seedling cannot or cannot orderly be conveyed into the clamping and conveying chain, and the garlic seedling cannot be aligned or easily pulled off, so that it is difficult to ensure the accuracy and uniformity of the handle length.

(2) The operating speed of the harvester has a significant influence on the operations quality. When the speed is too high, it easily leads to garlic leaking and clogging due to the garlic holder or backward transport untimely, and easily cause obstruction at the entrance of the align-cut device. At the same time, the garlic cannot be aligned and it is difficult to guarantee the length of the handle length.

(3) The main reason for damaging garlic is that the garlic makes friction and collision with the device in the process of clod removing and garlic cleaning. The harvester can be improved in terms of working surface, clod removing and parts cleaning with adopting rubber or plastic material to enhance its cushioning effect.

ACKNOWLEDGEMENT

The study was supported by Excellent Talents Training Program by the Ministry of Education (gxfx2017125), the National Natural Science Foundation of China (51375247) and planning project of Chuzhou University (2015GH43).

REFERENCES

[1] Badoiu D., Petrescu M., Toma G., (2014), On the Analysis and Synthesis of the Quadrilateral Mechanism, *J. Balkan Tibological Association*, Vol.20, Issue 2, pp.161-169, Ed. Elsevier, London/U.K;

[2] Guan M., Chen Z.Y., GaO L.X., (2015), Multifunctional modular full-feeding peanut picking testing device, *Transactions of the Chinese Society for Agricultural Machinery*, Vol.46, Issue 11, pp.88-94, Ed. Elsevier, London/U.K;

[3] Hu Z. C., Wang H.O., (2007), Summary of mechanized cultivation and processing of garlic in America, *Journal of Anhui Agricultural Sciences,* Vol.35, Issue 13, pp. 4059-4061, Anhui/CHN;

[4] Hu Z. C., Wu F., Wang H.O., (2007), The garlic harvesting machinery status in the world, *Farm Machinery,* Issue 6, pp. 47-49, Beijing/CHN;

[5] Hu Z.C., Wang H.O., Wang J. N., (2010), Experiment on 4HLB-2 Type Half Feed Peanut Combine Harvester, *Transactions of the Chinese Society of Agricultural Machinery*, Vol.41, Issue 4, pp.79-84, Ed. Elsevier, London/U.K;

[6] Jiang J.C., (2007), Present status of the technology and development direction of garlic harvesting mechanization, *Agricultural Equipment & Technology,* Vol. 33, Issue 12, pp.18, Jiangsu/CHN;

[7] Li B.F., (2008), Agricultural machinery study, *China Agriculture Press*, Beijing/CHN;

[8] Li S.X., Shang S.Q., (2015), Researching design and experiments of spring tined type peanut mechanism, *Journal of Agricultural Mechanization Research,* Vol. 3, Issue 2, pp.136-139, Heilongjiang/CHN;

[9] Li Z.X., Du S. K., (2010), Experimental optimization design and statistical analysis, Science press, Beijing/CHN;

[10] Liu J.J., Song J.N., (2008), Analysis and discussion of garlic harvesting machine, *Journal of Agricultural Mechanization Research,* Issue 1, pp. 32-39, Heilongjiang/CHN;

[11] Liu D.R., Wang X.J., Wang Y.S., (2010), Experiment and analysis on optimizing parameters of 4S-6 type garlic harvester, *Journal of Qingdao Agricultural University (Natural Science),* Vol.27, Issue 1, pp. 81-83, Shandong/CHN;

[12] Lu Z.M., Kuai J., Rao Y., (2011), Test and analysis of segmented garlic bulb harvest machine, *Agricultural Equipment and Vehicle Engineering,* Vol.234, Issue1, pp. 28-31, Shandong/CHN;

[13] Lü X. L., Hu Z.C., Zhang Y.H., (2015), Design and performance testing of the half-feed peanut picker, *Journal of Huazhong Agricultural University,* Vol.34, Issue 3, pp. 124-129, Hubei/CHN;

[14] Zhang H. J., HU Z. C., WU F., (2010), The planting and harvesting overview of garlic mechanization in China, *Jiangsu Agricultural Sciences,* Issue 3, pp. 460-461, Jiangsu/CHN.

A PRAGMATIC METHODOLOGY TO ESTIMATE HOURLY ENERGY DEMAND PROFILE OF A CASE STUDIED DAIRY FARM; PRIMARY STEP TOWARD PV APPLICATION

/

یک روش عملی برای تخمین پروفیل ساعتی برق مصرفی در یک گاوداری گاو شیری مورد مطالعه:
گام نخستین در بکار گیری برق فتوولتاییک

Ph.D. Stud. Eng.Sarnavi H.J.[1)], Assoc.Prof.Ph.D. Eng. Nikbakht A.M.[*1)], Assoc.Prof.Ph.D. Eng. Hasanpour A.[1)], Assoc.Prof.Ph.D. Eng. Shahbazi F.[2)], Assoc.Prof.Ph.D. Eng. Aste N.[3)], Assoc.Prof. Ph.D. Eng. Adhikari R.S.[3)]

[1)]Department of Mechanical Engineering of Biosystems, Urmia University / Iran,
[2)]Department of Mechanical Engineering of Biosystems, Lorestan University / Iran,
[3)]Department of Architecture, Built Environment and Construction Engineering, Politecnico di Milano University / Italy
Tel: +98 44 2770555, E-mail: a.nikbakht@urmia.ac.ir

***Keywords:** energy, dairy farm, demand profile, herd size, lactating capacity*

ABSTRACT

On-farm detailed electric load profile is becoming increasingly important in the context of renewable energy source implementation in livestock housing due to rising energy costs along with concerns over greenhouse gas emissions. This study aimed to propose and investigate a pragmatic methodology to determine detailed energy demand profile in dairy farm sizes of 20 to 100 cows as the most common size in Iran. A model was developed based on the case studied dairy farm conditions, including artificial lighting, milking, milk cooling and water pumping subsections. This research prepares the first step toward employing photovoltaic electricity in dairy farms and thereby encouraging sustainable dairy farming.

چکیده

با توجه به افزایش قیمت انرژی و نگرانی های ناشی از گازهای گلخانه ای ودر ارتباط با بکار گیری منابع انرژی های تجدیدپذیر در تامین نیاز گاوداری ها، بررسی مفصل پروفیل بار الکتریکی مصرفی از اهمیت روزافزونی برخوردار شده است. هدف از این تحقیق پیشنهاد و تشریح یک روش عملی و قابل اجرا برای تعیین دقیق پروفیل نیاز الکتریکی گاوداری های گاو شیری با گله هایی از 20 تا 100 گاو، که در محدوده غالب گاوداری های ایران هستند، است.بر مبنای شرایط موجود در یک مطالعه موردی انجام شده، مدلی شامل زیر بخش های روشنایی مصنوعی، شیردوشی، سرمایش شیر و پمپاژ ساخته شد. این تحقیق گام نخستین در بکارگیری برق فتوولتاییک در گاوداری های گاو شیری را فراهم می سازد که به واسطه آن کمک به توسعه پایدار گاوداری های گاو شیری می شود.

INTRODUCTION

Iran dairy farms are moving toward modern livestock systems equipped with specialized facilities and scientific management practices. Transition from traditional-scale dairy farms towards larger and more specialized dairy systems would result in a significant increase of on-farm electricity demand. Milk production in Iran dairy farms has reached 4,100 tons per year, during 1989-2015, with an eight-fold increase, along with a five-fold increase of herd size, thanks to implementing new technologies and management practices *(ISC, 2017)*. Holstein Friesian is the dominant breed of modern dairy cattle in Iran, with daily lactating capacity (LC) ranged in 20-30 kg *(Atashi et al, 2012)*. Moreover, Iran has begun to move toward deployment of decentralized small scale PV plants as a part of its renewable energy plans. Any attempts toward gaining the photovoltaic electricity or energy saving through optimization approaches need detailed understanding of demand load. The intermittent nature of solar energy highlights the importance of hourly demand profile which determines the PV system performance in lessening or entirely covering the demand load.

A considerable amount of literature has been published on electric energy audit in dairy farms all over the world *(Edens et al, 2003; Ludington and Johnson, 2003; Hörndahl, 2008; Murgia et al, 2008; Sefeedpari et al, 2014; Bartolome et al, 2015; Upton et al. 2015; Pradhanang, 2015; Hosseinzadeh et al, 2016)*. Energy Utilization Index (EUI) of kWh/cow/year and kWh/hl, which have been commonly used for benchmarking energy needs in dairy farms, are achieved in range of 142-1760 and 2.27-7.71, respectively. Reviewing the literature, it has been revealed that the results are not or are only partially comparable, due to different taken assessment boundaries, management practices, diversity of machinery, production systems, working habits and maintenance, as well as ambient conditions. As a matter of fact, generally applicable methods for calculating energy input in animal husbandry are still missing *(Kraatz 2012)*. On the other hand, most of these researches have only been led to results with time horizon of yearly or monthly resolution. These time horizons are originated from the fact that, the audit procedure of the researches is usually based on the farm electricity bill evaluation or through filling pre-designed questionnaires forms by farmers. To the authors' best knowledge, there has been relatively little literature focusing on the issues of hourly profile of on-farm electricity demands. Hörndahl measured the sub hourly profile of electricity use in four complete dairy farms in Sweden *(Hörndahl, 2008)*. Moreover, Murgia et al. analyzed a set of fourteen dairy farms ranging from 40 to 300 milking cows in Sardinia region of Italy, for one year with reference to the main operations (milking, milk cooling, lighting, ventilation, manure handling) and the equipment used *(Murgia et al, 2008)*. The first systematic study of hourly demand profile for dairy farms was reported by Upton *(Upton et al, 2014)*, however, there are a number of dairy farm hourly demand profiles which have been adopted through the use of real-time data recording *(Houston et al, 2014)* or by taking the robust assumptions*(Nacer et al, 2016)*. Nevertheless, Upton et al. developed a mechanistic model for demonstrating electricity consumption in Irish dairy farms on monthly average hours i.e. one day is a representative for a whole month, which may not be practical to implement in renewable energy plant. In this study, a new technique is suggested to extend the previous works.

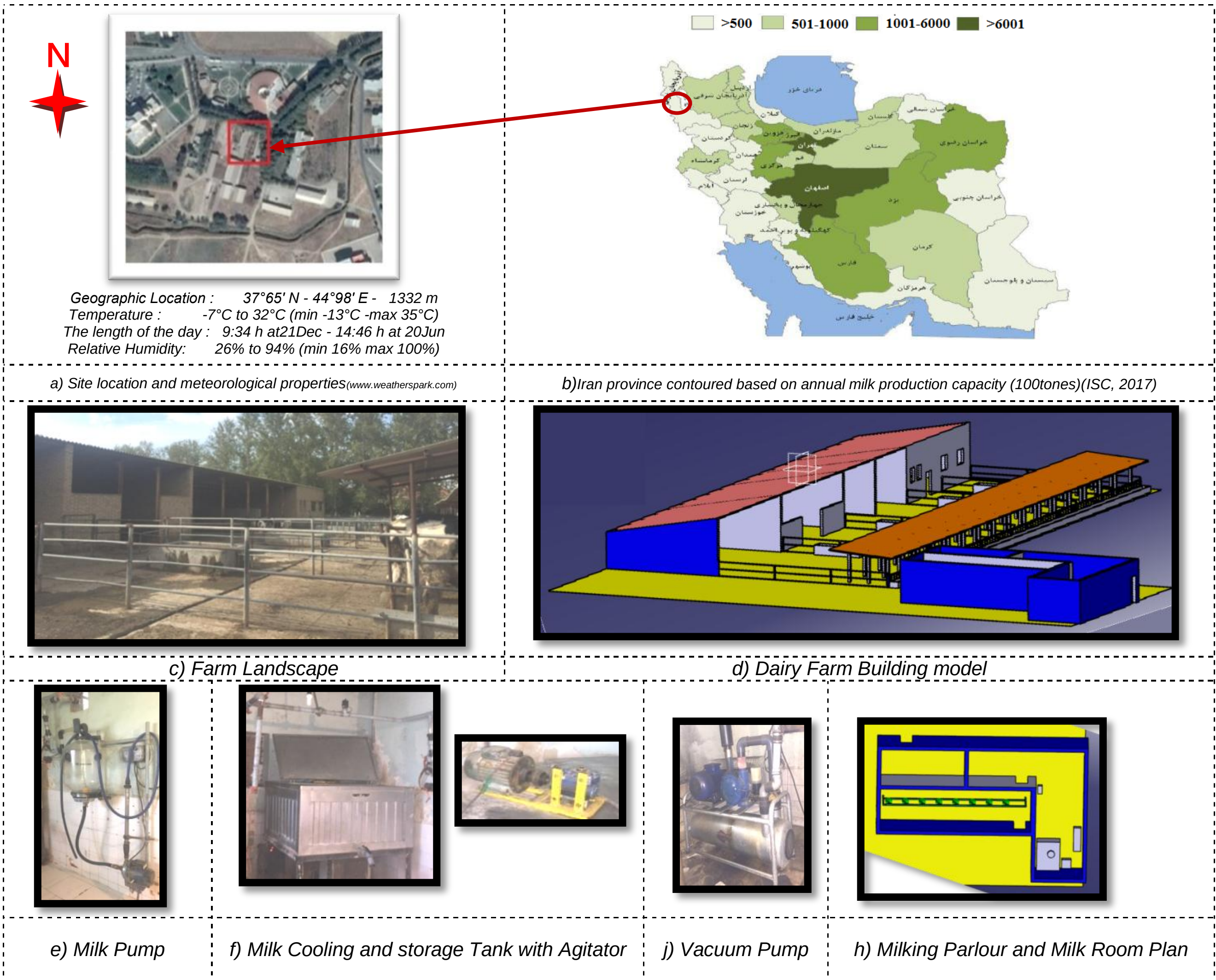

a) Site location and meteorological properties(www.weatherspark.com) | b)Iran province contoured based on annual milk production capacity (100tones)(ISC, 2017)

c) Farm Landscape | d) Dairy Farm Building model

e) Milk Pump | f) Milk Cooling and storage Tank with Agitator | j) Vacuum Pump | h) Milking Parlour and Milk Room Plan

Fig. 1 - Case Study; educational dairy farm, Urmia University

The original idea for writing this paper has been emerged as a primary step for conducting techno-economic analysis of grid-connected photovoltaic system in typical dairy farms in Iran. However, the case study of the farm, which is located on Urmia university site in north-west cold region of Iran as depicted in Fig. **1**-a,b, was applied to define the realistic framework of study. The geographical site location and meteorological properties of Urmia city were depicted in Fig. **1**-a. Indeed, the specific objective of this research is to develop a pragmatic mathematical methodology to represent energy consumption in major operational demand subsections to estimate the met electricity demand load by generated PV electricity. The presented methodology can be adopted on a range of Iran dairy farms, to feed the promise optimization approaches and to offer more detailed hourly load profile of electric energy demand.

MATERIAL AND METHODS

We started by investigating the technical specification of electrical appliances which exist in case studied farm. As most of dairy farms, the electrical appliances are comprised of artificial lighting lamps, water and milk pumps, milking system and milk cooling storage tank as shown in Fig.1. The required technical characteristics of different appliances are presented in Table 1. The selected dairy farm can keep 50 lactating cows; however, regarding its educational function, this amount is not fixed during the year. The proposed methodology to estimate energy consumption in the dairy farm is illustrated in Fig.2-bas a computational flowchart, where a time scheduling of farm activities is available (Fig.2-a). We consulted with expert opinions and considered the personal dairy staff judgments to choose the most prevalent and right activities timing. Regarding the aims and extent of this research, a computational model was developed to predict the electricity demand profile as a function of several parameters including farm location, ambient temperature, herd size and LC, as well as the technical specifications of electrical appliances presented in Table1. The calculation was performed on the basis of eight unit milking parlor as demonstrated in Fig.1-h. However, the applied methodology is independent of the number of milking units. Fig. **2**-a illustrated time scheduling of activities engaged in electricity demand profile of the dairy farm with twice milking per day within 10 hours, in the morning and evening. This time scheduling is strongly conditional on farm management plan. The model was then uploaded into the TRNSYS software. TRNSYS is an extremely flexible component-based software package used to simulate the behavior of transient systems. TRNSYS was selected based on both the time scheduling capability and the advantage of using TMY meteorological database. Additionally, a very useful feature in TRNSYS is the ability to define equations within the input file which are not in a component. According to Fig. 2-b, the calculation of each four sub sections was done by defining simple algebraic equations within input files and linking them to the TYPE109, as TMY reader, and several TYPE517, as hourly time scheduling components of different activities. Furthermore, TRNSYS provides a trustworthy simulation package to study the real-time interaction of the grid-connected PV electricity generation with farm demand load.

Table 1

Technical specification of electrical appliances demonstrated in Fig.1

Farm Activity	Electrical Appliance	Commercial Brand	Technical Specification
Milking	Vacuum Pump	CAMAK-AGM112M	4 kW - 1425 rpm
Milk Cooling	Compressor & Fan	Paykan	4.75 kW, Scroll Compressor
	Agitator	SYN MOTOR+Gearbox	0.75 kW - 1440 rpm
Pumping	Milk Pump	LOWARA-CEAM70/5/A	0.55 kW - 30~80 lit/min - 28.8~20.2 m
	Water Pump	PUMPIRAN	2 kW - 2 m^3/h - 50 m
Artificial Lighting	Fluorescent Tube Lamp		2× 32 W

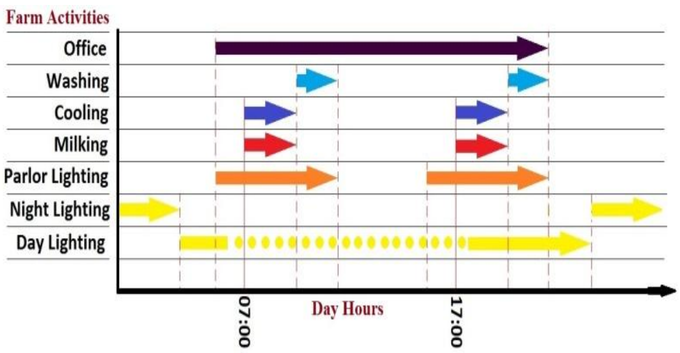

a) Farm Activities Time Scheduling

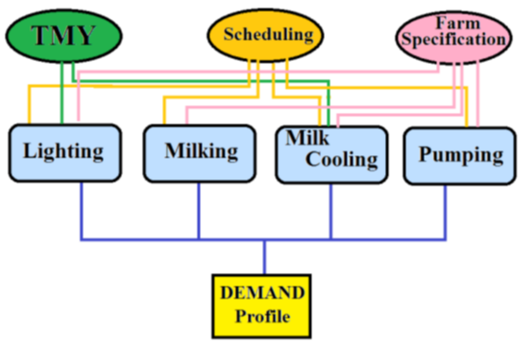

b) Computational flowchart

Fig. 2 - Activity time scheduling and computational model structure

Artificial Lighting Demand

In summary, a regime of 16 hours of light followed by 8 hours of darkness, with maximum illumination of 5 lux, is suggested for dairy farm barns to optimize cow activity, feed intake and milk production. There are also some recommendations in standards and regulations concerning the adequate illumination level and also technical specification of different lamps *(ASAE, 1996; Bickert et al., 2000; NMHC, 2006; INSO, 2013; CIGR, 2014; Rajaniemi et al., 2015; DairyNZ, 2015)* which give almost same suggestions for applying artificial lighting in different parts of dairy farms. There are different types of lighting lamp technologies. The fluorescent lamps prevail in Iran as all over the world because of their durability and affordable cost as recommended by Iranian national standardization organization *(INSO, 2013)*. Table 2 presents the detailed technical specification of the artificial lighting subsection of farm demand which would be used in TRNSYS calculation algorithms. According to the required level of illumination and considering the illumination characteristics of utilized lamps, the lighting share of electricity consumption profile can be calculated based on the time scheduling of farm activities and the number and lamp powers. Moreover, depending on the farm location and time of the year the length of daylight period varies and was taken into account in lighting consumption calculation.

Table2

Artificial Lighting characteristic details for studied dairy farm based on the recommendation by *(Bickert et al, 2000)*

Farm Areas	Recommended illumination level (lux)	Area (m^2)	Lamp Size	Illuminated Area*** (m^2)	Required Number	Wh/hour	Wh/hour PerCow
Barns day-light (feeding)	100 (day)	760	2 × 32W	16	47	3008	60.16
Barns day-light (resting)	150 (day)	366	2 × 32W	12	30	1920	38.4
Barns night-light (resting)	5 (night)	1126	2 × 32W	320	4	256	5.12
Milking Parlor	538	47	4 × 32W	8	6	768	independent of cow numbers
Milk & Utility Room	215	62	2 × 32W	8	8	512	
Staffroom	538	22	4 × 32W	8	3	384	

Milking Demand

Based on the current common technology in milking machines, the electric energy consumption referred to the electromotor which drives the vacuum pump, providing a vacuum that alternates with atmospheric pressure to draw milk from the teats, imitating the calf suckling. The oil lubricated centrifugal vane vacuum pumps without variable speed control and automatic shut-off valves are implemented here. The size of the milking machine defined with the volume rate of vacuumed air which needed to keep the drop of vacuum level lower than 2kPa *(Mein et al., 1992)*. It is assumed that a vacuum drop of 2 kPa has little or no effect on milking performance. ASAE standards suggest a constant value of 850 l/m for the milking systems with milking stalls less than 10 units *(ASAE, 1996).* This proposal would meet the current industry concern that small systems seem to be under-pumped but large systems are over-pumped. However, ISO standards proposed the base requirement 30 l/m per each milking unit plus extra amounts of 400 l/m for vacuum drop, altitude, leaks and wear *(ISO, 2007).* This extra value is recommended for the vacuum configuration without automatic shut-off valves in the cluster claw, for configuration with automatic shut-off valves it would be 200 liters per minute. For supplying the air volume rate of 640 liters per minute, based on the current Iran market brands, a machine with the nominal power about 3 or 4 kW would be needed. The vacuum pumps are used to wash the milking machine, as well. In TRNSYS calculations, electric energy consumption of the milking machine can be calculated simply by multiplying the nominal power consumption by its working time. On average, having an eight unit milking machine, each eight cows need 10-15 minutes to be milked and the washing process takes less than 30 minutes, as well.

Milk Cooling Demand

Fresh milk is normally harvested at 39°C and must be cooled down to 4°C within two hours since milking *(INSO, 2013)*, to arrest the bacterial growth and maintain the quality of harvested milk in order to meet the health and safety standards for human nourishment. Bulk milk coolers are used to chill the milk from its harvest temperature by consuming electric energy. The milk is pumped continuously to the insulated storage tank, where it can be kept, with occasional agitation, until collection. The cooled milk is collected in the insulated storage tanks which are able to keep the milk cool with 3 degrees temperature increase more than initial state, after 12 hours. The system cooling efficiency depends strongly on the cooling system coefficient of performance (COP). It was reported that, the COP value for a milk cooling system as a part of its research on energy audit process, was between the range of 1.62 to 2.43, for milk refrigeration units without any kinds of pre cooler *(Pradhanang, 2015)*. In addition, Sapali et al. declared COP of 3 for milk chilling as an energy intensive practice *(Sapali et al., 2014)*. However, the COP and the cooling capacity strongly depend on the ambient temperature and the chilled water temperature. To calculate milk cooling EUI in kWh/kg-milk, the procedure outlined in *(Upton et al, 2014)* was adopted here. Modified Carnot cycle (ideal refrigeration cycle) formula as described by *(Henze et al., 1997)*, was implemented to define COP as an ambient temperature dependent variable in Eq.1.

$$\mathrm{COP} = \left|\frac{\mathrm{T_{evp}}}{\mathrm{T_{am}} - \mathrm{T_{evp}}}\right| \times \alpha \tag{1}$$

$$\mathrm{Q_{mc}} = \frac{\mathrm{C_m} \times \Delta\mathrm{T}}{\mathrm{COP} \times 3600} \tag{2}$$

Eq.2 introduced $\mathrm{Q_{mc}}$ as EUI for milk cooling process as $\mathrm{kWh/kg}$ in hourly time horizon. The variable $\mathrm{T_{evp}}$ is the characteristic evaporator temperature of the refrigeration system, which assumed to be $268\ \mathrm{K^0}$ and $\mathrm{T_{am}}$ was the hourly ambient temperature which depends on the farm geographical location and time of the year, from TMY database implementing in TRNSYS simulations. Furthermore, the coefficient of α was considered as an adjustment factor to account for inefficiencies in real world systems according to *(Upton et al, 2014)*. Hence, the COP variation is bound to ambient temperature, evaporator temperature and insufficiency factor. The milk cooling share of total demand load would be calculated with respect to the number of milked cows in each hour and their LC.

Pumping Demand

Both milk and water must be pumped during a day in each dairy farm. Water usually used with the purpose of drinking, cows and milking machine washing and also in cleaning the farm. The amount of hot water required for washing purpose varies from farm to farm and depends on the size of the milking herd and the type and size of the milking system. The estimation of fresh water use for different farm sections is reported in literature with a wide variation *(Looper and Waldner, 2002; Kramer et al, 2008; CIGR, 2014; Schroeder, 2015; DairyNZ, 2015)*.

Table 2

Approximate required water volume for drinking, washing and cleaning in typical dairy farms
(Bickert et al, 2000)

Water Use	Water Volume	
Drinking	76-114	Liter/cow/day
Bulk Tank	113-151	Liter/wash
Milking Parlor Pipeline	283-473	Liter/wash
Miscellaneous Task	113	Liter/day
Cow preparation	7.5	Liter/washed cow
Parlor Floor	2100-8100	Liter/milking
Milk Room Floor	38-76	Liter/day
Toilet	19	Liter/flush

However, the studied farm uses the university network of water pipes; the electrical demand needed for pumping the required water amount was calculated regarding the specification of a centrifugal water pump, kept as an auxiliary setup. Therefore, energy used in this section focuses solely on pumping equipment operation. The amount of electricity consumption per each liter of pumped fluid (p) can be calculated in TRNSYS simply by applying Eq.3 regarding the corresponding schedule timing.

(3)

Where, Q is the nominal rate of pump in [m^3/h], P is the nominal power of pump in [kW] and η_{pump} is the pumping efficiency, according to Table 3.

RESULTS

We have introduced a new approach to estimate hourly electrical consumption in each subsection of artificial lighting, milking, milk cooling and pumping. As mentioned earlier, it has been adjusted in the methodology that the estimation of demand profile would be a function of herd size, LC of cows, geographical and meteorological parameters of farm location and time scheduling of farm activities. A positive correlation was found between estimated demands in subsections and the main inputs of the model, as demonstrated in Fig.3. As follows from the Fig.3-a,b,c, all subsections of current methodology are strongly depended on the farm herd size. However, for cooling subsection, there is also direct dependency of cooling demand on cow's LC, which is illustrated in Fig. 3-c as three values of LC which ranged on the regular Holstein LCs. It has been found that with increasing the herd size from 20 to 100 lactating cows, almost 2 fold of linear increase in milking and pumping shares of electric demand would be expected, as illustrated in Fig. 3-b. Furthermore, the dominant effect of meteorological factors also was depicted on the cooling and lighting demands, in Fig.3. From Fig.3-a, it can be seen that the variation of day length during the months of the year would cause significant changes in lighting electric demand of the farm. In addition, it has been perceived that deviation from flat trend with regard to herd size, in Fig.3-a, is justified by the fact that a portion of lighting is devoted to the milking parlor which is almost invariable through the year. The results thus demonstrated in Fig.3-c are compatible with the fact that the COP of cooling system is strongly influenced by the ambient temperature according to Eq.1-2, where, the smaller COP, the higher cooling electric demand would be expected.

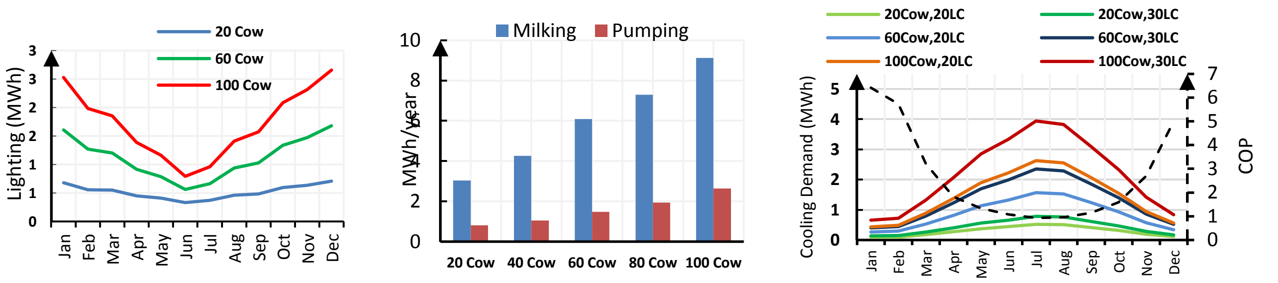

(a)Lighting demand (b) Milking and Pumping demand (c) Milk Cooling demand

Fig. 3 - The detailed and illustrated influence of different sub-sections

In Fig.4, the demand share of each subsection is plotted against herd size in varying LCs. The minimum around 5% share is devoted to pumping and maximum value to either lighting or cooling. The main point here is that cooling demand increases with expanding the herd size from 20 to 100 cows. Lighting, on the other hand, decreases by 5% as well. The cooling share overweighs the lighting share as pinpointed in Fig. 4b-c.

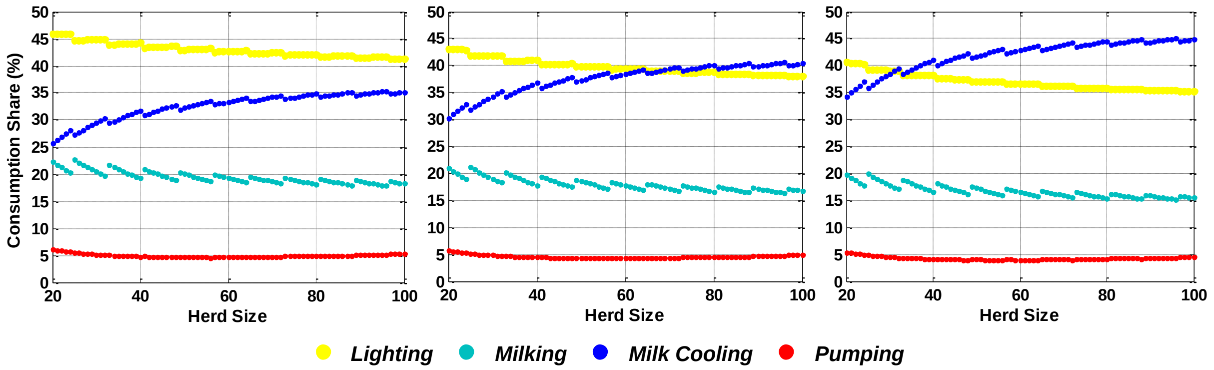

a) 20 kg/Cow/Day b) 25 kg/Cow/Day c) 30 kg/Cow/Day

Fig. 4 - Demand consumption share variation versus farm herd size for different LCs

Electric demand of Urmia university farm is detailed in Fig.5. The case studied farm consumes 29,435 kWh annually, its maximum value being in August. The profile is of critical significance in time scheduling and decision making strategies. As elucidated in Fig.5, top row, overall shape of daily electric demand is bimodal, i.e. two peaks around the milking time. The effect of day length on the demand in lighting subsection is well predicted (Fig.5); in midwinter and 4 hours before twilight 100 lux would be needed for barn lighting. In midsummer, however, only 2 hours of artificial lighting would be sufficient. In mid row of Fig.5, variation of lighting demand on daily resolution is showed. Milking parlor and pumping have constant load on the demand over the year despite considerable water consumption fluctuations.

As shown in the lowest row of Fig.5, the effect of ambient temperature on cooling demand is quite significant. Generally speaking, the dominant demand is dedicated to cooling in warm months of the year and lighting in cold months.

In the case studied project here, the lighting system consumes the most electricity, 42% of the farm total demand. This is of great importance in consumption optimization and control strategies to reduce energy demand.

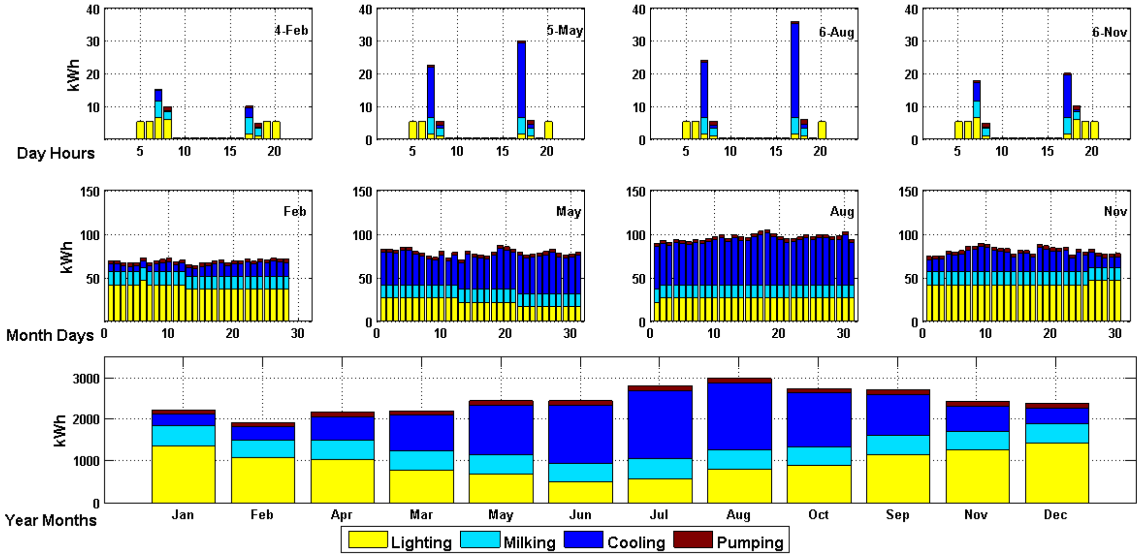

Fig. 5 - Electric demand load of case studied dairy farm
(herd size-50 cows, lactating capacity of 30 kg/Cow/Day);
Hourly, daily and monthly demand profiles for middle seasons days, middle seasons months and whole year, respectively

CONCLUSIONS

Estimating the hourly demand profile of electricity consumption in dairy farms was the main target as the primary step toward applying PV system in dairy farms. To achieve this objective, a typical dairy farm was selected as a reference to define the simulation framework. A methodology was presented as a computational program combining the models of artificial lighting demand, milking demand, milk cooling demand and pumping demand, which was developed in TRNSYS. Further investigation was conducted on farms with herd size of 20 to 100 cows as the most common size in Iran dairy farms.

It has been demonstrated that the electrical demand has the overall shape of bimodal, i.e. two peaks around the milking time in the morning and evening. Summing up the results, it can be concluded that the most part of electric energy is consumed in lighting and milk cooling sections. In small herd size and low LC, the lighting is dominant consumer and with increasing the LC the milk cooling would be the main consumer in smaller herd size. Moreover, the effect of ambient temperature and day length, respectively, on milk cooling demand and artificial lighting demand is quite significant and governs the total demand variation during a year, where the maximum demand is registered in August. The proposed method can be readily used in practice and the findings are of direct practical relevance. An important finding to emerge in this study is the detailed consumption share of each subsection which can be used in economical evaluation of equipment replacements through enhancement plans. This research was concerned with PV application; however, the results should be applicable also to energy efficiency intervention strategies.

REFERENCES

[1] Atashi H., Zamiri M.J., Sayyadnejad M.B., Akhlaghi A., (2012), Trends in the reproductive performance of Holstein dairy cows in Iran. *Tropical Animal Health and Production*, 44(8), pp.2001–2006;

[2] Bartolome D., Tabernero de Paz M.J., Posado R., Olmedo S., Garcia J.J., Bodas R., (2015), Daily electricity consumption in dairy cattle farms. *ITEA(http://dx.doi.org/10.12706/itea.2015.017.)* 111 (3): 259–71;

[3] Bickert W.G., Holmes B., Janni K., Kammel D., Stowell R., Zulovich J., (2000), Dairy free stall housing and equipment, *7th ed. Ames Iowa: MidWest Plan Service;*

[4] CIGR, (2014), Recommendations of dairy cow and replacement heifer housing (The design of dairy cow and replacement heifer housing). *Commission Internationale du Génie Rural International Commission of Agricultural and Biosystems Engineering;*

[5] Dairy NZ, (2015), Dairy cow housing-a good practice guide for dairy housing in New Zealand. *Dairy NZ Limited 2015;*

[6] Edens W.C., Pordesimo L.O., Wilhelm L.R., Burns R.T., (2003), Energy use analysis of major milking centre components at a dairy experiment station. *St. Joseph, Mich.: ASABE. doi:10.13031/2013.15659;*

[7] Henze G., Dodier R.H., Krarti M., (1997), Development of a predictive optimal controller for thermal energy storage systems. *HVAC&R Research 3 (3);*

[8] Hörndah lT., (2008), Energy use in farm buildings, *Swedish University of Agricultural Sciences Faculty of Landscape Planning, Horticulture and Agricultural Science,* Report 2008:8;

[9] Hosseinzadeh H., Safarzadeh D., Ahmadi E., (2016), Optimization of energy consumption of dairy farms using data envelopment analysis -a case study: Qazvin City of Iran, *Journal of the Saudi Society of Agricultural Sciences.* doi:10.1016/j.jssas.2016.04.006;

[10] HoustonC., Gyamfi S., Whale J., (2014), Evaluation of energy efficiency and renewable energy generation opportunities for small scale dairy farms: A case study in Prince Edward Island, Canada, *Renewable Energy 67: pp. 20–29.* doi:10.1016/j.renene.2013.11.040;

[11] INSO, (2013), Dairy cow milking parlor, *Iranian National Standardization Organization 16027;*

[12] ISC, (2017), Report of Industrial Cow Livestock section, Iran Statistics Centre,(www.amar.org.ir);

[13] ISO 3918, (2007), *Milking Machine Installations;*

[14] KraatzS., (2012), Energy intensity in livestock operations - modeling of dairy farming systems in Germany, Agricultural Systems 110. Elsevier Ltd: 90–106. doi:10.1016/j.agsy.2012.03.007;

[15] KramerE., Stamer E., Mahlkow K., Lüpping W., Krieter J., (2008), Relationship between water intake, dry matter intake and daily milk yield on a German research farm, *Livestock Science 115 (1): 99–104*;

[16] Looper M.L., Waldner D.N., (2002), Water for dairy cattle, *Oklahoma Cooperative Extension Service,* ANSI-4275. (www.osufacts.okstate.edu);

[17] Ludington D., Johnson E., (2003), Dairy farm energy audit summary. *New York State Energy Research and Development Authority*, New York,17 Columbia Circle Albany;

[18] Mein G.A., Reinemann D.J., Carrano J., (1992), ASAE, 3-A and ISO STANDARDS FOR MILKING SYSTEMS, *In Winter Meeting of the ASAE,* Nashville, Tennessee, ASAE Paper No. 923543;

[19] Murgia L., Caria M., Pazzona A, (2008), Energy use and management in dairy farms. *In Innovation Technology to Empower Safety, Health and Welfare in Agriculture and Agro-Food Systems*, Vol. 6. Sassari;

[20] Nacer T., Hamidat A., Nadjemi O., (2016), A comprehensive method to assess the feasibility of renewable energy on Algerian dairy farms, *Journal of Cleaner Production 112,* Elsevier Ltd: 3631–42. doi:10.1016/j.jclepro.2015.06.101;

[21] NMHC, (2006), Dairy lighting, *CowTime Project: National Milk Harvesting Centre,* www.cowtime.com.au;

[22] Pradhanang M.P., (2015), Modelling and benchmark development for electric energy use and energy efficiency on Nova Scotia dairy farms, *MS Thesis in Dalhousie University,* Nova Scotia*;*

[23] Rajaniemi M., Turunen M., Ahokas J., (2015), Direct energy consumption and saving possibilities in milk production, *Agronomy Research*, 13 (1): 261–68;

[24] Sapali S.N., Pise S.M., Pise A.T., Ghewade D.V., (2014), Investigations of waste heat recovery from bulk milk cooler, *Case Studies in Thermal Engineering* 4. Elsevier: 136–43;

[25] Schroeder J.W., (2015), Water needs and quality guidelines for dairy cattle, *NDSU extension service*, AS1369;

[26] Sefeedpari P., Rafiee SH., Akram A., Komleh S.H.P., (2014), Modelling output energy based on fossil fuels and electricity energy consumption on dairy farms of Iran: application of adaptive neural-fuzzy inference system technique, *Computers and Electronics in Agriculture 109,* Elsevier B.V.: 80–85. doi:10.1016/j.compag.2014.09.010;

[27] Upton J., Murphy M., Shalloo L., Koerkamp P.W.G., DeBoer I.J.M., (2015), Assessing the impact of changes in the electricity price structure on dairy farm energy costs, *Applied Energy 137*, Elsevier Ltd: 1–8. doi:10.1016/j.apenergy.2014.09.067;

[28] Upton J., Murphy M., Shalloo L., Koerkamp P.W.G., DeBoer I.J.M., (2014), A mechanistic model for electricity consumption on dairy farms: definition, validation, and demonstration, *Journal of Dairy Science*, 97 (8). Elsevier: 4973–84. doi:10.3168/jds.2014-8015;

[29] ***ASAE., (1996), Milking machine installations - construction and performance, *ASAE S518, Published by the American Society of Agricultural and Biological Engineers*, St. Joseph, MI.

RESEARCH ON THE DYNAMICS OF SAPROPEL UNLOADING FROM A CABLE INSTALLATION BUCKET
/
ДОСЛІДЖЕННЯ ДИНАМІКИ РОЗВАНТАЖЕННЯ САПРОПЕЛЮ ІЗ КОВША КАНАТНОЇ УСТАНОВКИ

Prof. Ph.D. Eng. Hevko B.M., Lect. Ph.D. Eng. Diachun A.Y., Lect. Ph.D. Eng. Dzyura V.O., Lect. Ph.D. Eng. Skyba O.P., Mel'nychuk S.L.
Ternopil Ivan Pul'uj National Technical University, Ruska Str., 56, Ternopil, Ukraine
E-mail: volodymyrdzyura@gmail.com

Keywords: *sapropel extraction, cable installation, dynamic model, buff load*

ABSTRACT
The new design of an installation for extracting sapropel is proposed. The theoretical background of sapropel extraction is developed. Based on the second order Lagrange equations and the standard program of numerical method Kunna-Tucker, the differential equation of bucket oscillation is derived. The graphic dependences of changing the angle of bucket deformation are developed as well as the linear horizontal and vertical deformation during unloading the bucket.

РЕЗЮМЕ
Запропоновано нову конструкцію установки для добування сапропелю. Теоретично обґрунтувано видобутку сапропелю на основі рівнянь Лагранжа другого роду і стандартної програми чисельного методу Кунна-Таккера, відтворені диференціальне рівняння коливань ковша. Представлені графічні залежності зміни кута деформації ковша, а також лінійної горизонтальної та вертикальної деформації при розвантаженні ковша.

INTRODUCTION
Agriculture of Ukraine plays a major role in providing people with food products and the industry with raw materials. The soil fertility, which is the foundation of agriculture, essentially contributes to obtaining high yields of crops with appropriate quality indicators.

Derno-podzolic soils dominate in Polissia of Ukraine, namely in Volyn and Rivne regions. They are characterized by low natural fertility; that is why fertilizers application, especially organic ones, is the determining factor in obtaining high yields. The use of sapropel as an organic fertilizer improves soil fertility in the mentioned regions. (*Shymchuk M.Y., 1966; Smyrnov A.V. 1973; Diduh V.F., Taraymovych I.V., and others, 2011; Tsyz' I.Y., Khomych S.M., 2009, 2013*) and others studied the issues of sapropel application for improving yields capacity. (*Tarasiuk V.V., 2012; Khomych S.M., 2014; Hlopetskyi R.A., 2014, 2016; Shymchuck O. 2014; Vanags R., 2015*) and others substantiated the production technologies of sapropel granules. (*Loveykin V.S., Nesterov A.P., 2002; Oleg Lyashuk, Zdenko Tkáč, and others, 2013; Lyubachivskij R. and others, 2013; Holubentsev A.N., 1959; Komarov M.S., 1989; Pavlovs'kyi M.A. 2002)*, and many others studied the parameters of transportation machinery used for sapropel extraction.

MATERIAL AND METHODS
Based on experimental studies, significant dynamic oscillation was found to occur during sapropel transportation. Besides, the oscillation amplitude decreases during the unloading process. Oscillations occur both in vertical and horizontal planes. Since the mechanical motion of the bucket affects the speed of its unloading and the performance of a cable installation, there is a need to study the dynamic loads on the cable installation elements and the nature of its components movement.

This movement can be calculated by solving differential equations of motion. To simplify calculations, some idealization of the system should be performed with rejection of minor factors.

The analytical model of unloading the bucket is shown in Fig. 1. This model is represented as the lumped masses connected by elastic ties. Elastic ties are considered permissible weightless and characterized by a constant stiffness coefficient.

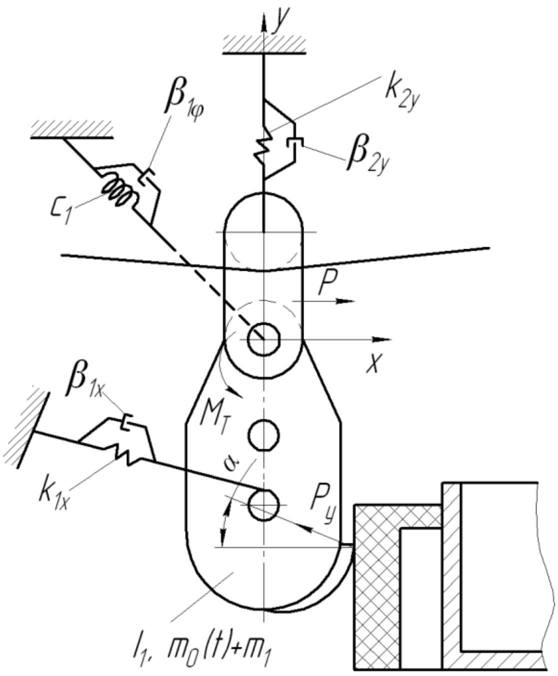

Fig. 1 - Analytical model of unloading the bucket of cable installation

Local stresses and strains in the joints of individual elements will be neglected. The lumped masses are: $m_0(t)$ - sapropel mass, m_1 - bucket mass, I_1 - moment of bucket inertia with sapropel. In addition, the figure shows stiffness coefficients: k_{1x} –given stiffness coefficient of unloading cable, k_{2y} –given stiffness coefficient of bearing cable, C_1 - given stiffness in torsion of the bucket. Besides, the damping coefficients are marked: $\beta_{1\varphi}$ – damping coefficient of torque oscillations of the bucket; β_{1x} – damping coefficient of linear oscillations of unloading cable in the direction of the axis *x*; β_{2y} – damping coefficient of linear oscillations of bearing cable in the direction of the axis *y*. The feed force of the bucket *P* and the impact force P_y are applied to a plate conveyor. The impact force P_y occurs during the unloading of sapropel. In addition, the frictional moment M_T, which prevents rotation of the bucket, is applied to it.

When unloading, the sapropel mass in the bucket is reduced. This process is defined by the dependence:

$$m_0(t) = m_p - \frac{t}{t_v} \cdot V_k \cdot \rho \tag{1}$$

where: m_p – mass of loaded sapropel;

t – time;

t_v – time of unloading sapropel from the bucket;

V_b – volume of loaded sapropel in the bucket;

ρ – sapropel density.

Similarly, the moment of bucket inertia with sapropel I_1 is changed. Having avoided negative values, the changes of sapropel mass into the dynamic model were implemented correctly with the aid of the auxiliary algebraic function:

$$m'_0(t) = \frac{m_0(t) + P_C - |m_0(t) - P_C| + \big|m_0(t) + P_C - |m_0(t) - P_C|\big|}{4} \tag{2}$$

where: P_c - auxiliary constant.

An example of the function application (2) is presented graphically in Fig. 2.

Our system has three degrees of freedom. Let us choose as generalized coordinates φ - angle of the bucket (it is considered positive in the counter-clockwise direction); x_1 – movement of the bucket mass centre in the direction of the axis *x*; y_1 - movement of the bucket mass centre in the direction of the axis *y*. Positive movement directions are shown in Fig. 1.

Differential equations of oscillations without taking into account the environmental resistance were deduced with the aid of second order Lagrange equations:

$$\frac{d}{dt}\left(\frac{\partial T}{\partial \dot{q}_j}\right)-\frac{\partial T}{\partial q_j}=-\frac{\partial \Pi}{\partial q_j}+Q_j \quad (j=1,3). \tag{3}$$

Then the kinetic energy of the system:

$$T=\frac{1}{2}I_1\dot{\varphi}^2+\frac{m_1+m_0(t)}{2}\left(\dot{x}_1^2+\dot{y}_1^2\right). \tag{4}$$

Potential energy of the system:

$$\Pi=\frac{1}{2}C_1\varphi^2+\frac{1}{2}k_{1x}\left(x_1-R\varphi\right)^2+\frac{1}{2}k_{2y}y_1^2\,, \tag{5}$$

where: R – distance from the bucket mass centre to the axis of rotation.

$$\frac{\partial T}{\partial \dot{\varphi}}=I_1\dot{\varphi};\quad \frac{d}{dt}\left(\frac{\partial T}{\partial \dot{\varphi}}\right)=I_1\ddot{\varphi};\quad \frac{\partial T}{\partial \varphi}=0;\quad -\frac{\partial \Pi}{\partial \varphi}=-C_1\varphi+k_{1x}R\left(x_1-R\varphi\right).$$

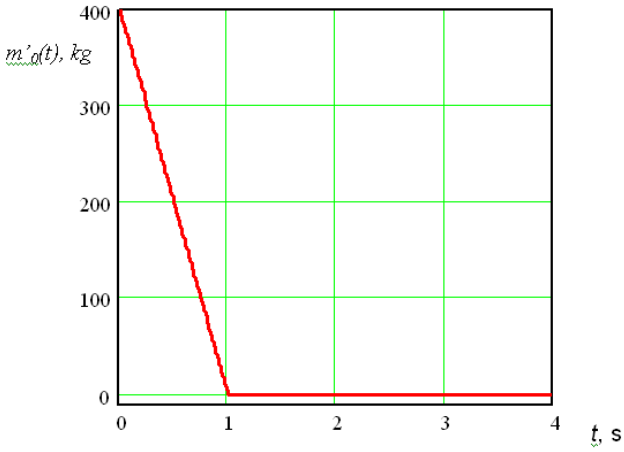

Fig. 2 - Graph of sapropel mass changes in the bucket in time

So, the first equation is

$$I_1\ddot{\varphi}+\left[C_1+R^2k_{1x}\right]\varphi-k_{1x}Rx_1=P_yR_1\cos\alpha-M_T$$

where: R_1 - distance from the point of the bucket and support interaction to the axis of bucket rotation; α - angle of the bucket and support interaction.

$$\frac{d}{dt}\;\frac{\partial T}{\partial \dot{x}_1}=\left(m_1+m_0(t)\right)\ddot{x}_1;\quad -\frac{\partial \Pi}{\partial x_1}=-k_{1x}\left(x_1-R\varphi\right);\quad Q_{x_1}=P_{x_1}\,.$$

$$\left(m_1+m_0(t)\right)\ddot{x}_1+k_{1x}\left(x_1-R\varphi\right)=P_y\cos\alpha-P$$

Similarly, the third equation is deduced. The final complete system of equations of the problem is:

$$\begin{gathered}I_1\ddot{\varphi}+\left[C_1+R^2k_{x1}\right]\varphi-k_{1x}Rx_1=P_yR_1\cos\alpha-M_T\\ \left(m_1+m_0(t)\right)\ddot{x}_1+k_{1x}\left(x_1-R\varphi\right)=P_y\cos\alpha-P\\ \left(m_1+m_0(t)\right)\ddot{y}_1+k_{2y}y_1=P_y\sin\alpha-\left(m_1+m_0(t)\right)g\end{gathered} \tag{6}$$

where: g – gravitational acceleration.

Taking into account the energy degradation, the following equations are deduced:

$$\begin{gathered}I_1\ddot{\varphi}+\left[\beta_{1\varphi}+R^2\beta_{1x}\right]\dot{\varphi}-\beta_{1x}R\dot{x}_1+\left[C_1+R^2k_{x1}\right]\varphi-k_{1x}Rx_1=P_yR_1\cos\alpha-M_T\\ \left(m_1+m_0(t)\right)\ddot{x}_1+\beta_{1x}\dot{x}_1-\beta_{1x}R\dot{\varphi}+k_{1x}\left(x_1-R\varphi\right)=P_y\cos\alpha-P\\ \left(m_1+m_0(t)\right)\ddot{y}_1+\beta_{2y}\dot{y}_1+k_{2y}y_1=P_y\sin\alpha-\left(m_1+m_0(t)\right)g\end{gathered} \tag{7}$$

While studying the impact interaction of the bucket and support, the only immediate impact force P_y is considered. This force is strong enough to create a pulse of finite size:

$$\vec{S}_1 = \int_{t_0}^{t_0+t_{K2}} \vec{P}_y dt \ , \tag{8}$$

where : t_0 - initial time, s;

t_{K2} - duration of impact, s.

During the collision of solids, the order of t_{K2} is 10^{-4}s.

As we know from theoretical mechanics:

$$\vec{S}_1 = m_1 \cdot \vec{V}_f - m_1 \cdot \vec{V}_i \ , \tag{9}$$

where : V_f - final relative velocity of the bucket, m/s;

V_i - initial relative velocity of the bucket, m/s.

RESULTS

For the case $t_0 = 0$, $V_\Pi = 0$, the final relative velocity of the bucket V_K equals the velocity of movement. As the impact is not absolutely elastic, the coefficient of renewal K_B should be considered. It defines physical and mechanical properties of materials and lies in the interval 0 K_B <1. The force of impact P_1 is assumed constant in the interval from t_0 to t_{K2} Therefore, equating equations (8) and (9), and considering the coefficient of renewal, after appropriate transformations the following formula is deduced:

$$P_1 = K_B \cdot \frac{m_1 \cdot V_K}{t_{K2}} \tag{10}$$

To implement the force of impact P_y into the dynamic model taking into account its short action, the auxiliary non-dimensional coefficient should be used:

$$F_9 = b \cdot \left(1 - \frac{t}{t_{K2}}\right) \tag{11}$$

where : b - coefficient in the order of magnitude higher than the value of impact force.

Then the force of impact can be explained by algebraic function:

$$P_y = \frac{F_9 + P_1 - |F_9 - P_1| + \left|F_9 + P_1 - |F_9 - P_1|\right|}{4} \tag{12}$$

The change of impact force in time t is shown in Fig. 3.

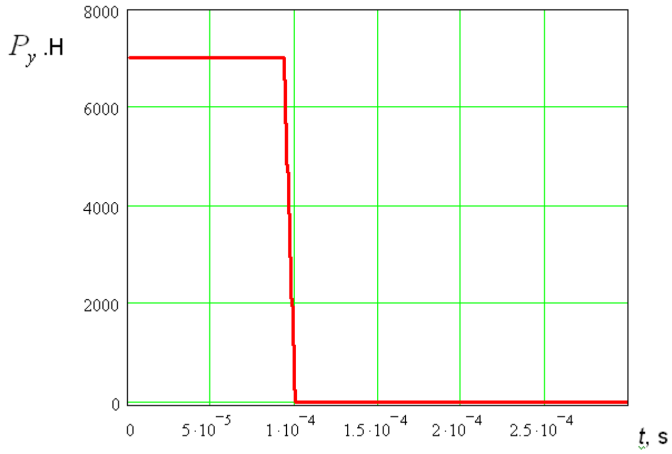

Fig. 3 - Graph of changing the force of bucket impact on the support $P_б$ in time t

The reasons to set down initial conditions for the system of equations are as follows. The time is counted from the moment of the bucket and support collision. During the movement of sapropel to that moment, the elastic elements of the system are not subjected to deformation. Therefore, the initial relative coordinates and velocities are assumed equal to zero. Further deformation occurs due to external forces. Therefore, if $t = 0$, the following formulae are deduced:

$$\varphi(0)=0\,,\ x_1(0)=0\,,\ y_1(0)=0\,,$$
$$\dot{\varphi}(0)=0\,,\ \dot{x}_1(0)=0\,,\ \dot{y}_1(0)=0\,. \tag{13}$$

The differential equations (7) with initial conditions (13) should be solved on the computer using a standard subprogram of numerical method Kunna-Tucker.

According to the research results, the graphic dependences of changing the angle of bucket deformation in time (Fig. 4) are developed, as well as the dependences of linear horizontal deformation of the bucket in time (Fig. 5) and linear vertical deformation of the bucket in time (Fig. 6) during unloading sapropel.

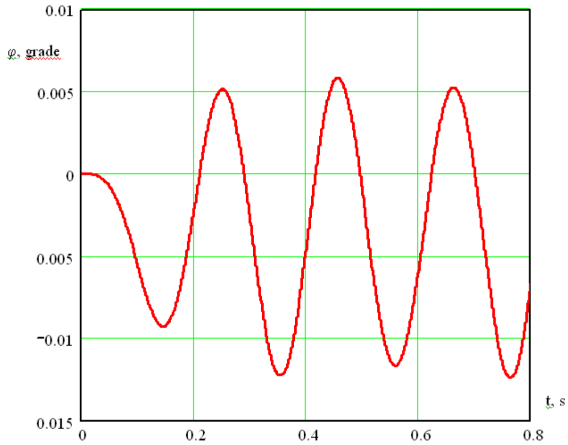

Fig. 4 - Graph of changing the angle of bucket deformation in time

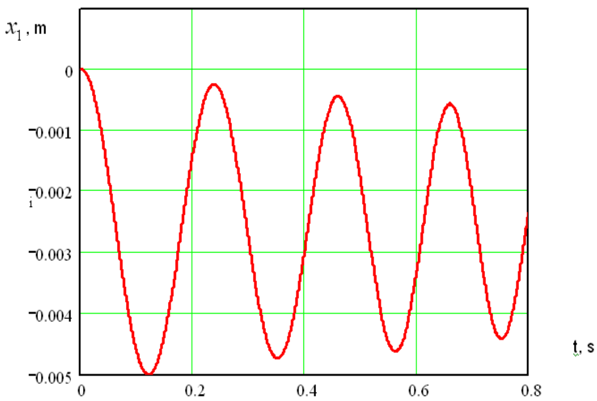

Fig. 5 - Graph of changing the linear horizontal deformation of bucket in time

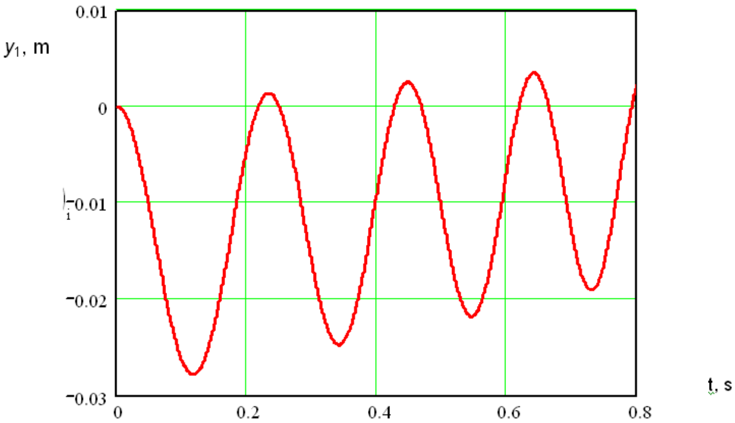

Fig. 6 - Graph of changing the linear vertical deformation of bucket in time

To test the adequacy of the proposed system of differential equations, all its components were determined experimentally. According to the presented graphic dependences, the change of vertical linear deformation of the bucket in time is greater than the change of horizontal linear deformation of the bucket in time and reaches 0.028m due to the smaller given stiffness coefficient of bearing cable as compared to the given stiffness coefficient of unloading cable.

The use of local organic raw materials will reduce the cost of the final product and will increase the amount of humus-forming plants. Sapropel from freshwater lakes as organic component should be appropriately used in the production of granular OMF (organic mineral fertilizer) in the areas of its significant resources. Sapropel is a universal substance that contains a set of elements necessary for plant nutrition. As experience shows, the use of sapropel instead of traditional organics can reduce the production cost. In addition, the development of sapropel recreational fields contributes much to the restoration of natural environment.

Thus, the impact of sapropel on soil fertility is multifaceted and complex. The effectiveness of sapropel on sandy soils is much higher than on heavy soils.

CONCLUSIONS

The new design of installation for extracting sapropel is proposed. The theoretical background of sapropel extraction is developed. Differential equations of oscillations, without taking into account the environmental resistance, were deduced with the aid of second order Lagrange equations and the standard program of numerical method Kunna-Tucker. The graphic dependences for changing the angle of bucket deformation are developed as well as the linear horizontal and vertical deformation during unloading the bucket.

REFERENCES

[1] Diduh V.F., Taraymovych I.V., and others, (2011), Research on formation of organic fertilizers granules by break-in method (Дослідження процесу формування гранул органо-мінеральних добрив методом обкачування), *Journal of Kharkiv P. Vasylenko Technical University of Agriculture. "Mechanization of agricultural production"*, Vol.1 №107, pp.387-309, Kharkiv;

[2] Holubentsev A.N., (1959), *Dynamics of transition processes in machines with multiple masses (Динамика переходных процессов в машинах со многими массами)*, MACHHIZ, p.180, Moscow;

[3] Komarov M.S., (1989), *Dynamics of machines (Динамика машин)*, Mechanical Engineering, p.342, Moscow;

[4] Khomych S.M., (2014), *Substantiation of intake device parameters for extracting sapropel (Обґрунтування параметрів забірного пристрою для добування сапропелю)*, Abstract of the PhD thesis, p. 21, Ternopil;

[5] Loveykin V.S., Nesterov A.P., (2002), *Dynamic force of lifting machines optimization (Динамическая сила оптимизация подьемных машин)*, LNU Press, p. 387, Luhansk;

[6] Lyubachivskij R., and others, (2013), Discovering of the dynamics of screw sectional conveyors (Дослідження динаміки гвинтового секційного конвеєра), *Journal of Mechanical Engineering the National Technical University of Ukraine "Kyiv Polytechnic Institute",* no 69, pp.45-50, Kyiv;

[7] Oleg Lyashuk, Zdenko Tkáč, and others, (2013), Results of experimental research of granular materials transportation by tubular scraper conveyors, *In acta technologica agriculturae*, no. 4, pp.101-105, Nitra, Slovak Republic;

[8] Pavlovs'kyi M.A. (2002), *Theoretical mechanics (Теоретична механіка)*, Tehnika, p.512, Kyiv;

[9] Shymchuk M.Y., (1966), *Sapropels of Ukraine. Stocks, quality and prospects of usage. (Сапропелі України. Запаси, якість та перспективи використання)*, Nadstyrya, p.383, Lutsk;

[10] Smirnov A.V., (1973), *Lacustral sapropels, their production and use in agriculture (Озерные сапропели, их добыча и использование в сельском хозяйстве)*, Kolos, p.170, Moscow;

[11] Tsyz' I.Y., Khomych S.M., (2009), The results of experimental studies of performance of pneumatic safety device for extracting sapropel (Результати експериментальних досліджень продуктивності пневматичного запобіжного пристрою для добування сапропелю), *Designing, manufacturing and exploitation of agricultural machinery*, №39, KNTU, pp.418-423, Kirovograd;

[12] Tarasiuk V.V., (2012), *Substantiation of technology and means of forming the granules from sapropel (Обґрунтування технології та засобу формування гранул на основі сапропелю)*, Abstract of the PhD thesis. p. 25, Ternopil;

[13] Hlopetskyi R.A., (2016), *Improvement of technology and mean for lacustrine sapropel extraction from the water layer (Удосконалення технології та засобу для добування озерних сапропелів з-під шару води)*, Abstract of the PhD thesis. p. 24, lviv;

[14] Tsyz' I.Y., Khomych S.M., (2013), Experimental research of working process of pneumatic intake device for sapropel extraction, *INMATEH – Agricultural Engineering*, vol.40, no.2, pp.67-72, Bucharest / Romania;

[15] Hlopetskyi R., Shymchuck O. (2014), Latest technologies and tools for lacustrine sapropel extraction from the water layer, *MOTROL. Commission of Motorization and energetics in agriculture*, vol.16, no.4, pp.255-257, Lublin –Rzezow / Poland;

[16] Vanags R., (2015), Research on sapropel extraction technical tools, *Engineering for rural development*, pp.151-154, Jelgava / Latvia.

STUDY OF THE PRESSURE REGULATOR WORK WITH A SPRING-DAMPER SYSTEM APPLIED TO MILKING MACHINE
/
ДОСЛІДЖЕННЯ РОБОТИ РЕГУЛЯТОРА ТИСКУ З ПРУЖИННО-ДЕМПФЕРНОЮ СИСТЕМОЮ СТОСОВНО ДО ДОЇЛЬНИХ УСТАНОВОК

Assoc. Prof., Dr.Sc.Eng. Dmytriv V.T.[*1)], Lect. Ph.D.Eng. Dmytriv I.V.[1)], Lect. Ph.D.Eng. Lavryk Y.M.[1)], Postgraduate Krasnytsia B.[1)], Assoc. prof., Dr.Sc.Eng. Bubela T.Z.[2)], Prof. Dr.Sc.Eng. Yatsuk V.O.[2)]
[1)] Lviv National Agrarian University, Faculty of Mechanic and Power Engineering, Lviv-Dubliany / Ukraine
[2)] Lviv Polytechnic National University, Department of Metrology, Standardization and Certification, Lviv / Ukraine
E-mail: Dmytriv_V@ukr.net

Keywords: *regulator, damper, attenuation coefficient, experiment, vacuum, model*

ABSTRACT
A mathematical model of a regulator for the vacuum gauge pressure with the dual mass valve-damper system was studied in the article. The differential equation was solved as well as eventual equations that simulate the valve and load moving depending on the following parameters: amplitude, oscillation of vacuum gauge pressure, load mass, valve diameter, springing of spring, damper environment description. The results of theoretical and experimental research of valve and load moving of vacuum gauge pressure regulator with the dual weight valve-damper was determined in conditions of different pressure and attenuation coefficient and also the characteristic oscillation frequency of the valve and load mass.

РЕЗЮМЕ
У роботі наведено математичну модель регулятора вакуумметричного тиску з двомасовою клапанно-демпферною системою. Розв'язано диференціальне рівняння та кінцеві рівняння, що моделюють переміщення клапана і вантажу залежно від амплітуди, частоти коливання вакуумметричного тиску, ваги вантажу, діаметра клапана, пружності пружини, характеристики демпферного середовища. Наведено результати теоретичних і експериментальних досліджень переміщення клапана і вантажу регулятора вакумметричного тиску з двомасовою клапанно-демпферною системою за різного тиску і коефіцієнта затухання, а також частоти власних коливань клапана і ваги вантажу.

INTRODUCTION
The stability of the vacuum gauge pressure is one of the basic parameters that provide quality of the cow milk ejection process. This index depends on conditions of regulator operating and must exclude the possible vibrations and resonant phenomena in the vacuum system under valve operation of the regulator and during work of the milking machines. Allowable oscillation of the vacuum gauge pressure must not be more than 2.0 kPa (*ISO 6690:2006, 2007; ASAE EP445.1, 1996*). Stability of the vacuum gauge pressure is provided by both the regulator construction and its descriptions that are formed by the construction parameters. To ensure the technological parameters it is necessary to have a mathematical tool that does possible the simulation of the modes of the vacuum regulator operation.

The stability of the vacuum gauge pressure has been estimated by the researchers group (*Pazzona A. et al, 2003*) depending on the method of pressure regulation in the vacuum hose. A group of researchers note that stabilizing the vacuum by a gravitational type regulator is more dynamic, the time constant is twice smaller of the computer-aided system (CAS). In particular, the typical regulator spends on the average 1.69 seconds on proceeding in stable pressure, while the system of the VSD-controller spends 3.75 seconds (*Pazzona A. et al, 2003*).

The vacuum gauge pressure is regulated by the rotation frequency of the vacuum pump rotor using the PID control digital systems with the amplification factors parameters of the proportion, integral and differential links accordingly: $K_p = 20$, $K_i = 0.05$, $K_D = 0.5$ at the vacuum gauge pressure of 35, 40, 45 kPa. Amplitude of vibrations does not exceed 0.3 kPa, time constant is τ = 5 s, maximal overcontrol is 2 kPa (*Radu R., Petru C., Ioan T., 2013*).

The research result of the vacuum-gauge pressure oscillations in a milking machine vacuum system did not show substantial differences between the regulators with the gravitational and digital control (*Pařilova M., Stadnik L., Ježkova A., Štolc L., 2011; Reinemann D. J., 2005*).

The vacuum-gauge pressure oscillations have been researched depending on: a) configuration of the vacuum and the milk duct systems (the length and diameter of pipelines, other parameters that influence on the pressure loss); b) milk flowrates in the milk pipelines; c) rates of air movement in vacuum pipelines (*Reinemann D.J., Schuring N., Badel R.D., 2007*).

The construction variants of milking machine vacuum regulators (*Vagin Yu T. and other, 2012*) differ in the load mass that is counted on the set vacuum gauge pressure at the appropriate area of valve seat (*Dmytriv V.T., Dmytriv I.V., 2012; Dmytriv V.T., 2015, 2016*). However, the dynamic descriptions of the valve-damper system are uncoordinated with the vacuum power oscillations and speed parameters of the air entering in the milking machine vacuum system. The milking machine caused the pressure oscillation of the milker vacuum system (*Dmytriv V.T., Dmytriv I.V., 2017*). The oscillation amplitude depends on the probability of phase coincidence and frequency of pulsators work.

Dynamic descriptions of the regulator work must provide the smoothing of pressure oscillations.

Therefore, researches on the work of vacuum gauge pressure regulators for the milking systems are up-to-date.

MATERIAL AND METHODS

Development of the mathematical model of vacuum gauge pressure regulators with the dual mass valve-damper system and research of influence of the regulator construction descriptions and technological parameters of a milking machine vacuum system on the dynamic descriptions of pressure adjusting by a regulator were the aim of this research work.

Let us consider the work of the vacuum gauge pressure regulator of spring-gravitational type with a hydraulic damper, which was showed in fig. 1.

The equilibrium of the system is provided (fig.1) when the force is created by the pressure difference that added to the valve (1) mass m_1 and the spring elastic force (2) equals the load mass m_2 (3) and the damper plate (4). Let us consider the work of the vacuum regulator as dual mass system, when the additional shaking force was applied to the valve. This force appeared as a result of increasing the vacuum-gage pressure by the size of Δp_{vp}. The scheme of forces applied to the valve as a result of the shaking forces is shown in fig. 1. Let us name this mode by the dynamic mode of regulator. During the valve 1 upwards movement on the y_1 size and the load 3 on the size of y_2, the spring will get of y_1-y_2 additional deformation.

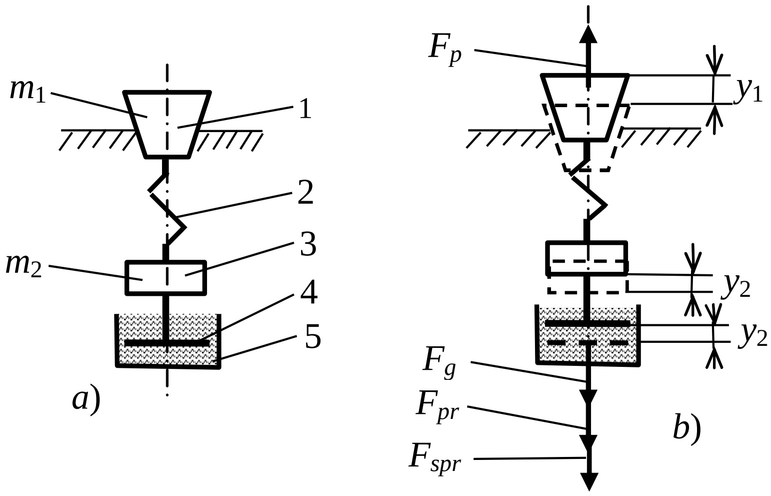

Fig. 1 - Scheme of vacuum gauge pressure regulator

a – equivalent scheme; b – functional scheme of action of forces;
1 - valve; 2 - spring; 3 - load; 4 – plate in a damper environment; 5 - damper environment;
F_p - force of the vacuum gauge pressure; F_{pr} – elasticity force; F_{spr} – the resistance force of damper environment; F_g - the force that is created by mass of regulator movable elements; m_1, m_2 – respectively the weight of the valve and the load with other elements

The system of differential equations of the motion and the load of valve should be written down:

$$\begin{cases} m_1 \cdot \ddot{y}_1 = -K_{pr} \cdot (y_1 - y_2) + \Delta p_{vp} \cdot S_{kl} \cdot f(t) \\ m_2 \cdot \ddot{y}_2 = K_{pr} \cdot (y_1 - y_2) - K_{spr} \cdot \dot{y}_2 \end{cases}, \tag{1}$$

where: K_{spr} – the integrated coefficient of resistance of the damping fluid, [N·s/m];

K_{pr} – the coefficient of elasticity of spring, [N/m];

S_{kl} – the sectional area of valve seat, [m^2];

$f(t)$ – characteristic of the applied force changes;

The notation was proposed: $K_1^2 = \dfrac{K_{pr}}{m_1}$, $K_2^2 = \dfrac{K_{pr}}{m_2}$ – square of free oscillations frequency accordingly the valve and load, [s^{-2}]; $2n_2 = \dfrac{K_{spr}}{m_2}$ – coefficient of oscillation attenuation, [s^{-1}]; $h_1 = \dfrac{\Delta p_{vp} \cdot S_{kl}}{m_1}$ – specific amplitude of the forced oscillation force, [m/s^2].

Then, the system of differential equations (1) will be:

$$\begin{cases} \dfrac{d^2 y_1}{dt^2} + K_1^2 \cdot (y_1 - y_2) = h_1 \cdot f(t) \\ \dfrac{d^2 y_2}{dt^2} + 2n_2 \cdot \dfrac{dy_2}{dt} + K_2^2 \cdot (y_2 - y_1) = 0 \end{cases} \tag{2}$$

Let the character of change of the vacuum-gage pressure Δp_{vp} meet the dependence (fig. 2) that is analytically described by the next equations:

$$f(t) = \begin{cases} 1, & n \cdot T < t < n \cdot T + \tau \\ 0, & n \cdot T + \tau < t < (n+1) \cdot T \end{cases}, \tag{3}$$

where: $n = [\tau / T]$ – aliquot of number τ / T.

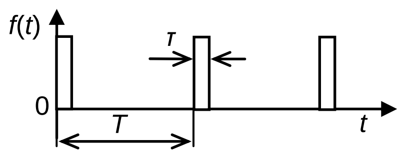

Fig. 2 - Impulse receiving character at vacuum gauge pressure changing Δp_{vp}

τ – duration of presence of vacuum-gage pressure impulse; T – impulse receiving period

After two differentiations of the second equation of the system (2), we shall get:

$$\frac{d^2 y_1}{dt^2} = \frac{1}{K_2^2} \cdot \left(\frac{d^4 y_2}{dt^4} + K_2^2 \cdot \frac{d^2 y_2}{dt^2} + 2n_2 \cdot \frac{d^3 y_2}{dt^3} \right). \tag{4}$$

Next, we will put the obtained equation (4) in the first equation of the system (2):

$$\frac{d^4 y_2}{dt^4} + 2n_2 \cdot \frac{d^3 y_2}{dt^3} + \left(K_1^2 + K_2^2\right) \cdot \frac{d^2 y_2}{dt^2} + K_1^2 \cdot 2n_2 \cdot \frac{dy_2}{dt} = K_2^2 \cdot h_1 \cdot f(t) \cdot \tag{5}$$

The characteristic equation that fits the homogeneous equation (5) looks like:

$$\lambda^4 + 2n_2 \cdot \lambda^3 + \left(K_1^2 + K_2^2\right) \cdot \lambda^2 + K_1^2 \cdot 2n_2 \cdot \lambda = 0 \tag{6}$$

The equation (6) is rewritten in the following way:

$$\lambda \cdot \left(\lambda^3 + 2n_2 \cdot \lambda^2 + \left(K_1^2 + K_2^2\right) \cdot \lambda + K_1^2 \cdot 2n_2\right) = 0 \tag{7}$$

One root of the equation (7) will be $\lambda_0 = 0$. Other roots will be obtained after solving the cube equation, with preliminary defining a discriminant:

$$D = \frac{4n_2^2}{9} - \frac{K_1^2 + K_2^2}{3} \tag{8}$$

A discriminant can take on two values, $D > 0$ and $D < 0$. To define the roots of the equation, additional determinant should be determined:

$$q = \left(\frac{2n_2}{3}\right)^3 - \frac{2n_2 \cdot \left(K_1^2 + K_2^2\right)}{6} + \frac{2n_2 \cdot K_1^2}{2} \tag{9}$$

The analysis of previous calculations shows that the difference of values of the expressions (8) and (9) is $D - q < 0$. Then for $D > 0$ it is necessary that the squares sum values of valve and load free oscillation frequency be below the oscillation attenuation coefficient, but a value of q determinant will be always higher than the D discriminant.

In this case the solution of equation (7) will be one actual and two complex roots:

$$\lambda_1 = -2 \cdot \operatorname{sgn}(q) \cdot \sqrt{|D|} \cdot ch(\alpha) - \frac{2n_2}{3}$$

$$\lambda_{2,3} = \operatorname{sgn}(q) \cdot \sqrt{|D|} \cdot ch(\alpha) - \frac{2n_2}{3} \pm j \cdot \sqrt{3} \cdot \sqrt{|D|} \cdot sh(\alpha) \tag{10}$$

where: $\alpha = \frac{1}{3} \cdot Arch\left(\frac{|q|}{|D|^{3/2}}\right) = \frac{1}{3}\ln\left(\frac{q}{\sqrt{D^3}} + \sqrt{\left(\frac{q}{\sqrt{D^3}}\right)^2 - 1}\right)$.

On condition of $D < 0$, the solution of equation (7) will be one actual and two complex roots:

$$\lambda_1 = -2 \cdot \operatorname{sgn}(q) \cdot \sqrt{|D|} \cdot sh(\alpha) - \frac{2n_2}{3}$$

$$\lambda_{2,3} = \operatorname{sgn}(q) \cdot \sqrt{|D|} \cdot sh(\alpha) - \frac{2n_2}{3} \pm j \cdot \sqrt{3} \cdot \sqrt{|D|} \cdot ch(\alpha) \tag{11}$$

where:

$$\alpha = \frac{1}{3} \cdot Arsh\left(\frac{|q|}{|D|^{3/2}}\right) = \frac{1}{3}\ln\left(\frac{q}{\sqrt{D^3}} + \sqrt{\left(\frac{q}{\sqrt{D^3}}\right)^2 + 1}\right).$$

To better understand the physical process of pressure adjusting we will point the analytical solution of the homogeneous system of equations (2) in view of $y_1 = A \cdot e^{\lambda t}, y_2 = B \cdot e^{\lambda t}$ (*Samoilenko A.M., Kryvosheja S.A., Perestiuk N.A., 1989*).

The analytical solution was put in the first equation of (2) the system. Then we get:

$$e^{\lambda t} \cdot \left(A \cdot \left(\lambda^2 + K_1^2\right) - B \cdot K_1^2\right) = 0 \tag{12}$$

Taking into account that $B=A\cdot(1+\lambda^2/K_1^2)$ from the (12) equation and the values of roots (10) and (11) the general solution of the homogeneous system of differential equations (2) is given bellow:

$$\begin{aligned} y_{10} &= A_0 + A_1 \cdot e^{\lambda_1 t} + A_2 \cdot e^{\lambda_2 t} + A_3 \cdot e^{\lambda_3 t} \\ y_{20} &= y_{10} + \frac{1}{K_1^2} \cdot \left(\lambda_1^2 \cdot A_1 \cdot e^{\lambda_1 t} + \lambda_2^2 \cdot A_2 \cdot e^{\lambda_2 t} + \lambda_3^2 \cdot A_3 \cdot e^{\lambda_3 t}\right) \end{aligned} . \tag{13}$$

The partial decision that satisfies the beginning conditions has been found for $t = 0$, $y_{10}(0) = 0$, $\dot{y}_{10}(0) = 1$, $y_{20}(0) = 0, \dot{y}_{20}(0) = 0$. On the basis of expressions (13) the system of algebra equations is formed:

$$\begin{cases} A_0 + A_1 + A_2 + A_3 = 0 \\ \lambda_1 A_1 + \lambda_2 A_2 + \lambda_3 A_3 = 1 \\ \lambda_1^2 A_1 + \lambda_2^2 A_2 + \lambda_3^2 A_3 = 0 \\ \lambda_1^3 A_1 + \lambda_2^3 A_2 + \lambda_3^3 A_3 = -K_1^2 \end{cases} . \tag{14}$$

The coefficients of equations (13) were determined from the system of the equations (14) as follows:

$$A_0 = -\frac{\Delta_1 + \Delta_2 + \Delta_3}{\Delta}; \quad A_1 = \frac{\Delta_1}{\Delta}; \quad A_2 = \frac{\Delta_2}{\Delta}; \quad A_3 = \frac{\Delta_3}{\Delta}$$

where:

$$\Delta=\lambda_1\cdot\lambda_2\cdot\lambda_3\cdot(\lambda_2-\lambda_1)\cdot(\lambda_3-\lambda_1)\cdot(\lambda_3-\lambda_2);\quad \Delta_1=\lambda_2\cdot\lambda_3\cdot(\lambda_3-\lambda_2)\cdot\left(\lambda_2\cdot\lambda_3-K_1^2\right)$$
$$\Delta_2=\lambda_1\cdot\lambda_3\cdot(\lambda_1-\lambda_3)\cdot\left(\lambda_1\cdot\lambda_3-K_1^2\right);\quad \Delta_3=\lambda_1\cdot\lambda_2\cdot(\lambda_2-\lambda_1)\cdot\left(\lambda_1\cdot\lambda_2-K_1^2\right).$$

The solution of the equation system (2) is the following:

$$y_1(t)=C_0+C_1\cdot e^{\lambda_1 t}+C_2\cdot e^{\lambda 2t}+C_3\cdot e^{\lambda_3 t}+h_1\cdot\int_0^t y_{10}(t-z)\cdot f(z)dz \tag{15}$$
$$y_2(t)=C_0+\left(1+\frac{\lambda_1^2}{K_1^2}\right)\cdot C_1\cdot e^{\lambda_1 t}+\left(1+\frac{\lambda_2^2}{K_1^2}\right)\cdot C_2\cdot e^{\lambda_2 t}+\left(1+\frac{\lambda_3^2}{K_1^2}\right)\cdot C_3\cdot e^{\lambda_3 t}+h_1\cdot\int_0^t y_{20}(t-z)\cdot f(z)dz$$

The constants of solutions (15) C_0, C_1, C_2, C_3 were determined from the initial conditions. If the $t = 0$, $y_1(0)=\dot{y}_1(0)=y_2(0)=\dot{y}_2(0)=0$, the constants C_0, C_1, C_2, C_3 are zero as well.

The integral constituents of (16) equations according to the solution are the following:

$$y_1(z)=h_1\int_0^t y_{10}(t-z)\cdot dz=h_1\cdot\left(A_0\cdot z-\frac{A_1}{\lambda_1}\cdot e^{\lambda_1(t-z)}-\frac{A_2}{\lambda_2}\cdot e^{\lambda_2(t-z)}-\frac{A_3}{\lambda_3}\cdot e^{\lambda_3(t-z)}\right) \tag{16}$$
$$y_2(z)=H_1(z)-\frac{h_1}{K_1^2}\cdot\left(A_1\cdot\lambda_1\cdot e^{\lambda_1(t-z)}+A_2\cdot\lambda_2\cdot e^{\lambda_2(t-z)}+A_3\cdot\lambda_3\cdot e^{\lambda_3(t-z)}\right)$$

Then, we will write down a (15) decision, taking into account the limitations of the system of (3) the function analytical expression and that in (16) the equations of the $z = t$ are:

$$y_1(t)=\begin{cases} y_1(t)-y_1(nT)+\sum_0^n\left(y_1(nT+\tau)-y_1(nT)\right), & nT\le t\le nT+\tau \\ \sum_0^n\left(y_1(nT+\tau)-y_1(nT)\right), & nT+\tau\le t\le(n+1)T \end{cases} \tag{17}$$

$$y_2(t)=\begin{cases} y_2(t)-y_2(nT)+\sum_0^n\left(y_2(nT+\tau)-y_2(nT)\right), & nT\le t\le nT+\tau \\ \sum_0^n\left(y_2(nT+\tau)-y_2(nT)\right), & nT+\tau\le t\le(n+1)T \end{cases} \tag{18}$$

RESULTS

We studied the regulator valve-damping systems of both the valve and load movement depending on the amplitude and frequency of the vacuum pressure oscillation. Initial data for calculating the square of characteristic oscillation frequency in accordance with the K_1^2 valve and K_2^2 load, $2n_2$ oscillation damper factor (attenuation coefficient), K_{op} resistance coefficient of the damper environment, K_{pr} spring elasticity coefficient were the following: the wire diameter of the regulator springs d_{dr} = 0.0018 [m]; the outer diameter of the spring D_{pr} = 0.021 [m]; the number of spring turns n = 10; elastic shear modulus for steel G_{pr} = 80.5 [GPa]; the diameter of the damper plate D_{pl} = 0.0874 [m]; plate shift in the damper environment x_{pl} = 0.01 [m]; dynamic viscosity of the damper environment μ_{dm} = 0.065 [Pa·s]; weight of the regulator load m_2 = 1.4 [kg]; weight of the regulator valve m_1 = 0.17 [kg].

The results of the calculation were the following: resistance coefficient of the damper environment K_{op} = 0.039 [N·s/m]; the spring elasticity coefficient K_{np} = 1134 [N/m]; specific amplitude of the forced oscillation force h_1 = 1,011 [m/s^2]; the square of characteristic oscillation frequency of the valve and the load is K_1^2 = 666.781 [s^{-2}] and K_2^2 = 80.966 [s^{-2}] respectively; oscillations attenuation coefficient $2n_2$ = 2.786 ·10^{-3} [s^{-1}]. The roots of the solution and equation coefficients: λ_1 = - 2.461·10^{-3}; λ_2 = - 1.494·10^{-4} + j·27.345; λ_3 = - 1.494·10^{-4} - j·27.345; A_0 = 43.995; A_1 = - 43.995; A_2 = - 3.564·10^{-7} - j·0.016; A_3 = - 3.564·10^{-7} + j·0.016. The numerical values of the discriminant at the given factors is D = - 249.249.

Taking into account the coefficients and roots of the $z = t$ and $t = \tau$ (fig. 2), the values of the (16) equations will be:

$$y_1(t) = 1.011 \cdot \left(43.995 \cdot t - \frac{43.995}{2.461 \cdot 10^{-3}} \cdot e^{-2.461 \cdot 10^{-3} \cdot (\tau - t)} - \frac{(-3.564 \cdot 10^{-7} - j0.016)}{(-1.494 \cdot 10^{-4} + j27.345)} \times \right.$$
$$\left. \times e^{(-1.494 \cdot 10^{-4} + j27.345) \cdot (\tau - t)} - \frac{(-3.564 \cdot 10^{-7} + j0.016)}{(-1.494 \cdot 10^{-4} - j27.345)} \cdot e^{(-1.494 \cdot 10^{-4} - j27.345) \cdot (\tau - t)} \right),$$
$$y_2(t) = y_1(t) - \frac{1.011}{666.781} \cdot \left(43.995 \cdot 2.461 \cdot 10^{-3} \cdot e^{-2.461 \cdot 10^{-3} \cdot (\tau - t)} - (3.564 \cdot 10^{-7} + j0.016) \times \right.$$
$$\times (-1.494 \cdot 10^{-4} + j27.345) \cdot e^{(-1.494 \cdot 10^{-4} + j27.345) \cdot (\tau - t)} +$$
$$\left. + (-3.564 \cdot 10^{-7} + j0.016) \cdot (-1.494 \cdot 10^{-4} - j27.345) \cdot e^{(-1.494 \cdot 10^{-4} - j27.345) \cdot (\tau - t)} \right) \quad (19)$$

Example of regulator pressure valve and load oscillation for the above-mentioned construction and technological parameters of 2.5 [kPa] pressure oscillation and its duration of 0.25 [sec] is shown in fig. 3. The maximum movement of the regulator valve for the 45-50 [kPa] of vacuum pressure and 1.0-1.4 [kg] load weight is shown in fig. 4.

Analysis of the regulator movement of the valve-damping system (fig. 3) by the p = 48 [kPa] vacuum pressure in the milking machines vacuum pipeline and the Δp_{vp} = 2.5 [kPa] permissible oscillations in vacuum pressure and the total weight of the load $m = m_1 + m_2$ = 1.57 [kg] shows that the maximum movement of the valve is y_1(0.112 [s]) = 3.093 [mm] and the total duration of the open state of the valve is t_{sum} = 0.225 [s]. Re-raising of the valve to a height y_1(0.315 [s]) = 0.5292 [mm] lasts $\sum t$ = 0.084 [s]. The τ = 0,225 [s] total duration of the pressure impulse is Δp_{vp} = 2.5 [kPa]; that exceeds the working vacuum gauge pressure of p = 48 kPa. Load has a single movement for y_2(0.08-0.13 [s]) = 0.394 [mm] height lasting t_{sum} = 0.225 [s]. Load is in a static state within the damping environment until next pressure impulse.

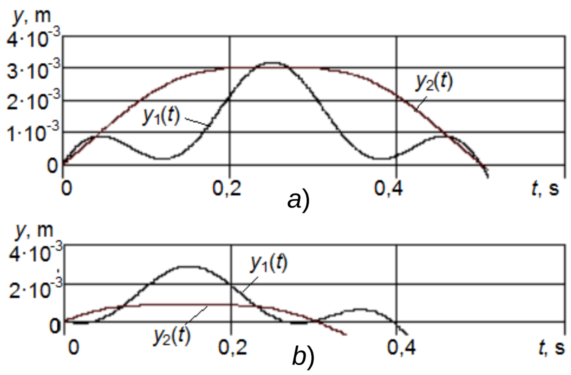

Fig. 3 - Oscillation of the regulator valve-damping system by impulse of vacuum pressure of Δp_{vp} = 2.5 kPa and τ of its duration:

a – τ = 0.25 s; *b* - τ = 0.15 s; $y_1(t)$ – valve oscillations; $y_2(t)$ – load oscillations in damping environment

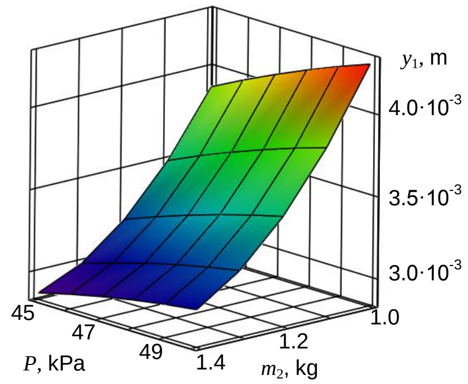

Fig. 4 - The maximum valve movement y_1 of the pressure regulator with spring-damper system depending on the p vacuum gauge pressure and the load mass m_2 for the impulse duration of τ = 0.25 [s]

For the duration of the impulse vacuum pressure of τ = 0.112 [s] the movement character of the valve and load has a single oscillation which is equal to the impulse duration. The maximum rise of the valve is y_1(0.056 [s]) = 1.329 [mm], the maximum movement of load in the damping environment is insignificant – y_2(0.056 [s]) = $3.101 \cdot 10^{-2}$ [mm].

For the load weight of m_2 = 10 [N] and impulse pressure duration of τ = 0.15 [s], the maximum valve movement is up to $y_1(t)$ = 2.783 [mm].

To confirm the results of theoretical studies the planned experiment was made considering the following factors: the K_2^2 square of characteristic oscillation frequency of the load mass and the oscillation attenuation coefficient $2n_2$. The square of characteristic oscillation frequency of the load mass was changed within K_2^2 = 80.966...174.927 [s^{-2}] according to the limits of the m_2 = 14…10.8 [N] of the weight load change. The oscillation attenuation coefficient was within $2n_2$ = $1.38 \cdot 10^{-3}$…$1.789 \cdot 10^{-3}$ [s^{-1}].

General view of the laboratory setup for the study of vacuum-gage pressure regulators is shown in fig. 5.
The graphical representation of the experimental results in a three-dimensional model view is described by the regression equation (20) (see fig.6).

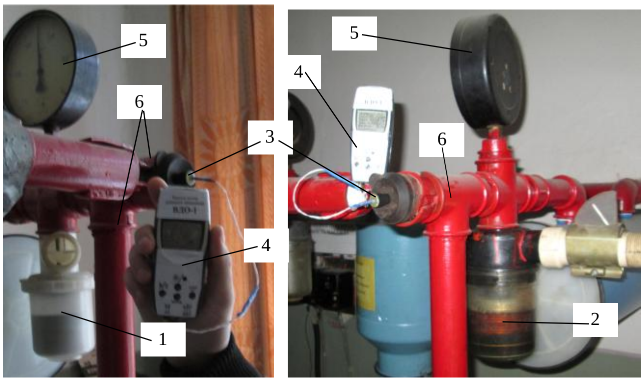

Fig. 5 - General view of the laboratory setup for the study of vacuum-gage pressure regulators
1, 2 – vacuum pressure regulators; 3 – vacuum-gage pressure sensor; 4 – vacuum analyser; 5 – vacuum gauge; 6 – vacuum pipeline

$$y_1 = 1.1147 + 0.0351 \cdot K_2^2 + 4350.5645 \cdot 2n_2 + 6.484 \cdot 10^{-5} \cdot K_2^4 - 0.293 \cdot K_2^2 \cdot 2n_2 - 8.0338 \cdot 10^5 \cdot 2n_2^2 \cdot \quad (20)$$

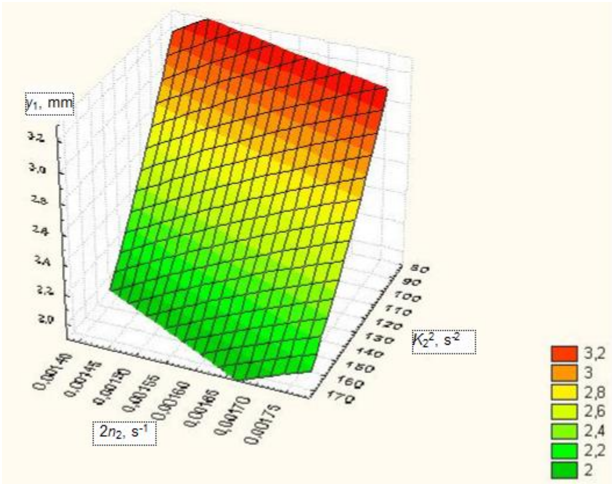

Fig. 6 – The maximum valve movement y_1 of the vacuum regulator with the spring-damper system depending on the $2n_2$ oscillation attenuation coefficient and the K_2^2 square of the natural oscillations frequency of the regulator load

For the square of characteristic oscillation frequency of K_2^2 = 104.956 [s^{-2}] valve movement amplitude is y_1 = 3.3 [mm] for the vacuum-gage pressure of p = 50 [kPa]. For the p = 45 [kPa] the oscillation parameters are K_2^2 = 131.195 [s^{-2}], y_1 = 2.8 [mm]. The reduction of the elasticity coefficient causes the lessening of the square of characteristic oscillation frequency. For the square of characteristic oscillation frequency of K_2^2 = 80.966 [s^{-2}] the amplitude of the valve movement is y_1 = 3.1 [mm] for the vacuum pressure of p = 50 [kPa]. For the p = 45 [kPa] the oscillation parameters are the following K_2^2 = 101.208 [s^{-2}], y_1 = 2.7 [mm].

CONCLUSIONS

The analysis of study results shows that the reduction of the square of characteristic oscillation frequency of the regulator load mass increases the amplitude of the regulator valve oscillation. The increase of the spring elasticity coefficient leads to increasing the square of characteristic oscillation frequency of the regulator load weight, and that increases the valve movement. Increase of the load mass causes the reducing of the valve movement and the lifting repeatability (oscillation) of the regulator valve was also increased. The lifting repeatability (oscillation) of the regulator valve was increased with the increase of the duration of vacuum-gage pressure impulse.

Increase of the load mass reduces the height of valve lifting and the air supply into the vacuum system of the milking machine. Rising the vacuum pressure up to 50 [kPa] increases the valve movement and the repeatability of its opening.

The oscillation of the regulator valve with spring-damper system of the valve is damping out. The amplitude of the single oscillation depends on the load mass and duration of the vacuum-gage pressure impulse.

REFERENCES

[1] ASAE EP445.1, (1996), Test Equipment and Its Application for Measuring Milking Machine Operating Characteristics, *Standard by the American Society of Agricultural and Biological Engineers*, St. Joseph, MI, USA;

[2] Dmytriv V.T., Dmytriv I.V., (2012), Diaphragm of the electromagnetic pulsator as time-setting element of transient processes in the milking machine (Мембрана електромагнітного пульсатора як часозадаючий елемент перехідних процесів в доїльному апараті), *Technical systems and technologies of animal husbandry,* Issue 108, pp. 183-188, Kharkiv, KNTUA;

[3] Dmytriv V.T., (2015), Modelling of work of the vacuum pressure regulator with the damper membrane (Моделювання роботи регулятора вакуумметричного тиску з демпферною мембраною), *Technical service of agriculture, forestry and transport systems*, Vol. 3, pp. 27-33, ISSN 2311-441X;

[4] Dmytriv V.T., (2016), Modelling of oscillations of the valve-damper system of the vacuum gage pressure regulator (Моделювання коливань клапанно-демпферної системи регулятора вакуумметричного тиску), *Technical service of agriculture, forestry and transport systems*, Vol. 5, pp.227-237, ISSN 2311-441X;

[5] Dmytriv V.T., (2016), Analytic study of the pressure regulator in conformity with pulsating vacuum systems, *MOTROL. Commission of Motorization and Energetics in Agriculture*, Vol.18, № 8. pp. 69-76 Lublin-Rzeszow;

[6] Dmytriv V.T., Dmytriv I. V.T., (2017), Modelling of pressure oscillations of the milking machines vacuum system (Моделювання коливання тиску вакуумної системи доїльної установки), *Mechanization of Agriculture*, Issue 180, pp. 115-123, Kharkiv/KNTUA;

[7] ISO 6690:2006, (2007), Milking Machine Installations – Mechanical Tests, *International for Standardization Organization*, 42 p. Geneva/Switzerland;

[8] Pazzona A., Murgia L., Zanini L. et all, (2003), Dry tests of vacuum stability in milking machines with conventional regulators and adjustable speed vacuum pump controllers, *ASAE Annual International Meeting, Riviera Hotel and Convention Center*, Las Vegas, Nevada, USA, [Electronic resource], Mode of access: http://www.academia.edu/14281287/Dry_Tests_of_Vacuum_Stability_in_Milking_Machines_with_Conventional_Regulators_and_Adjustable_Speed_Vacuum_Pump_Controllers, Date of call: 03.08.2015;

[9] Pařilova M., Stadnik L., Ježkova A., Štolc L., (2011), Effect of milking vacuum level and overmilking on cows' teat characteristics, *ACTA Universitatis Agriculturae et Silviculturae Mendelianae Brunensis*, LIX 23 (5), pp.193-202;

[10] Radu R., Petru C., Ioan T., (2013), Using a Computer Driven PID Regulator for Controlling the Vacuum Pump of a Mechanical Milking Machine, *Computer Technology and Application*, Vol. 4, pp. 395-399, [Electronic resource], Mode of access: http://www.davidpublishing.com/davidpublishing/upfile/11/19/2013/2013111907369927.pdf, Date of call: 03.08.2015;

[11] Reinemann D.J., (2005), The history of vacuum regulation technology, *Proceedings of the Annual Meeting of the National Mastitis Council*, pp.124-132 Orlando/USA;

[12] Samoilenko A. M., Kryvosheja S. A., Perestiuk N. A. (1989), *The differential equations: praxis and tasks (Дифференциальные уравнения: примеры и задачи)*, Higher school, 383 p., Moskva;

[13] Vagin Yu.T., Dobyshev A.S., Baranovskyi M.V., Strybuk A.A., Yarosh A.D, (2012), *Engineering assurance of milk production. Modern equipment for milking: practical textbook (Техническое обеспечение производства молока. Современное оборудование для доения: практическое пособие)*, pp.37, 50-56, ISBN: 978-985-6987-03-01 Minsk/Avoline.

KINETIC FEATURES OF VIBRATING AND FILTRATION DEWATERING OF FRESH-PEELED PUMPKIN SEEDS
/
ОСОБЛИВОСТІ КІНЕТИКИ ВІБРАЦІЙНО-ФІЛЬТРАЦІЙНОГО ЗНЕВОДНЕННЯ СВІЖЕОЧИЩЕНОГО НАСІННЯ ГАРБУЗА

Ph.D. Tsurkan O.V. [1], Eng. Gerasimov O.O.[1], Ph.D. Polyevoda Y.A.[1], Ph.D. Tverdokhlib I.V.[1], Ph.D. Rimar T.I.[2], Ph.D. Stanislavchuk O.V.[3]
[1]Vinnitsa National Agrarian University / Ukraine; [2]National University "Lviv Polytechnic" / Ukraine,
[3]Lviv State University of Life Safety / Ukraine
Tel: +380672152088; E-mail: igor_tverdokhlib@yahoo.com

Keywords: *vibration and filtration dewatering, pumpkin seeds, drying coefficient, vibration.*

ABSTRACT
Drying coefficients depending on the main process parameters of fresh-peeled pumpkin seeds (FPPS) vibration and combined dehydration and relative drying coefficient on the basis of the constructed graphic dependence are defined. Dependences for calculation of moisture and time of FPPS dewatering in the studied change range of drying process parameters are displayed.

РЕЗЮМЕ
Визначено коефіцієнти сушіння залежно від основних параметрів процесу вібраційно-фільтраційного зневоднення свіжеочищеного насіння гарбуза (СОНГ) та відносний коефіцієнт сушіння на основі побудованої графічної залежності. Виведено залежності для розрахунку вологості та часу зневоднення СОНГ в досліджуваному діапазоні зміни параметрів процесу сушіння.

INTRODUCTION
At present stage of industry development technical and economic policy of conserving resources becomes increasingly important. It requires the implementation of new scientific ideas and technologies in production intensification. Following a strict regime of economy of raw materials, fuel and energy with simultaneous intensification technologies can be up to 75...85% increase in inputs. Drying, as a process, is the main production stage and most significantly affects its economic indexes *(Rymar T., 2009)*, accounting for about 20% of total production costs *(Poperechnyj A., 2007)*.

It is known that high-intensity filtering dehydration is dispersed by drying and sheet material and has advantages over traditional methods of dehydration, such as: the availability period of the free moisture mechanical displacement; the use of thermal agent with low temperature capabilities; reducing costs of thermal energy in the process, increasing the speed of drying; improving the quality of drying materials, avoiding stage of cleaning agent heat *(Mykychak B. et al, 2012)*. Significant prospects for improving the efficiency of dehydration of fresh-peeled pumpkin seeds (FPPS), as a subject to final sowing and food (pharmaceutical) demands is a combination of filtration and dewatering vibrating action, requiring an in-depth theoretical and experimental study.

Many authors *(Hanyk Ya., 1992; Atamanjuk V., 2007; Stanislavchuk O., 2007)* have devoted their papers to the investigation of heat and mass transfer process during drying of materials of different nature, while *(Tsurkan O. et al, 2014)* researched the process vibration filtration dehydration of FPPS, a paper based on experimental data and where is obtained basic analytical dependence describing the process hydrodynamics. In the work *(Tsurkan O. et al, 2015)*, it is shown the time dependence of the critical speed and vibration-filtration dehydration, and proved dominant influence pressure drop and vertical oscillations of dehydration intensity of high damp fresh-peeled pumpkin seeds in the first drying period on the basic parameters of the process. Theoretical and experimental study of heat transfer processes during the second period of filtration, dispersed materials drying is considered in detail *(Atamanjuk V. and Gumnytskyj Ya., 2009)*. Energy and technical, technological aspects of drying process intensification of high damp seeds, including pumpkin seeds, are covered in *(Palamarchuk I. et al, 2016).*

In the article, we generalize the vibration kinetics and combined dehydration of FPPS in the second period and set dependencies for calculating humidity and FPPS dehydration time in the test range changing process parameters, in particular, the ratio of vertical and horizontal components of the vibration amplitude at a vibration frequency f = 15 Hz revs of stirrer-cleaner n from 0 to 1.2 r/min, as auxiliary operating parameters, in the vibrating dryer *(Palamarchuk I. et al, 2016)*.

MATERIAL AND METHODS

Based on own studies *(Tsurkan O. et al, 2009)* and the existing ones (*Holubkovych A., 1986*) we determined the type of relation of moisture and material and the corresponding interval limits of FPPS humidity, making it possible to justify the dehydration rational ways (table 1) and the corresponding constructive scheme of drying equipment *(Pravdjuk N. et al, 2011)*. In general, the process of combined dehydration of FPPS, of the 1st class of cleaning seeds and surface layer (according to the classification given in (*Holubkovych A., 1986*), also depending on the type of material, and moisture relation based on moisture intervals (table 1) can be divided into two conditional periods. In the first period of FPPS dehydration, humidity changes in the range 44 – 52% as typical mechanical removal of moisture through the channels between seeds (BSC) – macro pore layer of FPPS and pre-slight warming of seeds. For the second period of combined dehydration of FPPS humidity changes within 44 – 38% as typical decreasing drying speed and kinetic curves depicted curved sections, the angle of which indicates a slowdown in the process of dehydration (*Tsurkan O. et al, 2015*). This can be explained by the fact that the amount of moisture, delayed both by adsorption forces (bridging, drip, wet point) and surface tension forces on the seeds surface, is gradually reducing, and the process of evaporation due to heat small seeds is quite slow.

After removing moisture through BSC, the layer of FPPS still contains a significant amount of moisture that is delayed both by adsorption forces and due to the presence of blind channels from which moisture is replaced. In through BSC of complex form streams of drying agent turbilize, tear film of moisture in the form of small droplets of fog and render them out of material structure.

To reach the humidity range of about 38% cohesive-adhesive properties of seed layer are weakened, and seed acquires discrete properties (table 1).

Table 1

Rational methods of FPPS dehydration depending on type of relationship between moisture and the material

Type of moisture relation during dehydration	The hydrodynamic characteristics of FPPS	Rational way of dehydration: Filtration dehydration	Rational way of dehydration: Convection drying	The driving factors and the intensification of dehydration process
Capillary W_{ca} =(52- 47)%	**Local drag reduction adjacent to vibrating surfaces of LFPPS**	**Filtering displacement of moisture from cross-mating BSC "top-down"**	**Preheat of LFPPS, slight evaporation of moisture**	**Submission of a drying agent of FPPS "top-down" • Slight heating of the drying agent (t = 30°C) • Dilution under FPPS (P_d = 450 Pa) • Vibration action • Preferably vertical vibrations • The mechanical mixing of LFPPS • Cleaning of perforated surfaces of supply-drying agent selection**
	Fluidization, destruction of cohesive-adhesive bonds	**Displacement of moisture from the deadlock, non-connected BSC "top-down"**		
Rope W_r =(47- 44)%		**Two phase movement drip-air mixture "top-down"**		
Capillary-butt (glands) W_{cb}=(44-38)%				
Capillary-butt (spot) W_{cb} =(38-24)%	Reduction of hydrodynamic resistance, ability to aerovibroboiling	Two-phase movement drip-air mixture "bottom-up"	Intense convective drying in AVBL	Vibration performance, stable AVBL •Filing drying agent «bottom-up» • Heating drying agent (t_{da2} = 50°C) • Pre-heating of seeds (t_{s1} = 26°C)
Surface film-drop W_{sf} =(24-15)%				
Inside physico-chemical relation $W_{ph\ ch}$ =(15-10)%				

Note: *LFPPS – layer of fresh-peeled pumpkin seeds; AVBL – aerovibroboiling layer. Highlight: vibration filtration, dewatering study method.*

Under the influence of vibration and drying agent flow in the direction of "perforated bottom – a layer of seeds" created aerovibroboiling layer (AVBL), which can increase the temperature of the drying agent and significantly intensify the process of dehydration, which can be divided into two periods: the constant and the decreasing speed drying.

In this article, we studied the kinetics of the second period of vibration filtration dehydration of FPPS within the humidity range 44 – 38%.

Experimental studies were conducted using research and industrial design vibration dryers, developed and manufactured at the processes and equipment department for food processing industries named by Professor P.S. Bernik Vinnytsia, National Agrarian University, realizing vibration filtration dehydration and convective drying AVBL *(Pravdjuk N. et al, 2011)*.

To summarize the kinetics vibration filtration dehydration of FPPS in the second period we used the equation curve speed drying method proposed by A. Lykov, which has the form *(Lykov A., 1968)*:

$$-\frac{dW}{d\tau}=K\cdot\left(W-W_{\mathrm{m}}\right) \tag{1}$$

where:

$\frac{dW}{d\tau}$ – the moisture change over time (speed drying), %/s;

W – running material moisture, %;

W_{m} – the equilibrium moisture content, %;

K – drying rate (1/s), which is defined by the formula: $K=\chi\cdot N$;

χ – relative drying rate, %;

N – drying speed in the first period, %/s.

The integral form of equation (1) can be written:

$$\frac{W-W_{\mathrm{m}}}{W_{\mathrm{cr}}-W_{\mathrm{m}}}=e^{-K\cdot(\tau-\tau_{\mathrm{cr}})}\ . \tag{2}$$

Having logarithmic equation (2) we get:

$$\ln\left(\frac{W-W_{\mathrm{m}}}{W_{\mathrm{cr}}-W_{\mathrm{m}}}\right)=-K\cdot\left(\tau-\tau_{\mathrm{cr}}\right) \tag{3}$$

To determine the drying coefficient *K* for the research of kinetics vibration filtration dehydration of FPPS in the second period we built graphical dependence: $\ln\left(\frac{W-W_{\mathrm{m}}}{W_{\mathrm{cr}}-W_{\mathrm{m}}}\right)=f\left(\tau-\tau_{\mathrm{cr}}\right)$, (fig.1-4), which are linear.

RESULTS

Drying factor *K* is defined as the slope of the line to the vertical axis (fig. 1-4). The resulting figures are presented in table 2. The coefficient drying *K* is not a constant (the ratio increases with the vertical and horizontal components of vibration amplitude, with increasing temperature of the coolant and reducing the height of the material) (table 2).

To determine the drying length in the first period *(Tsurkan O. et al, 2015)* we considered the graphical dependence of the critical drying time τ_{cr} and the speed of drying *N* in the first period (fig. 5), according to which such an evident relationship results:

$$\tau_{\mathrm{cr}}=\tau_{\mathrm{I}}=\frac{28{,}1}{N^{0{,}83}} \tag{4}$$

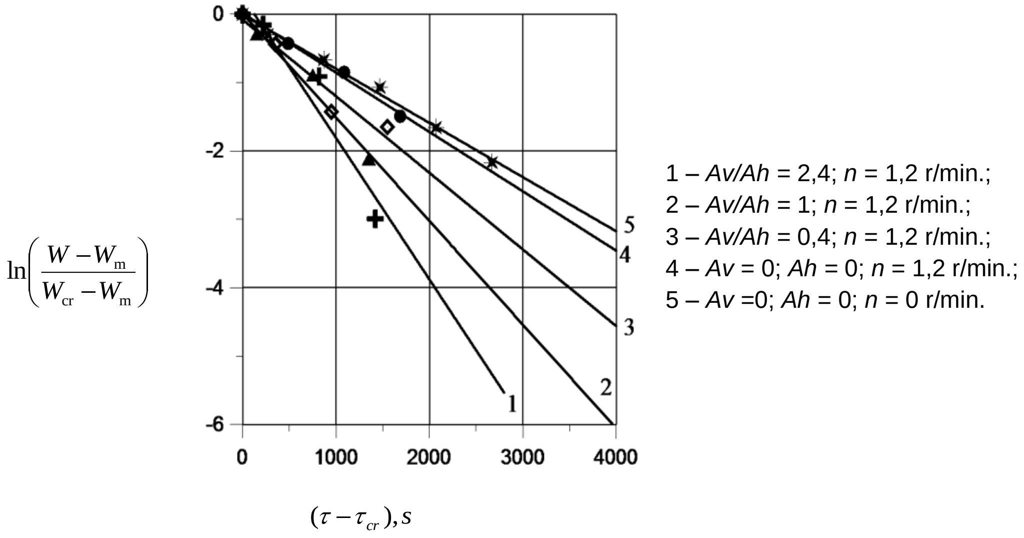

Fig. 1 – Determination of FPPS drying K by vibration filtration dehydration at different ratio of vibration amplitude vertical and horizontal components under the following conditions:

$A\omega^2$ = 55 m/s^2; t = 30°C; K_d = 0,75; ΔP = 1250 Pa

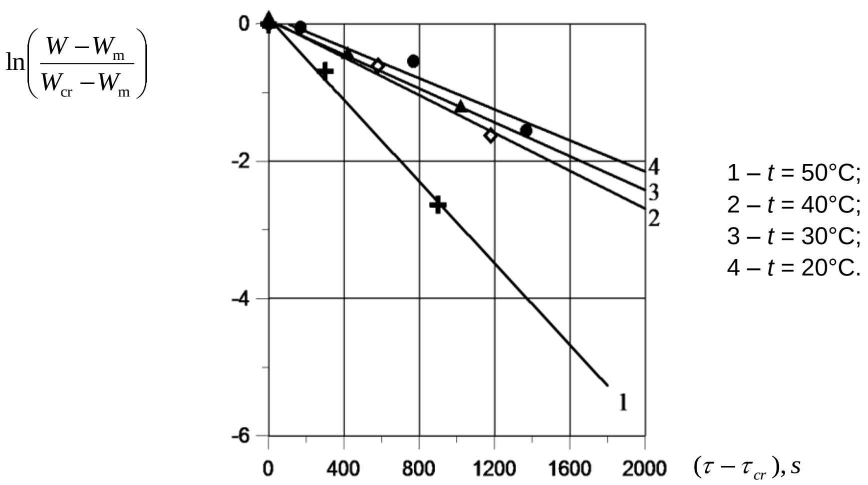

Fig. 2 – Determination of FPPS drying *K* by vibration filtration dehydration at different temperature of drying agent under the following conditions:

K_d = 0,75; ΔP = 1250 Pa; n = 1,2 r/min.; $A\omega^2$ = 55 m/s^2; Av/Ah = 2,4

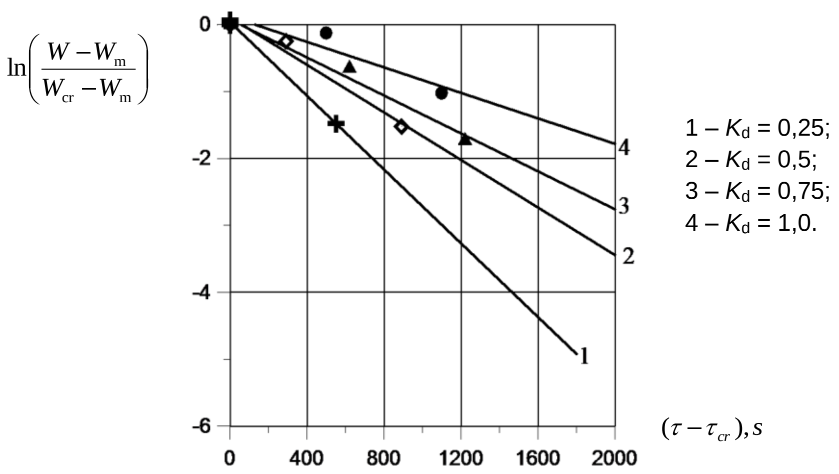

Fig. 3 – Determination of FPPS drying *K* by vibration filtration dehydration at different values of the drying chamber filling circuit K_d under the following conditions:

t = 30°C; ΔP = 1250 Pa; n = 1,2 r/min.; $A\omega^2$ = 55 m/s^2; Av/Ah = 2,4

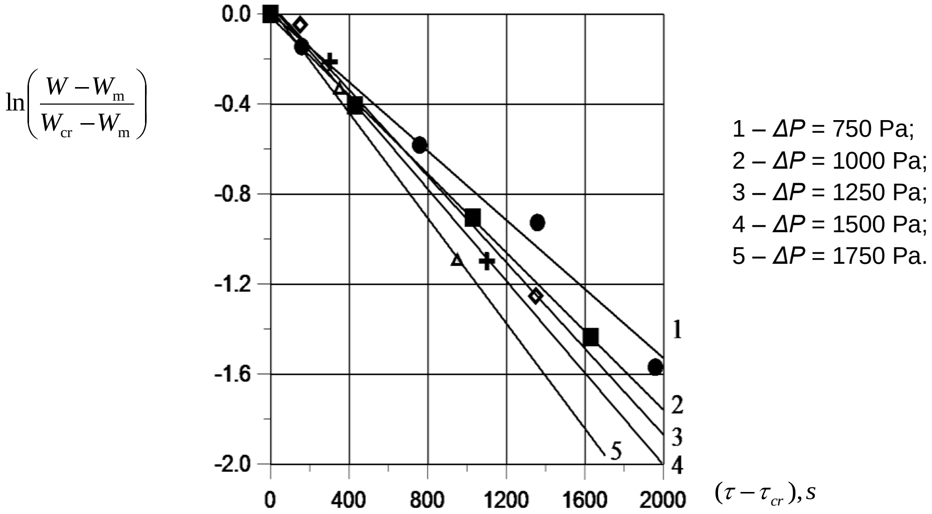

Fig. 4 – Determination of FPPS drying *K* by vibration filtration dehydration at different pressure drop under the following conditions:
$A\omega^2$ = 55 m/s^2, t = 30°C; K_d = 0,75; Av/Ah = 2,4

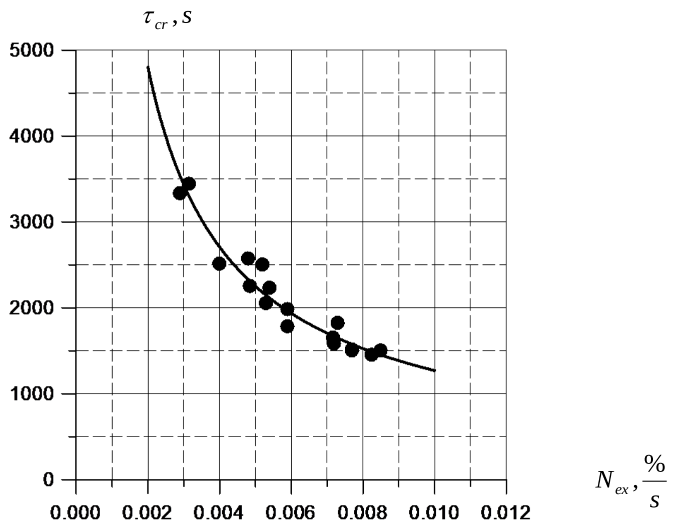

Fig. 5 – Dependence of FPPS drying (*N*) in the first period on vibration filtration dehydration critical time

The calculations built graphical dependence $K = f(N)$ (fig. 6), which is defined as the relative rate of drying slope given in the equation:

$$K = \chi \cdot N \tag{5}$$

Relative factor is drying χ = 0,157%.

Equation (2) is derived to calculate humidity depending on FPPS in time to test a range of parameters for the drying process of the second period:

$$W_{II} = \left(W_{cr} - W_m\right) \cdot e^{-0,157 \cdot N \cdot \left(\tau - \tau_{cr}\right)} + W_m \tag{6}$$

Substituting (4) into the equation (6) we have:

$$W_{II} = \left(W_{cr} - W_m\right) \cdot e^{-0,157 \cdot N \cdot \left(\tau - \frac{28,1}{N^{0,83}}\right)} + W_m \tag{7}$$

The investigations make it possible to track mutual parameters of first and second periods of FPPS vibration-process filtration dehydration (fig. 6).

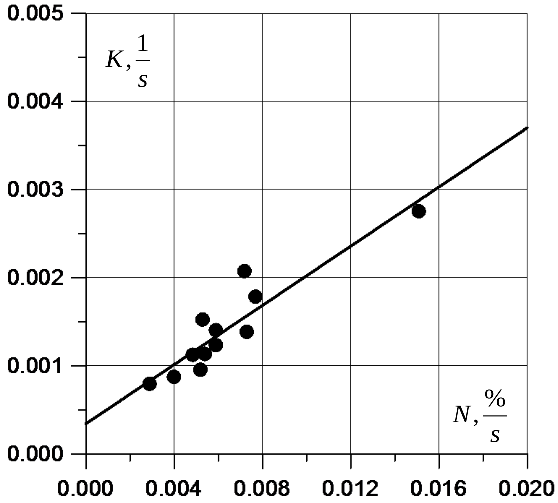

Fig. 6 – Dependence of drying *K* (the second period) on the rate of FPPS vibration filtration dehydration *N* (in the first period)

The drying time in the first period was determined by the formula (4), and the second – in the equation (7) and it is the following:

$$\tau_{II} = -\frac{1}{0{,}157 \cdot N} \cdot \ln\left(\frac{W - W_m}{W_{cr} - W_m}\right) \tag{8}$$

The duration of FPPS vibration filtration dehydration investigated the changes range of the process parameters is:

$$\tau_к = \tau_I + \tau_{II} = \frac{28{,}1}{N^{0{,}83}} - \frac{1}{0{,}157 \cdot N} \cdot \ln\left(\frac{W - W_m}{W_{cr} - W_m}\right) \tag{9}$$

This shows that the drying depends on the speed of drying *N* in the first period, running, and moisture equilibrium on FPPS movement.

Table 2

Determining factors of drying, depending on changing technological parameters of FPPS vibration-filtration dehydration

Process parameters				First drying period	Second drying period
t, °C	*H*, m	$\frac{A_V}{A_h}$	*n*, r/min	*N*, %/s	*K*, 1/s
30	0.026	2.4	1.2	0.0072	0.00207
		1	1.2	0.0053	0.00152
		0.4	1.2	0.00485	0.00112
		0	1.2	0.004	0.00087
		0	0	0.0029	0.00079
30	0.0075	2.4	1.2	0.0151	0.00275
	0.0175			0.0077	0.00178
	0.026			0.0059	0.0014
	0.03			0.0052	0.00095
50	0.026	2.4	1.2	0.0085	0.00297
40				0.0073	0.00138
30				0.0059	0.00123
20				0.0054	0.00113

Analysing the results of FPPS vibration filtration dehydration process of (table 2) we found that the increase in the ratio of vibration amplitude vertical and horizontal components of the drying $\frac{A_V}{A_h}$ chamber from 0 to 2.4 by the simultaneous increase in rpm stirrer-cleaner *n* from 0 to 1.2 r/min. speed the drying process in the first period increases by 2.4 times.

CONCLUSIONS

1. We determined the type of relation between moisture and the material and the corresponding interval of FPPS moisture limits reasonably rational methods of dewatering and drying constructive scheme appropriate equipment.

2. The increase of the process speed is limited by the maximum allowable temperature of FPPS heating (especially for sowing and pharmaceutical purposes), and fill coefficient of drying chamber volume is limited by compromise productivity values and specific energy equipment.

3. We summarized kinetics vibration filtration dehydration of FPPS in the second period by the method proposed by A. Lykov.

4. According to the research of kinetics vibration filtration dehydration of FPPS in the second period we built a tracker $\ln\left(\frac{W-W_{\mathrm{m}}}{W_{\mathrm{cr}}-W_{\mathrm{m}}}\right)=f\left(\tau-\tau_{\mathrm{cr}}\right)$ determined coefficient *K* and relative drying rate, which is χ = 0.157%.

5. We defined the changes of drying coefficient *K* in key technical parameters of the process: drying coefficient *K* increases with the ratio of vibration amplitude vertical and horizontal components, with increasing temperature of the coolant and reducing the height of the FPPS material.

6. We defined the dependence of calculating FPPS humidity in time to test the range change process parameters and the process of drying and its length depending on drying speed in the first period and running, and the moisture equilibrium on FPPS movement.

7. We confirmed the feasibility process of intensifying FPPS vibration filtration dehydration by increasing the ratio of vibration amplitude vertical and horizontal components of the drying chamber (in case of increase in the ratio $\frac{A_V}{A_h}$ of 0 to 2.4 by the simultaneous increase in rpm stirrer-cleaner *n* from 0 to 1.2 r/min. speed the drying process in the first period increases by 2.4 times).

REFERENCES

[1] Atamanjuk V., (2007), Hydrodynamics and a heat mass exchange during filtrational drying of disperse materials (Гідродинаміка і тепломасообмін під час фільтраційного сушіння дисперсних матеріалів): *Author. Dis. on competition sciences. Degree dock. Sc. Science*, p.46, Lviv/Ukraine;

[2] Atamanjuk V., Gumnytskyj Ya., (2009), Mathematical model of heat exchange process during the second period of dispersed materials drying filtration (Математична модель процесу теплообміну під час другого періоду фільтраційного сушіння дисперсних матеріалів), *The East European Journal of Advanced Technologies*, Vol.37(1/4), pp.20-24, Kharkov/Ukraine;

[3] Hanyk Ya., (1992), Filtrational drying of flat permeable materials (Фильтрационная сушка плоских проницаемых материалов), *Dis.Dr.Sc. Sciences*: 05.17.08, p.426, Lviv/Ukraine;

[4] Holubkovych A., (1986), Classification of seeds for drying (Классификация семян для сушки), *Vegetable e Farming (Овощное хозяйство)*, №. 2, pp. 33-36, Moscow/Russia;

[5] Lykov A., (1968), Theory of drying *(Теория сушки)*, p.472, Moscow/Russia;

[6] Mykychak B., Biley P., Kindzera D., (2012), Hydrodynamics of veneer packet filtration drying (Гідродинаміка фільтраційного сушіння пакета шпону), *Scientific Journal NLTU Ukraine (Науковий вісник НЛТУ України)*, Vol. 22.5, pp. 148-154, Lviv/Ukraine;

[7] Palamarchuk I., Tsurkan O., Hurych A., (2016), Prospects of vibromechanic combined action during processing and food production (Перспективы использования комбинированного вибромеханического действия в процессах перерабатывающих и пищевых производств), *Vibrations in Engineering and Technology*, Vol. 2(82), pp.100-108, Vinnitsa/Ukraine;

[8] Poperechnyj A., (2007), Scientific substantiation of mechanical vibrations influence on the processes intensification of food raw materials processing (Наукове обґрунтування впливу механічних коливань на інтенсифікацію процесів переробки харчової сировини): *Author. Dis. on sciences competition. Degree dock. Sc. Science*, p.36, Kharkov/Ukraine;

[9] Pravdjuk N., Tsurkan O., Koz I., Gerasimov O., (2011), Vibratory dryer (Вібраційна сушарка), *Patent № 64644*, Ukraine;

[10] Rymar T., (2009), Resource conservation in colloidal materials *drying (Ресурсозбереження під час сушіння колоїдних матеріалів)*, *VSN. eng. acad. of Ukraine (Вісн. інж. акад. України)*, Vol. 1, pp. 193-196; Kyiv/Ukraine;

[11] Stanislavchuk O., (2007), Drying of paste-like materials in a motionless layer (Сушіння пастоподібних матеріалів у нерухомому шарі): *Author. Dis. on sciences competition. Degree kand. Sc. Science*, p.22, Lviv/Ukraine;

[12] Tsurkan O., Gerasimov O., Rymar T., Stanislavchuk O., (2014), Hydrodynamics of dehydration filtration process of fresh-peeled pumpkin seeds with vibration activation (Гідродинаміка процесу фільтраційного зневоднення свіжеочищеного насіння гарбуза з вібраційною активацією), *Vibrations in Engineering and Technology*, Vol. 2(74), pp. 138-144, Vinnitsa/Ukraine;

[13] Tsurkan O., Gerasimov O., Polyevoda Y., Rymar T., Stanislavchuk O., (2015), Generalization of kinetics of fresh-peeled pumpkin seeds 1st period of dehydration filtration with vibration and pneumatic activation (Узагальнення кінетики 1-го періоду фільтраційного зневоднення свіжеочищеного насіння гарбуза з вібраційно-пневматичною активацією), *Journal Scientific Works of National University of Food Technologies*, Vol. 21, №. 2, pp. 151-159, Kiev/Ukraine;

[14] Tsurkan O., Yanovych, V., Gerasimov O., (2009), Results of theoretical and experimental studies of vibratory dryer dynamics (Результати теоретичних та експериментальних досліджень динаміки руху вібраційної сушарки), *Vibrations in Engineering and Technology*, Vol. 4(56), pp. 149-156, Vinnitsa/Ukraine.

RESEARCH ON REVERSIBLE HEAT PUMP INSTALLATION FOR GREENHOUSE HEATING
/
ИЗСЛЕДВАНЕ НА РЕВЕРСИВНА ТЕРМОПОМПЕНА ИНСТАЛАЦИЯ ЗА ОТОПЛЕНИЕ НА ОРАНЖЕРИИ

Lecturer Ph.D. Eng. Kolev Z. D.[1], Lecturer Ph.D. Eng. Kadirova S. Y.[*2], Student Nenov T. R.[3]
[1] Rousse University "Angel Kunchev", Agrarian – Industrial Faculty / Bulgaria
[2] Rousse University "Angel Kunchev", Faculty of Electrical Engineering, Electronics and Automation / Bulgaria
[3] Rousse University "Angel Kunchev", Faculty of Electrical Engineering, Electronics and Automation / Bulgaria
Tel: 00359 877 089537; E-mail: skadirova@uni-ruse.bg

Keywords: *greenhouse, heating, heat exchange, heat flow, performance coefficient*

ABSTRACT
The aim of the article is to investigate the influence of the airflow velocity on the main parameters of a reversible heat pump installation, as the airflow crosses the external surface of heat exchange apparatus of the "water – air" convector. The main installation parameters, working in "heating" regime at specific values of airflow velocity have been investigated. The investigated parameters are: heat convection coefficients and convector heat transfer coefficient; internal and external installation heat flows; heat pump performance coefficient.

РЕЗЮМЕ
Целта на публикацията е да се изследва влиянието на скоростта на въздушния поток, обтичащ външната повърхност на топлообменния апарат на „водо – въздушен" конвектор, върху основните параметри на реверсивна термопомпена инсталация. Изследвани са основните параметри на инсталацията, работеща в режим отопление, при конкретни стойности на скоростта на въздушния поток. Изследваните параметри са: коефициенти на топлопредаване и коефициент на топлопреминаване на конвектора; вътрешен и външен топлинни потоци на инсталацията; коефициент на трансформация на термопомпата.

INTRODUCTION
Nowadays, greenhouse farming is a growing industry in many countries because of world population increase. That is why greenhouse food production is an additional alternative for meeting increased food demand year around. The way to produce greenhouse crops is very expensive and there are many variables to consider before the farmer decides to take this route. All plant growth factors can be controlled and maintained at optimum level in year around in the greenhouses (*Esen M., Yuksel T., 2013)*.

In developing countries, greenhouses are small-size enterprises, which are generally established by farmers. In general, these are the ones that don't need heating or are heated by farmers through their own methods. The increase in nutrition needs and the rise in the standard of nutrition which is consumed have made greenhousing more important (*Benly H., 2010; Yang S., Rhee J., 2013).*

The energy consumption in agriculture has increased considerably with the introduction of high-yielding varieties and mechanized-crop production practices. A higher heating cost for greenhouses using natural gas or oil has resulted and many growers have preferred to choose alternative energy sources (*Benly H., 2010; Biris S. St. et al, 2009; Constantinescu D. M. et al, 2009; Russo G. et al, 2014).* This problem is very up-to-date, taking into account the significant price increase of natural gas in Europe at the moment.

Underground water source heat pumps are a highly efficient, renewable energy technology for space heating and cooling. These technologies rely on the fact that the underground water sources have a relatively constant temperature (*Benly H., 2010; Kurpaska S., 2011).*

Greenhouse heating is one of the fields requiring high energy consumption during the cold seasons *(Awani S. et al, 2015)*. It's important to optimize the heat pump performance coefficient in the heating installations, which is an indicator of their efficiency. This coefficient depends on the heat flow that the heaters give to the air in the greenhouse. On another hand, the heat flow depends on the settings of the heaters, which determine the coefficients of heat exchange.

In this article, the influence of the fan setting of "water–air" convector in a reversible heat pump installation on the main installation parameters has been investigated. The investigated parameters are: heat convection coefficients and convector heat transfer coefficient; internal and external installation heat flows; heat pump performance coefficient. The researches have been performed under laboratory conditions.

The aim of the article is to obtain results for quantitative change of the investigated parameters, which can be used for greenhouse microclimate maintenance, and optimization of the energy costs for heating.

MATERIAL AND METHODS

Object of research

The principal scheme of the heat pump installation is shown in Fig.1. The heat pump is of "water – water" type, CEAT brand, Aurea 20 model. The convector is of "water – air" type, BUMYANG brand, FVC20MLL2 model. Under "heating" regime, the heat pump heat exchanger in the external circle works as an evaporator, and the internal one works as a condenser. In the evaporator, the refrigerant takes heat energy from the cold water, circulating in the external circle, at the same time in the condenser the refrigerant gives heat energy to the hot water, circulating in the internal circle. The convector gives heat energy to the internal ambient air to ensure the required temperature (*Bobilov V. et al, 2011; Kolev Z. et al, 2015; Kolev Z. et al, 2015b*).

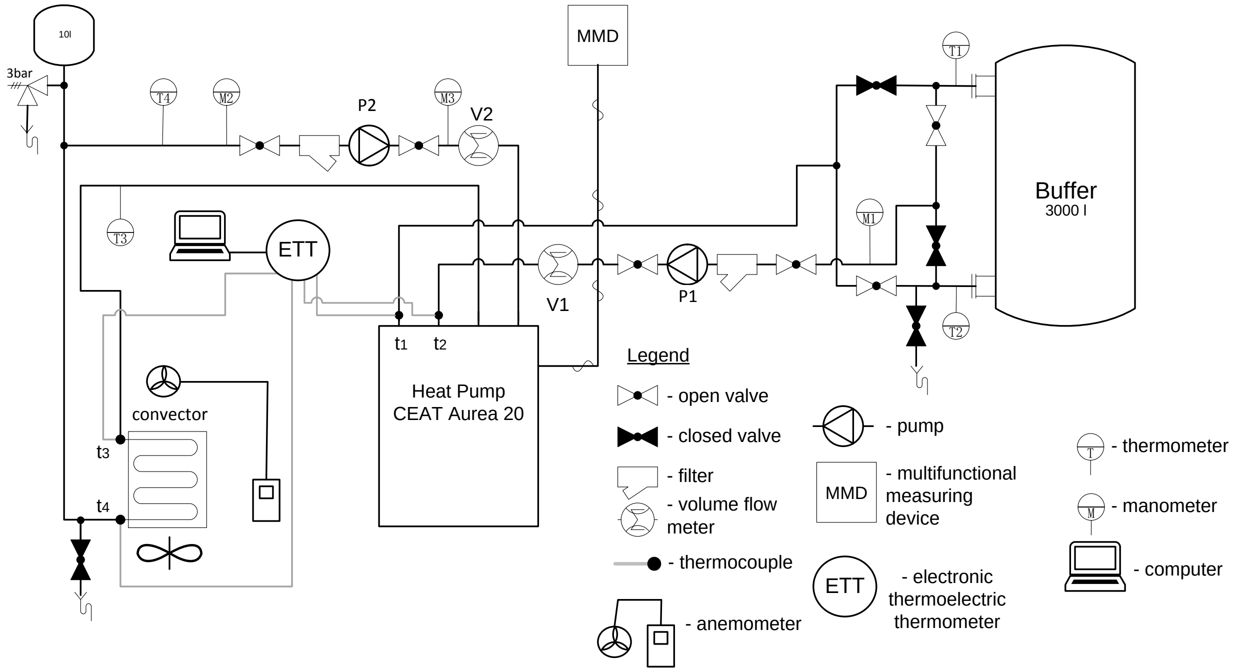

Fig. 1 - Main scheme of the heat pump installation

Under "heating" regime the water in the buffer represents the heat source, from which the installation takes heat energy, ensuring heat pump working. For the installation to work for a long time without reducing considerably the temperature of the buffer water, it is necessary to achieve a stratification of the water in the buffer. The work scheme presenting the "heating" regime is shown in Fig. 2.

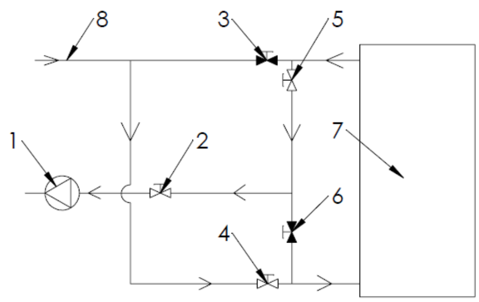

1 - circulation pump;

2, 4 and 5 - open valves;

3 and 6 - closed valves;

7 – water buffer;

8 – from heat pump

Fig. 2 - Work scheme presenting the "heating" regime

The convector's heat exchanger has been implemented as a two-pipe staggered ribbed tube sheaf. The tubes and ribs are made from a copper alloy. The main scheme of the convector's heat exchanger is shown in Fig. 3 *(Bobilov V. et al, 2011; Kolev Z. et al, 2015; Kolev Z. et al, 2015b)*.

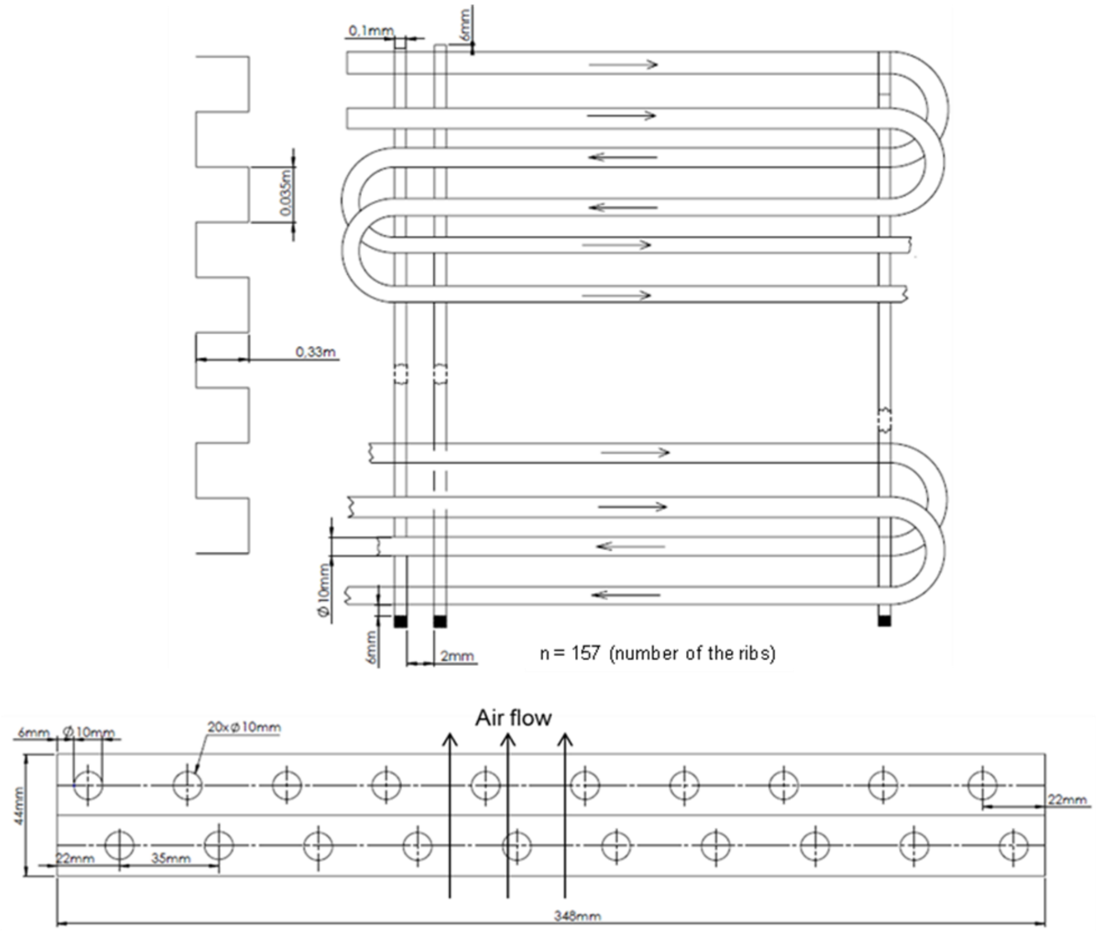

Fig. 3 - Main scheme of the convector's heat exchanger

In the convector's tubes is running water, which is heated or cooled by the heat pump, depending on the installation working regime. The pipe bundle is crossed by airflow, generated by the axial fan.

Methodology for determining the parameters

The actual velocity of the airflow in the air gap between heat exchanger tubes and ribs has been calculated by the equation (*Kolev Z. et al, 2015; Kolev Z. et al, 2015b*):

$$w_2 = w_{2-measured} \cdot \frac{S_2}{S_{2-air\,gap}} \text{ [m/s]} \tag{1}$$

where:

$w_{2-measured}$ is the measured airflow velocity at the convector's output, m/s;

S_2 - cross sectional area of the heat exchanger, crossed by the airflow, m^2;

$S_{2-air\,gap}$ - cross sectional area of the air gap between the tubes and ribs, m^2.

The heat convection coefficient between the water in the convector tubes and their internal surface has been determined by the equation (*Kolev Z. et al, 2015; Kolev Z. et al, 2015b*):

$$\alpha_1 = \frac{Nu_1 . \lambda_1}{d_{tube1}} \text{ [W/(m}^2\text{K)]} \tag{2}$$

where: the criterion of Nuselt has been calculated by the equation $Nu_1 = 0{,}021.Re_1^{0,8}.Pr_1^{0,43}$;

λ_1 - thermal conductivity coefficient of the water in tubes, W/(m.K);

d_{tube1} - internal diameter of the tubes, m.

The heat convection coefficient between the external surface of the convector and the airflow has been determined by the equation (*Kolev Z. et al, 2015; Kolev Z. et al, 2015b*):

$$\alpha_2 = \frac{Nu_2.\lambda_2}{d_{tube2}} \quad [\mathrm{W/(m^2K)}] \tag{3}$$

where: the criterion of Nuselt has been calculated by the equation $Nu_2 = 0{,}25.\left(\frac{d}{t}\right)^{-0{,}54}.\left(\frac{D-d}{2.t}\right)^{-0{,}14}.Re_2^{0{,}65}.Pr_2^{0{,}4}$;

λ_2 - thermal conductivity coefficient of the air crossing heat exchanger external surface, W/(m.K);

d_{tube2} - tubes external diameter, m.

The heat transfer coefficient between the water in the convector tubes and the airflow crossing the convector external surface has been determined by the equation for single layer flat wall, ignoring the thermal resistance of the tubes and ribs (*Kolev Z. et al, 2015; Kolev Z. et al, 2015b*):

$$U = \frac{1}{\frac{1}{\alpha_1} + \frac{1}{\alpha_2}} \, [\mathrm{W/(m^2K)}] \tag{4}$$

The heat flows $\dot{Q}_{con}$ and $\dot{Q}_{eva}$ have been determined by the basic calorimetric equation, (*Bobilov V. et al, 2011; Kolev Z. et al, 2015; Kolev Z. et al, 2015b*):

$$\dot{Q} = \dot{m}.c_{pm}.\Delta t \quad [\mathrm{W}] \tag{5}$$

where:

$\dot{m}$ is the water mass flow rate, kg/s;

c_{pm} - water mass heat capacity, J/(kg.K);

Δt - water temperature difference, K.

$\dot{Q}_{con}$ is the heat flow in the internal installation circle which has been exchanged in the heat pump condenser. On the other hand, this is the heat flow between the convector and the ambient air.

$\dot{Q}_{eva}$ is the heat flow in the external installation circle which has been exchanged in the heat pump evaporator.

The heat pump performance coefficient under "heating" working regime (winter regime) has been determined by the equation (*Bobilov V. et al, 2011*):

$$COP|_W = \left.\frac{\dot{Q}_{con}}{W_{comp}}\right|_W \tag{6}$$

where W_{comp} is the electric power, consumed by the heat pump, W.

The installation input parameters for the research are presented in Table 1.

Table 1

Installation input parameters

Set of the convector's fan	Set of the heat pump	Internal water volume flow rate	External water volume flow rate	Temperature of the ambient air	Actual airflow velocity
"LOW" Degree	The switch ON temperature of the heat pump is *t₄ = 42 °C* The switch OFF temperature of the heat pump is *t₄ = 45 °C*	$\dot{V} = 0.000148\, m^3/s$	$\dot{V} = 0.000411\, m^3/s$	$t_{ambientair} = 14.2\ ^oC$	$w_2 = 0.92\, m/s$
"MID" Degree				$t_{ambientair} = 15.2\ ^oC$	$w_2 = 2.51\, m/s$
"HIGH" Degree				$t_{ambientair} = 15.2\ ^oC$	$w_2 = 5.06\, m/s$

The ambient temperature $t_{ambient\ air}$ has constant value during the experiment.

The average temperature of the water in the buffer remains approximately equal to $t_{ambient\ air}$.

RESULTS

- **Research on the influence of airflow velocity w_2 on the heat convection coefficient α_1**

The change of the coefficient α_1 depending on the velocity w_2 of the airflow in the air gap between the heat exchanger tubes and ribs is presented in Fig. 4.

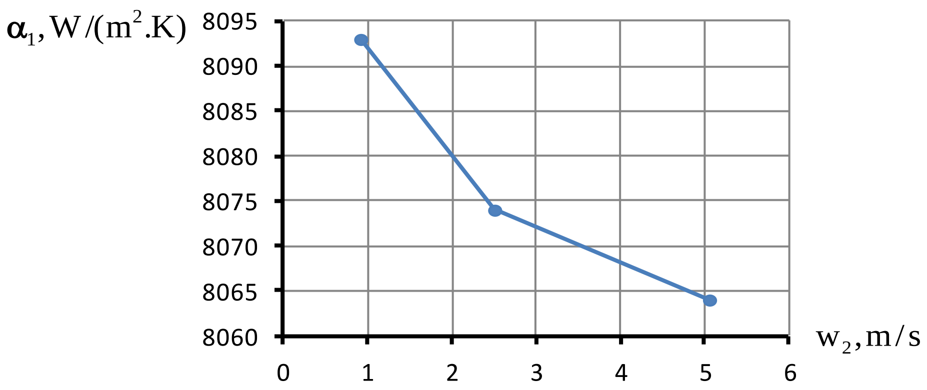

Fig.4 - Graphical dependence between α_1 and w_2

The reason for the decrease of the heat convection coefficient α_1 by increasing the airflow velocity is the decrease of the average water temperature in the internal circle. The increase of the water temperature leads to the increase of water kinematic viscosity, which in turn leads to the decrease of the Reynolds criterion.

- **Research on the influence of the airflow velocity w_2 on the heat convection coefficient α_2**

The change of the coefficient α_2 depending on the velocity w_2 is presented in Fig. 5.

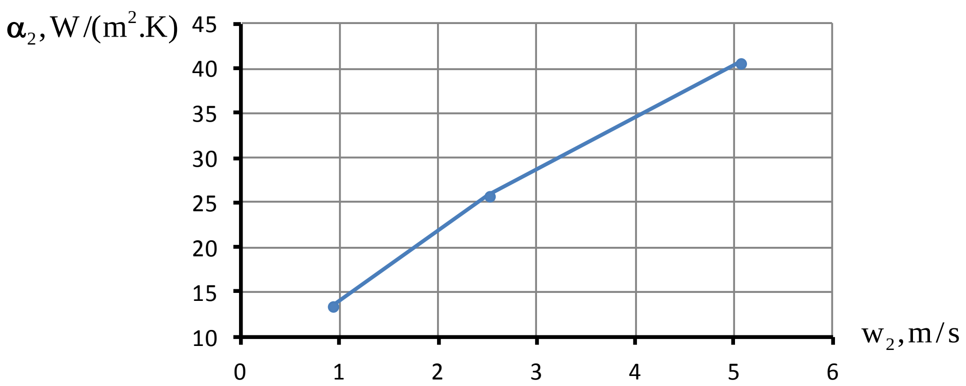

Fig. 5 - Graphical dependence between α_2 and w_2

The increase of the heat convection coefficient α_2 results from the significant increase of Reynolds criterion by the increase of the airflow velocity. On the other hand, the temperature of the air crossing the convector is decreased and leads to a decrease of the water kinematic viscosity.

- **Research on the influence of the airflow velocity w_2 on the heat transfer coefficient U**

The change of the coefficient U depending on the velocity w_2 is presented in Fig. 6.

The reason for the increase of the heat transfer coefficient U by increasing the airflow velocity w_2 is the increase of the external heat convection coefficient α_2, which has a more significant influence on U than the decrease of the internal heat transfer coefficient α_1. It can be concluded that the values of U have insignificant deviation comparing to those of α_2 (the differences are of the orders of tenths of 1 W/(m^2.K)).

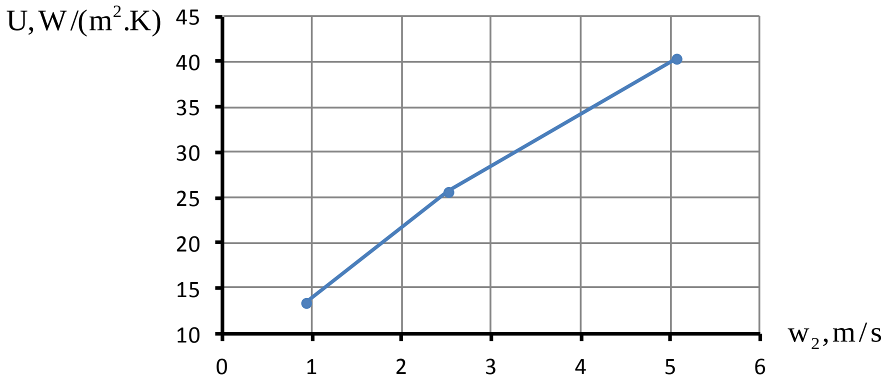

Fig. 6 - Graphical dependence between U and w_2

- **Research on the influence of the airflow velocity w_2 on the heat flow $\dot{Q}_{con}$**

The change of the heat flow $\dot{Q}_{con}$ depending on the velocity w_2 is presented in Fig. 7.

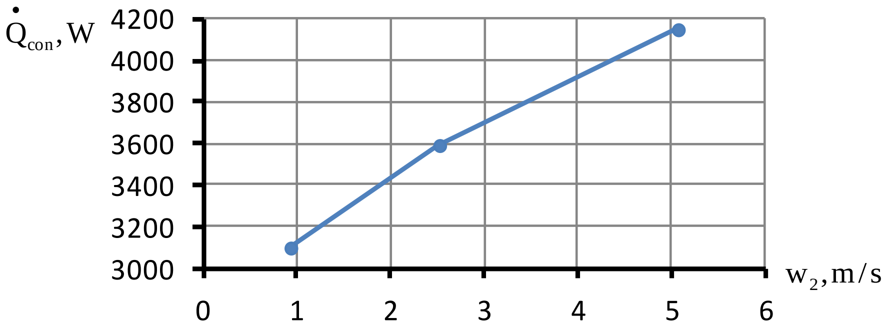

Fig. 7 - Graphical dependence between $\dot{Q}_{con}$ and w_2

The heat flow $\dot{Q}_{con}$ can be determined also based on the calculated heat convection coefficients and heat transfer coefficient.

Based on the basic calorimetric equation, the heat flow $\dot{Q}_{con}$ in the convector has been increased by increasing the airflow velocity, because the temperature difference "t_3(convector input) - t_4(convector output)" has increased. On the other hand, the water temperature in the internal circle has decreased, which leads to a decrease of the water density.

In terms of the "Newton – Rickman" law for the process of heat convection between the water and the internal surface of the tubes, the increase of the temperature difference "(average water temperature in the central section of tubes) - (average temperature of the inner tubes surface)" has a higher influence on the heat flow comparing to the decrease of the internal heat convection coefficient α_1.

From the perspective of the "Newton – Rickman" law for the process of heat convection between the external surface of heat exchange apparatus and the crossing airflow, the external heat convection coefficient α_2 has a significant influence on the heat flow.

Regarding the heat transfer process in the convector, the significant increase of the heat transfer coefficient U influences the heat flow.

- **Research on the influence of the airflow velocity w_2 on the heat flow $\dot{Q}_{eva}$**

The change of the heat flow $\dot{Q}_{eva}$ depending on the velocity w_2 is presented in Fig. 8.

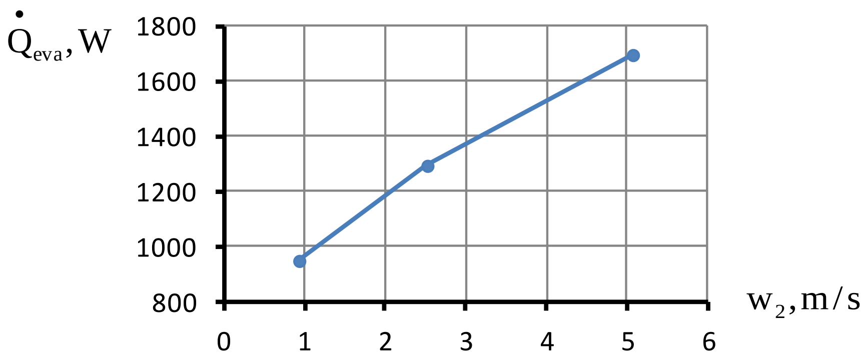

Fig. 8 - Graphical dependence between $\dot{Q}_{eva}$ and w_2

The heat flow $\dot{Q}_{eva}$ from the buffer water to the evaporating refrigerant in the evaporator increases with increasing airflow velocity through the convector, due to increased temperature difference "t_2 (buffer output) - t_1(buffer input)".

- **Research on the influence of the airflow velocity w_2 on the heat pump performance coefficient $COP|_W$**

The change of the performance coefficient $COP|_W$ depending on the velocity w_2 is presented in Fig. 9.

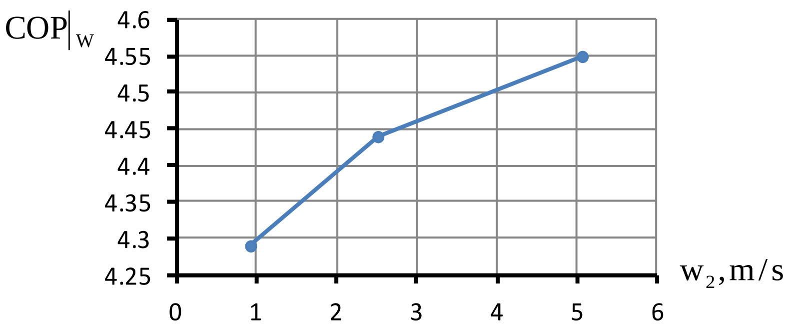

Fig. 9 - Graphical dependence between $COP|_W$ and w_2

The performance coefficient increases when increasing the airflow velocity. This results from the higher influence of the increase of the heat flow through the convector than the change of the average electrical power, consumed by the heat pump.

From the results observed, presented in Fig. 9 we can conclude that there is relatively low variation of the coefficient $COP|_W$ in terms of airflow velocity variation.

At a lower airflow velocity, i.e. less power consumption of the convector's fan, the operation efficiency of the heat pump heating installation will be obtained with a value close to that at a higher airflow velocity.

CONCLUSIONS

The main parameters of the installation working under "heating" regime at specific values of airflow velocity have been investigated. Based on them, the microclimate in greenhouses as well as the energy costs for heating can be optimized by correct control of the heat pump heating installation.

The change of the airflow velocity w_2 leads to a higher degree of change of the external heat convection coefficient α_2, respectively of the heat transfer coefficient U, comparing to the change degree of the internal heat convection coefficient α_1.

On the other hand the change of the airflow velocity w_2 leads to a higher change degree of the heat flow $\dot{Q}_{eva}$ exchanged by the heat pump evaporator, than the heat flow $\dot{Q}_{con}$ exchanged by the heat pump condenser.

At a lower airflow velocity, i.e. less power consumption of the convector fan, the operation efficiency of the heat pump heating installation will be obtained with a value close to that at a higher airflow velocity.

Last but not least, the used laboratory installation is suitable for additional researches about heat pump heating installations for greenhouses. The additional parameters of the installations which can be investigated are: the temperature of the ambient air, the temperature of the water energy source, the water volume flow rate in the internal installation circle, the settings of the heat pump (switch ON temperature, switch OFF temperature, as well as the temperature range between them).

REFERENCES

[1] Awani S., Chargiu R., Kooli S., Farhat A., Guizani A., (2015), Performance of the coupling of the flat plate collector and a heat pump system associated with a vertical heat exchanger for heating two types of greenhouses, *Energy Conversion and Management*, Vol.103, pp.266-275, https://doi.org/10.1016/j.enconman.2015.06.032;

[2] Benly H., (2011), Energetic performance analysis of a ground-source heat pump system with latent heat storage for a greenhouse heating. *Energy Conversion and Management,* Vol. 52 (1), pp.581-589, https://doi.org/10.1016/j.enconman.2010.07.033

[3] Biris S. St., Paraschiv G., Maican E., Ungureanu N., Manea M., Vlădut V., (2009), Present and future in the field of alternative energy use, *INMATEH-Agricultural Engineering*, Vol.27 (1), pp.1–8, Bucharest / Romania;

[4] Bobilov V., Genchev G., Mushakov P., Zlatev P., Kolev Z., (2011), Methodology for researching the performance coefficient of reversible “water-water” heat pump, *Proceedings of University of Ruse*, volume 50, series 1.2, ISSN 1311-3321, pp.8-12, Ruse / Bulgaria;

[5] Constantinescu D. M., Badescu M., Boruz S., (2009), Actualities and perspectives of clean energy using in agricultural. Case study. *INMATEH - Agricultural Engineering*, Vol.28 (2), pp.139–145, Bucharest / Romania;

[6] Esen M., Yuksel T., (2013), Experimental evaluation of using various renewable energy sources for heating a greenhouse. *Energy and Buildings,* Vol. 65, pp. 340-351;

[7] Kolev Z., Zlatev P., Mushakov P., Bobilov V., (2015), Research on the heat exchange parameters of water-air convector in laboratory heat pump installation. *Proceedings of University of Ruse*, volume 54, series 1.2, ISSN 1311-3321, pp. 111-115, Ruse / Bulgaria;

[8] Kolev Z., Zlatev P., Mushakov P., Bobilov V., (2015b), Methodology for determining heat exchange parameters of water-air convector in laboratory heat pump installation. *Proceedings of University of Ruse*, volume 54, series 1.2, ISSN 1311-3321, pp. 101-105, Ruse / Bulgaria;

[9] Kurpaska S., (2011), Utilisation of low temperature heat in agriculture using heat pumps – current state and prospects. *Agricultural Engineering* 7(132), pp. 65 – 72, Institute of Agricultural Engineering and Informatics, University of Agriculture in Krakow / Poland;

[10] Russo G., Anifantis A., Verdiani G., Mugnozza G., (2014), Environmental analysis of geothermal heat pump and LPG greenhouse heating systems, *Biosystems Engineering,* Volume 127, pp.11-23, https://doi.org/10.1016/j.biosystemseng.2014.08.002;

[11] Yang S., Rhee J., (2013), Utilization and performance evaluation of a surplus air heat pump system for greenhouse cooling and heating, *Applied Energy*, Vol. 105, pp. 244-251.

MODELLING THE WORK OF CLOSED SYSTEM OF HEATING AND VENTILATION OF GREENHOUSES
/
МОДЕЛЮВАННЯ РОБОТИ ЗАМКНУТОЇ СИСТЕМИ ОПАЛЕННЯ І ВЕНТИЛЯЦІЇ ТЕПЛИЦЬ

Doctor of Engineering Science Golub G.A.[1], Ph.D. Eng. Kepko O.I.[2]
[1]National University of Life and Environmental Sciences of Ukraine, Kyiv / Ukraine,
[2] Uman National University of Horticulture, Uman' /Ukraine
Tel: +380630499929, *E-mail kepko@meta.ua*

Keywords: *closed system of ventilation, energy preservation, greenhouses*

ABSTRACT
A simulation mathematical model is proposed for the analysis of energy intensity of mushrooms production and greenhouse plants in the closed system of heating and ventilation of greenhouses of the type "plant greenhouse - mushroom greenhouse".

РЕЗЮМЕ
Запропоновано статична математична модель для аналізу енергоємності виробництва грибів і тепличних рослин в замкнутій системі опалення і вентиляції теплиць типу "рослинна теплиця - грибна теплиця".

INTRODUCTION
Vegetable production in the greenhouses is connected with significant energy expenses to heat the incoming air and necessity for its saturation with carbon dioxide for plant greenhouses and with oxygen for mushroom greenhouses, so reducing the energy intensity of production is especially important for greenhouses *(Blasco X. et al, 2007; Kozhukhov V.A. et al, 2009; Golub G.A., 2010; Bakanova S.V., Haryna A.A., 2014; Demiynenko Y. et al., 2016)*.

This problem can be solved by using closed system of ventilation *(The request №3-65929; Copyright certificate of USSR №950241; Girchenko M. et al, 2003)*, which uses the opposite principle of plants and mushrooms respiration *(Grodzynsky D., 1982; Tkachenko V.A., Kondratiuk O.V., 2009)*.

In order to improve the energy efficiency in the greenhousesby using a closed system of ventilation, that allows the simultaneous growing of plants and mushrooms, we must organize the flow of air, saturated with carbon dioxide from the mushroom spawn in the plant greenhouse, and enriched with oxygen in the mushroom spawn. Substantiation of operating modes of such systems will provide their effective use in the production.

The nature and duration of transitional processes in the greenhouses at high production volumes require their modelling for the evaluation of the object in any area of the transitional process *(Horobets V.H., Yatsenko O.V., 2014; Dudnyk A.O., 2014)*. This question is particularly relevant for closed systems of ventilation, because of their complexity.

Let us consider fig. 1 showing a closed heating and ventilation system as an object of mathematical modeling. Accepted limitation: the apparent stream of heat from the substrate is constant; evaporation from a wetted surface does not depend on temperature. Also adopted assumptions: CO_2 in the outside air and the air coming from the adjacent greenhouses during the ongoing transition process; the outside temperature during transients is constant; air density does not depend on the temperature and pressure inside the room; moving of the air in the room is not included. We distinguish two main components of the model - the heat balance and gas balance.

MATERIAL AND METHODS
Due to the fact that plant and mushroom greenhouses are connected by a common ventilation system, the heat balance of greenhouses will be in the form of the set of equations (1), kW.

$$\begin{cases} -Q_{O.H.1} - Q_{hv.1} + Q_{hl.1} - Q_{if.1} + Q_{fe.1} = 0 \\ -Q_{O.H.2} - Q_{hv.2} + Q_{hl.2} - Q_{if.2} + Q_{fe.2} = 0, \end{cases} \tag{1}$$

Where:

$Q_{O.H.}$ is the general heat input to the room;

Q_{hv} is the capacity of the heating and ventilation system;

$Q_{hl}$is the capacity of heat losses;

Q_{if} is the flow of heat from input air;

Q_{fe} is the flow of heat from outlet air;

1 is the mushroom greenhouse; *2* is the plant greenhouse.

In the real conditions when growing the greenhouse crops, the air exchange in the room is actually different. It is also necessary to consider that in the air, during its circulation, contaminants accumulate in the closed system. Therefore, a mathematical model must take into account the air exchange with the external environment.

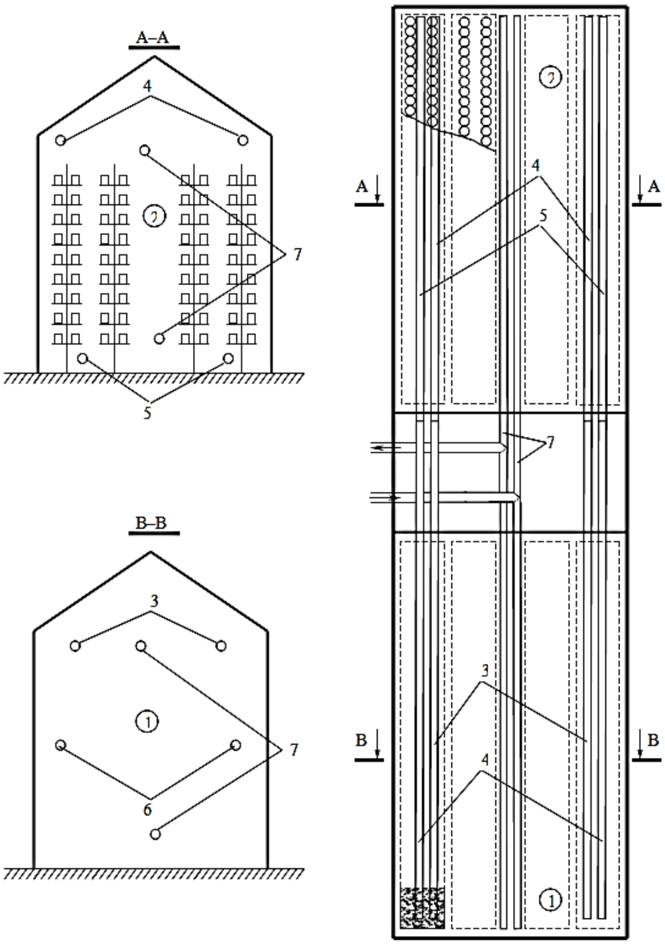

Fig. 1 - The layout of closed system of ventilation

1 - plant greenhouse; 2 - mushroom greenhouse; 3 - air ducts of intake air enriched with O_2; 4 - air ducts of input air enriched with O_2; 5 - air ducts of intake air enriched with CO_2; 6 - air ducts of input air enriched with CO_2; 7 - air ducts of air exchange with the external environment

Let us suppose that due to the technological requirements the air exchange in the rooms $G_{M.1}$ and $G_{M.2}$ is different - in the mushroom room, it is higher, but in the plant room, it is lower. Then, there is an excess of G_M in the first room, on the basis of which it is necessary to organize the air exchange with the external environment. In this case, after mathematical transformations we get the set of equations:

$$\begin{cases} -Q_{O.H.1} - Q_{hv.1} + Q_{hl.1} - c_p \cdot [G_{M.1.1}(t_{ai.2} - t_{в.1}) + G_{M.1.2}(t_{ae} - t_{ai.1})] = 0 \\ -Q_{O.H.2} - Q_{hv.2} + Q_{hl.2} - c_p \cdot G_{M.1.1} \cdot (t_{ai.1} - t_{ai.2}) = 0 \end{cases} \quad (2)$$

where:

$G_{M.1.1}$is the air exchange between the greenhouses (kg/s);

$G_{M.1.2}$is the air exchange with the external environment (*kg/s*);

t_{ai} is the air temperature in the greenhouse (°*C*);

t_{ae} is the outdoor air temperature (°*C*).

RESULTS

This is an example of using the simulation model (2) to determine the air exchange in the experimental greenhouse, where oyster mushroom was grown in the mushroom greenhouse and the leek in the plant greenhouse. The calculation was made for the winter period (t_{ae}=*-15 °C*, t_{ai1} = *16 °C*, t_{ai2} = *14 °C*).

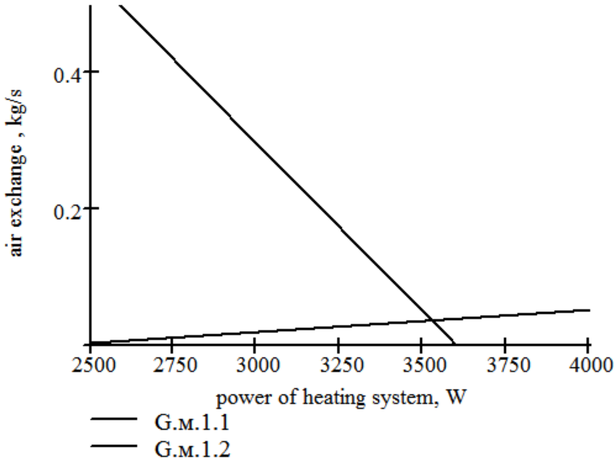

Fig. 2 - The dependence of the air exchanges on the capacity of the heating system

The example of the use of simulation model for determining the temperature is shown in Figure 3, (t_{ae} = *- 15 °C*, $G_{M.1.1}$ = *0.0346 kg/s*, $G_{M.1.2}$ = *0.0194 kg/s*).

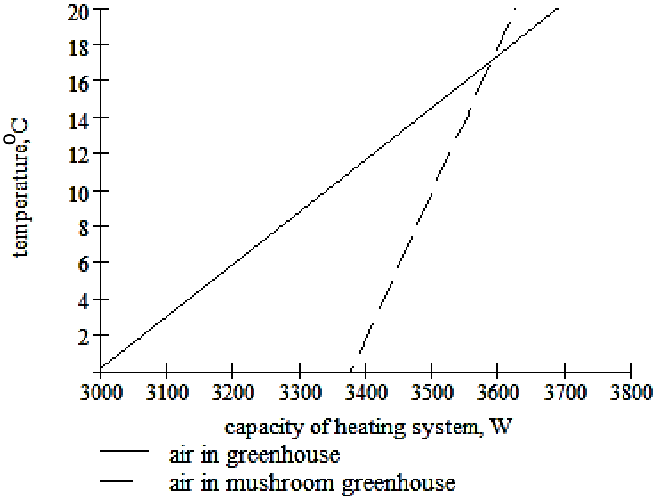

Fig. 3 - The dependence of the air temperature in the plant and mushroom greenhouses depending on the capacity of heating system

In fig.1 and fig.2 we can see that while reducing the capacity Q_{hv2}, the air exchange between the rooms $G_{M.1.1}$ increases and the exchange with the external environment $G_{M.1.2}$ is reduced, but the temperature in the plant and mushroom greenhouses goes down. Thus, the amount of air exchange and the room temperature can be controlled by changing the capacity of the heating system of the mushroom spawn.

Figure 4 shows the comparative dependence of total capacity of the open-loop and closed-loop system from the temperature of external environment, according to given example. For example, the heating capacity of closed system reduces to 1160 W (13%) at the outdoor temperature -15°C, by comparison with the open-loop system.

The heating capacity of closed heating and ventilation system of greenhouses reduces to 12.7–20.5% in the range of external temperature from – 20°C to+ 14°C.

The air-exchange with CO_2 in closed heating and ventilation systems in greenhouses is of great interest *(Pukhalskaia N.V., 2000; Bohdanov K.B., Uskov E.Y., 2005).*

For example, let us consider a system of “vegetable greenhouse-mushroom greenhouse” facilities, making assumption that the density of the air outside and inside is the same and does not change over time.

In this case, the system takes the form of the following equations:

$$\begin{cases} L_c^1 + L_{zv}^1 C_{zv} = L_v^1 C_v^1 \\ -L_c^2 + L_{zv}^2 C_{zv} = L_v^2 C_v^2 \end{cases} \quad (3)$$

Where:

L_C - consumption of CO_2, which is produced in the premises as a result of the process, ltr/sec;

L_{zv}, L_v - volumetric stream rate, respectively, outside and inside air, m^3/sec;

C_{zv}, C_v - respectively, concentration of CO_2 in the outside and inside air, ltr/m^3.

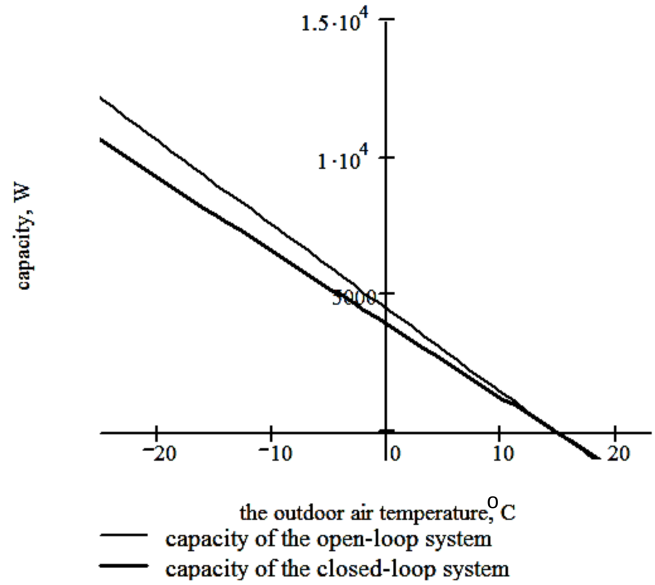

Fig. 4 - The dependence of heating system capacity on the outdoor air temperature

It is well-known that fungi respiration rate is higher, therefore there is an excess of CO_2 in the first room; in this case, air-exchange system should be based on mushroom greenhouse. After mathematical transformations, we form the following system:

$$\begin{cases} L^1_{\tilde{N}} + L^1_{PP^3} - L^1_{VP^3} + L^1_{PP.1.1} - L^1_{VP.1.1} + L^1_{PP.1.2} - L^1_{VP.1.2} = 0 \\ -L^2_{\tilde{N}} + L^2_{VP^3} - L^2_{VP^3} + L^2_{PP.1.1} - L^2_{VP.1.1} = 0 \end{cases} \quad (4)$$

Where:

$L_C = L_{CO2\ gr} \cdot m_C$ – CO_2 stream from substrate, m^3CO_2/h.;

$L_{PP\ 1.2} = C_{air} \cdot L_{M.1.2} \cdot m_C$ – carbon dioxide stream with tidal ventilation air, m^3 CO_2/h.;

$L_{VP1.2} = C_{gr} \cdot L_{M.1.2} \cdot m_C$ - carbon dioxide stream with blown off ventilation air m^3 CO_2/h.;

$L_{PPi} = C_{air} \cdot L_{infilt} \cdot m_C$ - carbon dioxide stream with tides of infiltrated air, m^3 CO_2/h.;

$L_{pp\ 1.1} = Cm\ L_{m1.1} \cdot m_c$ – carbon dioxide tidal stream from a greenhouse, m^3 CO_2/h.;

$L_{vp\ 1.1} = C_{gr} \cdot L_{M.1.1} \cdot m_C$ – carbon dioxide stream with incoming fresh air into a greenhouse, m^3 CO_2/h.; infiltration air-exchange, m^3-h · kg substrate mass;

$L_{M1.1}$ – air-exchange between rooms, m^3/h · kg;

$L_{M1.2}$ – air-exchange with outside surroundings, m^3/h · kg;

$L_{CO2\ gr}$ - carbon dioxide evaporation per 1 kg of substrate mass, m^3 CO_2/h· kg;

C_m – carbon dioxide concentration in tidal air, m^3 CO_2/m^3;

C_{gr} – carbon dioxide concentration in a mushroom greenhouse, m^3 CO_2/m^3;

m_c – substrate mass in kilograms.

Such a model helps determine the value of air between rooms and different environment, different values at different CO_2 concentration in a greenhouse or concentrations of carbon dioxide in areas with known values of air-exchange. If relevant changes and amendments are made, other parameters of the system can be determined.

The simulation model of the system (4) is used to determine the air-exchange when an experimental oyster mushroom is grown in an experimental room, and a hastening crop in a vegetable greenhouse - scallion, shown in Fig. 5, where the curve $L_{M.1.1}$– is the air-exchange between rooms and $L_{M.1.2}$–the air exchange with the environment. Calculations are made for winter period when the outdoor temperature $t_{outdr} = -15\ C^o$ and indoor air temperatures in a mushroom greenhouse $t_{indr}=16\ C^o$ and the greenhouse $t_{indr2} = 14\ °C$. By setting different values of CO_2 concentration in the greenhouse at a constant value of mushroom greenhouse concentration, the value of air exchange can be defined $L_{M.1.1}$ and $L_{M.1.2}$.

Fig. 5 clearly shows that by increasing concentration of CO_2 in the greenhouse, the air-exchange between rooms increases, while the air-exchange between mushroom greenhouse and outside environment decreases. In case we change the concentration of CO_2 in the mushroom greenhouse and its constant value in the greenhouse, we have the curves shown in Fig. 6.

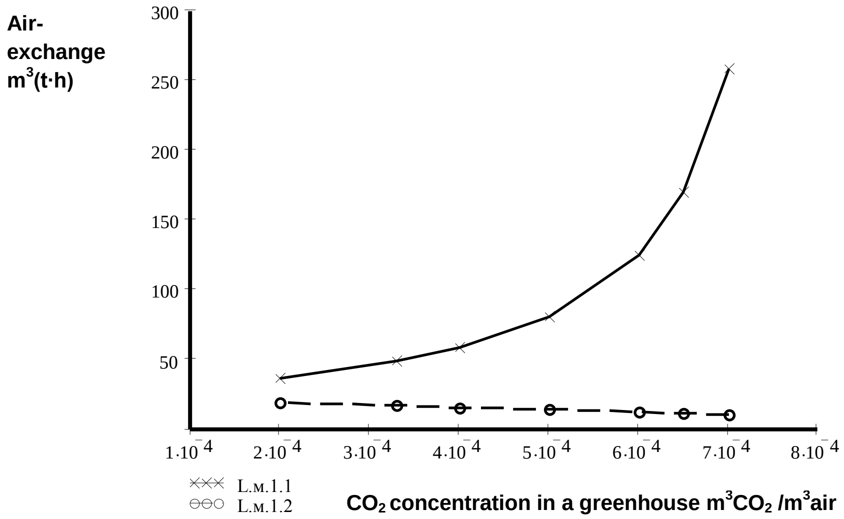

Fig. 5 - The relevance of air-exchange to CO_2 concentration in a greenhouse at C_{msh}= 0.0008 m^3 CO_2 / m^3_{air}

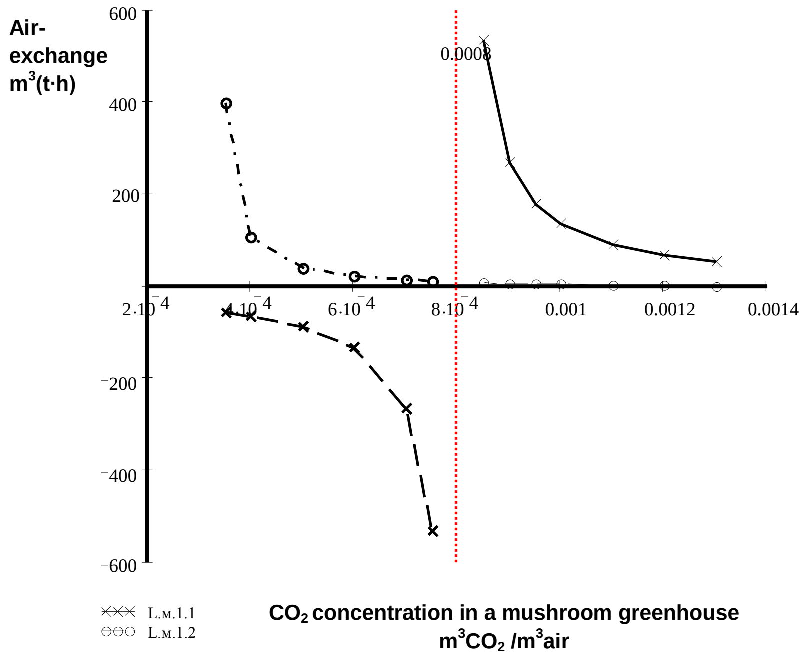

Fig. 6 - The relevance of air-exchange and concentration of CO_2 in the mushroom greenhouse at C_{wrth} = 0.0008 m^3CO_2 / m^3air

As shown in the graph (Fig. 6) the air exchange with the environment is reduced because of increasing the concentration of carbon dioxide in the mushroom greenhouse. At the same time, when the concentration is CO_2 = 0.0008 m^3CO2/m^3 air, the direction of air movement between rooms is changed and when the concentration is bigger than 0.0008 m^3CO_2/m^3 air, it takes the direction from the mushroom greenhouse to the greenhouse.

It quite clear, that the left part of the chart is irrelevant, due to the stated concentration of CO_2 (in our case: 0.0008m^3CO_2/m^3 air) as there is no need to direct the stream of CO_2 from the greenhouse to the mushroom greenhouse (in which carbon dioxide is consumed).

CONCLUSIONS

The research conducted by using simulation mathematical model of air exchange system shows that the highest efficiency of system work is at low temperature of outdoor air and at extremely large temperature difference in the greenhouses.

In terms of observing gas balance of a closed system, it must be included into the work to achieve accepted concentration value in one of the rooms. This condition can fail if the system is working and / or on thermal balance.

REFERENCES

[1] Bakanova S.V., Haryna A.A. (2014), Air heating greenhouses (Воздушноеотоплениетеплиц), *Penza State University of Architecture and Construction*, pp. 41-43, Russia;

[2] Blasco X. et al, (2007), Model-based predictive control of greenhouse climate for reducing energy and water consumption, *Computers and Electronics in Agriculture*, Volume 55, Issue 1, pp.49-70;

[3] Bohdanov K.B., Uskov E.Y., (2005), Ways to use carbon dioxide (CO_2) in the agricultural sector (Способы использования диоксида углерода (CO_2) в агропромышленном комплексе), *The role of the agricultural mechanics in the social development of society. Collection of scientific reports of the international Internet conference*, Volume 1, NSC UIMESKH, p.204, Kiev;

[4] Demiynenko Y., Gogol N., Martynovskyi V.S., (2016), The expediency of the heat pumps use for greenhouses heating, International conference "*Energy of Moldova regional aspects of development*" 29 September – 01 October, 2016, Chisinau, Moldova, *Educational & Scientific Institute of Cold, Cryotechnologies and Environmental Energy*, Odessa National Academy of Food Technologies, Odessa / Ukraine;

[5] Dudnyk A.O., (2014), Synthesis and research of mathematical models of energy costs for heating greenhouses in winter (Синтез та дослідження математичних моделей витрат енергоресурсів на опалення теплиць у зимовий період), *Scientific Journal NULiE Ukraine*, *Series: Engineering and Energy Agriculture*, № 194;

[6] GirchenkoM., GolubH., ZhorovV., Vdovenko, S., KepkoO., &Shapovalov L. (2003), The method of ventilation of closed soil structure (Спосіб вентиляції споруд закритого грунту)), *Patent No. 57956A*, Ukraine;

[7] Golub G.A., (2010), Energy autonomy of agricultural systems (Енергетична автономність агросистем), *Journal of agricultural science*, no.3, pp. 50-54, Kyiv;

[8] Grodzynsky D., (1982), Biophysics of plants (Биофизика растений), *Naukovadumka*, Kiev, pp.256, Ukraine;

[9] Horobets V.H., Yatsenko O.V., (2014), Creation of a heating system and a mathematical model of heat and mass transfer in greenhouses using alternative sources of energy (Розробка системи опалення та математичної моделі процесів тепло- і масопереносу в теплицях з використанням альтернативних джерел енергі), *Energy and Automation*, №1, National Agriculture University of Ukraine;

[10] Kozhukhov V.A., Mikheev N.B., Semenov A.F., (2009), Increase of greenhouse power supply efficiency, (Повышение эффективности энергообеспечения теплицы), *Bulletin of the Krasnoyarsk State Agrarian University*, № 6;

[11] Pukhalskaia N.V., (2000), Physiology fertilizing carbon dioxide in greenhouse horticulture (Физиология углекислотных подкормок в тепличном овощеводстве), *Ahrokonsalt*, Moscow;

[12] Tkachenko V.A., Kondratiuk O.V., (2009), Heating greenhouses Hangar (Системи опалення ангарних теплиць), *Ventilation, lighting and Heat,* Vol. 13, Kyiv National University of Construction and Architecture;

[13] *** Copyright certificate of USSR №.950241, (1982), *The greenhouse with artificial environment Теплица с искусственным микроклиматом)*;

[14] *** The request №3-65929, *Equipment for plant growing,* Japan (JP).

STRUCTURAL OPTIMIZATION OF A HANDHELD TILLER HANDRAIL BY VIBRATION MODAL ANALYSIS
/
基于振动模态分析的微耕机扶手架结构优化

Ph.D. Niu P.[1)], Prof. Yang M.J.*[1)], Prof. Chen J.[1)], Ph.D. Yang L.[1)], Prof. Xie S.Y.[1)], Prof. Chen X.B.*[2)]
[1)] Southwest University, College of Engineering and Technology, Chongqing Key Laboratory of Agricultural Equipment for Hilly and Mountainous Regions / P. R. China;
[2)] Agricultural Machinery Quality Control and Inspection Technology Centre, Nanjing Research Institute for Agricultural Mechanization Ministry of Agriculture / P. R. China
Tel: 8613883002509; E-mail: ymingjin@swu.edu.cn; chxibi@126.com

Keywords: *structural optimization, vibration modal analysis, handrail, handheld tiller*

ABSTRACT
Exposure to severe vibration while tilling presents a serious health and safety risk to a handheld tiller operator. Handrail of the tiller transfers vibration from tiller to operator with an essential extent. Taking handrail of Shineray SR1Z-80 tiller as a case study, its vibration characteristics were investigated by means of Computational Modal Analysis and Experimental Modal Analysis, resulting in good agreement on natural frequency and mode shape within interested frequency range of the vibration, and the average relative error of natural frequency between them is less than 4%. Handle, rod and cross bar are main sections of the handrail that affect the vibration with decreasing level of influence regarding displacements. Structural optimization of the handrail was obtained by orthogonal factorial experiment design technique and statistical analysis of variance. The optimal dimensions of the handrail are handle length 170 mm, rod length 470 mm, and cross bar length 390 mm.

摘要
耕作时的强烈振动对微耕机操作者造成严重的健康和安全危险。其中大部分的振动由扶手架传递给微耕机的操作者。本研究以鑫源 SR1Z-80 微耕机的扶手架为例，通过计算模态分析和试验模态分析研究了其扶手架的振动特性。在关注的频率段内，两种模态分析方法得到的扶手架固有频率和模态振型一致性很好，其中固有频率的相对误差小于 4%。扶手、扶手杆和横杆是影响扶手架振动性能的主要部分，他们对振动的影响程度（位移）依次降低。通过正交试验设计和方差分析，得到了扶手架的优化结构，其对应的优化尺寸参数为：扶手长度 170mm，扶手杆长度 470mm，横杆长度 390mm。

INTRODUCTION

Handheld tillers are typically propelled forward by the diesel or gasoline engine rotating rotavators and the power of the engine is normally less than 7.5 kW. The handheld tillers are widely used in hilly lands, greenhouses and orchards, due to their advantages of small volume, light weight, simple structure and easy transfer in the farm land. But for a handheld tiller, the connections between subsections (e.g. engine and transmission, transmission and frame, transmission and handrail, etc.) are rigid, thus operators are wholly exposed to severe vibration transmitted directly to their hands. Resulting from the engine, tilling rotavators and their coupling, the vibration is often pretty complex, contains many frequencies, occurs in several directions and changes over time, and it may cause injuries to sensory nerves, the vascular, muscles, bones and joints, influence the operators' performance capability, or present a serious health and safety risk to the operators *(Su et al., 1989)*. Under usual working conditions, in 10% of the exposed operators, vascular disorders of the hand, namely "vibration white finger", can appear after three years of continuous use of handheld tillers *(Ragni et al., 1999)*.

Many scholars studied the vibration characteristics of a handheld tiller handrail for better comfort level while operating. Goglia *et al.* (2004) studied the vibration of a small agricultural tractor transmitted to the driver's hands and body during work.

The transfer mechanism and the effects of vibration transmitted were analysed. *Li et al*. (2016) measured the acceleration at the handles of a handrail and engine cover along different directions under four working conditions, namely no-load idle speed, no-load half-throttle, no-load full throttle, and field operation full throttle. Yang and Meng (2005) employed the virtual prototype technology to study the vibration of the

GN31 cultivator and found that the vibration at the handles were reduced effectively by adding an object (1.5-3.0 kg) to the handrail-rod near the handrail cross-bar, with 79%-88% maximum acceleration reduction. Ying *et al.* (1994) designed a rubber vibration absorber on the handles of GN-5 walking tractor by increasing the damping and decreasing the vibration transmission. The vibration absorber reduced the acceleration by 41.1% and prolonged the tolerable time of daily exposure to vibrations by 126.4%. Yang (2005) developed a vibration isolation handle for the small-sized tiller on the basis of vibration mechanism, with 50%-80% reduction of vibration transmitted to the handle.

Currently, most studies of the vibration while tilling are focused on observation, evaluation and influence of vibration on the operators, etc., and the study on the handrails ergonomics is insufficient to provide the required information so as to decrease their vibration sensitivity and to improve tilling operation comfort. Taking the handrail of an SR1Z-80 handheld tiller as a case study, on the basis of vibration characteristics analysis and the corresponding statistics analysis of the handrail, structural optimization of the handrail was conducted, so as to provide available design theory and reference to develop new high quality tillers with features of high efficiency, low labour intensity, and good operation comfort.

MATERIAL AND METHODS

The SR1Z-80 handheld tiller was manufactured by Chongqing Shineray Agricultural Machinery Co., Ltd. The vibration characteristics of its handrail were studied by means of Computational Modal Analysis and Experimental Modal Analysis. The model parameters of these two modal analyses such as natural frequency and mode type were compared and validated. The optimal structure parameters were obtained by orthogonal factorial experiment design technique and statistical analysis of variance. The outline of the study was shown in fig. 1.

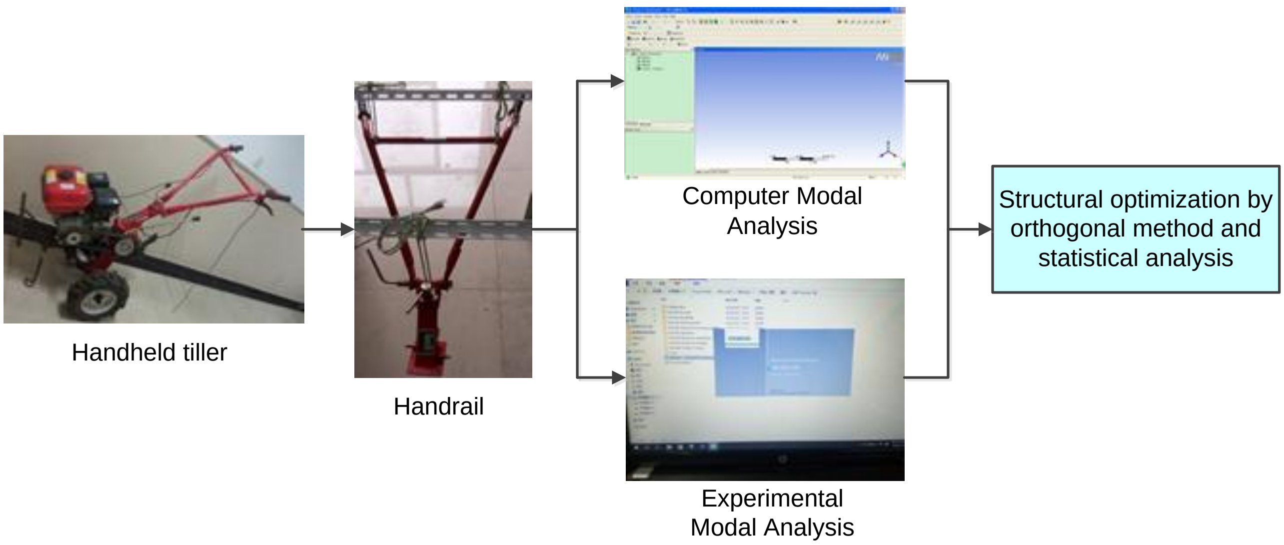

Fig. 1 - Outline of the study

Computational Modal Analysis

FEM model of the handrail

According to practical structure and parameters of handrail of the SR1Z-80 handheld tiller, the 3-D parametric solid model of the handrail was built in UG software package, as shown in fig. 2(a).

Import the solid model into ANSYS Workbench. By considering the effect of small sub-sections, such as chamfers, threads, etc. which were subjected to small forces during operation, on the meshing and solving of the handrail FEM model, some simplifications were made for the solid model. Then, the simplified 3-D model was obtained, as shown in fig. 2(b).

As triangle meshes have good performance for the vibration analysis, triangle meshing scheme was employed to mesh handrail of the tiller by automatic meshing method, with mesh size 3 mm. There are 51628 nodes and 27032 elements for the meshed handrail.

Handrail parameters were defined, as shown in table 1. Behaviour of handrail contact surface was defined as bonded. Then, the handrail FEM model was obtained, as shown in fig. 2(c).

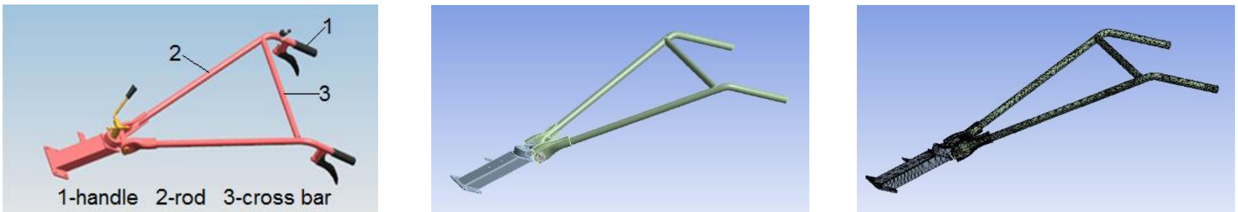

(a) 3-D model **(b) Simplified 3-D model** **(c) FEM model**

Fig. 2 - Finite element model of the handrail

Table 1

Parameters of the handrail

Material	Density/kg.m^{-3}	Poisson's ratio	Elastics modulus/Pa	Contact
Steel Q235	7.83e3	0.35	2.07e11	Bonded

Modal Analysis

The modal analysis was performed in Ansys Workbench. No constraints or loads were applied to FEM model for Computational Modal Analysis, namely a free modal analysis approach was employed to determine the vibration characteristics (natural frequencies and mode shapes) of the handrail. Frequency range from 2 Hz to 200 Hz was focused on for the analysis, with weighting factor W_h greater than 0.1 within the frequency range (the frequency-weighting characteristic for hand-transmitted vibration W_h reflects the assumed importance of different frequencies in causing injury to the hand).

In panel Details of “Analysis Settings”, specify Range Minimum and Range Maximum as 2 Hz and 200 Hz, respectively. Keep default option of “Solver Type” as “Program Controlled”. Then the modal analysis is available for carrying out. The qualified natural frequencies of different modes, non-rigid body modes, and the corresponding mode shapes were obtained. According to the modal analysis, there are 5 non-rigid body modes within the frequency range focused on.

Experimental Modal Analysis

Experiment setup

As the handrail was simple in structure and light in weight, it was hung by an elastic polyamide rope with 8 mm diameter for the experiment setup as shown in Fig. 3. Main equipment and instruments components were as follows: modal force hammer 086C03 of sensitivity 2.335 mV/N and sensor 356A16 of sensitivity 98.2mV/g, made by PCB Piezotronics, Inc., USA; signal analyser LMS SCADAS Mobile of 24 channels, made by SIEMENS, Germany.

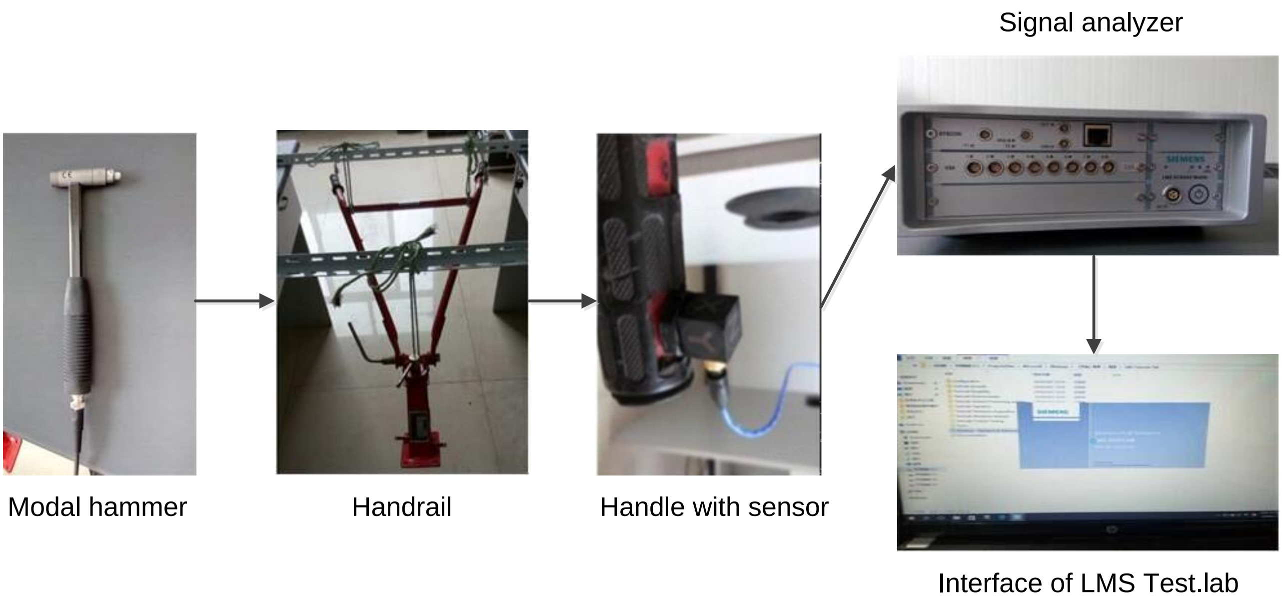

Fig. 3 - Experiment setup

Experiment procedure

According to exciting position sequences, information of 47 exciting points was defined in the testing system of the handrail investigated, by LMS Test.lab Impact Testing. The 3-D model of the handrail was built by combination of lines and surfaces determined by these exciting points in panel Geometry. Frequency 1024 Hz for the modal test was specified in panel Impact Scope. Driving points and average times for the exciting, trigger level, bandwidth, and window function were specified in panel Impact Setup through exciting trials, including auto-increment, roving hammer and auto reject with overload. The sensor locates at the 44th exciting point, and driving point starts from the first point and moves to the next sequentially, 5 times per driving point with 3-5 s intervals for the tapping excitation. Then, the frequency response function of each driving point can be obtained automatically in the LMS impact testing system.

Icons of Band, Stabilization, and Shapes are available for selection in panel PolyMax. Steady state diagrams were obtained after specification of frequency range by clicking the icon of Band, natural frequency characteristics were identified after enabling Automatic Modal Parameter Selection, Multivariant MIF or Complex MIF by clicking the icon of Stabilization, and the mode shapes of different order were obtained by clicking the icon of Shapes.

According to Modal Assurance Criterion (MAC) presented by West in 1986 *(Xiong, 2014)*, the values of MAC matrices were obtained by Auto-MAC method in panel Modal Validation. MAC is a dimensionless parameter, within a range of [0, 1]. The higher the MAC value, the greater the relevance.

Structural optimization

Experiment design

Orthogonal factorial experiment design technique based on Taguchi method was used to arrange experiments. Main control factors affecting vibration characteristics of the handrail were defined as follow: factor A: handle length; factor B: cross bar length; factor C: rod length. Levels of each control factor were shown in table 2. Experiments were designed in accordance with orthogonal array $L_9(3^4)$, a 3-level 4-factor array with 9 runs, and their arrangements were shown in table 3.

Table 2

Levels of control factor

Level	Handle length A /mm	Cross bar length B /mm	Rod length C /mm
1	170	390	470
2	200	420	520
3	230	450	570

Table 3

Experiment arrangements and results of natural frequency

No.	A	B	C	Blank column	Natural frequency /Hz
1	1	1	1	1	69.65
2	1	2	2	2	60.82
3	1	3	3	3	59.73
4	2	1	2	3	56.32
5	2	2	3	1	58.94
6	2	3	1	2	57.62
7	3	1	3	2	62.03
8	3	2	1	3	61.26
9	3	3	2	1	55.79

Optimization

Statistical analyses of range and variance were performed to obtain the impacts and their significance of each factor on the handrail vibration characteristics. Optimal engineering average was employed to obtain the optimal level combination of the control factors, and as a result, the structural optimization for the handrail was available.

RESULTS

Handrail vibration characteristics

The vibration characteristics (natural frequencies and mode shapes) of the handrail were obtained by means of Computational Modal Analysis and Experimental Modal Analysis.

Natural frequency

The natural frequencies of the non-rigid mode orders within the frequency range aforementioned were listed in table 4. As can be seen in the table, the natural frequencies by Computational Modal Analysis are in good agreement with those by Experimental Modal Analysis, with average relative error less than 4%. For the Experimental Modal Analysis, MAC values of each mode order are higher than 0.9, which shows that results by Experimental Modal Analysis are reliable. Therefore, Computational Modal Analysis can be used to analyse and optimize structure parameters of the handrail of a tiller from vibration characteristics.

Table 4

Comparison of natural frequency

Mode order	Natural frequency by Computational Modal Analysis /Hz	Natural frequency by Experimental Modal Analysis /Hz	Relative error /%
1	61.84	64.39	4.1
2	89.61	84.04	6.2
3	112.90	116.29	3.0
4	137.33	143.46	4.5
5	177.05	174.78	1.3

Mode shape

The mode shapes of the non-rigid mode orders within the frequency range can be extracted from results of Computational Modal Analysis and Experimental Modal Analysis, and animations of the vibration are also available. According to literature *(Zhou, et al., 1999)*, human hands are generally sensitive to vibration of frequency f_s about 50 Hz *(Wen, et al., 2002)*. Considering frequency range of (0.75-1.3) f_s, namely 37.5-65 Hz, human hands are relatively sensitive to the vibration within the range with respect to handrails of the small scale agricultural machinery. Because the natural frequency of the first non-rigid mode order of the handrail falls in the frequency range 37.5-65 Hz, only mode shapes of the first non-rigid mode order were extracted by Computational Modal Analysis and Experimental Modal Analysis, and their contours were shown in fig.4.

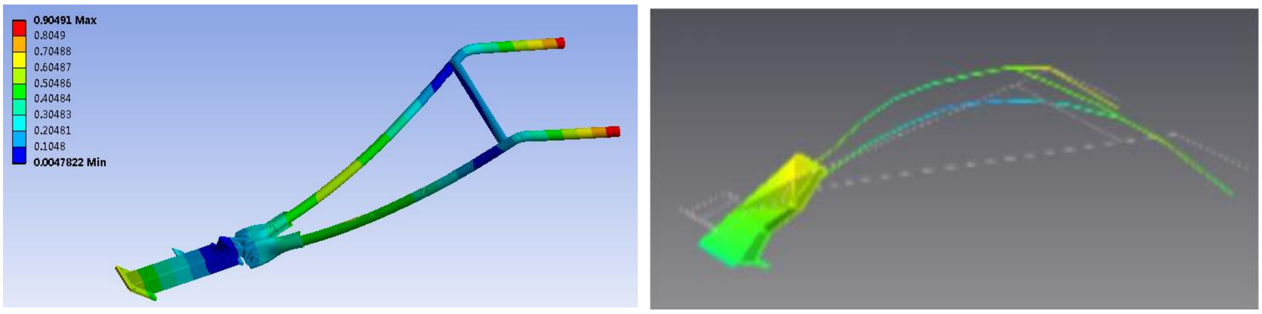

(a) Computational Modal Analysis **(b) Experimental Modal Analysis**

Fig. 4 - Mode shape of the first non-rigid mode order

From the vibration animations of the first non-rigid mode order, the handrail largely vibrates up and down. The maximum vibration is at handrail handle, with a displacement of 0.90491 mm, and the minimum vibration locates at connection part of the handle and cross bar, and at direction shift part of the handrail, with a displacement 0.0047822 mm, as shown in fig. 4 (a). The mode shape of the first non-rigid mode order from Computational Modal Analysis shows good agreement with that from Experimental Modal Analysis, as compared fig.4 (b) and fig.4 (a). Furthermore, the mode shapes of the other non-rigid mode orders within the frequency range also have agreement mutually.

Consequently, Computational Modal Analysis can well reveal vibration characteristics of the handrail, with small errors compared with Experimental Modal Analysis, and then it can be employed to analyse and optimize the structure of a handheld tiller handrail.

Structural optimization

As the natural frequencies of the first non-rigid mode order of the handrail fall in the frequency range 37.5-65 Hz, generally sensitive to human hands, the vibration characteristics of the first non-rigid mode order are necessary for the structural optimization, and it is better to shift the natural frequency of a handrail away from this frequency range for the comfortable reason to operators of the handheld tillers. The natural frequency results of the handrail first non-rigid mode order by Computational Modal Analysis were obtained as shown in table 3.

Statistical analyses of range and variance were performed to obtain the impacts and their significance of each control factor on the handrail natural frequency. Range analysis results were shown in table 5, and variance analysis results were shown in table 6. The values in cells of each level of the control factors in table 5 represent mean natural frequencies of the corresponding levels and factors. The delta values of each factor represent the biggest change of mean natural frequencies of the factor, namely the impact level of each factor. The numbers in the rank row indicate the impact significance of the control factors.

Table 5

Range analysis

Level	Factor A	Factor B	Factor C	Blank column
1	63.40	62.67	62.84	61.46
2	57.63	60.34	57.64	60.16
3	59.69	57.71	60.23	59.10
Delta	17.32	14.86	15.60	7.07
Rank	1	3	2	

Table 6

Variance analysis

Source of variance	Degree of freedom	Sum of squares	Mean sum of squares	*F*-ratio	Critical *F*-ratio
Factor A	2	51.34	25.67	6.14	$F_{0.25}(2,2)=3.0$
Factor B	2	36.85	18.42	4.41	$F_{0.10}(2,2)=9.0$
Factor C	2	40.56	20.28	4.85	
Blank Column	2	8.36	4.18	Error	
Total	8	137.11			

Range analysis and variance analysis shows that: factor of handle length has the highest significant impact level on handrail natural frequency and it is followed by factors of rod length and cross bar length, sequentially. The *F*-ratio of each control factor was compared to a critical value corresponding to a certain pre-selected probability, resulting in probabilities of 86.0%, 81.5% and 82.9% that control factors are in fact due to chance because of handle length, cross bar length, and rod length, respectively.

According to optimal engineering average strategy *(Wang, 2004)*, $A_1B_1C_1$ is the optimal level combination of the control factors that benefits to the handrail vibration characteristics and it shifts the natural frequency away from the frequency range 37.5-65 Hz.

Vibration characteristics of the optimized handrail

The parameters of the optimal level combination of $A_1B_1C_1$ are as follows: handle length 170 mm, cross bar length 390 mm, and rod length 470 mm. According to the national standard of the People's Republic of China (GB10395.10-2006), the parameters of the handrail optimal level combination qualify for the technical means for ensuring safety of walk-behind powered rotary tillers.

By Computational Modal Analysis, the mode shape of the first non-rigid mode order of the optimized handrail was obtained, as shown in fig.5. The natural frequency of the first non-rigid mode order is 69.65 Hz, and the maximum displacement and minimum displacement are 0.82063 mm and 0.0017485 mm, respectively, which shows good improvement in vibration characteristics compared to the original handrail.

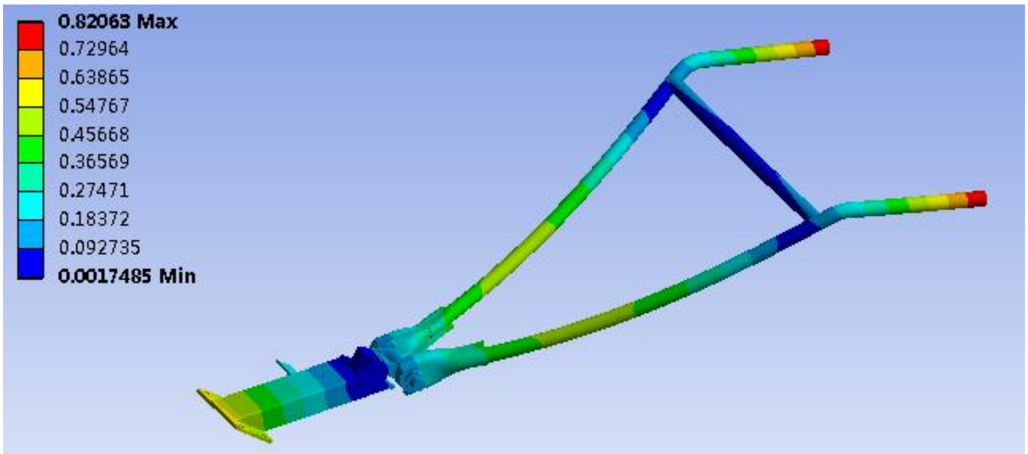

Fig. 5 - Mode shape of the first non-rigid mode order of optimized handrail

CONCLUSIONS

Hand-transmitted vibration presents a serious health and safety risk to operators of handheld tillers. Taking handrail of SR1Z-80 tiller as a case study, the vibration characteristics were investigated by means of vibration modal analysis. Structural optimization of the handrail was obtained by orthogonal factorial experiment design technique and statistical analysis. The main conclusions are as follows:

(1) Modal analysis can well reveal vibration characteristics (natural frequency and mode shape) of the handrail. The natural frequencies by Computational Modal Analysis are in good agreement with those by Experimental Modal Analysis, with average relative error less than 4%.

(2) Handle length has the highest significant level of impact on natural frequency of the handrail, and it is followed by rod length and cross bar length, sequentially. Their probabilities in fact due to chance are 86.0%, 82.9%, and 81.5%, respectively.

(3) The handrail optimal dimensions are handle length 170 mm, rod length 470 mm, and cross bar length 390 mm. The optimized handrail shows good improvement in vibration characteristics compared to the original handrail: natural frequency of the first non-rigid mode order 69.65 Hz, maximum displacement 0.82063 mm, and minimum displacement 0.0017485 mm.

ACKNOWLEDGEMENT

The study was funded by the National Natural Science Foundation of China (No. 51475385), Chongqing Science and Technology Commission (CSTC2016SHMSZX80037), Ph.D. Research Project of Southwest University (SWU115011), and Fund from Key Laboratory of Modern Agricultural Equipment, Ministry of Agriculture, P. R. China (201601001).

REFERENCES

[1] Goglia V., Gospodaric Z., Beljo-Lucic R, (2004), Vibration transmitted to small agricultural tractor driver. *Actual Tasks on Agricultural Engineering*, issue 4, pp. 23-27;

[2] Li G., Chen J., Xie H.J., and Wang, S.M, (2016). Vibration test and analysis of mini-tiller, *International Journal of Agricultural and Biological Engineering*, vol. 9, issue 3, pp.97-103;

[3] Li G., Chen J., Xie H.J., and Wang, S.M, (2016). Vibration test and analysis of mini-tiller, *International Journal of Agricultural and Biological Engineering*, vol. 9, issue 3, pp.97-103;

[4] Ragni L., (1999), Vibration and noise of small implements for soil tillage. *Journal of Agricultural Engineering Research*, issue 4, pp.403-409;

[5] Xiong F., Zou X.H, Shi X.H., Chang, S.L., (2014), Numerical simulation and test research on modal characteristics of motorcycle frame (摩托车车架模态特性数值模拟与试验). *Journal of Chongqing University of Technology (Natural Science),* vol. 28, issue 7, pp.15-20;
[6] Su Q.Z., Zhang Y.L., Xu Q., (1989), Dynamic modification applied to the design of a walking tractor handle (手扶拖拉机扶手架的减振设计). *Transactions of The Chinese Society of Agricultural Machinery*, issue 4, pp.9-14;
[7] Wang W.Z., (2004), Design of experiments and analysis (试验设计与分析), *Higher Education Press*, P. R. China;
[8] Wen B.C., Liu S.Y., (2002), Mechanical vibration theory and dynamic design method (振动机械的理论与动态设计分析), Mechanical industry press, P. R. China;
[9] Yang J., Meng X.W., (2005), Study on vibration mechanism and measures for vibration reducing to the handle of cultivator by virtual prototype technology (耕整机扶手架振动机理及减振措施的虚拟研究). *Transactions of the Chinese Society of Agricultural Machinery*, vol. 36, issue 2, pp.39-42;
[10] Yang X.L., Yang J., Dong Y., Meng X.W., (2005), A study on vibration mechanism of the cultivator handle by virtual prototype technology (耕整机扶手架振动机理的虚拟研究), *Journal of Agricultural Mechanization Research,* issue 6, pp.106-108;
[11] Ying Y.B., Zhang L.B., Dong M.D., Xu F., (1994), Study on absorber of vibration transmitted by walking tractor handles (手扶拖拉机手把减振装置的研究), *Transactions of the Chinese Society of Agricultural Engineering*, issue 4, pp.74-79;
[12] Zhou Y.M., Mao S.R., (1999), *Vehicle Ergonomics (车辆人机工程学)*, Beijing Institute of Technology Press, P. R. China;
[13] ***Ministry of Industry and Information Technology of the P. R. China, (2013), JB/T 10266-2013. Handheld Tiller (JB/T 10266-2013, 微型耕耘机). China Standards Press, P. R. China;
[14] ***Chinese Academy of Agricultural Mechanization Sciences, (2007), Agricultural machinery design manual (农业机械设计手册), China Agricultural Science and Technology Press, P. R. China;
[15] ***Chinese Standard Committee, (2006). GB10395.10-2006, Tractors and machinery for agriculture and forestry-Technical means for ensuring safety-Part 10: Walk-behind powered rotary tillers (GB10395.10-2006, 农林拖拉机和机械安全技术要求 第 10 部分: 手扶 (微型) 耕耘机). China Standards Press, P. R. China;
[16] ***ISO Copyright Office, (2001), ISO 5349-1:2001(E), Mechanical vibration-measurement and evaluation of human exposure to hand-transmitted vibration - Part 1: General requirements. Printed in Switzerland.

A THEORETICAL RESEARCH OF THE GRAIN MILLING TECHNOLOGICAL PROCESS FOR ROLLER MILLS WITH TWO DEGREES OF FREEDOM
/
ТЕОРЕТИЧНЕ ДОСЛІДЖЕННЯ ТЕХНОЛОГІЧНОГО ПРОЦЕСУ ПОДРІБНЕННЯ ЗЕРНА У ВАЛЬЦЕВИХ СТАНКАХ З ДВОМА СТУПЕНЯМИ ВІЛЬНОСТІ

Prof. PhD. Eng. Bulgakov V.[1], Prof. PhD. Eng. Holovach I.[1], Prof. PhD. Eng. Bandura V.[2], PhD.Eng. Ivanovs S.[3]
[1]National University of Life and Environmental Sciences / Ukraine,[2]Vinnytsia National Agrarian University /Ukraine,
[3]Latvia University of Agriculture / Latvia
Tel.: +37129403708, E-mail: semjons@apollo.lv

Keywords: *grain, milling, roller mill, oscillations*

ABSTRACT
The grain milling process, in which flour is produced, is very important since it radically changes the quality and quantity characteristics of products. The main milling machine used during the last two centuries in the leading branches of food industry is a roller mill. The way in which the materials are comminuted in the roller mills is based on the process of their shift under the impact of forces which cause tensions in one vertical plane while the particles of the material are passing through a gap between the rollers. As a result of the conducted research, theoretical prerequisites have been worked out for an improved method of grain milling according to which the particles of the material are comminuted at the expense of simultaneous impact upon them of the disintegrating forces in a vertical and a horizontal plane.

РЕЗЮМЕ
Процес помелу зерна для отримання борошна є дуже важливим, оскільки він суттєво змінює кількісно-якісні характеристики продуктів. Основною машиною для помелу зерна протягом двох останніх сторіч у передових галузях харчової промисловості є вальцьовий верстат. Спосіб подрібнення матеріалів у вальцьових верстатах ґрунтується на процесі їх зміщення під дією сил, які викликають напруження в одній вертикальній площині при проходженні часток матеріалу крізь щілину між вальцями, що обертаються. В результаті проведеного дослідження розроблені теоретичні передумови вдосконаленого способу помелу зерна, при яких частинки матеріалу подрібнюються за рахунок одночасного впливу на них сил, що подрібнюють у вертикальній і горизонтальній площинах.

INTRODUCTION
Since ancient times, humanity has been using various kinds of grain for food. In order to improve digestibility and the ability to further process the products, different methods of grain comminution have been used, the most widespread among them being grain grinding between stone surfaces.

The grain milling process, in which flour is produced for feeding cattle, as well as for baking bread products, is very important since it radically changes the quality and quantity characteristics of the products. By their structure, the grain products are non homogeneous, differing by their physical, chemical and biological properties.

Therefore, the milling process of the grain products is complicated, it involves many factors, and there are a significant number of different machines developed for its implementation. The main milling machine, used during the last two centuries to produce flour, has been a roller mill *(Butkovski, 1990; Merko and Morgun, 2001).* To produce feed for animals, hammer-type grain crushers *(Savinyh, 2016; Sysuev, 2015)*are also used, yet the comminution degree in them is much lower than it is required in order to obtain flour.

In order to make products from grain, the crushing and milling of it requires up to 70% of the electric energy consumed by all the technological line machines. The technological properties of grain are the determining criteria for the quality and the end product. Their improvement affects minimisation of the specific production energy consumption, as well as the share of higher quality products. A great number of original works have been devoted to the study of the grain material strength and mechanical destruction in which the main emphasis is on the grain strength theory and the mechanism of its comminution (kinetics of breaking the molecular bonds in elasto-plastic deformations, arising and increasing of cracks, stress relaxation, and so on *(Dal-Pastro et al.)*

Crushing and milling of the grain materials have made the object of constant long-term researches and engineering developments in many countries of the world *(Bavram and Oner, 2014; Dal-Pastro et al., 2016; Sysuev, 2016; Vaiculik, 2013).* A search for the best comminution method of the grain materials is going on even at the present time; new essential regularities of these processes have been revealed during the last period, as well as methodologies worked out for the calculation of the milling and industrial mills technological cycles. At present, the most recent and substantiated are the comminution laws of Kick, Rittinger and Bond; they remain, as before, a topic of discussion while looking for universal comminution laws taking into account the empirical correlations between energy consumption and dispersity of the comminuted materials *(Hodakov, 1972; Schonert,1986; Naimushin, 2013).* However, none of the above-mentioned theories describes to a full extent the sphere of such a thin dispersion; moreover, none of them takes into account the impact a number of factors has upon the comminution process and energetics. No fundamental researches, conducted in many countries during the last decades, were able to change this situation.

The aim of this work is a theoretical research of the grain movement and comminution process in the new roller mill with an improved design in order to raise its operation efficiency.

MATERIAL AND METHODS

In order to develop new designs of roller mills, a new method for materials comminution in roller mills was offered *(Pavlenko et al., 2007- patent UA 20251)* the essence of which is that oscillatory (vibratory) movement is attached to the operating surfaces of the rollers along their geometric axes simultaneously with rotary movement; a new roller mill *(Pavlenko et al.,2007-patent UA 20249)* has been developed implementing the indicated method.

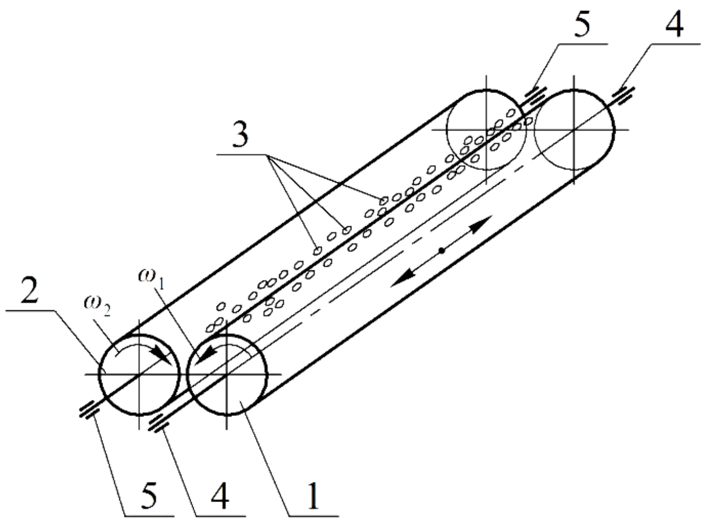

Fig. 1 - A design and technological scheme of the improved method of grain material comminution (Patent UA 20249):
1,2–rollers; 3–material particles; 4,5 – bearings

In order to raise the intensification of the grain material comminution process in the roller machines and to increase the output of the fine fraction in the end product, we have proposed an improved comminution method by means of rollers oscillatory movement in the direction of their horizontal axes. Fig.1 shows a technological scheme of the rollers operation which illustrates the essence of this method. The scheme in Fig.1 shows rollers *1,2* and material particles (grain) *3* as mentioned above. The drive shafts of the rollers *1,2* are mounted in the bearing units *4* and *5*. The method of comminuting the grain material is carried out in the following way. The rollers *1,2* set rotational movement towards each other with different angular velocities ω_1 and ω_2 . The rollers *1,2* rotate in bearings *4* and *5*. Besides, the roller *1* (or both rollers *1* and *2* at the same time) performs an oscillatory movement along its longitudinal axis. The mechanism of setting the rollers *1* and *2* in rotational or oscillatory movement is not shown in the scheme. Under the impact of the rotational movement of the rollers *1* and *2*, the particles of the material *3* are drawn under the forces of gravity and friction into the gap between the rollers *1* and *2* where their seizing and subsequent squeezing takes place, which leads to their crushing and flattening under the action of normal stresses in a vertical plane. Since the rollers *1* and *2* have equal external diameters but different angular velocities, shearing forces arise in a vertical plane causing tangential stresses, which results in grinding the material particles *3*. The oscillatory movement of the rollers *1* and *2* leads to the fact that the particles of the material *3* will occur under the impact of the forces, which cause tangential shear and crushing stresses acting in a horizontal plane, changing by their modulus and direction. Under the influence of these stresses the particles of the material *3* will additionally be ground in a horizontal plane. Besides, the material particles *3* will pass through the gap between the rollers *1,2* not along rectilinear paths in a vertical plane (as in the machines without an oscillatory movement of the rollers) but along paths which are certain curves (by their shape close to sinusoids), which, in its turn, will also raise the output of the fine fraction in the end product due to the increased time of the material particles being under the action of the crushing forces since any curvilinear path of the material particle movement will always have a longer path than the rectilinear path only in a vertical plane.

In order to carry out the improved method of the roller *1*oscillatory movement, a new design scheme of the roller itself was developed (Fig.2). As shown in the presented scheme, the roller consists of two parts: the roller centre *1* and the shell ring *2*, mounted on the roller centre with a possibility to move in either direction axially in relation to the roller centre *1*and the torque transfer from the roller centre *1* to the shell ring *2*. Such a possibility was achieved due to the fact that the internal diameter of the shell ring *2* is greater than the external diameter of the roller centre *1* but on the internal cylindrical surface of the shell ring *2*and on the external cylindrical surface of the roller centre *1* there are respectively formed three (or more) longitudinal grooves of triangular shape in which small balls *3* are inserted, separated by separators *4*. The balls *3* in the longitudinal grooves of the shell ring *2* and the roller centre *1* have a possibility of free rotation around their axes. Around the periphery of both end surfaces of the shell ring *2* there are fixed small balls *5* by means of rings *6*, with a possibility to rotate the balls *5* around their axes. The balls *5,* fixed to the left end of the shell ring *2* contact a space cam *7*, rigidly fixed to the frame *8*. The balls *5* which are fixed to the right end of the shell ring *2* contact a thrust ring *9* spring loaded by springs *10* to the frame *8*. To protect these mechanisms from penetration of the material particles to be comminuted, seals*11* are fixed on the frame *8***.**

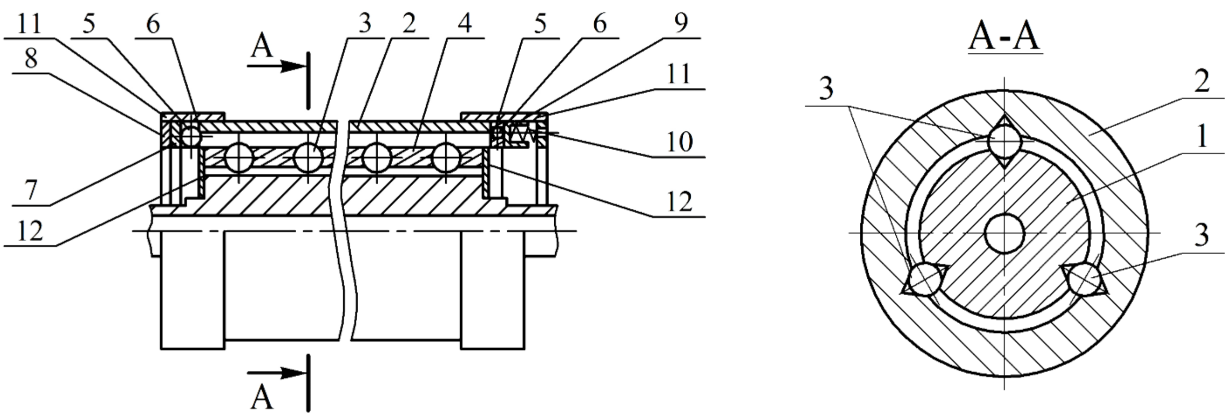

a) b)

Fig. 2 - A design principle scheme of the longitudinal section of roller axis 1(a) and its cross section (A-A) (b) (Patent UA № 20251)

1–roller centre; 2–shell ring; 3–balls; 4–separator; 5–balls; 6–rings; 7–cam; 8–frame: 9–thrust ring; 10 –spring; 11–seal; 12– protective ring

During the operation, the rotational movement is set to the rollers *1,2* of the frame in the direction towards each other with different angular velocities. The roller centre *1* rotating, the shell ring *2* will rotate with the same angular velocity and in the same direction as the roller centre *1* because the torque will be transferred by the balls *3*, inserted into the longitudinal grooves of the shell ring *2* and the roller centre *1* (Fig.2). The balls *5*, fixed by the ring *6* from the right end of the shell ring *2*, will receive through the thrust ring *9* forces from the side of the springs *10* which press the thrust ring *9* to the left of the frame *8*. These forces move the shell ring *2* to the left in an axial direction and, through the balls *5* fixed from the left end of the shell ring *2*, press the shell ring *2* to the space cam *7*. In further rotational movement the space cam *7* will determine the axial movement of the shell ring.

Consequently, as a result of the rotational movement of the roller centre *1*, the shell ring *2*, together with the roller centre *1*, will receive a rotational movement and, at the same time, an oscillatory movement along the axis of the roller centre *1*.

To conduct a theoretical research of the grain milling technological process in roller mills, there was built an equivalent scheme of the movement of a single grain (a material particle *M*) between two counter rotating rollers (Fig.3).

The material to be milled in the roller mills is conveyed between the rollers (Fig.1,*a*), on condition that:

$$f > tg\varphi_o \tag{1}$$

Where:

f – the coefficient of friction;

φ_o – an angle corresponding to the width of the milling zone (the operating zone) at which pulling of the material particle into the gap between the rollers is effectuated.

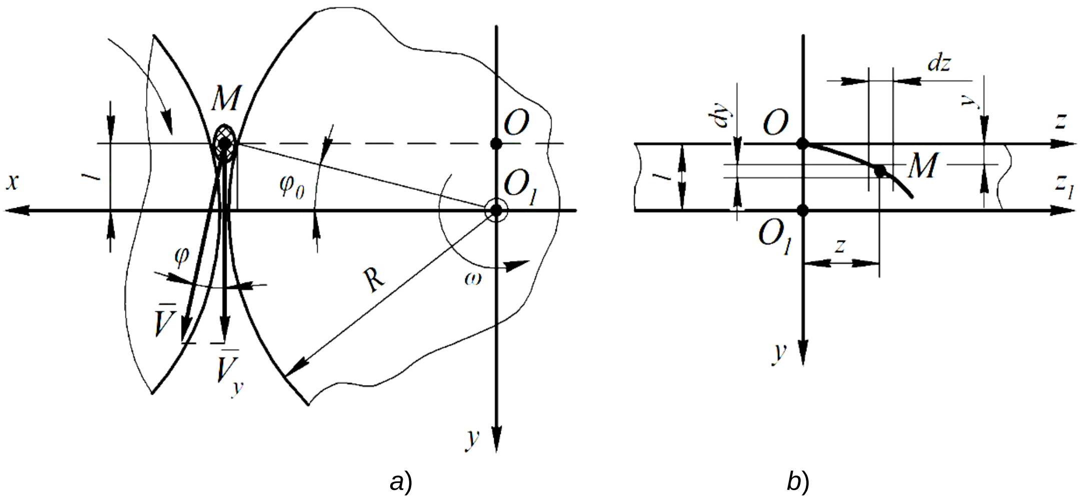

Fig. 3 - An equivalent scheme of a grain particle movement between the rotating surfaces of the milling rollers:

a) a view from above; *b*) a side view

In the scheme Point *M* – a symbolic representation of grain passing the route $OO_1 = l$, (Fig. 3 *b*).

The movement of the grain takes place in the direction of the axis Oy, perpendicular to the operating roller axis of rotation O_1z_1. In this case, there is no motion of the particle in the direction of the Ox axis. The movement in the direction of the Oy axis is the first degree of freedom. In addition, we assume that the particle between the rolls moves without slipping. Therefore, the motion of the particle M takes place with a forward velocity V_y, where

$$V_y = \omega R \cos \omega t \tag{2}$$

ω – the angular velocity of the roller rotation;

R – the radius of the roller.

As it is known $V_y = \frac{dy}{dt}$, therefore, taking equation (2) into account, we obtain:

$$\frac{dy}{dt} = \omega R \cos \omega t \tag{3}$$

Then:

$$dy = \omega R \cos \omega t \cdot dt \tag{4}$$

Integrating equation (4) in the range from *0* to *t,* we obtain:

$$y=\int_0^t \omega R\cos\omega t\cdot dt=\int_0^t R\cos\omega t\cdot d\left(\omega t\right)=R\sin\omega t \tag{5}$$

or

$$y=R\sin\varphi \tag{6}$$

where $\varphi=\omega t$.

In particular:

$$l=R\sin\varphi_o \tag{7}$$

The research was done by applying the methods of higher mathematics, theoretical mechanics, programming and numerical accounting on the PC.

RESULTS

Taking into consideration a proposed hypothesis about the expediency of additional oscillating (vibrating) movement along the geometric axes of the rollers (simultaneously with their rotary movement),we introduce the following additions into the design diagram.

We will consider that the oscillatory movement of the operating roller along the O_1z_1 axis is the second degree of freedom in agreement with the following law:

$$Z=H\sin\left(kt\right) \tag{8}$$

where:

H – the amplitude of the axial oscillations of the roller operating surface, m;

k – the cyclic frequency of these oscillations, s^{-1}.

In this case, point M of the milled grain will perform movement within the limits of the operating zone along a definite path which we will consider in the system of coordinates yOz , as shown in Fig.3*b*.

The parametric dependencies (5) and (8) make it possible to set the movement path of point M .

Let us find the elements of the arc of point M path– dy and dz during its movement in the operating zone of milling.

In this case we will obtain:

$$dy=\omega R\cos\omega t\ dt\,,\qquad dz=Hk\cos\left(kt\right)dt \tag{9}$$

Then, we will determine the length of the element of the arc path dL in the following way:

$$dL=\sqrt{\left(dy\right)^2+\left(dz\right)^2} \tag{10}$$

We will determine the length of the curve along which Point M is moving in a final interval of time t_1 through such an interval:

$$L=\sqrt{\left[\omega R\cos\left(\omega t\right)\right]^2+\left[Hk\cos\left(kt\right)\right]^2}\,dt \tag{11}$$

We will determine the value of the cyclic frequency k on condition that the oscillation period should correspond to the time of the movement of Point M on the path $OO_1=l$.

In the first approximation, we will assume that $V_y=\omega R$, and therefore the period T (the time of particle M displacement between the rollers) will be equal to:

$$T=\frac{l}{\omega R}=\frac{2\pi}{k} \tag{12}$$

so:

$$k = 2\pi\omega\frac{R}{l} \tag{13}$$

We will find out the width of the operating zone from condition (1).

Let us transform the right side of the expression (7), presenting it as a fraction in which the numerator and the denominator are multiplied by $2\cos\varphi_o$:

$$l = \frac{2R\sin\varphi_o \cdot \cos\varphi_o}{2\cos\varphi_o} \tag{14}$$

After corresponding transformations, we obtain:

$$l = \frac{2R\sin\varphi_o \cdot \cos\varphi_o}{2\cos\varphi_o} = \frac{R\sin 2\varphi_o}{2\cos\varphi_o} = \frac{2Rtg\varphi_o}{\left(1+tg^2\varphi_0\right)2cos\varphi_o} =$$
$$= \frac{Rtg\varphi_o}{\sqrt{1+tg^2\varphi_o}\cdot\sqrt{1+tg^2\varphi_o}\cdot\cos\varphi_o}. \tag{15}$$

Considering that $tg\varphi_o = f$, after the necessary transformations of the expression (15), we finally obtain:

$$l = \frac{Rf}{\sqrt{1+f^2}\cdot\sqrt{1+\frac{\sin^2\varphi_o}{\cos^2\varphi_o}}\cdot\cos\varphi_o} = \frac{Rf}{\sqrt{1+f^2}} \tag{16}$$

In order to make numerical calculations on the PC, it is necessary to use a program and set the numerical values of the constants. We will take such values of ω, R and f which agree with the data from the technical documentation of the working equipment *(Bavram and Oner, 2014; Butkovski, 1990).* At the values set for the parameters: f = 0.4; ω = 16π, s^{-1}; R =100 mm, and the arbitrarily selected $H = l$, using the parametric expressions (5) and (8), we perform the numerical calculations on the PC by means of the EXCEL program, on the basis of which we will construct the path of Point M when it is in the operating zone of milling.

Fig. 2*a* depicts a path which is a sinusoid with a cyclic frequency k and amplitude H .

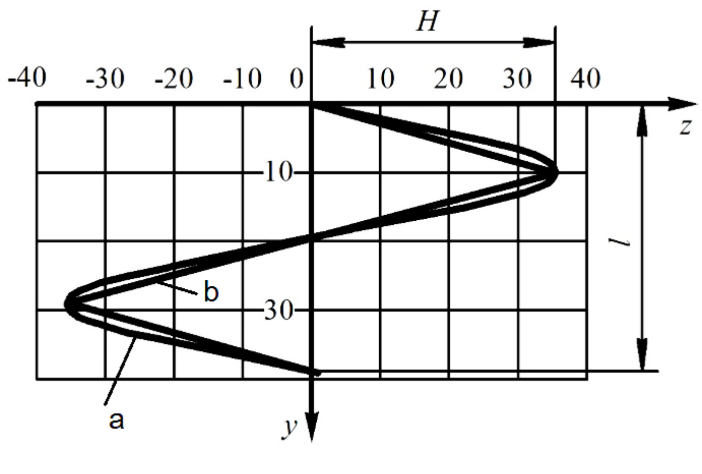

Fig. 4 - The path of a grain particle movement (Point M) in the milling operating zone

a) according to the obtained full calculated dependencies; b) according to a simplified method

The length of the curve L cannot be found in an elementary form because the integral (7) is elliptical *(Murray et al., 2015; Bulgakov et al., 2013),* which can be solved by any of the numerical methods.

The accuracy with which the path length will be determined depends on the integration step and time which we will spend using the computer. However, in the present work, the authors do not set it as an object to obtain exact numerical results, trying only to carry out an analysis of the essential factors affecting the grain milling process.

Therefore, the length of the path to be covered by Point M in the operation zone will be found using simplified methods.

The essence of the method is that the path depicted in Fig.4 (Curve ***a)*** will be presented as a broken line where the arc of the sinusoid is replaced by straight line segments, as shown in Fig.4 (Curve b). In such a case, we will find the length of the path L according to a considerably simplified formula:

$$L = \sqrt{l^2 + (4H)^2} \, . \tag{17}$$

The error with which the length of the path L will be determined makes only approximately 8%, by the way, towards underestimation in comparison with the exact formula envisaged for the integral application (7). This provides a possibility to establish that the second degree of freedom essentially affects the path length in the operating zone.

Assuming that $H = l$, the relation $\frac{L}{l} = \sqrt{17}$, but at $H = 2l$ – $\frac{L}{l} = \sqrt{65}$.

Consequently, the rollers oscillating movements in the direction of their axes of rotation considerably increase the length of the movement path and correspondingly improve the quality of the milled product. This statement is confirmed by researches in other similar technological processes *(Ertel, 2012).*

On the basis of a hypothesis that the intensity of the grain material milling process is proportional to the path covered by Point *M* in the operating zone, additional application of the second degree of freedom in the roller design will considerably raise efficiency in comparison with the roller mills using the conventional comminution method. In this case there arises a necessity also for theoretical research which would reveal the dynamics of the grain material milling process and a methodology for determining the optimal path to be covered by Point *M* in the operating zone in order to achieve the desired quality of the product.

An important issue is the choice and optimisation of the values *R, ω, H* and *k*, which can be finally established as a result of the conducted experiments.

In case the results of the experimental researches theoretical analysis and parameters optimisation are confirmed, there will be a possibility to create industrial designs of roller mills implementing the new comminution method of materials with oscillating rollers, which will give a remarkable economic effect.

CONCLUSIONS

An expression was determined in an analytical way of the width of the grain crushing operating zone and the path length of its movement through the rollers having an additional oscillating movement. The rollers oscillating movement in the direction of their rotation axes significantly increases the path length of the grain through the rollers and, correspondingly, raises the intensity and quality of the milled product.

REFERENCES

[1] Bavram M., Oner M., (2014), Bulgur milling using roller, double disc and vertical disc mills, *Journal of Food Engineering*, vol.79(1), pp.181-187;

[2] Butkovski V., (1990), *Flour Milling Production (Мукомольноепроизводство*), 381 p, Moscow / Russia;

[3] Dal-Pastro E., Facco P., Bezzo E., Zamprogna E., Barolo M., (2016), Data-driven modelling of milling and sieving operations in wheat milling process. *Food and Bioproducts Processing*, Vol.99, pp.99-108;

[4] Ertel W., (2015), *Advanced Mathematics for Engineers*, 227 p., Ravensburg-Weigarten / Germany;

[5] Hodakov G., (1972), *The Physics of Comminution (Физика измельчения)*, 240 p., Moscow / Russia;

[6] MerkoI., Morgun V. (2001), *Scientific Foundations and a Technology of Grain Processing (Научные основы и технология переработки зерна)*, 342 p., Odessa / Ukraine;

[7] Naimushin A., (2013), Engineering Support to the Innovative Development of Agricultural Production (Инженерное обеспечение для иновационного развития сельскохозяйственного производства),

Proceedings of the 8th International Scientific and Practical Conference, pp.173-178, Zernograd / Russia;

[8] Murray R., Spiegiel, Seymort Lipschutz, John Liu, (2015), *Mathematical handbook*, 293.p.;

[9] Naimushin A., (2013), *Experimental Research of the Grain Crushing Process on a Toothed Roll Grinder*. *(Экспериментальное исследование процесса измельчения зерна на зубчато-роликовом измельчителе)*. Herald of the Altay State Agrarian University, Vol. 12(110), pp.108-113., Barnaul / Russia;

[10] Pavlenko B., Bandura V., Pavlenko M., (2007*), A Roller Mill (Вальцовый станок)*, Patent No 20251, UA;

[11] Pavlenko B., Bandura V., Pavlenko M., (2007), *Method of Material Comminution in Roller Mills (Способ измельчения материалов в вальцовых станках)*, Patent No 20249, UA;

[12] Bulgakov V., Prisyzhniuk N., Adamchuk V. et al., (2013), *A Theory of Agricultural Production Vibratory Machines: A Monograph, (Теория вибрационных машин сельскохозяйственного производства)*, 324 p., Kyiv / Ukraine;

[13] Savinyh P., Nechaev V., Nechaeva M., Ivanovs S., (2016), Motion of grain particle along the rotor fan blade of hammer crusher. *Engineering for Rural Development, Proceedings of the 15th International Scientific Conference,* Vol. 15, pp.1072-1076, Jelgava / Latvia;

[14] Sysuev V., Savinyh P., Aleshkin A., Ivanovs S. (2016), Simulation of elastic deformation propagation of grain under impact crushing in crusher. *Engineering for Rural Development*, *Proceedings of the 15th International Scientific Conference,* Vol.15, pp.1065-1071, Jelgava / Latvia;

[15] Sysuev V., Ivanovs S., Savinyh P., Kazakov V., (2015), Grain movement and transformation in two-stage crusher. *Engineering for Rural Development, Proceedings of the 14th International Scientific Conference,* Vol.14, pp. 22-27, Jelgava / Latvia;

[16] Schonert K., (1986), *Advances in the physical fundamentals of comminution. Advances in mineral, Processing*, pp. 28;

[17] Vaculik P., Maloun J., Chladek L., Poikryl M., (2013), Disintegration process in disc crushers. *Research in Agricultural Engineering.* Vol. 59, Issue 3, pp. 98-104.

STUDY OF LONG HAUL TRUCK MOVEMENT ALONG THE CURVILINEAR TRAJECTORY WHILE STEERING A CARRYALL SEMI-TRAILER - CONTAINER BY BRAKING THE WHEELS OF ONE AXLE

/

ДОСЛІДЖЕННЯ РУХУ АВТОПОЇЗДА ПО КРИВОЛІНІЙНІЙ ТРАЄКТОРІЇ ПРИ УПРАВЛІННІ УНІВЕРСАЛЬНИМ НАПІВПРИЧІПОМ-КОНТЕЙНЕРОВОЗОМ ШЛЯХОМ ГАЛЬМУВАННЯ КОЛІС ОДНІЄЇ ОСІ

Prof. Dr. Eng. Sakhno V.P.[1)], Prof. Ph.D. Eng. Marchuk M.M. [2)], Lect. Ph.D. Eng. Marchuk R.M.[2)].

[1)] National Transport University, Suvorova Str., 1, Kiev / Ukraine

[2)] National University of Water and Environmental Engineering, Soborna Str., 11, Rivne / Ukraine

E-mail: r.m.marchuk@nuwm.edu.ua

Keywords: *long haul truck, semi-trailer, container, axle, bogie, trajectory, braking*

ABSTRACT

The long-haul truck movement along the curvilinear (in plan) trajectory is studied in this article. Braking the wheels of the bogie's one side is proved to lead to the fact that the absolute instantaneous centre of the bogie turn, when coming into a corner and coming out of a corner, will be on different sides of the semi-trailer bogie axles. The side force of the bogie is directed towards the transfer centre of semi-trailer angular velocity when coming into a corner and, in the opposite direction, when coming out of a corner. Therefore, braking the wheels of one side frame of a bogie rear axle is considered more efficient.

РЕЗЮМЕ

У статті розглядається рух автопоїзда по криволінійної (в плані) траєкторії. Встановлено, що гальмування коліс одного борту возика призводить до того, що абсолютний миттєвий центр обертання возика на вході в поворот і виході з повороту буде лежати по різні боки від осі возика. Показано, що на вході в поворот бічна сила на возику спрямована в бік центру переносної кутової швидкості напівпричепа, а на виході з повороту - в протилежну сторону. Тому доцільним є гальмування коліс одного борту задньої осі возика напівпричепа.

INTRODUCTION

The container transportation is known to be one of the most convenient and economic cargo delivery types, which is carried out by the local and international transportation organizations. The containers freight transportation is widely used around the world due to the high level of safety and the simplicity of customs registration. The volumes of such transportations grow from year to year (*Onishchuk V.P., and others 2011*). The modern motor-service for transporting containers has available a wide range of cars, trailers and semi-trailers. However, transportation of containers by carryall semi-trailers is more rational. For example, “Fliegl” Company produces a wide scale of container trucks, in particular, carryall ones for transporting all types of containers, including tank containers (from 20 to 45 foot) and HQ containers.

To transport the 45-foot containers by carryall container trucks, it is necessary to elongate the long haul trucks. Such elongation decreases the vehicles' cornering performance. The enlargement of the overall traffic lane (OTL) creates a danger to the oncoming transport, complicates the movement in the city conditions and reduces the average movement speed of the entire transport stream. It is possible to improve the long haul truck's cornering performance by means of steered (adjustable) axels (wheels) of the semi-trailer or by braking the wheels of the semi-trailer's one side (*Kuts N.G., and others 2003*).

Manoeuvrability indicators of a long-haul truck consisting of a carryall semi-trailer - container with an adjustable axle are defined in this work (*Bodnaruk V.B., and others 1998*). In particular, the long-haul truck with an adjustable axle is proved to meet the requirements of Council Directive 96/53/EC and Directive 2002/7/EC for manoeuvrability. However, its stability is insufficient. The objective of this work is to define the peculiarities of long haul truck pivoting movement when the carryall semi-trailer - container is steered by braking the wheels of one axle.

MATERIALS AND METHODS

To determine the semi-trailer turning radius when steering by braking the wheels of the bogie's one side, it is necessary to determine the normal reactions of the bearing surface to the wheels of the bogie's one side and the steering resistance coefficients inside and outside wheels. The wheels are functions of both normal load and braking torque acting on the bogie's wheel or side.

To determine the redistribution of vertical loads on the wheels of a semi-trailer bogie, the pivoting movement of a long-haul truck should be considered (*Pridyuk V.M., and others 2011*).

The centrifugal force acting on the semi-trailer bogie can be deduced by the formula:

$$P_{jn} = m_n \frac{v^2}{R} \quad [\mathrm{N}] \tag{1}$$

where m_n – weight acting on the semi-trailer bogie, kg;

v – long haul truck speed, m/s;

R – turning radius of the semi-trailer bogie, m.

Then, the centrifugal force acting on certain axles of the bogie is determined as:

$$P_{jni} = \frac{m_{ni} v^2}{R} \quad [\mathrm{N}] \tag{2}$$

where m_{ni} – weight acting on a certain axle of the bogie, kg.

Normal reactions of the bearing surface acting on the inside and outside wheels of the semi-trailer bogie are defined as:

$$Z_{\mathrm{int}} = \frac{a_n}{2L_{nn}} G_1 - \frac{h_{g1}}{2L_{nn}} P_{jxi} - \frac{h_{g1}}{2B} P_{jn} \quad [\mathrm{N}] \tag{3}$$

$$Z_{ext} = \frac{a_n}{4L_{nn}} G_1 - \frac{h_{g1}}{2L_{nn}} P_{jxi} + \frac{h_{g1}}{2B} P_{jn} \quad [\mathrm{N}] \tag{4}$$

where a_n – distance from the point of coupling the semi-trailer with the truck to the semi-trailer mass centre, mm;

h_{g1} – height of semi-trailer mass centre, mm;

G_1 – gravity of semi-trailer gross weight, H;

P_{jxi} – semi-trailer inertia force, H;

L_{nn} – semi-trailer wheelbase, mm;

B – bogie wheel tread, mm.

Therefore, as the force reactions along the semi-trailer bogie sides are changed, the resistance coefficient of steering the wheels of its axles from the normal load on the wheel is changed as well. In this case, D.A. Antonov dependence for determining the cornering force of the wheels of the semi-trailer bogie axles should be applied (*Antonov D.A., 1978*).

The braking torque, which occurs when braking the wheels of the semi-trailer bogie, is deduced by the formula:

$$M_{brk} = Z_{ext} \times \frac{B}{2} \times \varphi \quad [\mathrm{N{\cdot}m}] \tag{5}$$

where φ - adhesion coefficient of the semi-trailer bogie wheels, $\varphi = 0.6$;

B – semi-trailer bogie wheel-tread, mm.

In case of braking the one-axle wheels, the position of the axle is determined during the unstable pivoting movement of a long-haul truck. The change in the curvature sign is known to cause the change in the direction of normal acceleration, and hence, the side force (*Onishchuk V.P. and others, 2009*). The direction of normal acceleration is determined by the position of the absolute instantaneous turn centre, which (for the tri-axle semi-trailers under study) depends on the angles ratio of steering the bogie axle's wheels and its base. Braking the wheels of the bogie's one side can lead to the fact that the absolute instantaneous centre of a bogie turn, when coming into a corner and coming out of a corner, will be on different sides of the bogie axles. Changing the position of the absolute centre of a bogie turn relative to the semi-trailer movement trajectory indicates a change in the side force direction of the bogie mass centre, which coincides with the centre of the bogie relative angular velocity ω_T. Besides, when coming into a corner, the bogie side force is directed towards the centre of the bogie transfer angular velocity and when coming out of a corner - in the opposite direction.

The movement of the long-haul truck under study along the curvilinear (in plan) trajectory is the plane-parallel one. Therefore, the theorem on adding the rotations around parallel axles can be applied in studying the unsteady turn of the given long-haul truck (*Yablonsky A.A., 1971*). During the long-haul truck motion along the input transitional trajectory, Fig. 1 (a), the direction of relative angular velocity of the front steered axle coincides with the bogie transfer velocity direction. In this case, the magnitude of the axle absolute angular velocity is equal to the sum of the angular-rate components, that is:

$$\omega_1' = \omega_T' + \dot{\delta}_1' \tag{6}$$

where ω_T - relative angular velocity of the semi-trailer bogie;

$\dot{\delta}_1'$ – relative angular velocity of the bogie's front steered axle.

In this case, the absolute instantaneous turning centre is in the point O_{11}'.

Normal acceleration of the front axle can be determined as:

$$a_1' = V_1'\omega'_1 = V_1'\left(\dot{\delta}_1' + \omega_T'\right) \tag{7}$$

where V_1' - vector magnitude of the front axle velocity.

Additional side force $P_{\omega 1}'$ on the front axle acts from the rotation transfer centre O_2' and coincides in terms of direction with the force $P_{\omega c}'$.

Rear axle relative velocity $\dot{\delta}_3'$ does not coincide with the direction of the bogie's transfer velocity ω_T'. Therefore, at the beginning of a turn, the following ratio is deduced $\dot{\delta}_3' > \omega_T'$. Then, according to the theorem on adding the rotations around parallel axles, the absolute instantaneous turn centre in this section of the curvilinear motion will be at the point O_{31}', that is, further along the bogie longitudinal axle relative to its turn centre, at the point O_2'.

In this case, the magnitude of the rear axle absolute angular velocity is equal to the difference in the angular-rate components:

$$\omega_3' = \dot{\delta}_3' - \omega_T' \tag{8}$$

where $\dot{\delta}_3'$ – relative angular velocity of the given steered rear axle of the semi-trailer bogie.

Normal acceleration is deduced by the formula

$$a_3' = V_3'\omega_3' = V_3'\left(\dot{\theta}_3' - \omega_T'\right) \tag{9}$$

where V_3' - vector magnitude of the rear steered axle velocity;

$\dot{\theta}_3'$ - relative steering angle of the bogie rear steered axle.

The additional side force $P_{\omega 3}'$ on the rear steered axle will be directed from the absolute instantaneous centre of rotation O_{31}' to the centre O_2'. In this case, its direction is opposite to the direction of the side force on the semi-trailer bogie $P_{\omega c}'$.

The direction of relative velocity $\dot{\delta}_2'$ of a middle-steered axle depends on the angles ratio of steering the front and rear axles' wheels.

Whereas $\delta_1 > \delta_3$, the direction of the relative angular velocity $\dot{\delta}_2'$ coincides with the direction of the bogie's transfer velocity.

Then:

$$\omega_2' = \omega_T' + \dot{\delta}_2' \tag{10}$$

$$a_2' = V_2'\omega_2' = V_2'\left(\omega_T' + \dot{\delta}_2'\right) \tag{11}$$

where V_2' - vector magnitude of the middle axle velocity.

$\dot{\delta}_2'$ – relative angular velocity of the bogie's middle steered axle.

The direction of additional side force on the middle axle $P_{\omega 2}'$ coincides with force $P_{\omega c}'$ direction.

When $\delta_1 < \delta_3$, the direction of the middle axle $\dot{\delta}_2'$ relative angular velocity does not coincide with the bogie transfer velocity direction. For this case, the following formulae are deduced:

$$\omega_2' = \dot{\delta}_2' - \omega_T' \tag{12}$$

$$a_2' = V_2'\omega_2' = V_2'\left(\dot{\delta}_2' - \omega_T\right) \tag{13}$$

Moreover, the additional side force will act in the opposite direction of the side force on the semi-trailer bogie.

When coming out of a corner in the given section of bogie trajectory, Fig. 1 (b), the direction of relative angular velocity $\dot{\delta}_1''$ of the front axle does not coincide with the direction of the bogie transfer velocity ω_T''.

Thus, the ratio $\omega_T'' > \dot{\delta}_1''$ is quite obvious, therefore, the absolute instantaneous turn centre is at the point O''_{11}, that is, apart the point O''_2. The absolute angular velocity of the front axle in this section of the path can be determined as:

$$\omega_1'' = \omega_T'' - \dot{\delta}_1'' \tag{14}$$

where ω_T'' - semi-trailer bogie transfer velocity;

$\dot{\delta}_1''$ – relative angular velocity of the front steered axle when coming out of a corner.

The normal acceleration is deduced by the formula:

$$a_1'' = V_1'\omega_1'' = V_1'\left(\omega_T'' - \dot{\delta}_1''\right) \tag{15}$$

The additional side force $P_{\omega 1}''$ when completing a turn in the curve section will act in the same direction as in the previous case, namely, it will act from the centre of the rotation transfer O_2''. Its direction also coincides with the direction of the bogie side force $P_{\omega c}''$.

The truck-tractor Scania P230 CB6 × 4ENZ equipped with the front steered axle and two rear-driving axles, and the carryall semi-trailer - container produced by Fliegl Company in structure of a long-haul truck are studied in this work (Onishchuk V.P. and others (2010)). Equations for determining the parameters of the curvilinear motion of the given long-haul truck under study are developed.

Based on the conducted calculations, the following conclusions have been drawn. First, the long-haul truck can move along the circular trajectories if the curve radius is bigger than the semi-trailer base. Second, a long-haul truck with an uncontrolled bogie ensures the OTL permissible value, which equals 7.3 m, only if the length of the long haul truck does not exceed 16.8 m (the maximum base of the semi-trailer does not exceed 7.0 m).

Third, providing that the semi-trailer base exceeds the specified value, the bogie should be controlled both by the adjustable axle and by braking the wheels of one side.

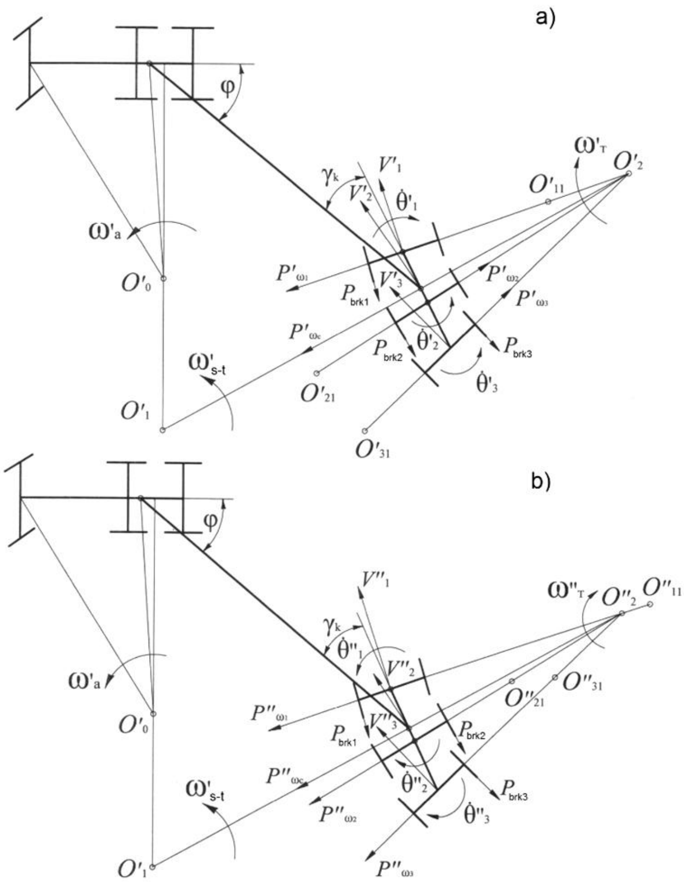

Fig. 1 - Scheme of turning a long haul truck with a dual control system of a semi-trailer bogie axle by braking the wheels of one side

RESULTS

The same change in the bogie trajectory curvature, Fig. 2, is achieved at various values of the braking forces applied to the wheels of its axles. At the same time, the weakest braking force should be applied to the rear axle wheels, somewhat stronger – to the front axle wheels, and much stronger – to the middle axle wheels.

The greatest rate of changing the trajectory curvature occurs during the first three seconds, and then its value stabilizes. It means the cessation of the transition process, meaning that the long haul truck goes to circular mode, Fig. 3.

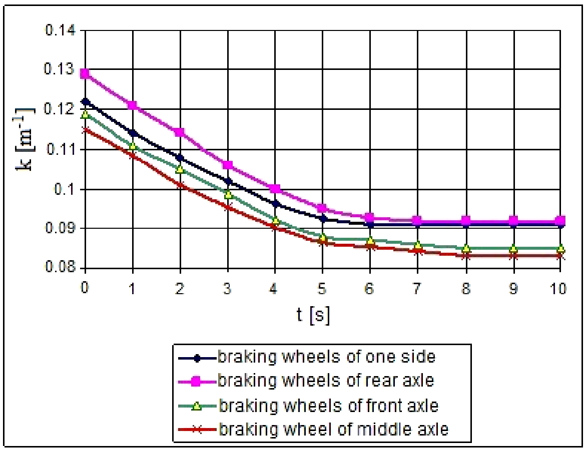

Fig. 2 - Dependence of semi-trailer trajectory curvature on the breaking torque of the bogie axles' wheels:
k – semi-trailer trajectory curvature, m^{-1}; t – time, s; braking torque, M_{brk} = 2,0 kH·m

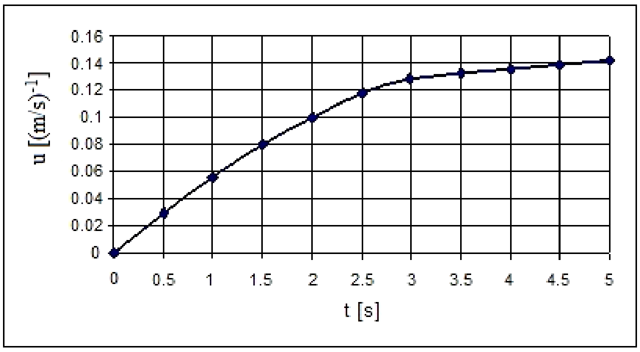

Fig. 3 - Rate of changing the trajectory curvature of a semi-trailer bogie in a time function of transition process:
u – rate of changing the semi-trailer trajectory, $(m/s)^{-1}$; t – time, s

The change in the semi-trailer bogie trajectory curvature due to braking the wheels of one side is advisable to use at the minimum turning radius of the tractor (from 15 to 20 m).

The turning radius increases, the efficiency of correcting the bogie trajectory by braking the wheels of one side decreases; after reaching 50 m, the difference in the turning radii of controlled and uncontrolled long-haul trucks does not exceed 10%.

CONCLUSIONS

The movement trajectory of the semi-trailer steered by braking the wheels of one side in an unsteady turn always consists of two sections, which differ in terms of curvature. Therefore, to correct the bogie trajectory, it is necessary to change the axle wheels that must be braked. Braking the wheels of the front axle changes the bogie movement trajectory the least. Therefore, braking the wheels of one side of the bogie rear axle is considered rational.

REFERENCES

[1] Antonov D.A., (1978), Stability theory of the multi-axle cars movement, (Теория устойчивости движения многоосных автомобилей), *Mechanical engineering*, p.216, Moscow;

[2] Bodnaruk V.B. and others, (1998). On definition of manoeuvrability indicators of long haul truck with the adjustable axle of semi-trailer, (До визначення показників маневреності автопоїзда із самоустановлювальною віссю напівпричепа), *System methods of management, technology and the organization of production, repair and operation of cars, Collection of scientific works.* UTU, TAU, pp.45-50, Kiev;

[3] Kuts N.G. and others (2003), Drives control of modern lorry convoys (Приводи керування сучасних автопоїздів), Avtoshliakhovyk Ukrainy, Separate release, *Bulletin of the TAU (Автошляховик України. Окремий випуск. Бюлетень ТАУ)*, Issue. 5, pp.78-79;

[4] Onishchuk V.P., and others (2010), The definition of manoeuvrability and stability movement of lorry convoy for container transportation, (До визначення показників маневреності і стійкості руху автопоїзда-контейнеровоза), *Bulletin of Zhytomyr State Technological University*, № 2 (53), pp.127-134, Zhitomir;

[5] Onishchuk V.P. and others (2009). On determination of design and layout options of lorry convoy for container transportation, *(*До визначення конструктивних і компонувальних параметрів автопоїзда-контейнеровоза*)*, *Bulletin of the National Transport University*, *NTU*, Issue 19, pp.80-83, Kiev;

[6] Onishchuk V.P. and others (2011), To the analysis of lorry convoy design for container transportation (До аналізу конструкцій автопоїздів-контейнеровозів), *Collection of reports 13 International scientific and practical conferences "Market of services of complex transport systems and applied problems of logistics"*, pp.180-182, Kiev;

[7] Pridyuk V.M. and others (2011), Manoeuvrability and stability of lorry convoy for container transportation movement, (Маневреність та стійкість руху автопоїзда-контейнеровоза), *Bulletin of the National Transport University*, *NTU*, Issue 23, pp.31-36, Kiev;

[8] Yablonsky A. A., (1971), The Course of theoretical mechanics (Курс теоретической механики), *The higher school,* p.496, Moscow;

[9] *** COUNCIL DIRECTIVE 96/53/EC of 25 July 1996 laying down for certain road vehicles circulating within the Community the maximum authorized dimensions in national and international traffic and the maximum authorized weights in international traffic, *Official Journal of the European Communities*, 1996, No L235/59-75;

[10] *** DIRECTIVE 2002/7/EC of European parliament and of the council of 18 February 2002 amending Council Directive 96/53/EC of 25 July 1996 laying down for certain road vehicles circulating within the Community the maximum authorized dimensions in national and international traffic and the maximum authorized weights in international traffic, *Official Journal of the European Communities*, No L67/47-49.

INFLUENCE OF ORGANIC OPERATION ENVIRONMENT ON CORROSION PROPERTIES OF METAL STRUCTURE MATERIALS OF VEHICLES
/
ВПЛИВ ОРГАНІЧНИХ РОБОЧИХ СЕРЕДОВИЩ НА КОРОЗІЙНІ ХАРАКТЕРИСТИКИ МАТЕРІАЛІВ МЕТАЛОКОНСТРУКЦІЙ ТРАНСПОРТНИХ ЗАСОБІВ

Prof. Ph.D. Eng. Popovych P.V. [1], Prof. Ph.D. Eng. Lyashuk O.L. [1], Lect. Ph.D. Eng. Shevchuk O.S. [1], Lect. Ph.D. Eng. Tson O.P. [1], Lect. Ph.D. Eng. Poberezhna L.Ya. [2], Bortnyk I. M. [1]
[1] Ternopil Ivan Pul'uj National Technical University, Ternopil / Ukraine
[2] Ivano-Frankivsk National Medical University, Ivano-Frankivsk / Ukraine
E-mail: ppopovich@ukr.net

Keywords: *organic fertilizers, corrosion rate, fixed capacity, depth indexes, corrosion current*

ABSTRACT.
The corrosiveness of cattle manure and mixed manure is considered to be low in relation to standard materials used in agricultural vehicles' metal structures – steels: standard steels (St.3 Steel, St.5 Steel) and quality steels (10 Steel, 15 Steel, 20 Steel, 25 Steel). Local corrosion damages caused by sticking particles (straw, etc.) are found. The corrosion rate of steels groups under investigation for the first day of exposure in filtered manure is found to be in the range of 0.031 to 0.042 mm/year. This rate is 3 to 4 times lower than the rate of corrosion caused by standard test rainwater solution where the further rate reduction up to 0.003 mm/year is caused by inhibitory properties of manure chemical components. In general, the corrosion of steels under study in liquid cattle manure and mixed manure occurs by an electrochemical mechanism. In comparison with distilled water, steady state potentials of the steels under study in these environments assume negative values, and the corrosion currents are to 5 times lower. Tafel constants are higher than in distilled water, which indicates the complexity of both electrode reactions as compared with the standard test environment.

РЕЗЮМЕ
Встановлено, що середовища гноївки великої рогатої худоби і гноївки змішаної мають низьку корозійну активність по відношенню до типових матеріалів металоконструкцій сільськогосподарських транспортних засобів - сталей: звичайної якості (Ст3, Ст5),також якісних сталей (Сталь 10, Сталь 15, Сталь 20, Сталь 25). Виявлено локальні корозійні пошкодження, спричинені налипанням частинок (солома, ін.). Швидкість корозії досліджених груп сталей за першу добу експозиції у відфільтрованих гноївках знаходиться в межах 0,031...0,042 mm/year, що є в 3…4 рази нижчим у порівнянні із модельним розчином дощової води, подальше зниження швидкості до 0,003 mm/year спричинене інгібувальними властивостями хімічних складових гноївок. Вцілому, корозія досліджених груп сталей в рідкому гної великої рогатої худоби та змішаному протікає за електрохімічним механізмом. Стаціонарні потенціали досліджуваних сталей у вказаних середовищах в порівняні з дистильованою водою зміщені в область від'ємних значень, а струми корозії до 5 разів нижчі. Константи Тафеля вищі, ніж у дистильованій воді, що свідчить про утруднення обох електродних реакцій у порівнянні з модельним середовищем.

INTRODUCTION
As a result of joint influence of aggressive environments and mechanical loads of tractor trailers and auger conveyors in agricultural production, about 70% of mechanisms get out of order, 20 to 25% of which are failures caused by operating overload due to the strength loss caused by corrosion damages *(Mykhaylovych Y., Pubets' A., 2008; Makarenko M., 2012; Tomashov N.D., Zhuk P.N., Titov V.A., Vedeneyeva M.A. ,1971; Popovych P.V., Mahlatyuk L.A., Kupovych R.B., 2014; Popovich P.V., Slobodyan Z.B., 2014; Ulig G.G.,1968; GTM 23.2.75.- 82., 1982; Starosvetsky J, Starosvetsky D, Amon R.,2007*). Despite the current study of influences of operating aggressive environments on the reduction of the strength and reliability of agricultural vehicles, the problems associated with the corrosion of metal structures caused by organic fertilizers are insufficiently studied (*Popovych P.V., Mahlatyuk L.A., Kupovych R.B., 2014; Popovich P.V., Slobodyan Z.B., 2014; Popovych P.V., Lyashuk O.L., et al., 2016*).

In particular, in *P. V. Popovych, et al. (2014*), only two types of steel are studied. It is well known that in the manufacture of metal structures of tractor trailers, the whole range of standard and quality steels is used (*GTM 23.2.75.- 82., 1982; Al-Otaibi M.S., Al-Mayouf A.M., Khan M., Mousa A.A., Al-Mazroa S.A., Alkhathlan H.Z., 2014; Raja P.B., Sethuraman M.G., 2008; Li X., Deng S., Fu H., 2012; Popovich P.V., Slobodyan Z.B., 2014)*). Therefore, there is a need to conduct experimental studies for a wider range of metal structure materials of tractor trailers. The reliability of transport machinery, in particular of agricultural trailers and auger conveyors, is ensured by their durability, failure-free operation, and maintainability and performance reliability. For vehicles, fertilizer spreaders, and others, the non-operating time is up to 80% (*Mykhaylovych Y., Pubets' A., 2008*) the performance of trailers is maintained during the storage; the efficiency of storage depends primarily on the quality of cleaning to ensure the removal of organic fertilizers residues and soil as well as on proper preservation of equipment. Even minor deviations from specified storage conditions can cause the corrosive damages. The rate of corrosion of the equipment made of standard and quality steels depends on the environment, time of contact, temperature, state of the metal and protective coatings, etc. The pit corrosion, oxygen concentration corrosion, fretting corrosion, contact corrosion, and corrosive cracking can be traced on some assemblies of tractor trailers (*Makarenko M., 2012*), Fig. 1, Fig. 2. Loss of metal is insignificant, however it most often occurs in significant conjugations of parts' surfaces that limit the reliability and serviceability of vehicles in general. Among organic fertilizers, the most corrosive are peaty composts, less aggressive – lowland and upland peats and caw manure. Thus, water acts as a catalyst of corrosion processes (*Makarenko M., 2012*; *Popovych P.V., Mahlatyuk L.A., Kupovych R.B., 2014*).

The purpose is to study the influence of exposure time on the corrosion rate of metal structure materials of agricultural vehicles, in particular, standard steel – St.3 Steel, St.5 Steel (DSTU 2651: 2005; DIN 17100) and carbon quality steel – 10 Steel, 15 Steel, 20 Steel, 25 Steel (GOST 1050-88; DIN 17200) as well as their electrochemical properties in cattle manure and mixed manure.

Fig. 1 – Corrosive damage of metal structure material of agricultural trailers

Fig. 2 – Corrosive damage of auger conveyor of agricultural materials

MATERIAL AND METHODS

Corrosion tests were carried out on samples of St.3 Steel, St.5 Steel and 10 Steel, 15 Steel, 20 Steel, 25 Steel under supply conditions. The samples were made in the form of discs with a diameter of 20 mm and with a surface polished to a roughness R_a = 0.63. Previously ungreased samples were weighed using a high-accuracy weighing machine to within ± 0.0004 g and stored in a desiccator up to 24 hrs.

As corrosive environments, the organic fertilizers were used: cattle manure and mixed manure in a ratio of 1/2 of caw manure + 1/2 of pig manure (their main content is given in Table 1 and distilled water as standard test condensation and rainwater. Before testing, corrosive environments were filtered using a paper filter to remove dispersed components.

Table 1

Content of major nutrients in fertilizers environments under study

Components / Environment	% mass								
	H_2O	**N General**	**N protein**	**N ammoniac**	**P_2O_5**	**K_2O**	**CaO**	**MgO**	**SO_3**
Cattle manure	86.7	0.38	-	-	0.12	0.22	0.25	-	-
Mixed manure	75.0	0.50	0.31	0.15	0.25	0.60	0.35	0.15	0.10

Before and after the experimental studies, the pH of solutions was measured using pH-meter I-160M. The rate of corrosion K_m (g/(sm^2·hr)) is determined by a gasometrical method after exposure for 1, 7, 12 and 24 days under natural aeration conditions and after the removal of corrosion products (*Tomashov N.D., Zhuk P.N., Titov V.A., Vedeneyeva M.A., 1971)*; calculations were performed using the known dependencies.

The calculations were performed using the following formula

$$K_m = \Delta m / S \cdot \tau\,, \tag{1}$$

where:

Δm – the sample weight change after exposure to the environment and removal of corrosion products, g;

S – the area of sample, m^2;

τ – the exposure time, hr.

The obtained value was converted using the depth index *P* (mm/year)

$$P = \frac{K_m \cdot k}{\gamma} \cdot 10^{-1}, \tag{2}$$

where: k – the conversion factor of hrs per year;

γ – the iron density 7.86 g/cm^3.

The percentage ratio of the degree of steel protection against corrosion *Z* was defined using the following formula

$$Z = \frac{K_m - K_i}{K_m} \cdot 100\% \tag{3}$$

where K_m and K_i – the corrosion rates of steel in distilled water and environments.

Polarization studies were conducted using the potentiostat IP-Pro. Samples of steel, pressed in PTFE, were used as the working electrodes; the working surface area is 0.0628 cm^2. Before each measurement, the sample was grinded by the abrasive paper №0, cleaned with acetone and dried. The comparison electrode is the saturated silver chloride electrode, the auxiliary – the platinum one. The corrosion current and Tafel constants of cathode and anodic reactions were determined from the straight sections of polarization curves.

The current-controlled indexes of corrosion rate were converted to the mass ones using the formula

$$K_i = i \cdot k \cdot A / n \cdot F \tag{4}$$

where: i – the corrosion current, A/cm^2;

k – the coefficient (*k* = 1, if the testing time is expressed in seconds, and the area – in cm^2);

A – the atomic mass of metal (iron and steel *A* = 56);

n – the valence of metal (iron 2 or 3);

F – the Faraday constant (*Ulig G.G., 1968*).

RESULTS

The nitrogen-containing compounds (see Table 1), which often have properties of corrosion inhibitors, were revealed during the chemical analysis of cattle and mixed manures. Corrosion tests of exposure studied at various times showed the following corrosion rates of steels in organic fertilizers (see Table 2). The corrosion rate of steel in both groups for the first day is 3 to 4 times lower in comparison with distilled water, and 8 to 10 times lower than in mineral fertilizer of ammonium phosphate and nitrophosphate when comparing, for example, St.3 Steel and 20 Steel.

Standard steels (St.3 Steel, St.5 Steel) corrode with greater speed than quality structural steels (10 Steel, 15 Steel, 20 Steel, and 25 Steel). The exposure time increases, the corrosion rate significantly decreases. After 24 days, the corrosion rates of steels under study in both environments equalize. Thus, for the first day, the inhibitory effect at the level of 60 to 70% occurs in manures as compared with distilled water. After 24 days, the degree of protection is over 90%. There is no difference between the corrosiveness of liquid cattle and mixed manures. Individual local corrosion damages of steels after exposure in unfiltered original manure is the result of the formation of galvanic couples due to sticking dispersed solid residues of straw, seeds and others on the surface of samples.

After 1 day testing, on the surface of samples only non-systemic single changes in the form of colour variation are found, corresponding to the thickness of the oxide film of the order 460 to 680 Å. After the further testing for 7 to 24 days, the sample surfaces are clean without any visible changes.

Before the corrosion test, pH of cattle manure and mixed manure was pH = 7.45 to 7.50. After exposure of steels in environments during 24 days, pH increased to 8.2.

Corrosion potentials of all steels under study in cattle and mixed manures are defined for 15 to 20 min. They assume more negative values in the standard test rainwater in comparison with distilled water (Fig. 2a, b). The nature of polarization curves on steel samples is the same (Fig. 3a, b). The quality steel cathode curves differ by the area and the value of boundary diffusion currents. In cattle manure the boundary diffusion current is $7 \cdot 10^{-2}$ A/sm^2 in the range of potentials –630 ... –920 mV; in mixed manure it is $3 \cdot 10^{2}$ A/sm^2 in the range of potentials –510... –810 mV. The standard steel cathode curves in both organic fertilizers differ extremely by the range of potentials of boundary diffusion current: –680 ... –1100 mV in cattle manure and –580... –1100 mV in mixed manure. The boundary diffusion current is higher than in quality steels – $9 \cdot 10^{-2}$ A/sm^2 and $7 \cdot 10^{-2}$ A/sm^2.

Table 2

Corrosion rate depth index of metal construction materials of tractor trailers in organic fertilizers

Steel	Time / Environment	*P*, mm/year			
		1 day	7 days	12 days	24 days
10 Steel	H2O	0.139	0.080	0.084	0.078
	Liquid manure	0.040	0.007	0.006	0.004
	Mixed manure	0.036	0.004	0.003	0.004
15 Steel	H2O	0.141	0.079	0.081	0.075
	Liquid manure	0.042	0.008	0.005	0.003
	Mixed manure	0.034	0.005	0.003	0.003
20 Steel	H2O	0.13	0.075	0.077	0.071
	Liquid manure	0.038	0.007	0.005	0.003
	Mixed manure	0.032	0.004	0.003	0.003
25 Steel	H2O	0.125	0.072	0.074	0.068
	Liquid manure	0.036	0.007	0.005	0.003
	Mixed manure	0.031	0.004	0.003	0.003
St.3 Steel	H2O	0.117	0.078	0.09	0.088
	Liquid manure	0.040	0.008	0.005	0.003
	Mixed manure	0.035	0.005	0.003	0.003
St.5 Steel	H2O	0.111	0.072	0.083	0.082
	Liquid manure	0.038	0.007	0.004	0.003
	Mixed manure	0.033	0.004	0.003	0.003

Anode curves for steels groups under study have a small area associated with the state of passivity: in liquid manure –480...–530 mV (20 Steel), –480...– 540 mV (St.3 Steel), and in mixed manure –250–320 mV (quality steels), –350...–420 mV (standard steels). The state of passivity is clearly traced in both environments when the potential assumes the values from –250 mV towards less negative ones at high currents of passivation about 10 A/sm^2.

Corrosion currents of all steels in both types of manure are 4 to 5.57 times lower than in distilled water (Table 3). Instantaneous values of current corrosion rates, listed in (4), satisfactorily correlate with the rates obtained by a gasometrical method for the first day under the condition of iron oxidation 3^+ (see Table 4). The low corrosiveness of manures under study is additionally confirmed by the analysis of Tafel areas of polarization curves.

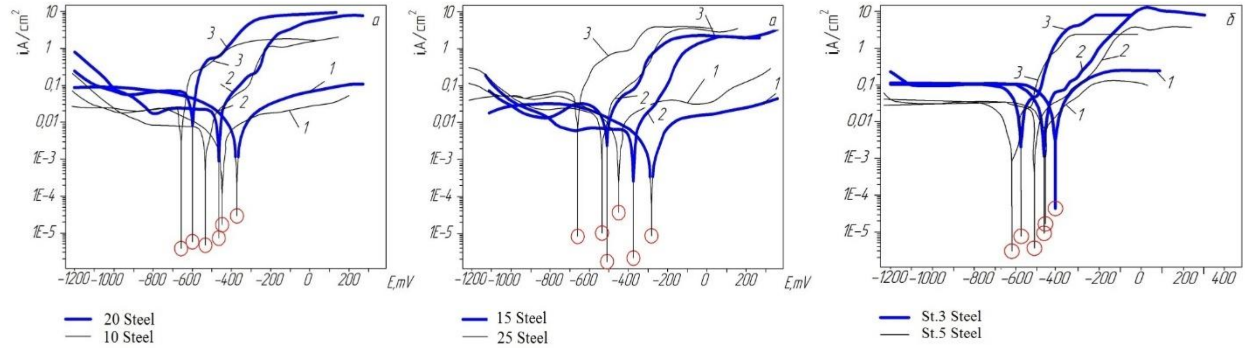

Fig. 3 - Polarization curves *a* – 10 Steel, 15 Steel, 20 Steel, 25 Steel; *b* – St.3 Steel, St.5 Steel
1 – distilled water; 2 – liquid manure; 3 – mixed manure.

Tafel constants of cathode and anodic reactions of these steels groups in environments under study are higher than the corresponding constants in distilled water (see Table 3). This fact ensures a greater over-potential of both electrode reactions compared with electrode reactions in water, resulting in low rates of electrochemical corrosion.

Table 3

Electrochemical properties of metal constructions materials of agricultural vehicles in organic fertilizers

Environment / prop. / Steel	Cattle manure				Mixed manure				Distilled water			
	$-E_{st}$, mV	$i_{cor}\cdot10^5$, A/cm^2	b_c, mV	b_a, mV	$-E_{st}$, mV	$i_{cor}\cdot10^5$ A/m^2	b_c, mV	b_a, mV	$-E_{st}$, mV	$i_{cor}\cdot10^5$, A/cm^2	b_c, mV	b_a, mV
10 Steel	597	0.8	30.8	28.6	454	0.7	36.1	28.8	392	3.7	22.4	19.8
15 Steel	604	0.7	31.3	29.2	457	0.7	37.2	30.2	380	3.5	23.1	20.2
20 Steel	610	0.7	33.3	30.0	460	0.6	38.5	460	372	3.0	25.0	22.3
25 Steel	617	0.7	34.8	32.1	472	0.5	40.1	33.8	452	3.9	36.2	30
St.3 Steel	590	0.9	30.2	28.1	450	0.8	35.0	27.9	401	4.1	21.3	18.3
St.5 Steel	592	1	30.4	28.4	452	0.9	36.2	30	410	4.3	22.0	19.1

Table 4

Comparing the corrosion rates of metals in organic fertilizers environments derived gravimetrically (K_m, (g/sm^2·s)), electrochemically (i_{cor}, A/cm^2) and listed from current parameters (K_i, (sm^2·s))

Environment / Steel	$H_2O_{distilled}$			Cattle manure			Mixed manure		
	$K_m\cdot10^9$	$i_{cor}\cdot10^5$	$K_i\cdot10^9$	$K_m\cdot10^9$	$i_{cor}\cdot10^5$	$K_i\cdot10^9$	$K_m\cdot10^9$	$i_{cor}\cdot10^5$	$K_i\cdot10^9$
10 Steel	3.32	3.70	5.85	0.99	0.70	1.45	0.85	0.70	1.25
15 Steel	3.30	3.50	5.88	1.01	0.8	1.48	0.87	0.70	1.28
20 Steel	3.25	3.00	5.80	0.94	0.70	1.40	0.80	0.60	1.20
25 Steel	3.20	2.80	5.76	0.90	0.80	1.36	0.76	0.50	1.16
St.3 Steel	3.50	4.10	7.80	1.10	0.90	1.70	0.90	0.80	1.50
St.5 Steel	3.42	4.30	7.73	1.03	0.90	1.63	0.84	1.00	1.42

Therefore, cattle and mixed manures are characterised by small corrosive aggressiveness to metal structure materials of agricultural vehicles, standard steels and quality steels. However, concentrators formed as a result of corrosion damages and combined with significant mechanical loads can reduce the equipment durability.

The corrosion in these environments occurs by an electrochemical mechanism at lower rates compared to distilled water, provided natural aeration. The obtained results allow to extend the operating time of agricultural equipment and to optimize its maintenance schedule. In addition, the results of the study of corrosion degradation can be used to create coatings for the metal surface protection.

CONCLUSIONS

1. The corrosion of standard steels and quality steels in cattle and mixed manures is exclusively local in nature. This property is caused by the formation of single galvanic couples as a result of sticking suspended solid particles (straw, etc.).

2. The metal structure materials of tractor trailers under study in both types of manure corrode by an electrochemical mechanism. In comparison with distilled water, steady state potentials of the steels under study in these environments assume negative values, and the corrosion currents are to 4 to 5.37 times lower. Tafel constants are higher than in distilled water, which indicates the complexity of electrode reactions. The values of current rates of corrosion satisfactorily coincide with the values obtained by a gasometrical method.

3. After the removal of suspended particles, the low corrosiveness can be traced in working environments under study in relation to the mentioned steels groups. The corrosion rate of studied metal structures materials of trailers for the first day of exposure is found to be in the range of 0.032 to 0.04 mm/year. This rate is 3 to 4 times lower than the rate of corrosion caused by standard test rainwater solution. The further rate reduction up to 0.003 mm/year is caused by inhibitory properties of manure chemical components.

REFERENCES

[1] Al-Otaibi M.S., Al-Mayouf A.M., et al., (2014), Corrosion inhibitory action of some plant extracts on the corrosion of mild steel in acidic media, *Arabian Journal of Chemistry*, vol 7(3), pp. 340-346;

[2] Li X., Deng S., Fu H., (2012), Inhibition of the corrosion of steel in HCl, H2SO4 solutions by bamboo leaf extract, *Corrosion Science*, vol 62, pp.163-175;

[3] Makarenko M., (2012), Pitting and other threats off seasons, *Agribusiness today*, № 22, p.245;

[4] Mykhaylovych Y., Pubets' A., (2008), The problem of storage of agricultural machinery, *Proposition*, №12, pp. 90–104;

[5] Popovych P.V., et al., (2014), Influence of Organic Fertilizers on the Corrosion-Electrochemical Characteristics of Low-Carbon Steels, *Journal of Mathematical Sciences*, Vol. 50, (2), pp. 284 –289;

[6] Popovich P.V., Slobodyan Z.B., (2014), Corrosion and Electrochemical Behaviors of 20 Steel and St.3 Steel in Ammonium Sulfate and Nitrophoska, *Journal of Mathematical Sciences*, Vol. 49, (6), pp. 819-826;

[7] Popovych P.V., Lyashuk O.L., et al., (2016), The service life evaluation of fertilizer spreaders undercarriages, *INMATEH Agricultural Engineering*, vol 50, no. 3, pp. 39-46, Bucharest/Romania;

[8] Raja P.B., Sethuraman M.G., (2008), Natural products as corrosion inhibitor for metals in corrosive media - A review, *Materials Letters*, vol 62(1), pp. 113-116;

[9] Starosvetsky J, et al.,(2007), Identification of microbiologically influenced corrosion in industrial equipment failures, *Engineering Failure analysis*, 14:1500-1511;

[10] Tomashov N.D., et al., (1971), Laboratory work on corrosion and protection of metals, *Metallurgy*, p.280, Moscow;

[11] Ulig G.G., (1968), Metal corrosion, *Metallurgy*, p. 306, Moscow;

[12] *** GTM (PTM) 23.2.75.-82, (1982), Guiding technical material, Welded frames of agricultural machines. Structural and technological design, *VISKHOM*, pp.111, Moscow.

QUERY ALGORITHM OF AGROMETEOROLOGICAL BIG DATA BASED ON DISTRIBUTED MATCHING
/
基于分布式匹配的农业气象大数据查询算法研究

Assoc. Professor Liu X.C.*[1], Ph.D. Chen S.[2], Ph.D. Wen L.Y.[3]
[1] Department of Information Engineering, Anhui Vocational and Technical College, Hefei / China;
[2] Institute of Intelligent Machines, Chinese Academy of Sciences, Hefei / China;
[3]Department of Computer Science and Electrical Engineering, West Virginia University, Morgantown / USA
Tel: +8613956016097; E-mail: liuxiaochuanmail@126.com

Keywords: *big data in agriculture, query system, distributed matching, storage cost, delay cost*

ABSTRACT
The query system established through integer linear programming (ILP) model can rapidly respond to query operation in agrometeorological data query service. However, related existing studies have only discussed about known network layer information, extremely high time complexity exists under complicated large-scale environment, and query result cannot be acquired. Therefore, a distributed matching-based heuristic ILP query algorithm was proposed in this study for large-scale network and unknown status of network layer information to improve distributed data query capability. The lower bound of space–time cost of the query system was certified under unknown status of network layer information, under which circumstance ILP model and algorithm design were proposed formally. Finally, disjoint path allocation and node replication allocation methods were used to design universal query system algorithms when network layer information was known and unknown, respectively. Experimental results showed that the distributed matching-based query system algorithm proposed in this study could obtain optimal solution in large-scale agrometeorological network and was not restricted to fixed network topology. When the cost ratio of storage to a unit delay cost was 10, the query system cost would present a linear growth; when the ratio was greater than 30, the storage cost would rapidly decrease, but the delay cost increased and the algorithm would run fast. Accordingly, the proposed algorithm could flexibly realize effective balance between storage cost and query delay. Conclusions of this study can provide theoretical and technical references for data query in intelligent agrometeorological service cloud system.

摘要
在农业气象大数据查询服务时，使用整数线性规划(Integer Linear Programming，ILP)模型构建查询系统能够快速响应查询操作。但现有相关研究仅讨论了已知网络层信息的情况，并且在大规模网络环境下，其时间复杂度过高甚至得不到查询结果。为了提升分布式数据查询能力，针对大规模网络以及网络层信息未知情况，本文提出了一种基于分布式匹配的启发式 ILP 查询算法。证明了在网络层信息未知时查询系统的时空开销下界，形式化地提出了在网络层信息未知时的整数线性规划模型和算法设计。最后，利用不相交路径分配和冗余结点分配方法设计了网络层信息已知和未知时通用的查询系统算法。研究结果表明：本文提出的基于分布式匹配的查询系统算法在农业气象大规模网络中能够得到优良的解，并且不受限于固定的网络拓扑结构，当单位存储开销与延迟开销的开销比为 10 时，查询系统开销会随之线性增长，大于 30 时，存储开销快速降低，延迟开销随之增大，算法运行时间会变快，这表明该算法可以灵活实现存储开销和查询延迟的有效平衡。本文的研究结论可以为智慧农业气象服务云系统中进行数据查询提供理论与技术参考。

INTRODUCTION
The Intergovernmental Panel on Climate Change once emphasized in the second and fourth evaluation reports that meteorological disaster would generate an enormous influence on the agriculture of China; if measures are not taken, the production capacity of the planting industry of China would drop by 5% to 10% up to 2030, and the sub-crop yield in 2050 would reduce by approximately 30% *(Yingjia et al., 2013)*. Therefore, China is vigorously developing precision agriculture and intelligence agriculture, which use modernized technologies and the use of agrometeorological big data is playing an increasingly significant role. The use of meteorological big data is significant to improving agricultural productivity and realizing high yield, high quality, high efficiency, safety and ecological and sustainable agricultural development *(Guangsheng, 2015)*. Agrometeorological big data feature mass distribution, timeliness and diversity. Agrometeorological data, which are acquired through ground automatic meteorological

observation, radar remote sensing monitoring, and satellite meteorological monitoring, are usually stored in hundreds of host computers. Then, saved data under geographical distribution are formed. Distributed query system is an extensively applied method to simultaneously analyse data on these different host computers and acquire real-time agrometeorological information.

When distributed query system is used to analyse and query high-correlation datasets, even damage of one patch of data will result in failure of the entire data analysis process; therefore, compared with traditional query system, distributed query system lays more emphasis on data survivability *(Mckendrick, 2014)*. In terms of the present distributed query technologies, integer linear programming (ILP) is superior to existing algorithms, such as A-star, in establishing query system *(Dokeroglu et al., 2014)*. However, most studies have ineffectively processed the space–time cost problem of query system in large network. Yangming studied distributed matching-based query system and proposed an improved ILP query system model that could effectively balance query system cost and storage cost under a few constraints *(Yangming et al., 2011)*. Nevertheless, only the ILP model of distributed matching query when network layer information was known was given in this study while effectively realizing and implementing the proposed scheme in large network system were difficult. In a large network environment, the query system design problem when network layer information was unknown was formally expressed as ILP model in this study. A universal algorithm when network layer information was known and unknown was also designed, which effectively improved the performance of distributed query system in large-scale network, enhanced agrometeorological service accuracy and data-supporting capacity, timely implemented intelligent data analysis of agrometeorological situation, and provided excellent scientific service for agricultural scientific research, agricultural production, and meteorological disaster prewarning.

The present research on distributed query system mainly aims at algorithm improvement and optimization. Bruno used aggregate method to control query system and data statistics under system operation and proposed an optimization method for distributed query processing of big data ***(****Bruno et al., 2013****)***. Marin introduced a metadata-based indexing strategy to improve the efficiency of inquiring mobile object in large-scale system *(Marin and Rodríguez, 2010)*. Sharma proposed a random decision support system of query optimization based on heuristic method, and this system significantly improved the query performance ***(****Sharma et al., 2016****)***. However, these optimization algorithms have lacked research on rapid big data matching, and they cannot effectively solve the bottleneck problem that restricts the operation efficiency of query system.

Wittmann-Hohlbein discussed the entire solution of the multi-parameter mixed ILP problem of uncertain items in constraint matrix, right-hand vector, and objective function coefficients *(Wittmann-Hohlbein and Pistikopoulos, 2013)*; neither this algorithm, nor the scheme proposed by Yangming *(Yangming et al., 2011)* was restricted to fixed network topology and both could realize fault-tolerant backup and were thus of favourable extendibility. However, these schemes could barely be implemented and applied under large-scale network environment with the following deficiencies: (1) Only the circumstance when network layer information is known is considered, but that when information is unknown is disregarded; (2) When the delay is not so important and the storage constraint is very strict, the distributed match making cannot find the tradeoffs between the used storage capacity and the response delay.

In view of the preceding analysis, the lower bound of the space–time cost of the query system when network layer information was known was analysed in this study. The ILP model and algorithm design of the query system design problem when network layer information was unknown was formally proposed. For the excess complicacy problem of ILP in large-scale network, a universal heuristic algorithm when network layer information was known and unknown was designed based on disjoint path allocation (DPA) and node replication allocation (NRA) algorithms, and this algorithm was named DPA-NRA-ILP. The algorithm framework proposed in this study did not rely on specific topological structure and could effectively realize balance of storage cost and query delay.

MATERIAL AND METHODS

ILP Formulation for The System Without Network Layer Information

In distributed matching query system of agrometeorological big data, two node sets $P(v)$ and $Q(v)$ are defined for each node v: $P(v)$ is the redundant node set of node v, namely, data of node v should be backed up on all nodes in $P(v)$, and $Q(v)$ is the node set that should be queried when node v generates query request. For each node pair (v,v'), the intersection $|P(v) \cap Q(v')|$ is calculated. If the intersection is non-null, then some nodes in $P(v)$ can be queried by node v', and node v' can query node v.

The objectives of distributed matching are to (1) minimize the average of $|P(v)\cap Q(v')|$ taken over all node pairs (v,v') and (2) find the tradeoffs between the lower bound of objective (1) and the average number of elements (or worst case number of elements) in $S(v)$, where $S(v)=\{j : v\in P(j)\}$.

For quantifying the optimization efficiency of the query system, the query system cost is set as C, the storage cost is C_{memory}, the delay cost is C_{delay}, the number of storage equipment is N_{memory}, the algorithm parameter γ is the cost ratio of a storage to a unit delay cost, and the query system cost is formally defined as

$$\begin{aligned} C &= C_{memory} + C_{delay} \\ &= \gamma \times N_{memory} + C_{delay} \end{aligned} \tag{1}$$

p_{ik} is set as binary variable. When $p_{ik}=1$, data of node i are backup of node k, and $p_{ik}=\begin{cases}1 & k\in P(i)\\ 0 & k\notin P(i)\end{cases}$. q_{jk} is the binary variable, and $q_{jk}=\begin{cases}1 & k\in Q(j)\\ 0 & k\notin Q(j)\end{cases}$. m_{ij}^{k} is the binary variable, and $m_{ij}^{k}=\begin{cases}1 & k\in P(i)\cap Q(j)\\ 0 & k\notin P(i)\cap Q(j)\end{cases}$. S is the maximum storage space of each node. B is the maximum number of communication times in each query. When network layer information is unknown, the following (2)–(7) ILP problems can be used to describe the distributed matching-based query system.

Objective Minimize:
$$\sum_i\sum_k p_{ik} + \sum_j\sum_k q_{jk} \tag{2}$$

Subject to:

$$p_{ik} \ge m_{ij}^{k} \quad \forall i,j,k \tag{3}$$

$$q_{jk} \ge m_{ij}^{k} \quad \forall i,j,k \tag{4}$$

$$\sum_k m_{ij}^{k} \ge K \quad \forall i,j \tag{5}$$

$$\sum_i p_{ik} \le S \quad \forall k \tag{6}$$

$$\sum_k q_{jk} \le B \quad \forall j \tag{7}$$

Function (2) means to make minimum storage cost and communication cost, $\sum_i\sum_k p_{ik}$ expresses the storage cost, and $\sum_j\sum_k q_{jk}$ expresses the communication cost. Formula (3) expresses $m_{ij}^{k}=1 \Rightarrow p_{ik}=1$, namely, $k\in P(i)\cap Q(j) \Rightarrow k\in P(i)$. Formula (4) expresses $m_{ij}^{k}=1\Rightarrow q_{jk}=1$, namely, $k\in P(i)\cap Q(j)\Rightarrow k\in Q(i)$. Formula (5) means that the system can reliably operate even when $K-1$ nodes are failing in the system. Formulas (6) and (7) represent that the maximum number of storage units in each node is S and the maximum number of communication times in each query is B.

In this model, N is the node number in the network, and $2NK+KN^2$ variables and $2KN^2+N^2+K+N$ constraint conditions exist. This problem is difficult to directly solve in large-scale network. Therefore, the lower bound of objective function (2) will be discussed and the algorithm will be designed to achieve this lower bound.

Query System Design Algorithm Without Network Layer Information

Lower Bound of Objective Function

A graph with $2n+v$ nodes called $a(1)\ldots a(n)$, $b(1)\ldots b(n)$, $r(1)\ldots r(v)$ is constructed to study the lower bound of the objective. $a(i)$ stands for the arguments of P, $b(i)$ stands for the arguments of Q, and $r(i)$ stands for the rendezvous elements. Whenever j is the rendezvous element of $P(i)\cap Q(k)$, an edge is put from $a(i)$ to $r(j)$ and the edge is from $r(j)$ to $b(k)$.

For the triples (i,j,k), if the path $a(i)\to r(j)\to b(k)$ exists, then they are called good triples. At least

Kn^2 good triples can then be obtained from constraint condition (5).

$d(j)$ is set as the total edge number from $a(i)$ to $r(j)$; $e(j)$ is the total edge number from $r(j)$ to $b(k)$; and for any j, at most $d(j)e(j)$ good triples include j ($r(j)$ is taken as intermediate node). $|P(i)+|Q(i)||$ is the size of the node set, $d(i)$ and $e(i)$ meet the following relational expression:

$$\sum_{i=1}^{v}[d(i)+e(i)]=\sum_{i=1}^{n}(|P(i)+|Q(i)||)$$

which is referred to as objective function (2), and

$$\sum_{i=1}^{v}d(i)\geq Kn$$

The storage unit number of each node is S. At most, S i s satisfy $j\in P(i)$, that is, $d(j)\leq S$, and

$$s\sum_{i=1}^{v}e(i)\geq\sum_{i=1}^{v}e(i)d(i)\geq Kn^2$$

Define $m=\sum_{i=1}^{v}[d(i)+e(i)]$, then

$$\begin{aligned}ms&=s\sum_{i=1}^{v}[d(i)+e(i)]=s\sum_{i=1}^{v}d(i)+s\sum_{i=1}^{v}e(i)\\&\geq s\sum_{i=1}^{v}d(i)+Kn^2\ \geq sKn+Kn^2\end{aligned}$$

Thus, the lower bound of the objective is obtained as

$$m\geq Kn(1+\left\lceil\frac{n}{s}\right\rceil) \tag{8}$$

where n is the total node number, K is the number of nodes responding to each query, and s is the storage unit number of each node.

Construction of Query Algorithm

Definition: Convergent matrix R is an n×n matrix, and each of its matrix element r_{ij} is a set including intersection $P(i)\cap Q(j)$.

The definition implies that

$$\bigcup_{j=1}^{n}r_{ij}=P(i)\quad and\quad \bigcup_{i=1}^{n}r_{ij}=Q(j)\cdot$$

Convergent matrix R of the following form is constructed:

$$R=\begin{bmatrix}\{1..K\} & \{1..K\} & \cdots & \{1..K\}\\ \vdots & \vdots & \vdots & \vdots\\ \{1..K\} & \{1..K\} & \cdots & \{1..K\}\\ \{K+1,..2K\} & \{K+1,..2K\} & \cdots & \{K+1,..2K\}\\ \vdots & \vdots & \vdots & \vdots\\ \{K+1,..2K\} & \{K+1,..2K\} & \cdots & \{K+1,..2K\}\\ \cdots & \cdots & \cdots & \cdots\end{bmatrix}.$$

All elements of the first S rows in the matrix are $\{1,\ldots,K\}$, all elements from the $(S+1)$ row to $2S$ row are $\{K+1,\ldots,2K\}$, and so on; then,

$$P(i)=\{K\left\lceil\frac{i}{s}\right\rceil+1,\ldots,K(\left\lceil\frac{i}{s}\right\rceil+1)\}\ ,\ Q(j)=\{1,\ldots,K\left\lceil\frac{n}{s}\right\rceil\}\ .$$

In this case, $\sum_{i=1}^{n}(|P(i)|+|Q(i)|)=nK+nK\left\lceil\frac{n}{s}\right\rceil$,

namely, the lower bound of objective function (2) certified in the preceding section. Thus, the query system constructed through the above-mentioned method is optimal.

DPA-NRA-ILP Query System Design

Main Idea

The heuristic query system design method proposed in this study ensures that the query paths of any two nodes will not intersect, the redundant node position of each node is calculated, and a feasible solution can be certainly obtained only by finding disjoint paths in this method.

DPA and NRA are used in this method. In the DPA, the legal path needs to meet the constraints of node disjoint and shared risk link groups (SRLG). For each node pair, k groups of legal path should be determined to meet the reliability requirement (at the moment, $(k-1)$ mistakes can be allowed in the system) *(Dijkstra, 1959)*. The total delay cost of the k groups of paths should be as small as possible. In the NRA, paths used for query are constructed, and the query delay and storage costs of the algorithm should be adjusted. The redundant node location of each node should be determined until paths of the same group are at different nodes to ensure system survivability. If residual spaces exist to store a large amount of data, then an attempt can be made to use these spaces to reduce overall cost in Equation (1). When the overall cost cannot be further optimized or no residual data storage space exists, then the algorithm ends.

Algorithm Process

The process of DPA-NRA-ILP is shown in Figure 1. The overall query system cost in Equation (1) is used to determine the quality of feasible solution. The left half in the figure (steps 1–7) is the DPA process, and k groups of legal paths are found for each node pair. The right half in the figure (steps 8–13) is the NRA process, which is used to construct a feasible solution and reduce the system cost.

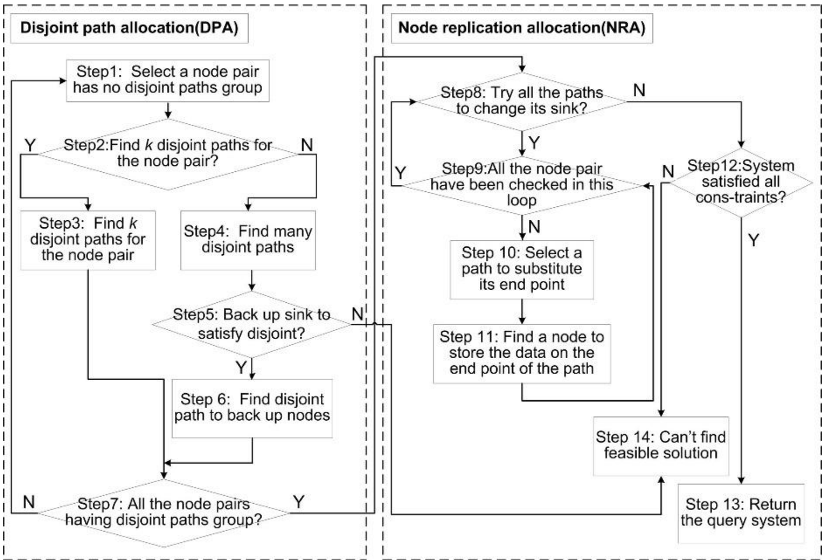

Fig. 1 - Main process of DPA-NRA-ILP

Description of detailed steps: steps 1–2 of the DPA select source node and sink node of the path, and an attempt is made to find k groups of legal paths. If yes, then step 3 will be executed; otherwise, steps 4–5 will be executed and under this circumstance, redundant sink nodes will be transferred onto other nodes to amplify legal paths. If legal paths are insufficient to constitute k groups yet, then the feasible solution cannot be found under the present reliability requirement, and the algorithm ends. The above-mentioned steps should be repeated until k groups of legal paths are found for all node pairs. Under abundant data operation, data should be replicated onto nodes nearby original node as far as possible.

If k groups of legal paths are found for all node pairs, then the NRA steps should be started (space substitution for time): step 8 judges whether a space is available to optimize time efficiency. Steps 10–11 modify the sink nodes of existing paths, as specifically described in the next paragraph. After redundancy is used to optimize the conversion of time efficiency, step 12 will be finally executed to test whether the present result meets all reliability requirements; if yes, then result will be output; otherwise, the algorithm ends.

Construction and Optimization of Feasible Solution

The following definitions are given:

Disjoint Path Set (DPS_{uv}): disjoint path set DPS_{uv} refers to the path set of query request from node

u to node v. All paths must take u as starting node (source node) but not certainly take v as end node (can end at redundant node of v). p_{uv}^{k} is the k path between nodes u and v, and $DPS_{uv} = \{p_{uv}^{k}\}$.

Weighted Path Delay (WPD_{uv}^{k}): it is related to the overall delay cost of p_{uv}^{k}. Under most circumstances, WPD_{uv}^{k} is rightly the overall delay cost, but if p_{uv}^{k} is not the only path with end node being v, then a large number should be superposed onto WPD_{uv}^{k}.

In step 8 of the NRA process, the algorithm will attempt to modify sink nodes for all paths to construct a feasible solution or optimize solutions. Steps 9–11 constitute an internal loop. Step 9 calculates $l = \arg\max_{k}\{WPD_{uv}^{k}\}$ for each node pair (u,v) and prepares to modify path l to optimize existing solutions. Step 10 finds the path that has not been tried but with maximum delay. Step 11 backs up sink node data onto node v', which is most adjacent to it and meets the following constraint conditions:

- Node v' is not the backup node of node v.
- The path exists between nodes u and v' and it does not intersect with other path except l in the present DPS set (allowed to intersect with l because l will be substituted). Delayed input parameter γ is lower than WPD_{uv}^{k}. The path meeting the above-mentioned conditions is $p_{uv}'^{l}$.

If this node v' can be found, then $p_{uv}'^{l}$ is used to substitute p_{uv}^{l} in the DPS set: $DPS_{uv} / p_{uv}^{l} \cup p_{uv}'^{l} \to DPS_{uv}$, or we will return to step 10, and another path is used for further trial. The cost to back up onto other nodes will be great because the selected new backup node is a legal node most adjacent to the original end point. Consequently, end point substitution of each path can be implemented once only.

Performance Analysis

The key idea of the DPA-NRA-ILP is to optimize results by steps on the condition that feasible solution is guaranteed. As shown in Figure 2, three disjoint paths exist between nodes 1 and 2: 1→2, 1→3→2, and 1→4→2. The three paths cannot be directly used for query because all paths take node 2 as end point. When single-node fault occurs to node 2, the system cannot maintain reliability. If the data redundancy of node 2 is put onto nodes 3 and 4, then the three paths can be transformed into 1→2, 1→3, and 1→4 to solve the reliability problem. This transformation can be realized by substituting sink node (end point).

During the path optimization process through the NRA steps, if the path with end point being v is not unique, then a large number will be superposed onto the overall query system cost WPD_{uv}^{k}. In this way, paths can be dispersed to different nodes by the algorithm to constitute feasible solution as a priority. When searching for substituting nodes, this algorithm will judge whether delayed input parameter γ of new path is lower than present delayed WPD_{uv}^{k}. The delay cost and storage cost of the algorithm can be controlled by inputting parameter γ. As γ increases, the consumption of storage units will be reduced and the delay cost will correspondingly increase.

$O(N^2)$ time complexity is needed to calculate the shortest path. Therefore, for each node pair, $O(KN^2)$ time complexity is needed to calculate K disjoint paths. During the NRA process, the end point of each path should be substituted, $O(N^2)$ is needed by the Dijkstra method *(Dijkstra, 1959)* to calculate all of the shortest paths from one node, and $O(N\log N)$ is needed for sorting. Substitution is tried successively for each node, and the substitution needs to be repeated for $O(N)$ times under the worst circumstance. Given N^2 node pairs in the system, the upper bound of overall time complexity of the algorithm is $O(K^2N^5\log N + 2KN^4 + KN^3)$, namely, $O(K^2N^5\log N)$. The shortest path is also calculated when the main time is used for substitution.

RESULTS

Experimental Scheme

The experiment time was selected in June in 2016, and the place was the Chaohu Lake in Anhui Province, China. This period comprised great meteorological change, mass meteorological data, and high requirement of agricultural production for real-time meteorological information. Data were acquired through field sampling, ground automatic meteorological observation, and radar remote sensing monitoring, as shown in Figure 3.

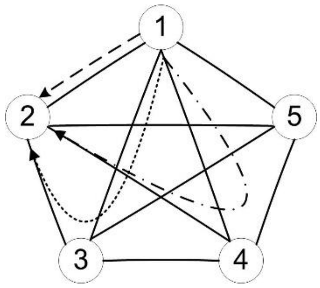

Fig. 2 - Disjoint paths from nodes 1 to 2

Fig.3 - Meteorological Data Acquisition

The algorithm in this study was implemented based on intelligent agrometeorological service cloud system and its system framework is shown in Figure 4 *(Xiang et al., 2015)*.

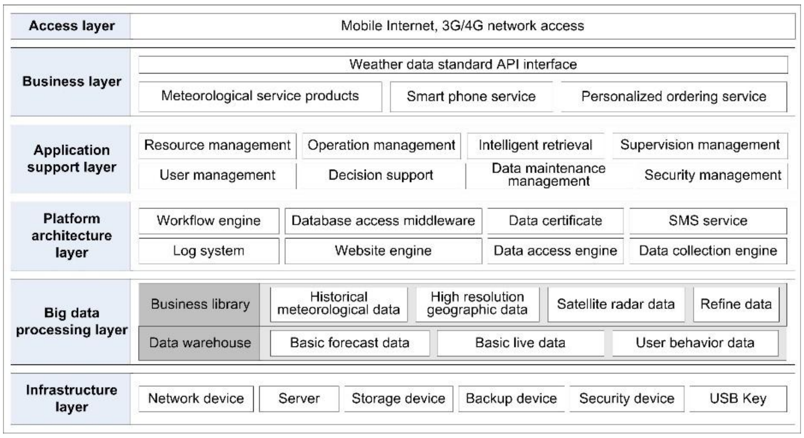

Fig. 4 - System Framework of Intelligent Agrometeorological Service Cloud

The experimental objective was to explore the influences of network scale and algorithm parameter, namely, cost ratio γ of storage to unit delay cost, on the algorithm execution. Section 2 proved that the algorithm in this study could still obtain optimal solution when network layer information was unknown. The experimental emphasis here was laid on the testing algorithm performance in simulation environment of known network layer information.

Experimental Result Analysis

Influence of Network Scale

Five network nodes were selected from agrometeorological network to construct a small-scale network test DPA-NRA-ILP algorithm, as shown in Figure 2. The execution process of the algorithm is shown in Figure 5.

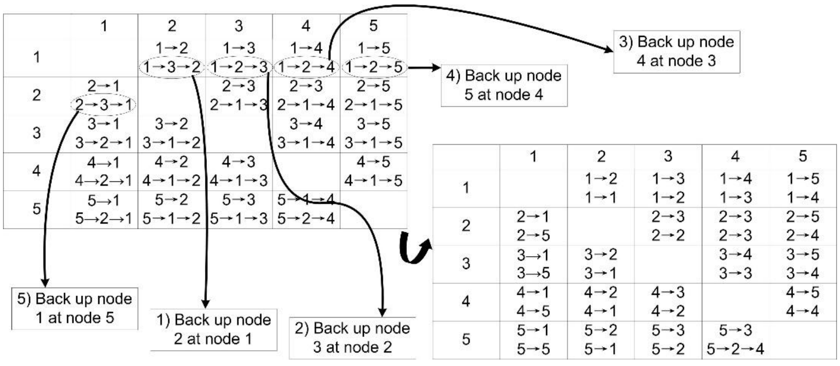

Fig. 5 - Example of DPA-NRA-ILP execution based on the network in Fig. 2

The delay cost between any two nodes was set 1, except the delay cost on (4, 5) was set 100, and the algorithm parameter $\gamma = 2$. The left table in Figure 5 shows the DPA results. After disjoint paths were found for each node pair, NRA was started for path adjustment. For example, in the first loop, the algorithm adjusted the second path from nodes 1 to 2, and the data on node 2 were backed up on node 1. Each path was queried through sequential substitution, and redundancy was created. The obtained results are shown in the right table in Figure 5. The algorithm generated the optimal solution.

The influence of network scale on the algorithm was analysed. A large number of network nodes were selected from agrometeorological network, a large-scale analog network was constructed through the method of Waxman *(Cheng et al., 2000)* and X and Y coordinate values of nodes were within 0 and 100. The shortest paths of all node pairs were calculated, and these lengths were taken as the delay cost between two nodes.

The influences of network scale on algorithm running time and query system cost are shown in Figures 6 and 7. Each node in the figure is the average cost of hundreds of query systems designed through DPA-NRA-ILP. In all simulations, the algorithm parameter γ was set as 10 and each node could store five copies of data of other nodes (namely, the storage unit number was 6). The storage spaces of all nodes in the result were used, and Figure 6 reflects the influence of network scale on algorithm running time. Figure 7 shows that the cost of query system largely presented a linear growth and the algorithm running time increased rapidly because the time complexity of DPA-NRA-ILP under the worst circumstance was $O(K^2N^5 \log N + 2KN^4 + KN^3)$, which was much faster than the linear growth.

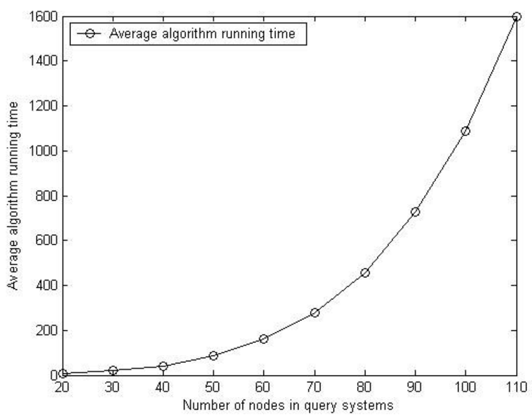

Fig. 6 - Influence of Network Scale on Algorithm Time

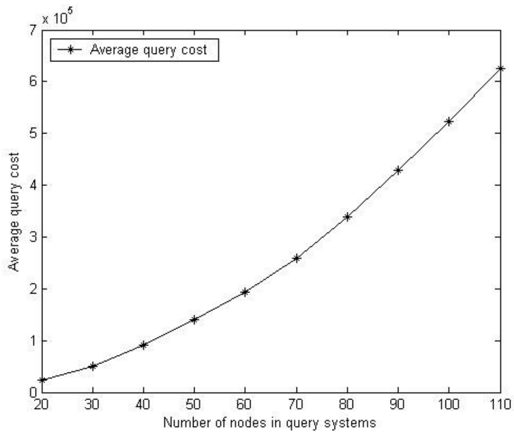

Fig. 7 - Influence of Network Scale on Query System Cost

Impact of Cost Ratio γ

An important feature of algorithm framework in this study was that it could conveniently adjust the time and space cost of the algorithm, which is significant in practical application. The influence of algorithm parameter γ on the space–time cost of the algorithm is shown in Figures 8–11.

Figure 8 reflects the relationship between γ and algorithm cost under system scales. The results showed that, when γ increased, the algorithm cost kept increasing. This finding was unrelated to system scale because, when γ increased, much space was needed to store redundant data.

Figure 9 shows the relationship between γ and storage cost. The results indicated that, if γ was small, all usable space would be used by the algorithm to reduce delay cost. When γ increased to a large degree (approximately 30), the storage cost would rapidly decline because using space to store redundant data was cost effective.

Figure 10 indicates that the change in delay cost was unobvious because all storage space was used, and the location of redundant data approximated to the original node considerably. As γ increased, the change in location of redundant data would result in slight reduction in delay cost. When γ increased to above 30, the delay cost increased with γ. The reason was that time was used to substitute space by the algorithm at the beginning, which indicated that the algorithm could realize conversion between time and space costs.

Figure 11 reflects the relationship between algorithm running time and γ. At the beginning, the algorithm running time would increase with γ because when γ increased. A large number of nodes should be tried by the algorithm to obtain optimal node with small cost. When γ was large, the algorithm operated fast because the number of nodes needing calculation reduced at the moment.

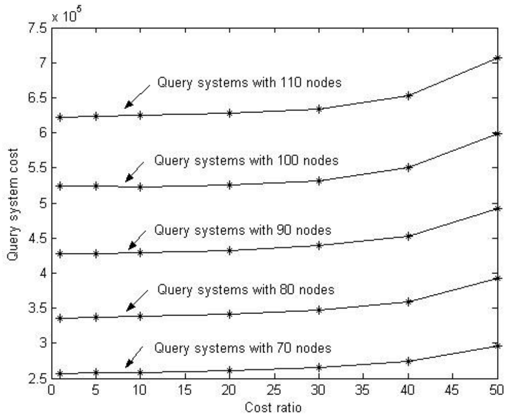

Fig. 8 - Influence of γ on Algorithm Cost

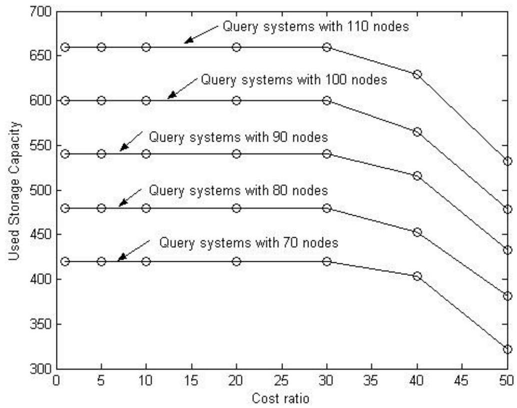

Fig. 9 - Influence of γ on Storage Cost

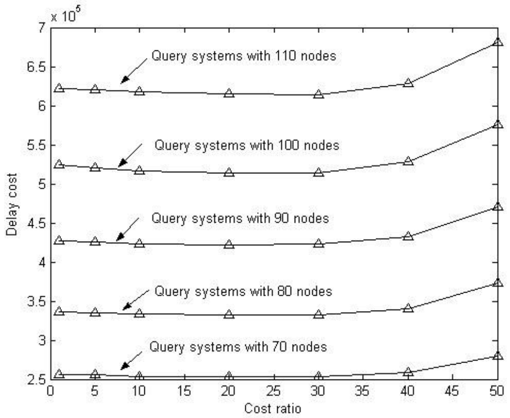

Fig.10 - Influence of γ on Delay Cost

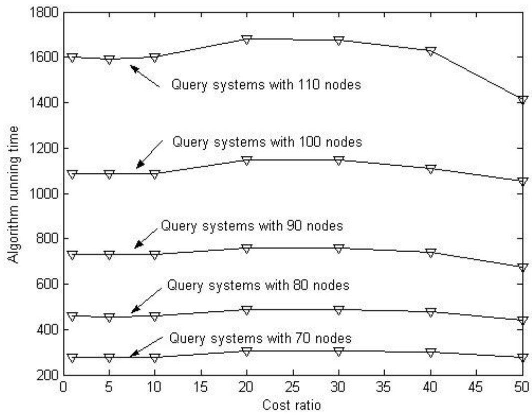

Fig.11 - Influence of γ on Algorithm Running Time

Performance Comparison Between the Algorithm in this Study and the ILP Algorithm

The performance comparison between the DPA-NRA-ILP algorithm proposed in this study and the ILP algorithm of Yangming *(Yangming et al., 2011)* is shown in Table 1. Large-scale network test data were the result based on network, as shown in Figure 2. As under large-scale network environment and when no network layer information was available, the ILP algorithm was not applicable. An emphasis was laid on comparing the performance of the two in small-scale network.

Table 1

Comparison between the algorithm in this study and ILP

Algorithm	Small-scale network		Large-scale network	Without network layer information
	Delay cost	Storage cost		
ILP	36	10	Not applicable	Not applicable
DPA-NRA-ILP	36	10	Applicable	Applicable

The test analysis in the previous paragraph implied that the solution obtained by DPA-NRA-ILP was different from that obtained by the ILP algorithm. However, Table 1 indicates that the two had the same cost. Thus, both were optimal solutions of the problem. However, the algorithm in this study could still obtain an excellent solution when network layer information was unknown in large-scale network.

CONCLUSIONS

Distributed matching-based query algorithm was investigated in this study under large-scale network environment based on theoretical analysis to improve the performance of data query system in intelligent agrometeorological service cloud system. The obtained main conclusions were as follows:

(1) When network layer information was unknown, using the ILP problem to describe the distributed matching-based query system model could obtain optimal query system at minimum system cost.

(2) The lower bound of objective function, which was related to the total number of nodes, the number of storage units in each node, and the number of nodes responding to each query, should be defined to realize optimization of query system in large-scale network. When the objective function achieved lower bound, the space–time cost of the query system was the minimum and the algorithm was optimal.

(3) The constraint conditions in distributed matching-based query system model were separated in different algorithm processes and a flexible algorithm framework could be obtained. Thus, adjusting the time and space costs of the algorithm would be convenient.

An important supplementation was made for distributed query system design of agrometeorological big data. However, when an attempt was made for node substitution, the calculated shortest path had certain impact on the time cost of the system. Therefore, reasonable experimental design and accurate numerical simulation should be developed, which will be used for in-depth analysis of the above-mentioned problem. These influencing factors should be considered in future studies.

ACKNOWLEDGMENTS

This study was supported by the National Natural Science Foundation of China (No. 61273329), and Natural Science Research Project of Anhui Vocational and Technical College (No. AZY2016KJ04).

REFERENCES

[1] Bruno N., Jain S., Jingren Z., (2013), Recurring job optimization for massively distributed query processing, *Bulletin of the IEEE Computer Society Technical Committee on Data Engineering*, Vol. 36, Issue 1, IEEE, USA, pp.46-55;

[2] Cheng J., Qian C., Sugih J., (2000), Inet: internet topology generator, *IEEE Transactions on Magnetics*, Vol. 19, Issue 3, University of Michigan, USA, pp.960-963;

[3] Dijkstra E. W., (1959), A note on two problems in connexion with graphs, *Numerische mathematik*, Vol. 1, Issue 1, Springer, Heidelberg/German, pp.269-271;

[4] Dokeroglu T., Bayır M. A., Cosar A., (2014), Integer linear programming solution for the multiple query optimization problem, *Information Sciences and Systems 2014*, Springer, Switzerland, pp. 51-60;

[5] Guangsheng Z., (2015), Research prospect on impact of climate change on agricultural production in China, *Meteorological and Environmental Sciences*, Vol. 38, Issue 1, Henan Meteorological Bureau, Zhengzhou/China, pp.80-94;

[6] Marin M., Rodríguez M. A., (2010), A meta-index for querying distributed moving object database servers, *Information Systems,* Vol. 35, Issue 6, Elsevier, Oxford/England, pp.637-661;

[7] Mckendrick J., (2014), Data integration in the era of big data, *Database Trends and Applications*, Vol. 28, Issue 1, Information Today Inc., New Jersey /USA, pp.4-6;

[8] Sharma M., Singh G., Singh R., (2016), Design and analysis of stochastic DSS query optimizers in a distributed database system, *Egyptian Informatics Journal*, Vol. 17, Issue 2, Elsevier, Oxford/England, pp.161-173;

[9] Wittmann-Hohlbein M., Pistikopoulos E. N., (2013), On the global solution of multi-parametric mixed integer linear programming problems, *Journal of Global Optimization*, Vol. 57, Issue 1, Springer, Netherlands, pp. 51-73;

[10] Xiang S., Huarui W., Qingxue L., (2015), Design and implementation of massive agricultural information resource management platform, *Computer Applications and Software*, Vol. 32, Issue 3, Shanghai Institute of Computing Technology, Shanghai/China, pp.75-78;

[11] Yangming Z., Sheng W., Huacheng C., et al., (2011), A new framework to design distributed query system, *International Conference on Advanced Intelligence and Awareness,* IET, Shenzhen/China, pp.270-274;

[12] Yingjia Z., Yaohui L., Yuhua C., (2013), Major progress of global and China regional climate change projection, *Journal of Arid Meteorology*, Vol. 31, Issue 4, Chinese Meteorological Society, Lanzhou/China, pp.803-813.

A PRODUCTIVE POTENTIAL ESTIMATION OF FIVE GENOTYPES OF THE MISCANTHUS ANDERSS GENUS IN THE UKRAINIAN STEPPE ZONES CONDITIONS
/
ОЦІНКА ПРОДУКТИВНОГО ПОТЕНЦІАЛУ П'ЯТИ ГЕНОТИПІВ МІСКАНТУСУ ANDERSS GENUS В УМОВАХ СТЕПОВОЇ ЗОНИ УКРАЇНИ

Prof. Ph.D. Agri.Sci. Kharytonov M.[1)], Dr. Ph.D. Biol.Sci.Martynova N.[1)], Dr. Assoc. Prof. Ph.D. Biol.Sci.Sitnyk S.[1)], Dr. Assoc. Prof. Ph.D. Eng.Sci. Naumenko M. [1)], Prof. Ph.D. Biol.Sci. Pidlisnyuk V.[2)], Assoc. Prof. Ph.D. Biol.Sci.Stefanovska T.[3)],

[1)] Dnipropetrovsk State Agrarian and Economic University, Dnipro / Ukraine
[2)] Jan Evangelista Purkyne University in Ústí nad Labem, Ústí nad Labem / Czech Republic
[3)] National University of Life & Environmental Sciences, Kiev / Ukraine
Tel: 380973456227; E-mail: envteam@ukr.net

Keywords: *weather conditions, Miscanthus species, productivity parameters, biomass yield, soluble sugars*

ABSTRACT
Five genotypes of the Miscanthus Anderss genus have been studied. M. sacchariflorus has very long rhizomes which quickly colonize the big areas. M. Giganteus, M. oligostachyus and particularly M. sinensis are more cespitose, their spread is slow and there is little risk of uncontrolled invasion of hedges or field, compared to the M. sacchariflorus. Despite that stands of M. sacchariflorus tend to be larger but less dense than stands of other Miscanthus species, M. s. "Gracillimus" has the highest stem density per unit of area. The biomass yield of Miscanthus per area in the earliest years of cultivation depends on the planting density. Under steppe conditions, optimal planting density is 14800 piece/ha for M. sacchariflorus and M. Giganteus and 20000 piece/ha for other species. Harvesting of above-ground biomass was made in the end of a growing season in October. It was revealed that during the drying process, plants lost up to 44% of water. Nevertheless, this indicator varies among species from 37.3% - M. sacchariflorus to 43.9% - M. oligostachyus. During the second year, substantial growth of productivity was observed for all species. Yield increased from 2.5 (M. sinensis) to 3.6 times (M. oligostachyus). In absolute measures, the largest values were noted for M. Giganteus (6.76 t/ha).
The work results show that optimum time for biomass harvesting is late autumn (November) for the solid types of fuel production or the end of the growing season (October) for the bioethanol production.

РЕЗЮМЕ
Вивчено п'ять генотипів роду Miscanthus Anderss. Висока вегетативна рухомість властива M. sacchariflorus, середня – M. Giganteus і M. oligostachyus, низька – M. sinensis. При визначенні щільності стояння пагонів спостерігається зворотна залежність: висока щільність – у M. sinensis (особливо у сорту Gracillimus), середня – у M. Giganteus, M. oligostachyus і низька – у M. sacchariflorus. Врожайність біомаси міскантуса з одиниці площі в перші роки вирощування залежить від щільності посадки рослин. В умовах степу оптимальним представляється середня щільність посадки: 14800 шт/га для M. sacchariflorus і M. Giganteus і 20000 шт/га для інших видів. Прибирання надземної біомаси проводилося в кінці вегетативного сезону в жовтні. Виявлено, що в процесі сушіння рослини втрачають до 44 % води. Тим не менш, цей показник трохи варіює між видами від 37,3% (M. sacchariflorus) до 43,9% (M. oligostachyus). Протягом другого року спостерігалося значне збільшення врожайності для всіх видів. Продуктивність збільшилася від 2,5 (M. sinensis) до 3,6 разів (M. oligostachyus). Щодо абсолютних показників, найбільші значення були зафіксовані для M. Giganteus 6,76 т/га. За проведеними дослідженнями оптимальний час для збирання врожаю є пізня осінь (Листопад), для виробництва біопалива або біоетанолу – кінець періоду вегетації (у Жовтні).

INTRODUCTION
Search for renewable energy sources is an integrated part of the general sustainable development of society. Today, the share of renewable energy in the world is about 13%. For example, in the European Union, the current potential of energy crops is estimated as 44-47 Mtoe/year. Until 2020, it is planned to increase biomass in gross final energy consumption to 138 Mtoe. According to recent data, in the EU the total area under lignocellulosic energy crops (Willow, Poplar, Miscanthus, Switchgrass, Reed canary grass)

is about 130-140 th. ha. At the same time, the cultivation area for energy crops intended for liquid biofuels production (grain crops and rape) is much bigger and exceeds 2.5 Mha. *(AEBIOM Report, 2011)*.

In Ukraine, the issue of sustainable bioenergy development is still at a relatively early stage of discussion, understanding and implementation. Currently, the share of biomass in the total primary energy input in the country is only 1.2% *(Geletukha et al., 2014, 2016)*. Miscanthus is a promising crop for the production of cellulose containing biomass *(Dohleman et al., 2009; Zub & Brancourt-Hulmel, 2010; Brosse et al., 2012)*. It is a perennial rootstock grass that originates from East Asia. Only 8-9 Miscanthus species of 16 known can grow in the temperate climate zone. They have a well-developed root system (up to 2.5 m deep), are characterized by fast growth and good resistance to low temperatures. Currently, four species of *Miscanthus* are actively studied and grown as an effective source of bioenergy raw materials. First of all, it concerns *Miscanthus Giganteus* - J.M.Greef et Deuter ex Hodk. et Renvoize. – spontaneous sterile hybrid cross between *Miscanthus sacchariflorus* (Maxim.) Hack. and *Miscanthus sinensis* Anderss. Along with other energy crops, this species takes rather large industrial areas in Western Europe and the USA. There is a lot of information about cultivation and productivity of giant miscanthus in these regions *(Nixon & Bullard, 2001; Caslin et al., 2010; Williams & Douglas, 2011; Anderson et al., 2011)*. There are also numerous researches devoted to the study of existing and creation of new genotypes of M. Giganteus, M. sacchariflorus and M. sinensis for obtaining more resistant and productive varieties *(Hodkinson et al., 2002; McKervey et al., 2008; Shumny et al., 2010; Nishiwaki et al., 2011; Yu et al., 2015; Cichora et al., 2015)*. The potential of other *Miscanthus* species is almost unknown, at a time when the possibilities of using them as an energy culture are sufficiently extensive.

The quantitative and qualitative indicators of the *Miscanthus* biomass depend not only on the species genetic component, but also on a large number of different external factors: the geographical location of the farming area, climatic conditions, water relationships, cultivation technology, availability of mineral elements etc. *(Lewandowski & Schmidt, 2006; Glowacka et al., 2013; Arnoult & Brancourt-Hulmel, 2015; Matyka & Kus, 2016)*. It is believed that medium-dense soils with low groundwater levels are suitable for growing Miscanthus. The plant has a relatively small demand for water, corresponding to an annual rainfall of 600-700 mm. However, this demand may enhance as the amount of biomass increases. For instance, 4-5-year-old plants of *M. Giganteus*, for normal growth and development, can absorb water amount corresponding to 900 mm and more annual precipitation. Investigations of different *Miscanthus* species were carried out mainly in Western Europe and Russia in regions with sufficient water supply *(Lewandowski et al., 2000; Clifton-Brown et al., 2001; Jezowski, 2008; Milovanovic et al., 2012; Kalinina et al., 2017)*. For example, in Germany, Denmark, Northern Ireland, England, Austria and the Centre of European Russia, the average annual precipitation varies from 550 to 700 mm, in Serbia from 850 to 900 mm, in Switzerland from 900 to 1000 mm, in Northwest Spain from 1800 to 1950 mm. In Ukraine studies of Miscanthus were carried out under the conditions of wooded district and forest-steppe, where the annual precipitation reaches 650-750 mm and 600-680 mm, respectively *(Tziporenko & Rakhmetov, 2013; Rakhmetov et al., 2015; Skachok & Kvak, 2016; Kalinina et al., 2017)*. In the steppe zone of Ukraine, where this work was conducted, the average annual rainfall does not usually exceed 500-550 mm. Deficiency of moisture can negatively affect the yield and biomass quality. Therefore, there is a need to study and select drought-tolerant and productive genotypes of Miscanthus for economically substantiated cultivation under conditions of insufficient water supply.

MATERIALS AND METHODS

Five genotypes of the Miscanthus Anderss genus have been studied: *M. sacchariflorus* (Maxim.) Hack., *M. sinensis* Anderss., *M. Giganteus,* J.M. Greef et Deuter ex Hodk. et Renvoize., *M. oligostachyus* Stapf. and *M. sinensis* “Gracillimus”. The planting stock for the trial was taken from the collection plants of the Oles Gonchar Dnepr National University Botanical Garden and from the Institute of Bioenergy Crops and Sugar Beet (*M. Giganteus*). The seedlings with 3-4 shoots were chosen for planting (Fig.1). Plants were set in the spring of 2015 on experimental sites according to the following scheme: for *M. sinensis, M. sinensis* "Gracillimus" and *M. oligostachyus*, the interval between the rows is 75 cm, the interval between the plants in the row is 60 cm (planting density is 2 pieces per m^2); for *M. sacchariflorus* and *M. Giganteus* the interval between the rows is 90 cm, the interval between the plants in the row is 75 cm (planting density is 1.5 pieces per m^2).

The soil of experimental plots is medium loam, low-humus black soil on loess. The physicochemical and agronomic parameters of this soil type are optimal for the normal growth and development of the

Miscanthus. Fertilizers and irrigation were not used. The morphometric parameters and biomass productivity were subject of study.

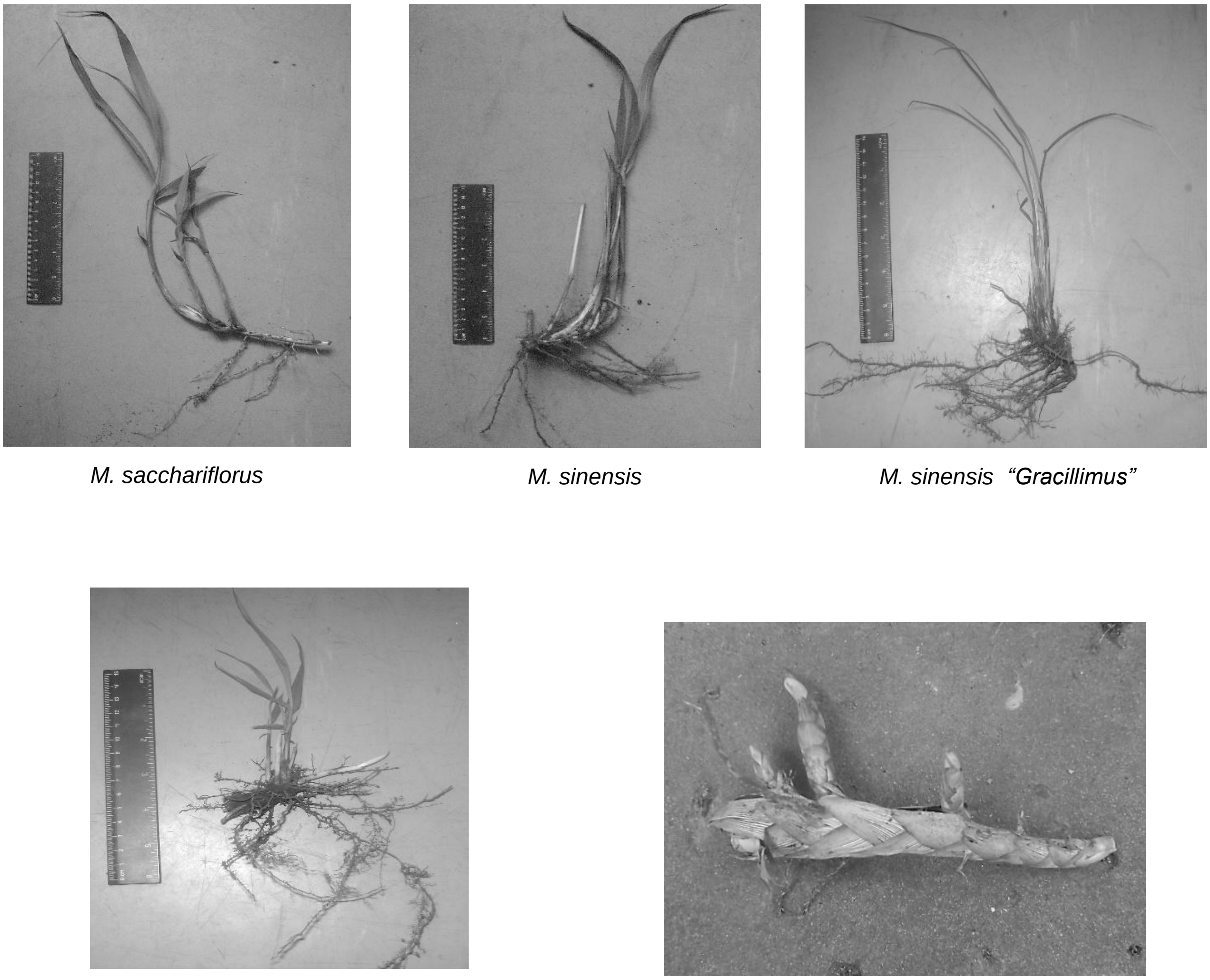

M. sacchariflorus *M. sinensis* *M. sinensis "Gracillimus"*

M. oligostachyus *M. Giganteus*

Fig. 1 - Miscanthus saplings

Culm height from the soil surface to the collar of the flag leaf of a representative culm for each plant was measured with a measuring ruler during the second week of October. Calliper was used to determine stem diameter by clamping it on to a random plant tiller 15 cm above the ground surface. Stem number per plant was counted during the first week of October. The inflorescence length was measured by means of a ruler in August in the flowering period.

For above-ground biomass determination, the whole plants were cut by hand, using a knife, at the end of each growing season at a stable height of 10 cm and they were weighed. Then they were dried until a constant weight was achieved. These dry samples were weighed to estimate the above-ground dry matter yield. Thus fresh weight (FW) and dry weight (DW) were determined and moisture (M) was calculated as: M(%)=100 × (FW – DW) / FW.

The soluble carbohydrates were estimated by photometric methods (*Naiem and Abdelatif, 2001*). Samples were quantified photometrically by measuring the change in wavelength at 660 nm. The amount of soluble carbohydrates was calculated with the help of standard curve obtained by using different concentration of standard glucose solution. The amount of sucrose was estimated as difference between total sugar content and reducing sugar content and multiplied with coefficient 0.95. Statistical analysis was conducted using the software package StatGraphics Plus5 with all tests of significance being made at a type 1 error rate of 5%.

RESULTS

The climate of the Dnepropetrovsk region is moderately continental. Over the course of a year, the temperature typically varies from -8°C to +31°C. The cold season lasts from December to March with an average daily temperature -3.1°C. In winter, air temperature can sometimes fall till -20-25°C. The warm season lasts from May to September 15 with an average daily temperature above +24°C. Often, the average day temperature in summer reaches +30-34°C, maximum +37-40°C. In recent years, there has been an increase in the average monthly temperature in comparison with the long-term data (Fig. 2a). Average annual precipitation is moderate. During the warm season, precipitation occur most often in the form of thunderstorms (63%), light rain (31%), and moderate rain (6%). The rainfall varies significantly over the course of the warm season (Fig.2b).

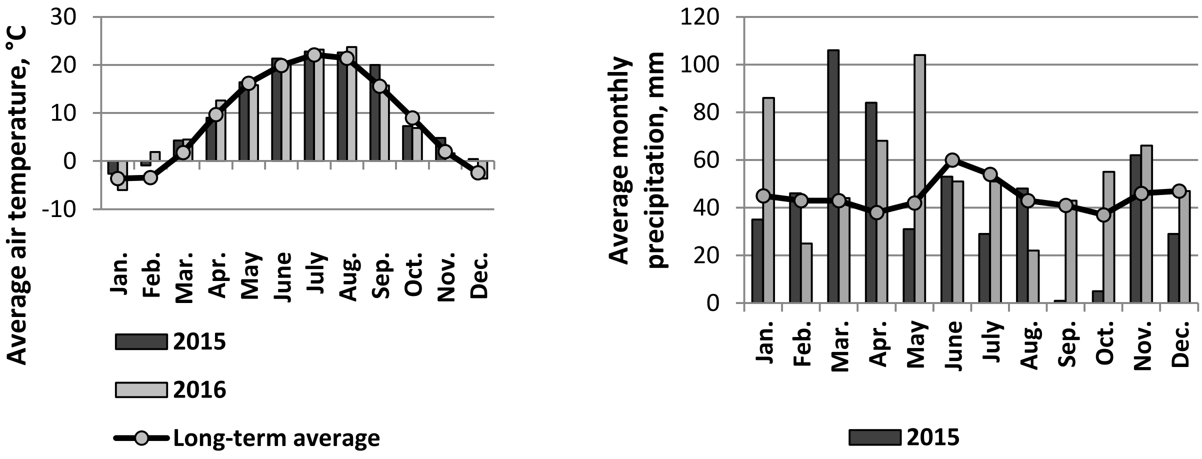

a) b)

Fig. 2 - Monthly average of air temperature and precipitation in the Dnipropetrovsk region

Considering that the spring in the steppe zone is short, planting of the *Miscanthus* must be made as soon as possible so that the plants can use the soil moisture accumulated in winter and grow stronger. The optimal dates for spring planting are the first and second decades of April. Autumn planting in October is also possible. Observing the planting time, we noticed that the survival rate of saplings in the first year of cultivation is high from 80% (*M. Giganteus*) to 100% (*M. sacchariflorus*).

According to long-term phenological observations in the steppe zone of Ukraine, spring growth *Miscanthus* begins mainly at the end of April. In some years, it starts in early May. Growing season continues until the third decade of October. *Miscanthus* plants reach the greatest height in a flowering stage, which comes in August-September.

The vegetation period of *M. s.* “Gracillimus” is longer than that of other varieties. Its leaves yellowing continue during December. The flowering stage also begins later, in November, and may remain unfinished in the event of early autumn frosts.

The studied *Miscanthus* species under introduction conditions do not form seed and can only be propagated vegetatively. *Miscanthus* spreads naturally by means of underground rhizomes. *M. sacchariflorus* has very long rhizomes which quickly colonize the big areas. *M. Giganteus, M. oligostachyus* and particularly *M. sinensis* are more cespitose, their spread are slow and there is little risk of uncontrolled invasion of hedges or field, compared to *M. sacchariflorus*. Despite that stands of *M. sacchariflorus* tend to be larger but less dense than the stands of others *Miscanthus* species, *M. s.* “Gracillimus” has the highest stem density per unit of area.

In the first year after planting, all *Miscanthus* species actively increased aboveground and underground biomass.

Plants of *M. sinensis, M. Giganteus* and *M. sacchariflorus* had a stem height of about 1 m at the end of the growth season. The highest was *M. sinensis* (106.1 cm), the lowest – *M. oligostachyus* (56.5 cm). In the second year of cultivation, the most active growth was observed for *M. Giganteus* and *M. sacchariflorus*. Their height was about 2 m (Table 1). This parameter for *M. sinensis* and *M. sinensis* "Gracillimus" was less by 25-32%. The height of *M. oligostachyus* did not exceed 1 m. In the first year, the flowering phase was absent in two species: *M. Giganteus* and *M. sinensis* "Gracillimus". The latter species did not bloom in the second year either. Measurements of the panicle length showed that this indicator is constant, it is determined by the genotype and does not depend on the age of the plants (Table 1). Plants of *M. sacchariflorus* have the longest inflorescence, and *M. oligostachyus* - the shortest.

Table 1

Culm height and inflorescence length of Miscanthus

	Culm height, cm		Panicle length, cm	
	First year	Second year	First year	Second year
M. sacchariflorus	80.0 ± 1.23	188.8 ± 2.93	33.36 ± 0.49	34.22 ± 0.52
M. sinensis	106.1 ± 2.42	142.5 ± 1.66	26.02 ± 0.40	26.88 ± 0.31
M. sinensis "Gracillimus"	73.1 ± 1.70	135.7 ± 2.33	–	–
M. Giganteus	86.7 ± 0.98	198.4± 2.91	–	27.08 ± 0.38
M. oligostachyus	56.5 ±1.63	93.7 ± 1.86	14.52 ± 0.34	14.70 ± 0.35

The formation of new culms occurred during the entire vegetation period. During the first year of cultivation, the stem number per plant increased on average by 3-4 times (Table 2). At the end of the year, the smallest number was observed in *M. oligostachyus* plants. The clump growth intensity in the second year of cultivation was less than that in the first year and for most species it was from 95 to 120%. Plants *M. oligostachyus* showed the greatest stem number increase (by 3 times) compared to the previous year.

Measurement of the stem diameter detected the highest indicators in *M. Giganteus*, and the smallest in *M. oligostachyus* (Table 2). This parameter increases with age, but not much, from 1.4% (*M. Giganteus*) to 10.7% (*M. sinensis* "*Gracillimus*").

Table 2

Season-end stem number and stem diameter of Miscanthus

	Stem number per plant		Stem diameter, mm	
	First year	Second year	First year	Second year
M. sacchariflorus	11.97 ± 0.54	26.2 ± 0.44	4.2 ± 0.15	4.4 ± 0.13
M. sinensis	15.21 ± 0.52	30.3 ± 1.25	4.22 ± 0.11	4.3 ± 0.11
M. sinensis "Gracillimus"	17.74 ± 0.95	34.48 ± 1.21	4.12 ± 0.10	4.56 ± 0.10
M. Giganteus	16.80 ± 0.64	33.12 ± 0.82	8.1 ± 0.21	8.21 ± 0.17
M. oligostachyus	10.22 ± 0.54	33.7 ± 1.14	3.3 ± 0.12	3.4 ± 0.10

The biomass yield of *Miscanthus* per area in the earliest years of cultivation depends on the planting density. If the planting density becomes greater than the yield also increases. However, planting more saplings can increase the cost of a plantation making from 50 to 150%. Especially as in the next years the difference between productivity on the plots differing in planting density is levelled. Usually the planting density of *Miscanthus* can vary from 10000 to 25000 pieces per hectare *(Himken et al., 1997; Christian et al., 2009; Williams & Douglas, 2011; Kalinina et al., 2017)*. Under steppe conditions optimal planting density is 14800 piece/ha for *M. sacchariflorus* and *M. Giganteus* and 20000 piece/ha for other species. Harvesting of above-ground biomass was made in the end of a growing season in October. It is revealed that during the drying process, plants lose up to 44% of water. Nevertheless, this indicator varies among species from 37.3% - *M. sacchariflorus* to 43.9% - *M. oligostachyus*. The yield of dry biomass was moderate in the first year of cultivation. Among tall species this parameter varies from 0.79 to 2.3 t/ha. Productivity of undersized *M. oligostachyus* was the lowest, only 0.33 t/ha (Fig.3). During the second year, substantial growth of productivity was observed for all species. Yield has been increased from 2.5 (*M. sinensis*) to 3.6 times (*M. oligostachyus*). In absolute measures the largest values were noted for *M. Giganteus* (6.76 t/ha). Nevertheless, these data somewhat lower than similar indicators of Miscanthus productivity, received for the European and East Asian regions where there is sufficient water supply *(Zub et al., 2010; Feng et al., 2015; Richter et al., 2016)*. In Ukraine, such comparison can be done only for *M. Giganteus* because other species practically are not studied. The comparative estimation has shown that in a steppe zone of Ukraine the productivity of *M. Giganteus* in the first years of cultivation is less by 20-50 % than in wooded district and forest-steppe *(Gumentyk et al., 2013; Rakhmetov et al., 2015)*. Thus, there is an obvious unfavourable influence of droughty conditions on biomass yield. The aboveground biomass of Miscanthus can be a significant source for bioethanol production. Usually technologies of bioethanol production by Miscanthus biomass includes following stages: pre-treatment remove hemicellulose and get reactive cellulose; hydrolysis for fermentable sugars; fermentation for production of ethanol (*Lien et al., 2005, Alvira et al, 2010, Huang et al., 2010*).

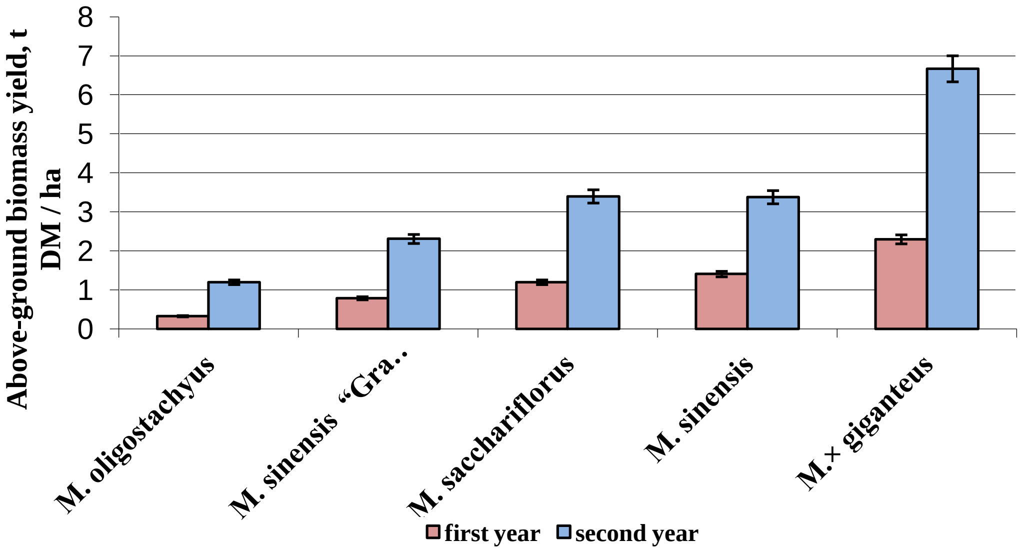

Fig. 3 - Above-ground biomass yield of *Miscanthus* under steppe zone conditions

At the same time, the biomass of *Miscanthus*, besides lignocellulosic components, contains water soluble carbohydrates and their total content is almost the same as in the case of traditional sacchariferous crops: *Sorghum*, *Eclrinochloa frumentacea*, *Setaria italica* et. *(Almorades and Hadi, 2009)*. The soluble sugar content was estimated in the end of the growing season (Fig.4).

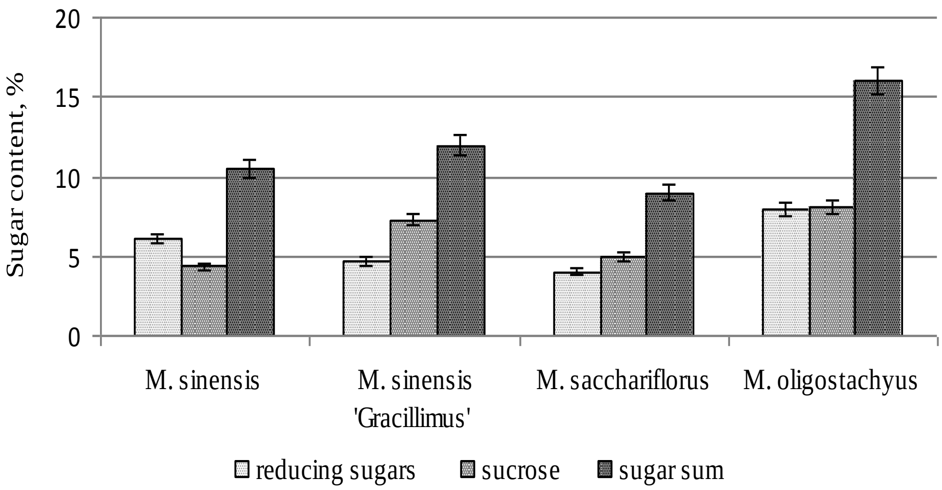

Fig. 4 - Soluble sugar content in aboveground biomass of *Miscanthus*

In this period, vegetation is still in progress. However, plants have already accumulated enough nutrients necessary for normal wintering and a cut of aboveground biomass will not damage the plant.

The sugar sum content varies in different species in range from 9.0 (*M. sacchariflorus*) to 16.05% (*M. oligostachyus*). Reducing sugars-sucrose ratio was nearly 50:50 at *M. oligostachyus*. At the *M. sinensis* reducing sugar content was greater than that of sucrose content by 40-60% and vice versa the biomass of *M. s. cv. Gracillimus* accumulates greater quantity of sucrose than reducing sugars by 56% and at *M. sacchariflorus* by 22.5%.

CONCLUSION

It is revealed that optimum terms of *Miscanthus* planting in a Ukrainian steppe zone are the first and second decade of April, and also from first to third decade of October. In the first year of cultivation, plants actively increase biomass. By the end of a vegetative season, the plants of the majority species reach heights about 1 m and stem number per plant increases at an average of three-four times. The intensity of clumps growth in the second year slightly decreases and ranges from 95 to 120%. The height of plants in the end of this period varies from 140 to 190 cm. The exception is the undersized *M. oligostachyus*, which had stems height only over 90 cm in the second year. The stem diameter also increases with age, but not greatly (from 1.4% to 10.7%). The yield of dry biomass in the first year among tall species varies from 0.79 to 2.3 t/ha. Productivity of *M. oligostachyus* was the lowest, only 0.33 t/ha. The yield of the second year is much higher. The highest productivity was noted for *M. Giganteus* (6.76 t / ha). The average measures are characteristic for *M. sacchariflorus and M. sinensis*. The yield of *M. oligostachyus* does not exceed 1.2 t/ha. Arid conditions of the steppe zone have a negative impact on the biomass productivity of Miscanthus. A comparative assessment showed that the yield of *M. Giganteus* in the first years of cultivation is 20-50% lower than in other regions of Ukraine with a higher level of water supply.

Determination of soluble carbohydrates in *Miscanthus* leaves and stems has shown high values of reducing sugars and sucrose.

REFERENCES

[1] Anderson E. Arundale R., Maughan M., et al, (2011), Growth and agronomy of Miscanthus Giganteus for biomass production, *Biofuels,* Vol. 2(1). pp.71-87;

[2] Annual Statistical Report on the contribution of biomass to the energy system in the EU 27, AEBIOM, 2011, http://ru.scribd.com/doc/73012151/2011-AEBIOM-Annual-Statistical-Report;

[3] Arnoult S., Brancourt-Hulmel M., (2015), A Review on Miscanthus biomass production and composition for bioenergy use: Genotypic and environmental variability and implications for breeding, *Bioenerg. Res*. Vol. 8, pp.502-526;

[4] Brosse N., Dufour A., Meng X., Sun Q., Ragauskas A., (2012), Miscanthus: a fast-growing crop for biofuels and chemicals production, Review, *Biofuels, Biorpod. Bioref*. P. 1–19;

[5] Caslin B., Finnan J., Easson L., (2010), Miscanthus best practice guidelines. Teagasc, *Crops Research Centre, AFBI*, Northen Ireland, 48 p;

[6] Cichorz S., Goska M., Rewers M., (2015), Miscanthus: Inter- and intraspecific genome size variation among M. Giganteus, M.sinensis, M. sacchariflorus accessions. *Acta Biologica Cracoviencia. Series Botanica,* Vol. 57(1), pp.104-113;

[7] Clifton-Brown J.C., Lewandowski I., Andersson B., et al, (2001), Performance of 15 Miscanthus genotypes at five sites in Europe, *Agronomy journal,* Vol.93, pp.1013-1019;

[8] Christian D.G., Yates N.E., Riche A.B., (2009), Estimation of ramet production from Miscanthus Giganteus rhizome of different ages, *Industrial Crops and Products,* Vol.30. P. 176-178;

[9] Dohleman F.G., Heaton E.A., Leakey A.D.B., Long S.P., (2009), Does greater leaf-level photosynthesis explain the larger solar energy conversion efficiency of Miscanthus relative to switchgrass? *Plant, Cell and Environment*, Vol. 32, pp.1525-1537;

[10] Feng X., He Y., Fang J., Fang Z., Jiang B., Brancourt-Hulmel M., Zheng B., Jiang D., (2015), Comparison of the growth and biomass production of Miscanthus sinensis, Miscanthus floridulus and Saccharinum arundinaceum, *Spanish Journal of Agricultural Research,* Vol.13 (3), pp.1-10;

[11] Geletukha G., Zheliezna T., Tryboi O., (2014), Prospects for the growing and use of energy crops in Ukraine, *UABio Position Paper,* No.10, 30 p;

[12] Geletukha G., Zheliezna T., Tryboi O., Bashtovyi A., (2016), Analysis of criteria for the sustainable development of bioenergy, *UABio Position Paper,* No.17, 30 p;

[13] Glowacka K., Jezowski, Kaczmarek Z., (2013), Gas exchange and yield in Miscanthus species for three years at two locations in Poland, *Canadian Journal of Plant Science*, Vol. 93, pp.627-637;

[14] Gumentik M., Kvak V., Zamoisky O., (2013), Yield of Miscanthus biomass, depending on the climatic conditions, timing and depth of rhizome planting in the Western Forest-steppe of Ukraine. / Урожайність біомаси міскантусу залежно від кліматичних умов, строків і глибини садіння ризомів у Західному лісостепу України, *Bulletin of Lviv National University. Series of Agronomy*, Vol.17(1), pp. 76-82;

[15] Himken M., Lammel J., Neukirchen D., Czipionka-Krause U., Olfs H-W., (1997), Cultivation of Miscanthus under West European conditions: seasonal changes in dry matter production, nutrient uptake and remobilization, *Plant and Soil,* Vol. 189, pp.117–143;

[16] Hodkinson T.R., Chase T.R., Takahashi C., Lietch I.J., Bennett M.D., Renvoize S.A., (2002), The use of DNA Miscanthus (Poaceae) sequencing (ITS and trnL-F), AFLP, and fluorescent in situ hybridization to study allopolyploid, *American Journal of Botany*, Vol.89, pp. 279-286;

[17] Jezowski S., (2008), Yield traits of six clones of Miscanthus in the first 3 years following planting in Poland, *Industrial Crops and Products,* Vol.27, pp.65-68;

[18] Kalinina O., Nunn Ch., Sanderson R., Hastings A.F.S., Weijde T. et al., (2017), Extending Miscanthus cultivation with Novel Germaplasm at six contrasting sites. *Frontiers in Plant Science*, Vol. 8, pp. 1-15;
[19] Lewandowski I., Schmidt U., 2006, Nitrogen, energy and land use efficiencies of miscanthus. reed canary grass and triticale as determined by the boundary line approach, *Agriculture, Ecosystems & Environment*, Vol.112, pp. 335-346;
[20] Lewandowski I., Clifton-Brown J.C., Scurlock J.M.O., Huisman W., (2000), Miscanthus: European experience with a novel energy crop, *Biomass and Bioenergy*, Vol.19, pp. 209-227;
[21] Matyka M., Kus J., (2016), Influence of soil quality for yielding and biometric features of Miscanthus × giganteus, Polish Journal of Environmental Studies, Vol.25, No 1, pp.231-219;
[22] Milovanovic J., Drazic G., Ikanovic J., Jurekova Z., Rajkovic S., (2012), Sustainable production of biomass through Miscanthus giganteus plantation development, *Annals of faculty engineering Hunedoara,* Tome X, pp. 79-82;
[23] McKervey Z., Woods V.B., Easson D.L., (2008), Miscanthus as energy crop and its potential for Northern Ireland. *Global Research Unit AFBI Hillsborough, Occasional publication*, Vol.8, p.37;
[24] Nixon P., Bullard M., (2001), *Planting and growing Miscanthus*, London: DEGRA Publications, 20 p;
[25] Naiem A.A., Abdelatif A.H., (2001), Chemical measurement of total soluble sugars as a parameter for cotton lint stickiness grading, *Seminar of the project "Improvement of the marketability of cotton produced in zones affected by stickiness"*. *Proceedings of the seminar*, pp.112-117;
[26] Nishiwaki A., Mizuguti A., Kuwabara S., Toma Y. et al., (2011), Discovery of natural Miscanthus (Poaceae) triploid plants in sympatric populations of Miscanthus sacchariflorus and Miscanthus sinensis in southern Japan. *American Journal of Botany,* Vol. 98, pp.154-159;
[27] Rakhmetov D.B., Scherbakova T.O., Rakhmetova S.O., (2015), High-potential energy plants of Miscanthus Anderss. genus introduced in M.M. Gryshko National Botanical Garden of the NAS of Ukraine (Перспективні енергетичні рослини роду Miscanthus Anderss., інтродуковані в Національному ботанічному саду ім. М.М. Гришка НАН України), *Plant introduction,* Vol. 1(65), pp. 3-18;
[28] Rakhmetov D.B, Shcherbakova T.O, Rakhmetov S.D., (2015), Miscanthus in Ukraine: introduction, biology, bioenergetics (Міскантус в Україні: інтродукція, біологія, біоенергетика), *Kiev: Phytosociocenter*, p.158;
[29] Richter G. M., Agostini F., Barker A., Costomoris D., Qi A., (2016), Assessment on-farm productivity of Miscanthus crops by combining soil mapping, yield modelling and remote sensing. *Biomass and Bioenergy,* Vol.85, pp. 252-261;
[30] Shumny V., Veprev S., Nechiporenko N., Goyachkovskaya T., et al., (2010), A new form of Miscanthus (Chinese silver grass, Miscanthus sinensis Andersson) as promising source of cellulosic biomass. *Advance in Bioscience and Biotechnology*, Vol.1, pp. 167-170;
[31] Skachok L.M., Kvak V. M., (2016), Comprehensive assessment of growing bioenergy crops as affected by various fertilization system (Комплексна оцінка вирощування біоенергетичних культур залежно від різних систем удобрення), *Scientific works of the Institute of Bioenergetic Crops and Sugar Beet,* Vol. 24, pp. 86-92;
[32] Tsiporenko O.L., Rakhmetov D.B., (2013), Prospects for the genus Miscanthus introduction under conditions of the Zhytomyr Polessye (Перспективи інтродукції видів роду Miscanthus в умовах Житомирського Полісся), *Bulletin ZhNAEU*, Vol. 1(1), pp. 275-280;
[33] Yu J., Zhang J., He M., Fu C., Nevo E., Peng J., (2015), Biology, pre-treatment and genetic development of Miscanthus sinensis, a biomass crop with great potential in China, *Research & Reviews: Journal of Botanical Sciences,* vol. 4(1), pp. 8-17;
[34] Zub H.W., Brancourt-Hulmel M., (2010), Agronomic and physiological performances of different species of Miscanthus, a major energy crop. A review. *Agron. Sustain Dev*., vol. 30(2), pp. 201-214;
[35] Williams M.J., Douglas J., (2011), Planting and Managing Giant Miscanthus as a Biomass Energy Crop, *Technical Note*, no 4, pp.1-22.

SYNTHESIS OF SELF-CENTRING GRIPPERS
/
SINTEZA MECANISMELOR DE PREHENSIUNE AUTOCENTRANTE

Prof. Ph.D. Eng. Moise V., Asoc.Prof. Ph.D.Eng.Tabără I., Lect. Ph.D. Eng. Dudici C.L., As. Ph.D. Stud. Eng. Bănică E., As. Ph.D. Stud. Eng. Rotaru Al., Eng. Boureci Gh. A., Eng. Stroe I.
University Politehnica of Bucharest,
E-mail: victor.moise@yahoo.com

ABSTRACT
The manipulation of cylindrical and spherical parts and blanks by using robots, to move them from a working place to another requires that the gripper fulfils certain conditions. This mechanism must be self-centring, to avoid the deterioration of the robots. In this paper, we made a synthesis of some self-centring grippers, by amplification with simple modular groups, usually RRR dyads. The grippers in the synthesis are considered to be with rigid fingers and with movable catching point.

REZUMAT
Manipularea pieselor si semifabricatelor de formă cilindrică si sferică folosind robotii industriali, pentru a le muta dintr-un loc de lucru in altul, necesita anumite condiţii pentru mecanismul de prehensiune. Acest mecanism trebuie sa fie cu centru de prindere fix, pentru a evita deteriorarea robotilor. În aceasta lucrare este realizata sinteza unor mecanisme de prehensiune cu centru de prindere fix, prin amplificarea cu grupe modulare simple, de obicei diade RRR. Mecanismele de prehensiune pentru care este făcută sinteza sunt considerate a fi cu degete rigide si cu punctul de prindere deplasabil.

INTRODUCTION
Manipulators and industrial robots can manipulate the pieces and blanks of different shapes. In the case of cylindrical or spherical parts or blanks, it is necessary that the gripping mechanism be self-centring, to avoid damaging the robot.

Lately, a lot of studies and researches have been made on the analysis and synthesis of the mechanisms of grippers with rigid fingers for industrial robots or anthropomorphic catching mechanisms (*Azlan N.Z., Yamaura H., 2012; Mesaros-Anghel V. et al., 2016; Chen W., Xiong C., 2016; Tarliman D., 2014; Tilli J. et al., 2014; Zhou X. et. al., 2015; Wu L., Carbone G., Cecarelli M., 2009; Wu L., Kong Y., Li X., 2015).*

In this paper, we will refer only to gripping mechanisms with stiff fingers.

Movements of fingers belonging to gripping mechanisms can be pure rotation, pure translation or planar complex motion.

As a result of this, the gripping centre of cylindrical or spherical parts is movable, depending on the diameter of the parts and on the gripper kinematic dimensions.

Figure 1 shows the kinematic scheme of the mechanisms gripping fingers presented in two different positions. The two fingers are articulated at points A and C and they have prismatic jaws.

The fingers are symmetrically related to axis *OX* and form the angles φ_1, respectively φ_2 with the positive direction of the axis *OX*. The diameters of the two cylindrical parts are *D*1 and *D*2.

The error between the positions of the two centres of the parts is:

$$\Delta L = XO2 - XO1 \tag{1}$$

where:

$$XO1 = R\cos\varphi_1 + BO1\sin\varphi_1$$
$$XO2 = R\cos\varphi_2 + BO1\sin\varphi_2 ; \tag{2}$$

$$BO1 = a + D1/2/\cos\alpha$$
$$BO2 = a + D2/2/\cos\alpha ; \tag{3}$$

$$\sin\varphi_1 = \frac{-R.\cdot e + BO1\sqrt{BO1^2 + R^2 - e^2}}{BO1^2 + R^2}$$
$$\cos\varphi_1 = \frac{BO1\cdot e + R\sqrt{BO1^2 + R^2 - e^2}}{BO1^2 + R^2} \tag{4}$$
$$\sin\varphi_2 = \frac{-R.\cdot e + BO2\sqrt{BO2^2 + R^2 - e^2}}{BO2^2 + R^2}$$
$$\cos\varphi_2 = \frac{BO2\cdot e + R\sqrt{BO2^2 + R^2 - e^2}}{BO2^2 + R^2} \tag{5}$$

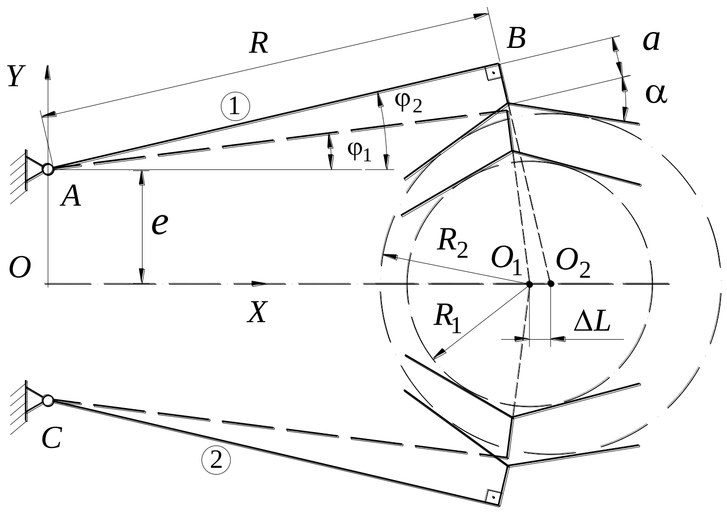

Fig. 1 - Highlighting centres of the cylindrical parts

In the literature related to this field is to be remarked the achievement of various self-centring mechanisms in several ways, namely:
- by kinematic synthesis of the entire mechanism taking into account the self-centring requirements *(Dudita Fl. and Staretu I, 1987; Konstantinov M., 1978; Kovacs Fr. and Cojocari G., 1982; Simionescu et al., 1987)*;
- by the synthesis of cams for actuating jaws in order to fulfil the centring condition *(Huang Qingsen, 1982)*;
- by shaping the caching jaws of the gripping mechanism, so that the gripping centre to remain fixed *(Simionescu et al., 1988).*

MATERIAL AND METHODS

In the present paper, we made a synthesis of self-centring gripping mechanisms, by amplifying the gripper with movable self-centring catching mechanism with simple modular groups, typically RRR dyads.

Figure 2.a shows the kinematic scheme of a gripper with bars, lower pairs and movable gripping centre, and Figure 2.b presents its schematic multipolar diagram.

Considering the multipolar scheme, it results that the gripper contains, besides to base group Z(0), a motohexade with lower pair (motor group with a hexagonal contour).

The mechanism gripping shown in Figure 2 can be transformed into a self-centring gripper, like the one presented in Figure 3, by amplifying it with two dyads RRR, which are designed to guide the nippers of the fingers so that the catching centre to remain fixed for a certain range of diameters of parts to be caught between its fingers.

Determination of elements dimensions contained in the modular groups involves two steps, namely:
a) establishing the old mechanism kinematic parameters for a given number of diameters to be gripped, considering point P as being fixed;
b) synthesis of the new mechanism from the self-centring conditions.

The synthesis equations are determined by using the contour *OT’TDEFPO*. By projecting the vector equation:

$$\overline{OT'} + \overline{T'T} + \overline{TD} + \overline{DE} = \overline{OP} + \overline{PF} + \overline{FE}\,, \tag{6}$$

on the axes of the coordinates system results the system presented below:

$$\begin{cases} S_i + b - XP + DE\cos\varphi_{3i} + EF\sin(\varphi_{4i} + \alpha - \beta) - \\ \qquad\qquad - FP\cos\varphi_{4i} = 0; \\ d + DE\sin\varphi_{3i} - EF\cos(\varphi_{4i} + \alpha - \beta) - FP\sin\varphi_{4i} = 0; \\ i = \overline{1, p}, \end{cases} \tag{7}$$

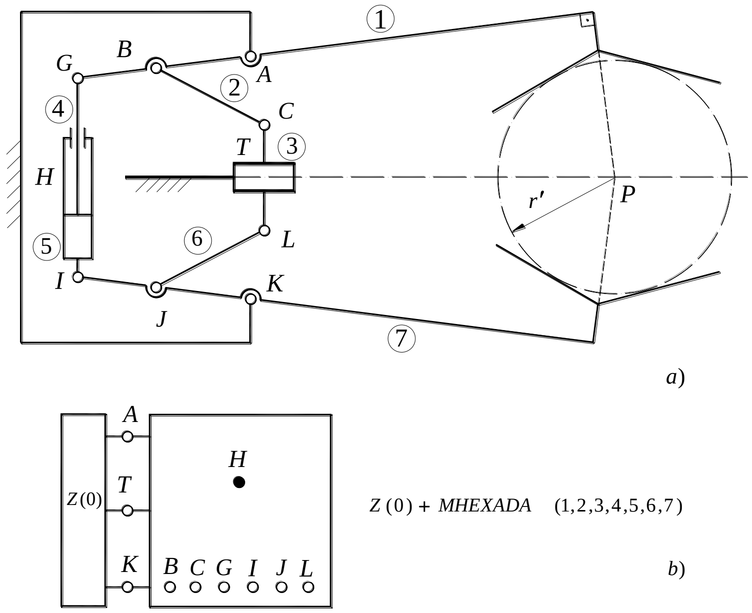

Fig. 2 - Gripper with movable gripping centre depending on the gripping parts diameter
a) kinematic scheme b) multipolar scheme

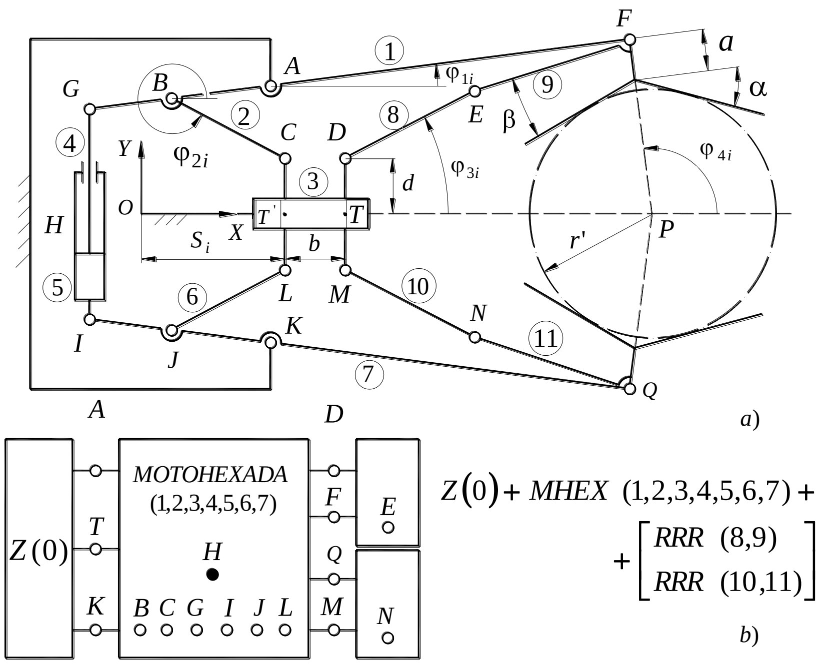

Fig. 3 - Self-centring gripper with bars
a) kinematic scheme; b) multipolar scheme

In the above system, ***p*** represents the number of positions for which the gripping is exact.

We obtained a system of non-linear equations which has the unknowns: *b*, *d*, *DE*, *EF*, β, φ_{3i}, $i = \overline{1, p}$ Starting from the condition of compatibility: 2*p* = 5+*p*, results *p* = 5, so there are 5 possible solutions for which the gripping is done accurately.

The accomplished system of non-linear equations is solved by using an adequate numerical method (Newton-Raphson, gradient etc.); *(Bakvalov, N., 1976; Dorn W.S., Mc Cracken D.D., 1976; Demidovitch, B.P., Maron I.A., 1981)*. The number of system equations can be reduced from 10 equations to 5 equations by eliminating the angle φ_{3i}. In this way is achieved a system of non-linear equations which has the unknowns: *b*, *d*, *DE*, *EF*, β namely:

$$\begin{cases} b11 + 2b1[EF\sin(\varphi_{4i} + \alpha - \beta) - FP\cos\varphi_{4i}] - \\ \quad - 2d[EF\cos(\varphi_{4i} + \alpha - \beta) + FP\sin\varphi_{4i}] \\ \quad - 2EF.FP\sin(\alpha - \beta) = 0; \\ i = \overline{1, p}, \end{cases} \tag{8}$$

where:

$$b11 = b1^2 - DE^2 + EF^2 + FP^2 + d^2,$$
$$b1 = b + S_i - XP.$$

In figure 4 is presented the kinematic scheme a) and multipolar scheme b), of a self-centring gripper fulfilled from a gripping mechanism with moveable centre and composed from a motor tetrad with bars and gears, amplified with two dyads *RRR*.

The system of equations used for the synthesis of the mechanism is:

$$\begin{cases} XE - XP - EF\cos(\varphi_{1i} + \gamma) + FG\cos\varphi_{2i} - HP\cos\varphi_{3i} - \\ \quad + HG\sin(\varphi_{3i} + \alpha - \beta) = 0; \\ YE - YP + EF\sin(\varphi_{1i} + \gamma) + FG\sin\varphi_{2i} - HP\sin\varphi_{3i} - \\ \quad - HG\cos(\varphi_{3i} + \alpha - \beta) = 0; \\ i = \overline{1, p}, \end{cases} \tag{9}$$

where:

HP = a+D/2/cosα.

The unknowns of obtained system non-linear equations are: *EF*, *FG*, *HG*, β, γ, φ_{2i}, $i = \overline{1, p}$.

Taking into account the condition of compatibility results the solution p = 5. The variable dimensions φ_{1i}, φ_{3i} are determined previous to synthesis by taking into account the kinematic analysis of the initial mechanism. By eliminating the angle φ_{2i} the nonlinear system is reduced from 10 to 5 nonlinear equations as follows:

$$\begin{cases} b22 + 2EF(HP\cos(\varphi_{1i} + \varphi_{3i} + \gamma) - HG\sin(\varphi_{1i} + \varphi_{3i} + \alpha - \beta + \gamma) + \\ + (XE - XP)\cos(\varphi_{1i} + \gamma) + (XE - YP)\sin(\varphi_{1i} + \gamma)) - \\ - 2HP(HG\sin(\alpha - \beta) + (XE - XP)\cos\varphi_{3i} + (YE - YP)\sin\varphi_{3i}) - \\ - 2HG((XE - XP)\sin(\varphi_{3i} + \alpha - \beta) - (XE - YP)\cos(\varphi_{3i} + \alpha - \beta)) = 0; \\ i = \overline{1, p}, \end{cases} \tag{10}$$

where:

$$b22 = EF^2 - FG^2 + HP^2 + HG^2 + (XE - XP)^2 + (YE - YP)^2$$

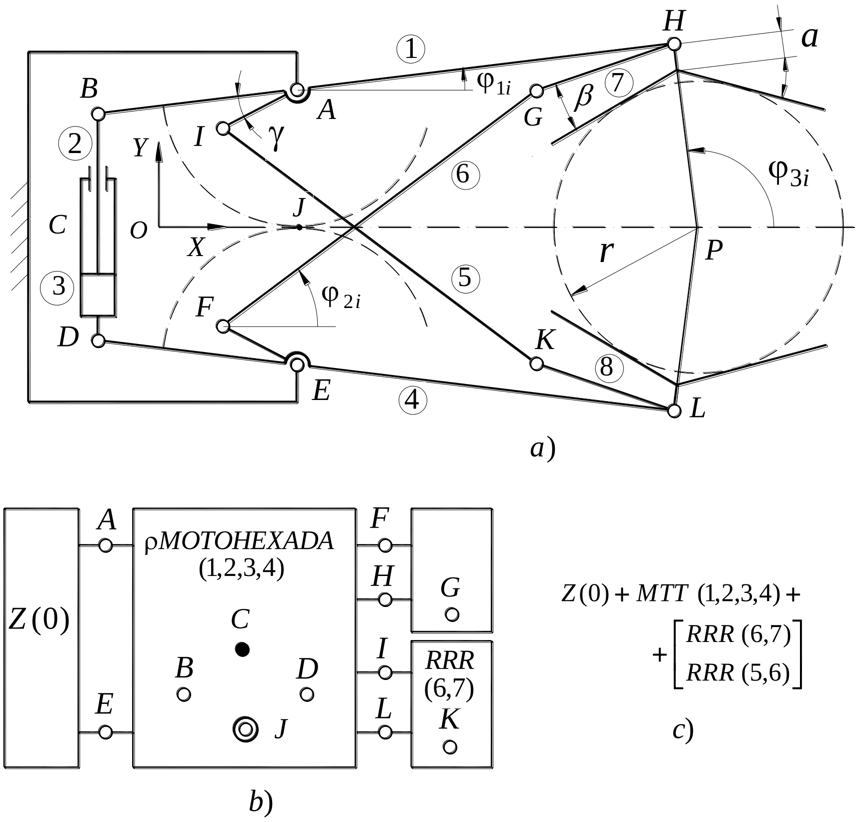

Fig. 4 - Self-centring gripper with bars and gears
a) kinematic scheme; b) multipolar scheme

RESULTS

To convert the gripper with the movable catching centre depending on the diameter of the caught parts into a self-centring gripping mechanism were considered:

- the diameter range of the griped parts between 0.040 and 0.08 [m].
  - α = 0.5235987 [rad];
  - *a* = 0.010 [m];
  - *XP* = 0.165 [m]
  - *XA* = 0.065 [m];
  - *YA* = 0.040 [m];
  - *AB* = 0.030 [m];
  - *BC* = 0.053 [m];
  - *AF* = 0.102 [m];
  - *CT'* = 0.010 [m].

Analysing the mechanism shown in figure 2, the resulted angles are φ_{1i}, φ_{2i} as well as the variable parameter in the prismatic pair T.

Solving the system of linear equations, afferent to the mechanism considered for synthesis, we have:

b = -0.03725 [m];
d = 0.02719 [m];
DE = 0.07294 [m];
EF = 0.05435 [m];
β= 0.52336 [rad].

The results below represent the links dimensions of RRR attached dyad as well as the connection elements with the initial mechanism.

CONCLUSIONS

The method of synthesis presented in this paper allows an easy adaptation of some gripping mechanisms with mobile gripping centre, into ones with fixed gripping centre, by development through simple modular groups, usually RRR dyads.

The presented method is very simple, clear, intuitive and easy to use.

Gripping mechanisms can be used successfully in the construction of agricultural machinery.

REFERENCES

[1] Azlan N.Z., Yamaura, H., (2012), Anthropomorphic finger with optimized geometric parameters for pinching and grasping tasks, *Mechanism and Machine Theory,* vol.49, pp.52-66;

[2] Chen W., Xiong C., (2016), On adaptive grasp with under actuated anthropomorphic hand, *Journal of Bionic Engineering*, vol. 13, pp.59-72;

[3] Bakvalov N., (1976), *Numerical methods* (*Methodes numeriques*), Mir Press, Moscow/Russia;

[4] Carbone G., (2013), *Grasping in Robotics*, vol. 10, Springer Publisher;

[5] Demidovitch B.P., Maron I.A., (1981), *Computational mathematics*, Mir Publicher, Moscow/Russia;

[6] Dudiţă Fl., Stareţu I., (1987*),* Synthesis and structural systematisation of the three-jaws gripping mechanisms (Sinteza şi sistematizarea structurală a mecanismelor de prehensiune cu trei bacuri)*, 7th National Symposium of Industrial Robots (Al VII-lea Simpozion Naţional de Roboţi industriali)*, vol. I, pp. 192-198, Bucharest/Romania;

[7] Dorn W.S., Mc Cracken D.D., (1976), *Numerical methods with FORTLAN programs (Metode numerice cu programe în FORTRAN)*, Technology Press, Bucharest/Romania;

[8] Konstantinov M., (1978), *Criteria for designing the gripping mechanism for manipulators and industrial robots (Kriterien zum Entwurf von Greifmechanism fur Manipulatoren. und Industrierobotor),* Maschinenbautechnik 27;

[9] Kovacs Fr., Cojocaru G., (1982)*, Manipulators, robots and their industrial applications (Manipulatoare, roboţi şi aplicaţiile lor industriale)*. “Facla” Publishing House, Timisoara/Romania;

[10] Huang Qingsen, (1982), A linkage mechanism for the concentric gripping of cylindrical components, *12 th International Symposium on industrial Robots*, 9 -11 June, Paris/France;

[11] Mesaros-Anghel V., Lovasz E.-C., Gruescu C.M., Moldovan C.E., (2016), Optimal design of a Grasping Device Through Simplified Pose Synthesis of a Four-Bar Linkage, *The Joint International Conference of the XII International Conference on Mechanisms and Mechanical Transmissions (MTM) (MTM) and the XXIII International Conference on Robotics (Robotics’16), pp. 3-14, Aachen / Germany;*

[12] Simionescu I., Moise V., Ene M., Neacșa M., Spanu A., Pascu S., (1988), Self-centred prehension mechanisms, (Mecanisme de prehensiune autocentrante), *7th National Symposium of Industrial Robots (Al VII-lea Simpozion Naţional de Roboţi industriali)*, vol. I, pp. 284-287, Bucharest / Romania;

[13] Simionescu I., Ion I., Ciupitu L., (2010), *Mechanisms of Industrial Robots, vol II. Gripping Mechanisms, Mechanisms for Ordering, Orientation and Transfer*, A.G.I.R. Publishing House, Bucharest/Romania;

[14] Simionescu I., Moise V., Ene M., Ion I., (1988), Prehension mechanisms with profiled jaws (Mecanisme de prehensiune cu bacuri profilate), *7th National Symposium of Industrial Robots (Al VIII-lea Simpozion Naţional de Roboţi industriali)*, vol. II, pp. 799-802, Cluj Napoca / Romania;

[15] Tarliman D., (2014), *Researches on industrial robots gripping systems using pneumatic muscles*, Ph. D. Thesis, Brasov / Romania;

[16] Tilli J., Brando A., Fantoni G., (2014), Gripping device for heavy and deformable materials handling: concept, design, selection and test, *Procedia CIRP* 21, pp.373-378;

[17] Zhou X., Majidi C., O’Reilly O.M., (2015), Soft hands: an analysis of some gripping mechanisms in soft robot design, *International Journal of Solids and Structures*, 64-65, pp.155-165;

[18] Wu L., Carbone G., Cecarelli M., (2009), Design an under-actuated mechanism for a 1 active DOF finger operation, *Mechanism and Machine Theory,* 44(2), pp.336-348;

[19] Wu L., Kong Y., Li X., (2015), Review and research Issues on under-actuated finger mechanism. In *Proceedings Chinese Intelligent Automatic Conference*, p.171, Springer.

DETERMINATION OF RATIONAL OPERATING PARAMETERS FOR A VIBRATING DYSK-TYPE GRINDER USED IN ETHANOL INDUSTRY
/
ВИЗНАЧЕННЯ РАЦІОНАЛЬНИХ ЕКСПЛУАТАЦІЙНИХ ПАРАМЕТРІВ ВІБРОДИСКОВОЇ ДРОБАРКИ СПИРТОВОЇ ГАЛУЗІ

Ph.D. Yanovich V.P., Assist. Kupchuk I.M.
Vinnitsa National Agrarian University / Ukraine
Tel: +380978173992; E-mail: kupchuk.igor@mail.ru

Keywords: *grinding, vibration, performance, angular velocity, humidity*

ABSTRACT
The article shows a schematic diagram of a vibrating disk-type grinder for chopping corn starch substance in ethanol production, achieving the idea of a combined interaction between vibrational and rotational motion of the working body, a combination of shock and cutting impact of working bodies on the material, which will handle both certified substance and substance materials with a high moisture content without significantly reducing equipment bandwidth and ensuring the timely product withdrawal from the grinding zone.
Also, were determined the rational vibration modes of the disk cutters by experimental evaluation of equipment performance, which resulted in a performance charts depending on the angular speed of the rotor, sieve orifice diameters and humidity.

РЕЗЮМЕ
У статті приведена принципова схема вібродискової дробарки для подрібнення зернової крохмалевмісної сировини спиртового виробництва, яка реалізує ідею комбінованого взаємодії вібраційного і обертального руху виконавчого органу, поєднання ударного і ріжучого впливу робочих елементів на матеріал, що дозволить обробляти як кондиційну сировину так і сировину з підвищеним вмістом вологості без значного зменшення пропускної здатності обладнання та забезпечити своєчасне виведення продукту із зони подрібнення.

Також було визначено раціональні режими роботи вібраційної дискової дробарки, шляхом експериментальної оцінки продуктивності обладнання, в результаті чого було отримано графічні залежності продуктивності від кутової швидкості ротора, діаметра перфорації сита та вологості.

INTRODUCTION
One of the most important and energy-intensive processes in ethanol production is material grinding, which is usually performed by a hammer grinder. Therefore, effective implementation of constructive machines to perform the designated operations and study their parameters determines the relevance of these studies.

Based on the analysis of processes*(Turshatov M.V., 2011; Abramova I.M., 2012; Billomyttcev A.S., Druzhynin E.I., Morachkovsky O.K. 2016; Dudnikov A.A., Belovod A.I., Pasyuta A.G., 2015; Toneva P., Epple P., Breuer M., 2011)*and structural schemes of existing equipment*(Turshatov M.V., 2011; Abramova I.M., 2012; Kuzo I.V., Lanets O.S., Gursky V.M., Shpak Y.V., 2015; Sydorenko I.I., Kushnir A.Y., Baidzhanov S.M., 2015)*for implementing the process of grinding and weight loss, we offer a better way of grinding grain substance for alcohol production, the essence of which is in the development of a fundamentally new grinder scheme, which could achieve a combination of shock and cutting impact of workingbodies on the material, which will handle both certified substance and substance materials with a high moisture content without significant reductting equipment bandwidth and the timely product withdrawal from the crushing zone, by levelling the excessive air circulation on product layer, and consequently reducing specific energy consumption for the mentioned treatment *(Deinychenko G.V, Samoichuk K.O., Ivzhenko A.O., 2016; Wang Y., Wang S., 2007)*.

However, to achieve high rates of energy efficiency, it is necessary to prove rational equipment operation by experimental evaluation of the productivity of equipment developed for the process of grinding starch containing grain materials.

MATERIAL AND METHODS

The experimental part of the work was conducted at the laboratory processes and equipment, processing and food production department in Vinnitsa National Agrarian University and in the "Ovechatske MPD" SE "Ukrspirt" specialized laboratory, using experimental and industrial design of the vibrating disk-type grinder *(Palamarchuk I.P., Yanovych V.P., Kupchuk I.M., Solomko I.V., 2013)* (Fig.1) for which when switching on the motor *5*, torque moment is transmitted through the clutch *6,* to the kinematic shaft *7* and counter weights *8*, the rotation of which leads to the creation of a combined power and torque placed on the unbalanced axles of rotor *9* and vibrating disk *10*. The material to be grinded continuously goes through the inlet *2* and is crushed due to the rotating and oscillating movement of disk *10*. When particle size decreases, the material is crushed under the influence of centrifugal forces and alternating loads undergo intense classification on the sieve surface: particles with diameters equal to or smaller than sieve *4* openings are discharged through the outlet *3*, the rest are re-grinded *(PalamarchukI.P., YanovychV.P., KupchukI.M., SolomkoI.V., 2013)*.

For the study on the technological characteristics of the equipment developed for the grinding process, a series of experiments to change the properties of the dispersed material (maize) under shock-cutting impact in the "vibration force field" were conducted.

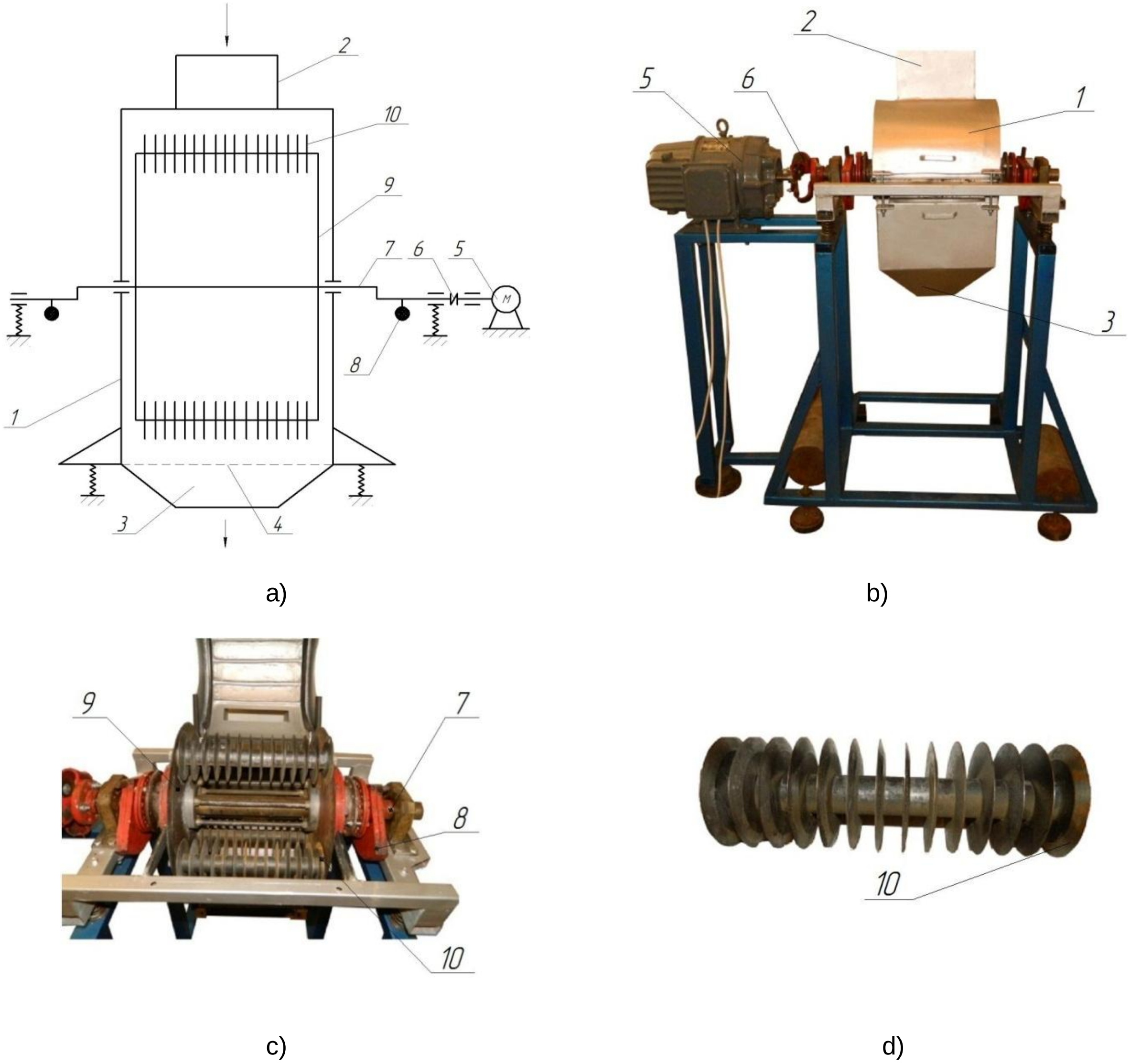

Fig. 1 - Vibration disk-type grinder

a) the basic scheme; b) general view; c) the working body; g) disc beat;
1 - the case; 2, 3 –material inlet and outlet; 4 - sieve; 5 - electric motor; 6 - elastic sleeve;
7 - kinematic shaft; 8 - counterweight; 9 - rotor; 10 –vibrating disk

Performance evaluation was performed by weighing the shredded material that passed through the mill for an hour. To determine the material mass, a BTA-60 / 30-5-T electronic laboratory technical balance (Fig. 2) was used.

Fig. 2 - BTA-60 / 30-5-T Electronic laboratory technical balance

1 - weighing pan; 2 - panel calibration; 3 - display indicator

Table 1

Technical characteristics of laboratory scales BTA-60 / 30-5-T

Parameter	Range
Maximum weighing, kg	30
The lowest weight, kg	0.02
Readability charging mass, g	1/2/5/10
Operating temperature range	+10 ... +40
Power supply, W	187 ... 242
Power consumption, W	15
Weighing pan dimensions, mm	220 x 340
Weights overall dimensions, mm	325 x 345 x 95

To record the rotational speed of the drive shaft, aUNI-T UT372 wireless tachometer (Fig.3) was used, and its operation principle is described in the technical documentation.

Fig. 3 - UNI-T UT372 Tachometer

1 - laser scanner; 2 - digital display; 3 - control panel

To manage and change the rotation frequency of the motor shaft, an AOSN-20-220-75 autotransformer (Fig.4) is used, which is designed to work with alternating current. It contains current down taking movable contact in the form of graphite roller, allowing infinitely variable voltage from zero to the maximum. Also, the autotransformer has several terminals, through which one can get different current output characteristics.

AOSN-20-220-75 performance laboratory autotransformer enables real-time analysis on performance, power consumption and number of motor revolutions.

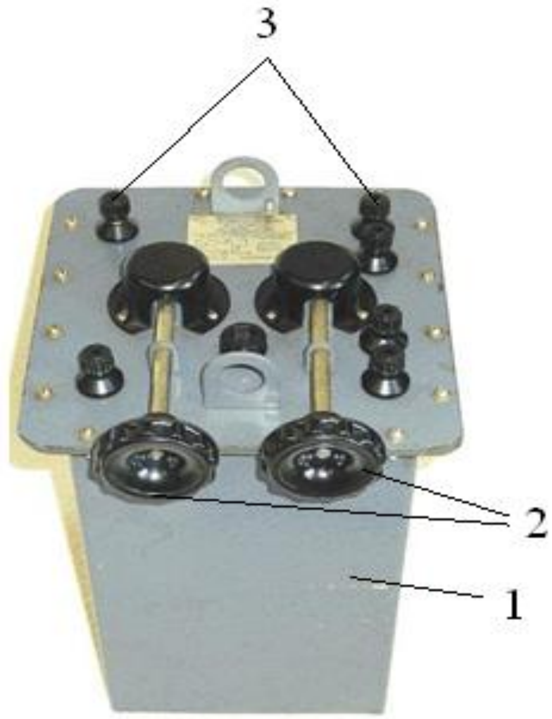

Fig. 4 - AOSN-20-220-7 laboratory autotransformer
1 - outer casing; 2 - voltage regulators; 3 - input and output terminals

To determine the relative humidity of the material, the Wile 55 Moisture analyser (Fig.5) was used, which can measure the relative humidity of various types of grains and seeds, recording the results in the device’s memory.

Fig. 5 - Wile-55 moisture analyser
1 - housing cover; 2 - digital display; 3 - control panel; 4 - capacity for sample

Technical characteristics of the device are shown in table 2, the working principle and rules of operation in the technical documentation.

Table 2

Wile-55 moisture analyser technical characteristics

Index	Value
Grain and seeds, %	8 ... 35%
Oilseeds, %	5…25
Operating temperature, ^{0}C	0 ... 40
Accuracy,%	± 0.1%
Power, W	9 (IEC 6F22)
Length, mm	120
Width, mm	80
Height, mm	210
Weight, kg	0.8

RESULTS

The data obtained from the experimental studies was processed and interpreted using Microsoft Excel software.

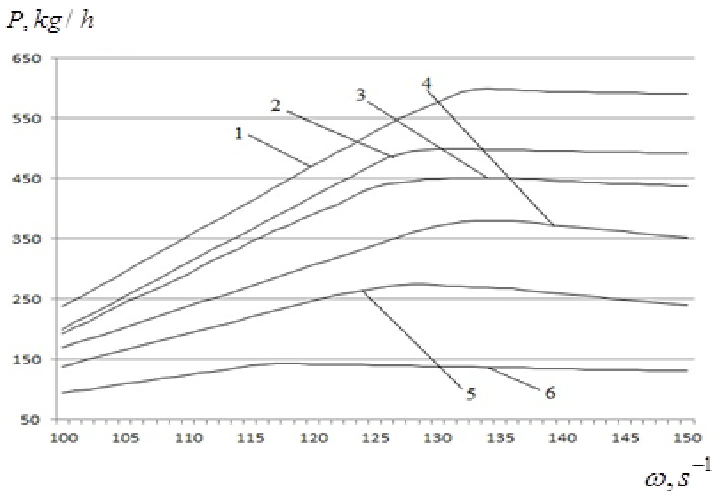

Fig. 6 -Productivity depending on the speed of the rotor and sieve orifice sizes (*d*):
1 - with d = 2 mm; 2 - with d = 1.8 mm; 3 - with d = 1.6 mm; 4 - with d = 1.4 mm; 5 - at d = 1.25 mm; 6 - with d = 1 mm

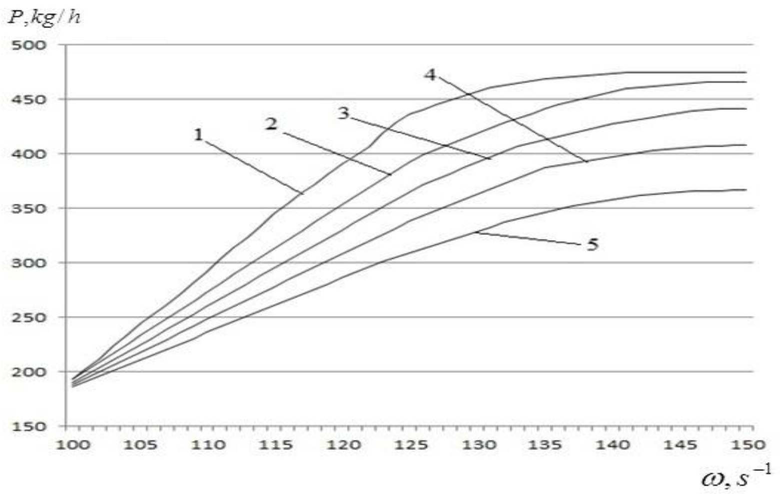

Fig. 7 - Productivity depending on the speed of the rotor and humidity (*H*):
1 - when H = 13 - 14%; 2 - when H = 15 - 16%; 3 - when H = 17-18%; 4 - when H = 19 - 20%; 5 - when H = 21 - 22%.

Fig. 6 shows the change in grinder productivity depending on the angular velocity of the rotor and the diameters of orifices in the separation surface (sieve) of the grinder. The results of experimental studies on changes in equipment productivity depending on the angular velocity of the rotor and the relative humidity of the material are shown in Fig. 7.

CONCLUSIONS

Analysing the dependence charts obtained, we can conclude that the productivity *P* increases with increasing the frequency of rotation, but when reaching the rotation frequency of 125-135 rad/s or more, a decrease of productivity growth is observed. This indicates excessive recirculation of re-grained material and unreasonableness of the machine operation, when the rotor angular velocity is greater than 125-135 rad/s. In addition, it was found that material moisture significantly affects the performance, especially at the same frequency (rad/s), performance decreased by more than 25%, namely from 450 kg/h to 325 kg/h during the grinding of materials with 13- 14 %, respectively 21-22% humidity, which allows selecting the optimal flow of material. Productive works should not exceed the experimentally installed capacity ranges of the equipment.

REFERENCES

[1] Abramova I.M., (2012) Features of wheat raw materials processing, ensuring the production of alcohol with high quality indicators (Особенности переработки пшеничного сырья, обеспечивающие производстваспирта с высокимипоказателямикачества), *Production of ethanol and alcoholic beverages (Производство спирта и ликероводочных изделий),* № 1, pp. 4–10;

[2] Gusev Y.I., Karasjov I.N., Kolman E.E., (1985), Design and calculation of machines for chemical industries: a textbook for machine building. Universities on spec. "Chemical engineering and instrumentation" (Конструирование и расчетмашинхимичискихпроизводств: учебникдлямашиностроит. вузовпоспец. «Химическоемашиностроение и аппаратостроение»*), Mechanical engineering (Машиностроение)*, p. 408;

[3] Islam M.N., Matzen R., (1988), Size distribution analysis of ground wheat by hammer mill, *Powder Technol*, № 54, pp.235–241;

[4] Palamarchuk I.P., (2008), *Scientific and technical bases of development of energy-efficient mechanical vibration action of food and processing industries (Науково-технічні основи розроблення енергозберігаючих вібромашин механічної дії харчових і переробних виробництв*), Dr.hab.dissertation, National University of Food Technologies, Kiev/Ukraine;

[5] Palamarchuk I.P., Kupchuk I.M., (2012), Prospects of low-frequency vibrations in the grinding of raw alcohol production (Перспективи застосування низькочастотних коливань в процесі подрібнення сировини спиртового виробництва), *Vibration in engineering and technology (Вібрації в техніцітатехнологіях)*, № 4 (68), pp. 5–13;

[6] Palamarchuk I.P., Yanovych V.P., Kupchuk I.M., (2013), Justification of technology and equipment for the pre-treatment of raw starch in the production of alcohol (Обґрунтування технології та обладнання для попередньої обробки крохмалевмісної сировини при виробництві спирту), *Vibration in engineering and technology (Вібрації в техніцітатехнологіях)*, № 4 (72), pp. 112–116;

[7] Palamarchuk I.P., Yanovych V.P., Kupchuk I.M., Solomko I.V., (2013), Development of the structural technological scheme of vibrating rotor grinder (Розробка конструктивно-технологічної схеми вібророторної дробарки), *Vibration in engineering and technology* (*Вібрації в техніцітатехнологіях*), №1(69), pp.125-129;

[8] Palamarchuk I.P., Yanovych V.P., Kupchuk I.M., (2013), *Grinder rotor vibration (Вібророторнадробарка)*, Patent № 85270, UA;

[9] Turshatov M.V., (2011), Modern technology of ethanol production (Современная технология производства спирта), *Production of ethanol and alcoholic beverages (Производство спирта и ликероводочных изделий),* № 1, pp. 24-30;

[10] Palamarchuk I.P., Yanovych V.P., Kupchuk I.M., (2015), Experimental evaluation of energy parameters vibration rotary grinder of starch raw materials in the ethanol industry (Експериментальна оцінка енергетичних параметрів вібророторної дробарки крохмаловмістної сировини спиртової промисловості), *Vibration in engineering and technology* (Вібрації в техніцітатехнологіях), № 3(79), pp.133–136;

[11] Pimentel D., Patzek T.W., (2005), Ethanol production using corn, switchgrass, and wood; biodiesel production using soybean and sunflower, Natural resources research, Vol.14, pp. 65–76;

[12] Toneva P., Epple P., BreuerM., (2011), Grinding in an air classifier mill, *Powder Technology,* № 211, pp.19–27.

WRITING NORMS

Article Types

Three types of manuscripts may be submitted:

1. **Regular articles:** These should describe new and carefully confirmed findings, and experimental procedures should be given in sufficient detail for others to verify the work. The length of a full paper should be the minimum required to describe and interpret the work clearly (max.10 pages, even number);
2. **Short Communications:** A Short Communication is suitable for recording the results of complete small investigations or giving details of new models or hypotheses, innovative methods, techniques or apparatus. The style of main sections has not necessarily to be in accordance with that of full-length papers (max. 6 pages, even number);
3. **Reviews:** Submissions of reviews and perspectives covering topics of current interest are welcome and encouraged (max.10 pages, even number).

Manuscripts should be written in English (American or British usage is accepted, but not a mixture of these) and submitted **electronically** at the following e-mail addresses: ***inmatehjournal@gmail.com***
Please be sure to include your full affiliation and e-mail address (see Sample manuscript)
The authors are responsible for the accuracy of the whole paper and references.
There are allowed 2 papers by each first author.
The text layout should be in single-column format. To avoid unnecessary errors it is strongly advised to use the "spell-check" and "grammar check" functions of your word processor.

Review Process

All manuscripts are reviewed by 2 members of the Scientifically Review Office. Decisions will be made as rapidly as possible and the journal strives to return reviewers' comments to authors in approx.3 weeks.
The editorial board will re-review manuscripts that are accepted pending revision.

NOTE:

Submission of a manuscript implies: that the work described has not been published before (excepting as an abstract or as part of a published lecture or thesis) that it is not under consideration for publication elsewhere.

1. REGULAR ARTICLES

- Manuscripts should be concise, in ***1.15 line spacing***, and should have 2 cm all over margins. The font should be ***Arial 10 pt.*** Ensure that each new paragraph is clearly indicated, using **TAB at 1 cm**.
- Title will be ***Arial 12 pt***. and explicit figures will be ***Arial 9 pt***.
- Text will be written in English.
- Chapters' titles are written by ***Arial 10 pt, Bold, Uppercase*** (e.g. **INTRODUCTION, MATERIAL AND METHODS**), between chapters is left a space for 10 pt. At the beginning of each paragraph, TAB of 1 cm.
- The paper body will be written in ***Arial 10 pt., Justify alignment***.

TITLE ***Arial 12 pt., Uppercase, Bold, Center*** *(in English language)* and ***Bold Italic*** *(in native language)*.
Should be a brief phrase describing the contents of the paper. Avoid long titles; a running title of no more than 100 characters is encouraged (without spaces).

AUTHORS ***ARIAL 9, Bold, Centre alignment***
Under the paper's title, after a space (enter) 9 pt., write ***authors' names*** and ***affiliations (Arial 8 pt.-Regular)***
When the paper has more than one author, their name will be followed by a mark (Arabic numeral) as superscript if their affiliation is different.
Corresponding author's name (next row), ***(Arial 8 pt.)***. Should be added also: phone, fax and e-mail information, for the paper corresponding author (***font: 8 pt., Italic***).

KEYWORDS ***(In English)*** about 4 to 7 words that will provide indexing references should be listed (title: ***Arial 10pt, bold italic,*** text ***Arial 10 pt., italic***).

A list of non-standard *Abbreviations* should be added. In general, non-standard abbreviations should be used only when the full term is very long and used often. Each abbreviation should be spelled out and introduced in parentheses the first time it is used in the text. Standard abbreviations (such as ATP and DNA) need not to be defined.

ABSTRACT ***(in English and Native language, Arial 10 pt.)***, the title *bold*; the text of abstract: *italic*) should be informative and completely self-explanatory, briefly present the topic, state the scope of the experiments, indicate significant data, and point out major findings and conclusions. The Abstract should be max.250 words. Complete sentences, active verbs, and the third person should be used, and the abstract should be written in the past tense. Standard nomenclature should be used and abbreviations should be avoided. No literature should be cited.

INTRODUCTION (***Arial 10 pt.***) should provide a clear statement of the problem, the relevant literature on the subject, and the proposed approach or solution. It should be understandable to colleagues from a broad range of scientific subjects. We should refer to the current stage of researches performed in the field of the paper to be published, by quoting up-to-date specialty studies, preferably published after 2006, excepting certain referential specialty books/studies, especially papers issued in magazines/journals/conferences/ISI quoted symposia or in other international data bases, which are well known and available.

MATERIALS AND METHODS (***Arial 10 pt.***) should be complete enough to allow experiments to be reproduced. However, only truly new procedures should be described in detail; previously published procedures should be cited, and important modifications of published procedures should be mentioned briefly. Methods in general use need not be described in detail.

RESULTS (***Arial 10 pt.***) should be clarity presented. The results should be written in the past tense when describing findings in the authors' experiments. Results should be explained, but largely, without referring to the literature. Discussion, speculation and detailed interpretation of data should not be included in the Results, but should be put into the Conclusions section.

CONCLUSIONS (***Arial 10 pt.***) The main conclusions drawn from results should be presented in a short Conclusions section. Do not include citations in this section.

Formulae, symbols and abbreviations: Formulae will be typeset in Italics (preferable with the Equation Editor of Microsoft Office 2003) and should be written or marked as such in the manuscript, unless they require a different styling. They should be referred to in the text as Equation (4) or e.g. (4). The formulae should be numbered on the right side, between brackets ***(Arial 10 pt.)***:

$$P = F \cdot v \tag{1}$$

Terms of the equation and the unit measure should be explained, e.g.

P is the power, [W];
F – force, [N];
v – speed, [m/s]

SI units must be used throughout.

Tables should be self-explanatory without reference to the text. The details of the methods used in the experiments should preferably be described in the legend instead of in the text. The same data should not be presented both in table and graph form or repeated in the text.

Table's title will be typed***Arial 9 pt, Bold, Centered***

In the table, each row will be written Arial 9 pt, single-spaced throughout, including headings and footnotes.

The table should be numbered on the right side, between brackets ***(Arial 10 pt)***:

Figure (Arial 9 pt., Bold, Center)should be typed in numerical order (Arabic numerals). Graphics should be high resolution (e.g.JPEG).Figure number is followed by what represent the figure or graph e.g.:

Fig.1 – Test stand

Legend: ***Arial 8 pt, Italic, Center,*** e.g.

1 - plansifter compartments; 2- break rolls; 3 – semolina machines; 4 – reduction rolls; 5 – flour

ACKNOWLEDGMENTS (***Arial 10 pt.***) of people, grants, funds etc should be brief (*if necessarily*).

REFERENCES (***Arial 10 pt.***)

(In alphabetical order, in English and in the original publication language).
Minimum 10 references, last 10 years, minimum 3 references from the last 2 years

It can be used"*References*" tool from the *Word Editor*.

References should be cited in the text in brackets as in the following examples:

(Babiciu P., Scripnic V., 2000)

All references must be provided in English with a specification of original language in round brackets.

Authors are fully responsible for the accuracy of the references.
References should be alphabetically, with complete details, as follows:
Examples:

Books: Names and initials of authors, year (between brackets), title of the book (Italic), volume number, publisher, place, pages number or chapter, ISSN/ISBN:

[1] Vlădut V., (2009), *Study of threshing process in axial flow apparatus (Studiul procesului de treier la aparatele cu flux axial),* vol.1, ISSN/ISBN …………, “Terra Nostra" Publishing House, Iaşi/Romania;

Journal Article: Names and initials of authors, year (between brackets), full title of the paper, full name of the journal (Italic), volume number, publisher, place, ISSN, page numbers:

[1] Lizhi Wu, Yan Di., (2005), Demonstrational study on the land consolidation and rehabilitation (LCR) project of saline-alkali soil in arid areas: a case study of Lubotan LCR project in Pucheng County, Shaanxi Province（干旱区盐碱化土地整理工程实证研究-以陕西蒲城县卤泊滩土地整理项目为例）, *Transactions of the Chinese Society of Agricultural Engineering*,vol.21, no.1, pp.179-182, Madison/Wisconsin;

[2] Leonov I.P., (1973), Basic machine theory for tobacco stringing. Post-harvest care of tobacco and rustic tobacco (Основы теории машин для закрепления табака на шнуры. Послеуборочная обработка табака и махорки), *Collection of scientific articles (сборник научно-исследовательских работ)*, pp.37-45;

Conference or Symposium: Names and initials of authors, year (between brackets), full title of the paper (Regular), full name of the conference/symposium (Italic), volume number, publisher, place, ISSN, page numbers

[1] Bungescu S., Stahli W., Biriş S., Vlăduţ V.,Imbrea F., Petroman C., (2009), Cosmos program used for the strength calculus of the nozzles from the sprayers (Program Cosmos folosit pentru calculul de rezistență la zgomot al aparatelor de distribuție), *Proceedings of the 35 International Symposium on Agricultural Engineering "Actual Tasks on Agricultural Engineering",* pp.177-184, Opatija / Croatia;

Dissertation / Thesis: Names and initials of authors, year (between brackets), full name of the thesis (Italic), specification (PhD Thesis, MSc Thesis), institution, place;

[1] Popa L., (2004), *Research on the influence of structural and functional parameters of the braking system on the braking performance of agricultural trailers (Cercetări privind influența caracteristicilor constructive şi funcționale ale sistemelor de frânare asupra performanțelor de frânare ale remorcilor agricole)*, PhD dissertation, Transylvania University of Braşov, Braşov / Romania.

Patents: Names and initials of authors, year (between brackets), patent title (Italic), patent number, country:

[1] Grant P., (1989), *Device for Elementary Analyses*. Patent, No.123456, USA.

Legal regulations and laws, organizations: Abbreviated name, year (between brackets), full name of the referred text, document title/type (Italic), author, place:

[1] *** EC Directive, (2000), Directive 2000/76/EC of the European Parliament and of the Council of 4 December 2000, on the incineration of waste, Annex V, *Official Journal of the European Communities*, L332/91, 28.12.2000, Brussels.

Web references: The full URL should be given in text as a citation, if no other data are known. If the authors, year, and title of the documents are known and the reference is taken from a website, the URL address has to be mentioned after these data:

The title of the book, journal and conference must be written in Italic, the title of the article, chapter of the book, must be written Regular.

Citation in text

Please ensure that every reference cited in the text is also present in the reference list (and vice versa). Do not cite references in the abstract and conclusions. Unpublished results, personal communications as well as URL addresses are not recommended in the references list.

Making personal quotations (one, at most) should not be allowed, unless the paper proposed to be published is a sequel of the cited paper. Articles in preparation or articles submitted for publication, unpublished, personal communications etc. should not be included in the references list.

Citations style

Text: All citations in the text may be made directly (or parenthetically) and should refer to:

- ***single author***: the author's name (without initials, unless there is ambiguity) and the year of publication:
  “as previously demonstrated *(Brown, 2010)*”.
- ***two authors***: both authors' names and the year of publication: *(Adam and Brown, 2008; Smith and Hansel, 2006; Stern and Lars, 2009)*
- ***three or more authors***: first author's name followed by "et al." and the year of publication: “As has recently been shown *(Werner et al., 2005; Kramer et al., 2000)* have recently shown ...."

Citations of groups of references should be listed first alphabetically, then chronologically.

Units, Abbreviations, Acronyms

- Units should be metric, generally SI, and expressed in standard abbreviated form.
- Acronyms may be acceptable, but must be defined at first usage.

Edited by: INMA Bucharest
6 Ion Ionescu de la Brad Blvd., sect. 1, Bucharest, ROMANIA
Tel: +4021.269.32.60; Fax: +4021.269.32.73
http://www.inmateh.eu
e-mail: ***inmatehjournal@gmail.com***